Calcium Activated Chloride Channels In Olfactory Transduction

Thesis submitted for the degree of

Doctor Philosopiae

CANDIDATE

Simone Pifferi

SUPERVISOR

Prof. Anna Menini

Declaration

The work described in this Thesis was carried out at the International School for Advanced Studies, Trieste, between November 2004 and August 2008.

The work described in this Thesis is included in:

Pifferi Simone[*], Pascarella Giovanni[*], Boccaccio Anna, Mazzatenta Andrea, Gustincich Stefano, Menini Anna, Zucchelli Silvia.
Bestrophin-2 is a candidate calcium-activated chloride channel involved in olfactory transduction
Proc Natl Acad Sci U S A 103:12929-12934 (2006).
[*] P.S. and P.G. contributed equally to this work.

Other experiments performed during this Thesis are included in:
Giulietta Pinato, Juraj Rievaj, Simone Pifferi, Michele Dibattista, Lara Masten and Anna Menini.
Electroolfactogram Responses from Organotypic Cultures of the Olfactory Epithelium from Postnatal Mice
Chem. Senses 33: 397–404 (2008)

Simone Pifferi, Anna Boccaccio, Anna Menini
Cyclic nucleotide-gated ion channels in sensory transduction
FEBS Letters 580: 2853–2859 (2006)

Abstract

Ca^{2+}-activated Cl^- channels are an important component of olfactory transduction. Odorant binding to odorant receptors in the cilia of olfactory sensory neurons (OSNs) leads to an increase of intraciliary Ca^{2+} concentration by Ca^{2+} entry through cyclic nucleotide-gated channels. Ca^{2+} activates a Cl^- channel that leads to an efflux of Cl^- from the cilia, contributing to the amplification of the OSN depolarization. The molecular identity of this Cl^- channel remains elusive. Recent evidences have indicated that bestrophins are able to form Ca^{2+}-activated Cl^- channels channels in heterologous systems. Immunohistochemistry revealed that mBest2 was expressed on the cilia of OSNs, the site of olfactory transduction, and co-localized with the main subunit of cyclic nucleotide-gated channels, CNGA2. We performed a functional comparison of the properties of Ca^{2+}-activated Cl^- channels from native channels expressed in dendritic knob/cilia of mouse OSNs with those induced by heterologous expression of mBest2 in HEK-293 cells. Even if the two channels did not display identical characteristics, they have many similar features such as the same anion permeability, the Ca^{2+} sensitivity in micromolar range and the same side-specific blockage of the two Cl^- channel blockers commonly used to inhibit the odorant-induced Ca^{2+}-activated Cl^- channels in OSNs, niflumic acid and 4-acetamido-4'-isothiocyanato-stilben-2,2'-disulfonate (SITS). However electroolfactogram recording from mBest2 null mice showed a normal sensitivity to odorant stimulation. Therefore mBest2 is a good candidate for being a molecular component of the olfactory Ca^{2+}-activated Cl^- channels but its precise role in olfactory transduction remains to be clarified.

Contents

Abbreviations

AC	adenylyl cyclase
BVMD	Best vitelliform macular dystrophy
CaCC	calcium-activated chloride channel
CFTR	cystic fibrosis transmembrane regulator
CNG	cyclic nucleotide-gated
DRG	dorsal root ganglion
EOG	electroolfactogram
GPCR	G-protein coupled receptor
ID	inner diameter
LP	light peak
OD	outer diameter
OR	odorant receptor
OSN	olfactory sensory neuron
PLC	phospholipase C
RPE	retinal pigment epithelium
TM	transmembrane domain

1. Introduction

1.1 The sense of smell

Chemosensation can be defined as the ability of a living organism to detect and discriminate different chemical molecules in the external environment. Its precursors can be found in the most primitive unicellular organisms, reflecting the need of every organism to sense its chemical milieu. This task is essential for survival of the individual and of the species, indeed it enables animals to locate nutritious food and suitable mating partners, and to avoid being eaten by predators or eating toxic substances.

Chemosensory systems (smell, taste) are distinguished from the other senses (vision, hearing, touch) by the qualitative heterogeneity of the stimuli: the chemical senses are responsible for detecting molecules of immense chemical variety. The olfactory repertoire contains aliphatic and aromatic molecules with varied carbon backbones and diverse functional groups, including aldehydes, esters, ketones, alcohols, alkenes, carboxylic acids, amines, imines, thiols, halides, nitriles, sulphides and ethers. A “normal” odor is usually composed by a mixture of different molecules in which the relative concentrations of each component participate to determine the particular perception response.

Moreover the olfactory system is also responsible for the sensing of pheromones, chemicals released by animals that act on conspecifics to regulate populations of animals and their social actions (Karlson & Luscher, 1959). Pheromones are detected by the vomeronasal organ and elicit programmed neuroendocrine controlled behaviors mediated by activation of the amygdala and the hypothalamus (Dulac & Wagner, 2006).

1.2 Anatomical organization of the olfactory system

1.2.1 The olfactory epithelium and the olfactory sensory neurons

The general features of the olfactory system are remarkably conserved across vertebrates. The primary receptor cells are organized to form a neuroepithelium, the olfactory epithelium that lines a series of cartilaginous outcroppings, called turbinates, located in upper reaches of the nasal cavity in mammals. The olfactory epithelium is usually situated posterior to vestibular and respiratory regions (Fig 1.1 A).

The olfactory epithelium is a columnar pseudo-stratified epithelium and it contains essentially three types of cells: olfactory sensory neurons (OSNs), the primary receptor cell, supporting cell (also called sustentacular cells) and basal cells. Moreover the olfactory epithelium of all vertebrate except fish has tubulo-alveolar glands called Bowmann's glands with the alveoli lying in the lamina propria and opening their ducts at the epithelial surface. The olfactory epithelium is thicker than the surrounding respiratory epithelium as seen in histological sections. Its thickness varies from one animal to the other ranging from 30 μm in moles to 150-200 μm in frogs and turtles. The nuclei of the three cellular components are directly arranged in separate layers as can be seen in Fig 1.1 B and C. The epithelial surface is normally covered by layer of mucus 10 to 40 μm thick that is produced by the secretion of Bowmann's glands.

The olfactory sensory neurons are typical primary sensory neurons with bipolar morphology. The receptor cell has a flask-like shape, its length is directly proportional to the thickness of the epithelium, while the diameter of its processes remains more constant (Fig 1.1 D) The cell body has a diameter of 5-8 μm located within the lower two thirds of neuroepithelium. The dendrite, 1-2 μm in diameter, reaches up to the surface of the tissue and ends in a knob-like swelling with an approximate diameter of 2-3 μm. Tens of very fine cilia, usually 20-30, project from the knob and are embedded in mucus covering the epithelium (Fig 1.2). The OSNs of lower vertebrates typically have about 6 motile cilia that can be as long as 200 μm (Menco, 1980). The diameter of a frog cilium tapers from 0.28 μm near the base of the cilium to 0.19 μm in the distal portion (Menco, 1980). In mammals, the cilia are shorter (15–50 μm), thinner (tapering to 0.11 μm), more numerous (averaging 17 per neuron), and nonmotile (Menco, 1980; Lidow & Menco, 1984; Menco, 1997). Graziadei

and Bannister (1967) have estimated that cilia of duck may increase the cell bare surface some one thousand or more times. The cilia are the site of the sensory transduction apparatus (Fig 1.2).

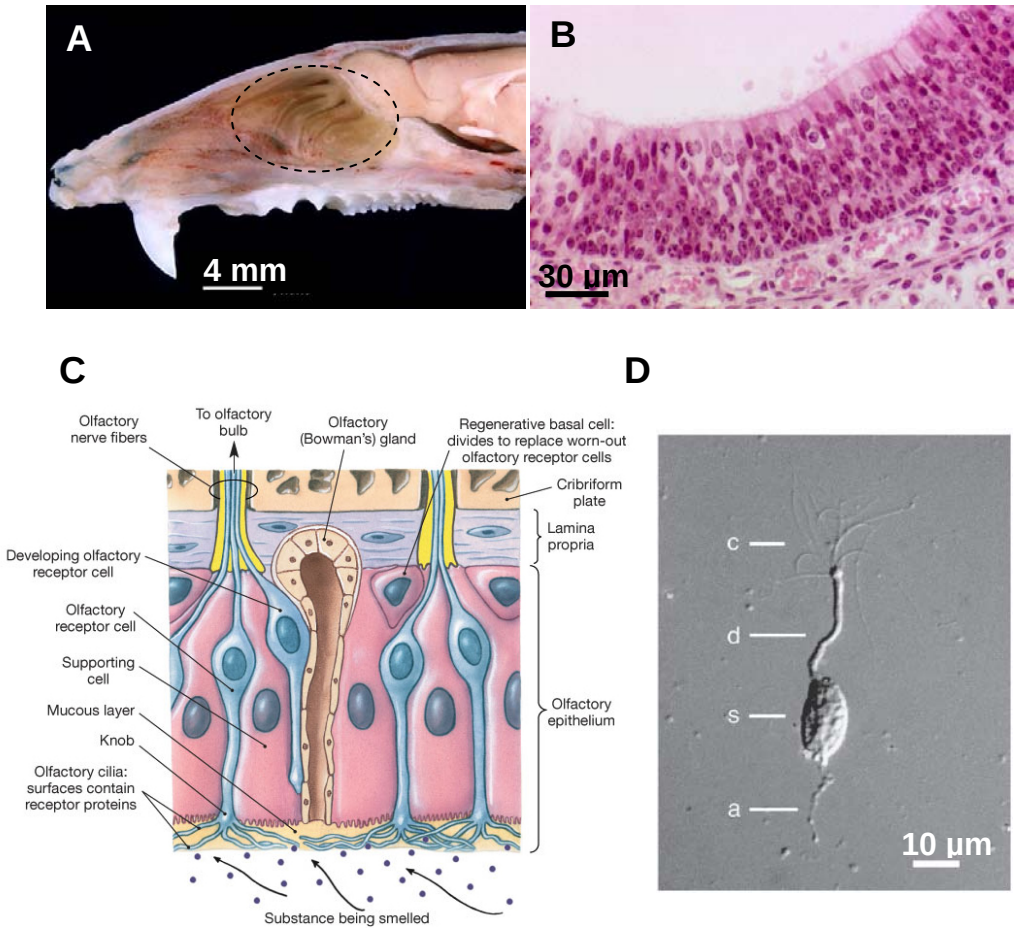

Figure 1.1 Olfactory epithelium and olfactory sensory neurons.

The olfactory epithelium in rodents is located in the upper part of the nasal cavity and lines on convolute cartilaginous structures called turbinates (A, from www.apuche.org/OIA/). Histological section of mouse olfactory epithelium stained with eosin (B, from http://education.vetmed.vt.edu/-curriculum/VM8054/Labs/Lab25/lab25.htm) and schematic diagram showing the various cell types and structures composing the neuroepithelium (C, from Anatomy and Physiology Laboratory Manual, Benjamin Cummings). Photograph of an isolated frog olfactory sensory neuron under differential interference optic, c: cilia; d: dendrite; s: soma; a: axon, (D, from Kleene & Gesteland, 1981).

The supporting cells are columnar epithelial cells and they extend vertically from the epithelial surface, where they show a series of irregular microvilli at the apical surface and they contact the basal lamina with branched digitiform processes.

The olfactory neuroepithelium undergoes a constitutive turnover of the neuronal population analogous to cellular replacement in other non-neural epithelia, as well as a wholesale reconstitution of that population after lesion as a kind of wound healing (Graziadei et al., 1978)

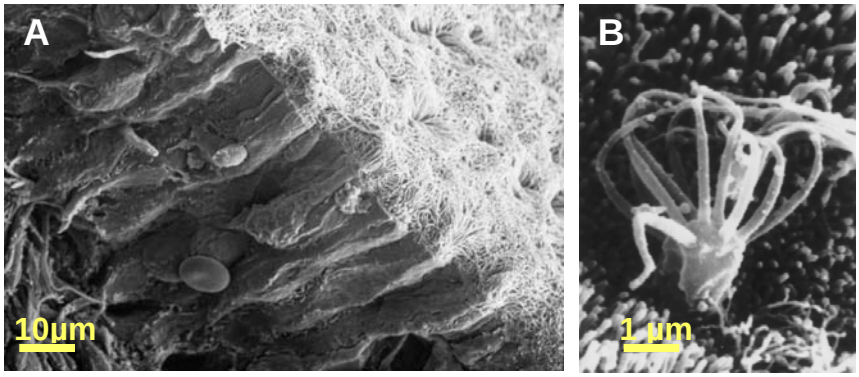

Figure 1.2 Cilia of olfactory sensory neurons are the site of olfactory transduction.
Microphotograph of human olfactory epithelium obtained with scanning electron microscopy. The cilia in mammals are tiny structures with diameter of 100-200 nm and length of 15-50 µm (B, Morrison & Costanzo, 1990).

1.2.2 Beyond the olfactory epithelium

The axons of OSNs cross the cribriform plate and directly reach the most rostral part of the brain known as the olfactory bulb. Molecular-genetic studies using transgenic mice have shown that all the neurons expressing a particular receptor, no matter where they are found on the epithelial sheet, converge to a single 'target' in the olfactory bulb (Mombaerts et al., 1996b), for review see (Mombaerts, 2004a; Fig. 1.3). These targets are the glomeruli, spherical conglomerates of neuropil some 50–100 µm in diameter that consist of the incoming axons of OSNs and the dendrites of the main projection cell in the bulb, the mitral cells (Fig. 1C). In the olfactory bulb complex processing of olfactory information is also taking place. Indeed, each glomerulus contains the axons of several thousands of OSNs and the dendrites of ~50 mitral and tufted cells, which are the output neurons of the olfactory bulb. These neurons are activated by OSNs, but odorant information is further processed by the activity of inhibitory interneurons, periglomerular cells, and granule cells (Lowe, 2003;

Schoppa & Urban, 2003) The axons of mitral and tufted cells project through the lateral olfactory tract to the olfactory cortex.

The olfactory cortex is composed of several anatomically distinct areas: the piriform cortex, olfactory tubercle, anterior olfactory nucleus, and specific parts of the amygdala and the entorhinal cortex. Further projections from the olfactory cortex, reach through the thalamus the orbitofrontal cortex, that are thought to be responsible for perception and discrimination of odors. In contrast the pathways leading to the amygdala and hypothalamus are thought to be involved in the emotional and motivational aspects of smell as well as the behavioral and physiological effects of odors (Menini *et al.*, 2004; Buck, 2000).

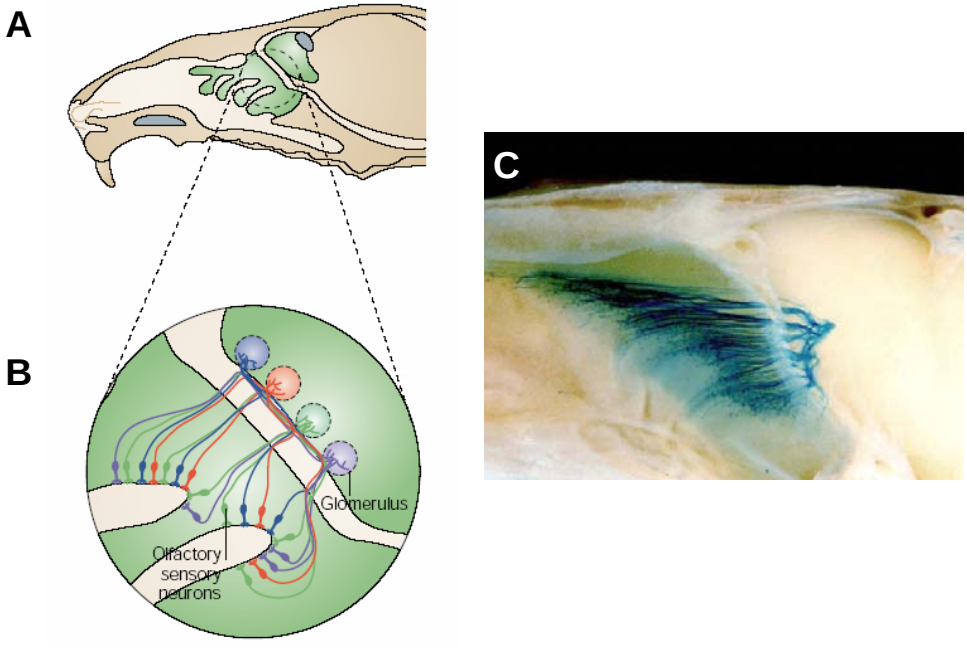

Figure 1.3 Projection of olfactory sensory neurons to the olfactory bulb.
All olfactory sensory neurons in the olfactory epithelium expressing the same odorant receptor project to the same glomerulus in the olfactory bulb (A-B, from Mombaerts, 2004b). Genetic labeled olfactory sensory neurons expressing the odorants receptor P2 send their axons to a specific glomerulus in the olfactory bulb (C, from Mombaerts et al., 1996a)

1.3 Odorant receptors

The identification of the genes encoding for odorant receptors opened the molecular era in olfactory research and it allowed the comprehension of the basis of olfactory system organization and its physiology.

In the late 1980s, it was becoming evident that the main pathway of olfactory signal transduction involved heterotrimeric G proteins. Indeed it has been shown that exposure of isolated cilia from rat olfactory epithelium leads to the rapid stimulation of adenylyl cyclase and an increase in cyclic AMP that is dependent on the presence of GTP (Pace *et al.*, 1985; Sklar *et al.*, 1986; Jones & Reed, 1989; Breer *et al.*, 1990). Moreover in 1987 (Nakamura & Gold, 1987) Nakamura and Gold reported that a cation channel that can be directly activated by cAMP is present in olfactory cilia.

This implied that receptors for odorants have a seven-transmembrane domain (7TM) structure, as we now know is the case for all other G protein-coupled receptors (GPCRs). The few GPCRs that had been cloned at that time showed conserved motifs. By application the novel strategy at that time, degenerate polymerase chain reaction (PCR), a diverse superfamily of ~1,000 genes that encoded 7TM proteins was identified in the rat and RNA transcripts were localized to the olfactory mucosa (Buck & Axel, 1991).

Degenerate PCR with pan-OR primers has permitted the cloning of OR genes from many vertebrate species (Mombaerts, 1999). The intronless structure of OR coding regions greatly facilitates this endeavour, as it is much easier to obtain genomic DNA from an animal than cDNA of the olfactory mucosa. In human, 50–60% of OR sequences are pseudogenes (Del Punta *et al.*, 2002; Del Punta *et al.*, 2002; Zozulya *et al.*, 2001; Niimura & Nei, 2003; Mombaerts, 1999; Mombaerts, 2001). Only ~350 human OR sequences have an intact open reading frame, and are potentially functional. As expression in OSNs remains to be demonstrated for any human OR gene, some receptors might not qualify as 'ORs'. The massive pseudogenization of the OR repertoire in humans and Old World primates (Gilad *et al*., 2004) is preceded by a moderately high level of pseudogenes (28–36%) in lower primate species (Gilad *et al*., 2003). By contrast, of the 1,300–1,500 OR sequences in the mouse genome (Zhao & Firestein, 1999; Godfrey *et al.*, 2004; Young *et al.*, 2002; Young *et al.*, 2003), only 20% are pseudogenes, and at least 419 are expressed in the olfactory epithelium (Young *et al.*, 2003). The mouse repertoire of ~1,000 potentially functional OR genes is by

far the largest gene superfamily in a mammalian genome, and perhaps in any genome. The intact mouse OR genes can be grouped into families, defined by an amino-acid identity of >40% (Zhang & Firestein, 2002) and containing between 1 and 50 member genes. Class I genes (~10% of the mouse repertoire) resemble the OR genes of fish, but class II genes are, so far, unique to terrestrial vertebrates. The amino-acid similarity is 37% on average across the OR repertoire, but it can be as low as 25% between two ORs. Of the plethora of short motifs that can be discerned among mouse ORs (Liu *et al*., 2003), certain combinations are diagnostic for ORs as opposed to other GPCRs, and this also extends to other vertebrate species. The genomic organization of the human and mouse OR repertoires is diffuse and complex. OR genes are spread over ~50 clusters localized on nearly all chromosomes.

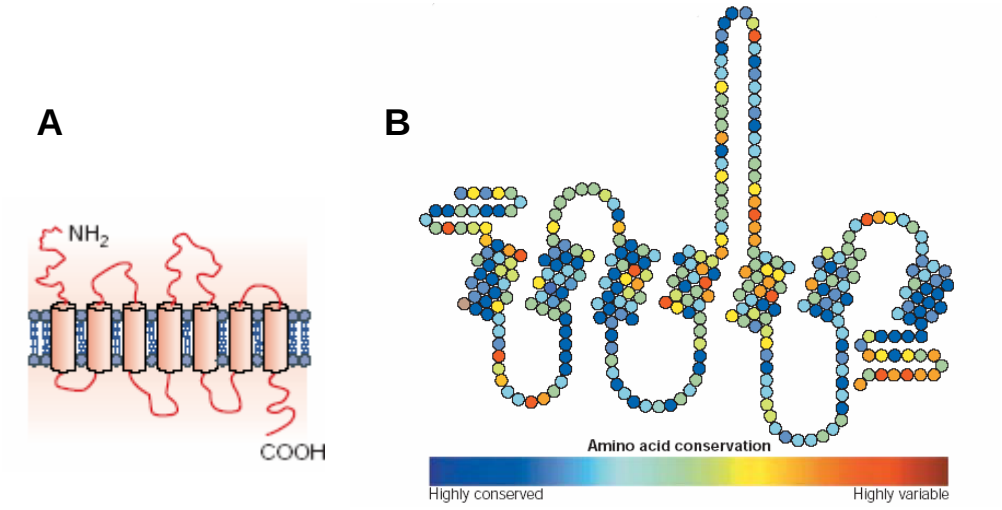

Figure 1.4 Odorant receptors.
Schematic topology of ORs with the typical 7 transmembrane domains of G-protein coupled receptor (A). Different regions of OR proteins show a different level of variability. The odorant binding domain is located in variable region of TM3, TM5 and TM6 (B, from Mombaerts, 2004b)

Every OSN expresses a single OR gene and in each OSN only one allele is expressed. (Chess *et al.*, 1994; Serizawa *et al.*, 2003; Serizawa *et al.*, 2004; Malnic *et al.*, 1999; Shykind, 2005). Moreover, based on the spatial distribution of OR genes, the olfactory epithelium can be divided in four zones along the antero-posterior axis. Each OR gene is expressed only in one zone but, inside it, the OSNs expressing that OR gene are randomly scattered (Ressler *et al.*, 1993; Sullivan *et al.*, 1994; Vassar *et al.*, 1993; Strotmann *et al.*, 1992).

The transcription regulation of OR genes is not yet fully understood. It is known that multiple levels of regulation exist, both at the gene, at the gene cluster, and more global levels (for review see Rodriguez, 2007). The choice of OR gene is apparently a stochastic process, which when stabilized is likely to remain stable during the entire life of the OSN. However not all ORs are chosen at the same frequency. Two models, not necessarily exclusive, have been proposed to explain the expression pattern of OR genes: (i) a proximal and gene-specific activation element and (ii) sequence acting over longer distances and shared among OR genes. At the moment the only long acting sequence that has been identified is the H element, a sequence of about 2 Kb. All data support a model in which the regulatory element loops and interact with specific OR genes to promote receptor choice, which is able to interact with one single promoter at a time. Some of these elements have been identified, such as homeodomain and O/E binding site just upstream of the transcription start site (Vassalli *et al.*, 2002; Rothman *et al.*, 2005; Hoppe *et al.*, 2003; Hoppe *et al.*, 2006; Michaloski *et al.*, 2006).

A more complex question is to understand why OSNs express just one receptor. It is not due to a non reversible genomic rearrangement occurring after OR gene choice as shown by nuclear transfer experiments (Eggan *et al.*, 2004; Li *et al.*, 2004). A model that has been proposed is the negative selection by which the neurons that express more than one gene are more sensitive to apoptosis and die. At present there is no evidence that support this model. The current and most obvious explanation for monogenic expression involves the expressed receptor itself, similar to what is observed in the immune system (Martensson et al., 2007). After the choice of the first OR gene either directly or indirectly a feedback loops prevent expression of other OR genes. The expression of nonfunctional OR alleles allows the cotranscription of novel OR genes, pointing to a role played by the protein itself rather than by its corresponding transcript. However, the mechanism by which the expressed OR mediates this feedback is still unknown (Serizawa *et al.*, 2003; Sato *et al.*, 2007; Lewcock & Reed, 2004; Shykind, 2005; Feinstein & Mombaerts, 2004). Vertebrate ORs share many features with other GPCRs, including a structure that predicts seven α-helical membrane-spanning domains connected by intracellular and extracellular loops of variable lengths, and numerous conserved short sequences. Other characteristics are specific to ORs, such as: an unusually long second extracellular loop, an extra pair of conserved cysteines in this loop, and other short sequences (see Fig 1.4 B, Mombaerts, 1999). Katada *et al*. (2005) found that

the most critical residues involved in odor binding are hydrophopic and are located in TM3, TM5 and TM6. Spatial localization of the binding pocket was similar to that for other biogenic GPCRs (Rivkees *et al.*, 1999; Church *et al.*, 2002; Manivet *et al.*, 2002; Berkhout *et al.*, 2003) however the environment was quite different. For example the catecholamines have been shown to form multiple electrostatic interactions with adrenergic receptors (Klabunde & Hessler, 2002). In contrast, the interaction of odorants in odor binding pockets in ORs is based on hydrophobic and van der Waals interaction, generating less rigid binding. This causes a higher EC_{50} but is still selective for shape, size and length of the ligand and its selectivity is due to the environment of the binding site.

Up to now the identification of the ligands for ORs is still very limited (Mombaerts, 2004b). This is due to the difficulty to express ORs in heterologous systems suitable for high-throughput screening. The main difficulty seems to be the OR protein trafficking to the plasma membrane. Indeed, the OR protein, although produced in transfected cells, remains trapped in the endoplasmic reticulum, Golgi and endosomal compartments, with little or no receptor finding its way to the membrane (Gimelbrant *et al*., 2001). This issue will be likely resolved by the discovery of accessory proteins that are involved in processing and trafficking of OR proteins. Indeed, it has been found that members of the RTP protein family, RTP1L, RTP1S and RTP2, and REEP1 were able to interact both in vivo and in vitro with OR proteins and induced their functional expression in heterologous systems (Saito *et al.*, 2004; Zhuang & Matsunami, 2007). Moreover Von Dannecker *et al*. (2005; 2006) reported that also Ric-8B, a putative guanine nucleotide exchange factor interacts with $G_{\alpha olf}$ and is able to promote the expression in heterologous systems.

1.4 Olfactory transduction: an overview

Once the receptor has bound an odor molecule, a cascade of events is initiated that transforms the chemical energy of binding into a neural signal (that is, a change in the membrane potential of the OSN). Although for a long time two possible mechanisms have been proposed, involving the production of cAMP or of IP_3, there are now converging evidences for only one common pathway for transduction of odorant stimulation in OSNs (Schild & Restrepo, 1998; Gold, 1999; Kleene, 2008; Menini *et al.*, 2004).

Odor molecules bind to odorant receptor proteins, and this interaction triggers an increase in the ciliary concentration of cAMP through the activation of a receptor-coupled G protein and an adenylyl cyclase. Cyclic nucleotide-gated (CNG) channels located in the ciliary membrane are directly activated by cAMP, causing a depolarizing influx of Na^+ and Ca^{2+} ions (Nakamura & Gold, 1987). The increase of $[Ca^{2+}]_i$ generated by Ca^{2+} entry through CNG channels directly gates a Ca^{2+}-activated Cl^- channels (Lowe & Gold, 1993b; Kleene, 1993; Kleene & Gesteland, 1991; Kurahashi & Yau, 1993). OSNs maintain an unusually high internal concentration of Cl^- that is in the same range of the Cl^- concentration present in the mucus at the external side of the ciliary membrane (Kaneko *et al.*, 2001; Reuter *et al.*, 1998; Nakamura *et al.*, 1997; Kaneko *et al.*, 2004). Therefore in physiological conditions, the opening of Ca^{2+}-activated Cl^- channels causes an efflux of Cl^- ions from the cilia, corresponding to an inward current that further contributes to the depolarization of OSNs (see Fig 1.5, Kurahashi & Yau, 1993; Kleene, 1993; Kleene & Gesteland, 1991; Lowe & Gold, 1993b).

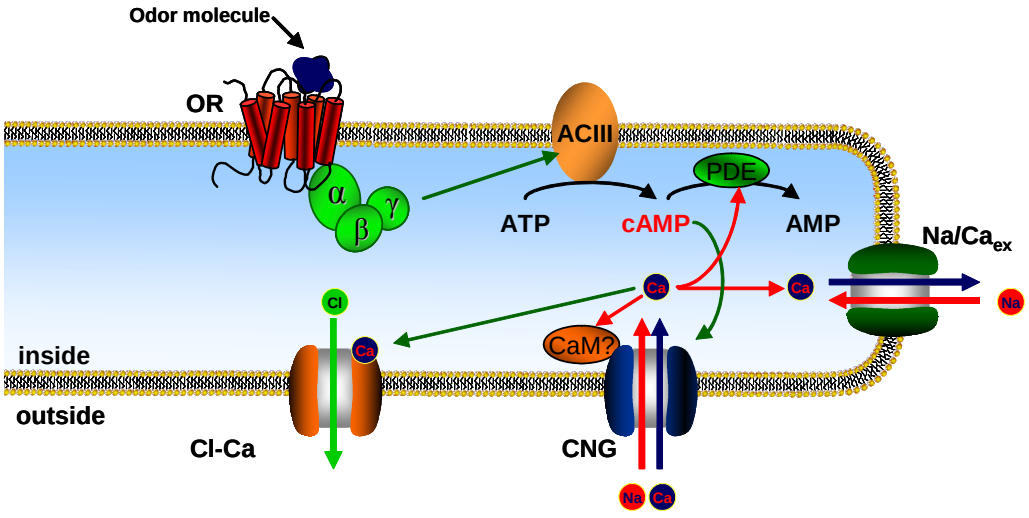

Figure 1.5 Olfactory transduction.
The binding of odorant molecules to ORs induces the G protein mediated activation of adenylyl cyclase. cAMP directly gates CNG channels generating a depolarizing influx of Na^+ and Ca^{2+}. $[Ca^{2+}]_i$ increase mediates both excitatory and inhibitory events. Ca^{2+} gates a Cl^- channel that produces a depolarizing efflux of Cl^-. On the other hand Ca^{2+}, through calmodulin and/or other Ca^{2+}-binding proteins, mediates the reduction of cAMP sensitivity of CNG channels and activates the PDE that hydrolyzes cAMP to AMP. $[Ca^{2+}]_i$ returns to basal level through the activity of a Na^+/Ca^{2+} exchanger.

1.5 Olfactory sensory neurons at rest: electrical and ionic conditions

The resting electrical proprieties of OSN as well as the ion gradient across the ciliary membrane play a fundamental role in shaping the proprieties of odor-induced responses.

1.5.1 Electrical resting condition

The membrane capacitance was measured in OSN of many vertebrates: it ranges from 0.7 pF in zebrafish (Corotto et al., 1996) to 35 pF in newt (Schild & Restrepo, 1998), with a value of 2-4 pF in rat (Lynch & Barry, 1989; Okada *et al.*, 1994). With the assumption of a standard value of 1 $\mu F/cm^2$, the membrane surface of OSNs is thus in the range between 70 and 3,500 μm^2.

The input resistance of OSNs was estimated to be 4-6 GΩ in frog (Pun & Kleene, 2004), 3-4 GΩ in mouse (Ma *et al.*, 1999; Liman & Corey, 1996) and a bigger value, 26 GΩ was found in rat (Lynch & Barry, 1991). This high input resistance allows a great depolarization for very small receptor currents. Indeed Lynch and Barry (1989) reported that in rat OSN the opening of a single channel was enough to induce the generation of action potentials.

The resting membrane potentials in mouse OSNs measured with whole cell recording ranges from –45 to –90 mV, with a mean value of –55 mV (Lagostena & Menini, 2003). Maue & Dionne (1987) using the cell-attached technique estimated a membrane potential in the range from –30 to –80 mV, with a mean of –52 mV. Ma *et al*. (1999) using the perforated patch technique found a mean value of –55 mV. In the rat, the resting membrane potential measured by Lynch & Barry (1991) was in the range –40 to –73 mV, with a mean of –52 mV, while in amphibians measurements of the resting membrane potential in the whole-cell configuration gave values ranging from –30 to –72 mV (Trotier, 1986; Firestein & Werblin, 1987; Kawai *et al.*, 1996; Schild, 1989). However, these measured membrane resting potentials are likely to be underestimations. In fact, to have a reliable measurement of the membrane resting potential, it is necessary that the resistance of the seal between the patch pipette and the cell membrane is much higher than the resistance of the cell membrane (Lynch & Barry, 1991; Lynch & Barry, 1989; Schild & Restrepo, 1998; Schild, 1989). However OSNs have a very high membrane resistance and, since seal resistances have a

similar value, usually a few GΩ (with occasional higher values up to 50 GΩ), the measured membrane resting potential is often underestimated and the real resting potential is more negative than the measured one (Schild & Restrepo, 1998). As a result, it is likely that the mean value does not have a physiological relevance and that the real resting potential is near the more negative measured values between –70 and –90 mV.

1.5.2 Ionic environment of olfactory transduction

Olfactory cilia are embedded in mucus covering the olfactory epithelium and therefore the understanding of ionic fluxes according during the odor-induced response requires the knowledge of ion concentrations in the mucus and inside the cilia. Data available about the intra- and extra-ciliary concentrations of major physiological ions are summarized in Table 1.1. Two features are immediately obvious: both $[Na^+]_{in}$ and $[K^+]_{out}$ are unusually elevated. There is no single ion with an equilibrium potential as negative as the neuronal resting potential. Such apparent discrepancies may be misleading. Although the estimates shown in Table 1.1 are the best available, the free ionic concentrations across the ciliary membrane are still not known with high precision. It may also be that the resting potential in the cilium is determined in the cell body, where the ionic gradients are unknown. Alternatively, it may depend on an electrogenic, multi-ion transport system with a negative reversal potential. In frog vomeronasal neurons, for example, activity of the Na^+,K^+-ATPase sets a negative resting potential (Trotier & Doving, 1996).

With the exception of Cl^-, the mechanisms of ionic homeostasis at rest have not been studied. Cl^- is accumulated by OSNs (Table 1.1). A Na^+,K^+,$2Cl^-$ cotransporter (NKCC1) contributes substantially to Cl^- uptake at rest as shown using knock out mice for NKCC1 (Reisert *et al.*, 2005; Kaneko *et al.*, 2004), but other still unidentified Cl^- transporters are also involved (Nickell *et al.*, 2006; Nickell *et al.*, 2007).

Ion	$[Ion]_{in}$ (mM)	$[Ion]_{out}$ (mM)	E_{Nernst} (mV)
Na^+	53 ± 31	55 ± 12	+1
K^+	172 ± 23	69 ± 10	-24
Free Ca^{2+}	40 ± 9 nM	4.8	+156
Cl^-	54 ± 4	55 ± 11	0

Table 1.1 Resting electrochemical gradients at the apical end of olfactory sensory neurons. Most of the ionic concentrations shown were measured by energy-dispersive X-ray microanalysis in dendritic knobs of rat OSNs (Reuter *et al*., 1998). Those values represent total rather than free ionic concentrations. Three of the concentrations were measured by other methods, as follows. $[Ca^{2+}]_{in}$ was measured in salamander cilia with a Ca^{2+}-sensitive fluorescent dye (Leinders-Zufall *et al*., 1997). $[Ca^{2+}]_{out}$ was determined with a Ca^{2+}-sensitive microelectrode in olfactory mucus of rat (Crumling & Gold 1998); the value shown is the midpoint of the reported range (2.6–7.1 mM). $[Cl^-]_{in}$ was measured in dendritic knobs of rat OSNs with a Cl^--sensitive fluorescent dye (Kaneko *et al*., 2004)

1.6 The odorant-induced response in olfactory sensory neurons

Even if OSNs are physiologically devoted to detect odors, measuring an odor response in a single OSN has been very demanding. Since each OSN expresses only one OR, a given neuron responds to a small and unpredictable subset of the many available odorants (Fig 1.6). Grosmaitre *et al*. (2006) reported that all tested OSNs expressing the MOR23, identifiable by coexpression of EGFP, respond to lyral, a known MOR23 ligand. Even among isolated OSNs from rat, every neuron tested that was found to express the I7 receptor responded to *n*-octanal (Zhao *et al*., 1998). However, in a mouse engineered to express the same receptor in every mature OSN, only 20% of the OSNs responded to an appropriate ligand (Reisert *et al.*, 2005). One can imagine that many cilia break off during dissociation. However, 94% of murine OSNs respond when cAMP is released inside the neuron (Lagostena & Menini, 2003). Because most of the cAMP-gated channels are on the cilia, this suggests that the cilia remain after isolation of the neurons. Most often, an effective stimulus must be found by trial and error. In this case, anywhere from 2% to 30% of isolated amphibian OSNs respond, depending on the choice of odorant (Fig 1.6; (Kurahashi, 1989; Firestein *et al.*, 1993; Takeuchi *et al.*, 2003; Takeuchi & Kurahashi, 2005). Success rates are lower in mouse, typically ranging from 3% to 12% (Lagostena & Menini, 2003; Oka *et al.*, 2004; Reisert *et al.*, 2007). Some evidence suggests that more neurons respond to odors when the epithelium is intact. In frog, rat, and catfish, several odorants elicited responses in 30–80% of single OSNs in situ (Sicard & Holley, 1984; Kang & Caprio, 1995; Duchamp-Viret *et al.*, 2000).

In isolated OSNs, the response to odor stimuli in solution has been well characterized. Most often, the response has been measured under voltage-clamp upon presentation of a brief pulse of odor. The odor stimulation generates a transient inward receptor current that would be expected to depolarize the neuron in situ (Fig 1.6). The response typically lasts 1 s or more. In amphibians, the latency between arrival of the stimulus and the onset of the current ranges from 150 to 600 ms (Kurahashi, 1989; Firestein & Werblin, 1987; Firestein *et al.*, 1990; Takeuchi & Kurahashi, 2003; Tomaru & Kurahashi, 2005). In mouse and rat, the latency is at most 160 ms (Reisert & Matthews, 2001a; Grosmaitre *et al.*, 2006). This shorter latency is observed even in the intact epithelium, which requires that the odorant diffuses through the mucus (Grosmaitre *et al*., 2006). For a strong stimulus, the amplitude of the peak receptor current can be of several hundred pA: 700 pA in salamander (Firestein *et al.*, 1990); 950 pA (Lowe & Gold, 1993b) to 1.5 nA in rat (Ma *et al.*, 1999). By directing the stimulus to various parts of the cell, it has been shown that the sensitivity to odorants is largely restricted to the cilia (Kurahashi, 1989; Firestein *et al.*, 1990; Lowe & Gold, 1991; Takeuchi & Kurahashi, 2003). During the odor response, cytoplasmic Ca^{2+} increases transiently (Omura *et al.*, 2003; Restrepo *et al.*, 1990; Leinders-Zufall *et al.*, 1997; Reisert & Matthews, 2001b; Hirono *et al.*, 1992) with a time course that parallels that of the odor induced current (Leinders-Zufall *et al.*, 1997; Reisert & Matthews, 2001b). The Ca^{2+} increase is first seen in the cilia, and the Ca^{2+} signal decays faster in the cilia than in the dendrite or soma (Leinders-Zufall *et al.*, 1998; Leinders-Zufall *et al.*, 1997). The amplitude of the peak of the receptor current can be increased by increasing either the concentration or the duration of the stimulus pulse (Takeuchi & Kurahashi, 2002). The relation between odor dose and peak receptor current is generally well fitted by a Hill equation:

$$I = I_{\max} \frac{C^n}{C^n + K_{1/2}^n} \qquad \text{eq 1.1}$$

where I_{max} is the maximum macroscopic current, C is the concentration of odorant, $K_{1/2}$ is the half-maximally effective concentration, and n is the Hill coefficient. In isolated salamander OSNs under whole-cell recording conditions, $K_{1/2}$ for the 3 odors isoamylacetate, cineole and acetophenone ranged from 3 to 90 μM (Firestein *et al.*, 1993). A similar range (4–104 μM) was observed when mouse OSNs were studied under more

physiological conditions (Grosmaitre *et al.*, 2006). However, some neurons in that study responded to as little as 10 nM of the odor lyral. In frog, some OSNs in intact epithelium responded to just 1 pM cineole (Frings & Lindemann, 1990). The other Hill parameter, n, describes the slope of the dose–response relation. As n decreases, the slope also decreases, causing an increase in the range of stimulus strengths over which the neuronal response varies (dynamic range). In isolated amphibian OSNs under whole-cell recording conditions, n ranges from 2.7 to 9.7 (Firestein *et al.*, 1993; Takeuchi & Kurahashi, 2005; Tomaru & Kurahashi, 2005). When recordings are made without disrupting the neuronal membrane, with suction electrode recordings or perforated patch analysis, n is much smaller (between 0.8 and 1.8; frog: (Reisert & Matthews, 1999), mouse: (Grosmaitre *et al.*, 2006), and rat: (Ma *et al.*, 1999), and the neurons respond over as much as a 1000-fold range of odorant concentration. For a given odorant, the dose–response relation varies considerably from one neuron to the next (Firestein *et al.*, 1993; Tomaru & Kurahashi, 2005), even among neurons known to express the same odorant receptor (Grosmaitre *et al.*, 2006).

The relation between odor dose and frequency of action potentials in OSNs is similar to that for the receptor current. However, the relation for action potentials is shifted to somewhat lower odorant concentrations (Tomaru & Kurahashi, 2005; Reisert & Matthews, 1999). In physiological solutions, the current-voltage relation of the odor-induced current is nearly linear with a slight outward rectification (Kurahashi, 1989; Takeuchi & Kurahashi, 2003; Kurahashi & Shibuya, 1990). The reversal potential ranges from 0 to +2.8 mV (Lowe & Gold, 1993a; Takeuchi & Kurahashi, 2003; Takeuchi *et al.*, 2003).

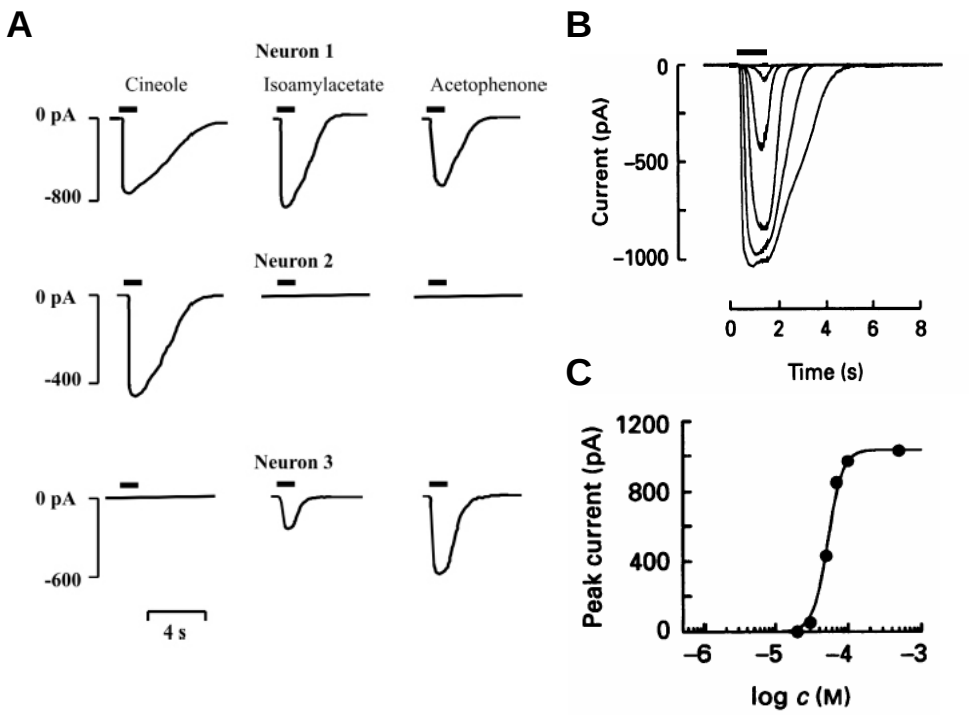

Figure 1.6 Odorant responses of olfactory sensory neurons under voltage-clamp.
Responses of isolated salamander OSNs to odorant stimulation measured with the voltage-clamp whole-cell configuration at -55 mV holding potential. Different OSNs respond to a specific subset of odorants (A). Responses of an OSN to various concentration of isoamyl acetate presented for 1.2 s (B). Plot of the odorant-induced current versus the odor concentration. The solid line is the best fit of the Hill equation to the data with $K_{1/2}$ = 53 µM and n= 4.2 (C, from (Firestein *et al*., 1993)

1.7 The G protein

The first evidence that olfactory transduction involved the increase of cAMP in olfactory cilia was the finding that adding GTP to purified olfactory cilia caused the production of cAMP (Pace *et al.*, 1985; Sklar *et al.*, 1986). This suggested that the production of cAMP is G protein dependent. Jones & Reed (1989; 1987) reported that OSNs express a new variant of the G_s protein, named $G_{\alpha olf}$, which is able to stimulate the adenylyl cyclase in vitro. Menco *et al*. (1992) with ultrastructural experiments found that $G_{\alpha olf}$ is localized in rat olfactory cilia. Electrophysiological experiments using non hydrolysable GTP and GDP analogs confirmed the role of a G protein in odor signaling in OSNs. Indeed, in the presence of GTP-γ-S the response was prolonged (due to long lasting activation of G proteins), whereas addition of GDP-γ-S to the patch pipette progressively reduced the response to repetitive stimulations (due to block of the G protein, Firestein *et al.*, 1991a).

The essential role of $G_{\alpha olf}$ in olfactory transduction was finally proven by Belluscio *et al*., (1998) who showed that knock out mice for $G_{\alpha olf}$ are anosmic.

Various β and γ G-protein subunits have been found in catfish (Bruch *et al.*, 1997). Kulaga et al. (2004) reported that in the cilia of OSNs was express the γ13 subunit. Moreover Tirindelli & Ryba (1996) reported that γ8 was expressed in developing rat OSNs.

1.8 The adenylyl cyclase

The first evidence that olfactory transduction involved a cAMP signaling cascade was the discovery in olfactory cilia of rat and frog of an odor-induced adenylyl cyclase activity (Pace *et al.*, 1985; Sklar *et al.*, 1986; Shirley *et al.*, 1986).

After a report that some odor did not activate AC (Sklar *et al.*, 1986), it was demonstrated that odors activate either AC or phospholipase C (PLC) alternatively (Boekhoff *et al.*, 1990). However, this interpretation seems to have been revised: the odor-induced cAMP formation showed a different time course and different Ca^{2+}-dependence between types of receptors. When the experiments were carefully designed in consideration of the Ca^{2+} concentration and its kinetics, all the odors activated the AC (Jaworsky *et al.*, 1995). The primary structure of this AC, obtained by screening the cDNA library of olfactory epithelium by PCR, was distinct from AC type I or II (Bakalyar & Reed, 1990) and it was named type III (ACIII).

The rapid production of cAMP was revealed by a more detailed look at the time course of odor-induced cAMP generation in a cilia preparation. Using rapid quench methods it was shown that cAMP concentration increases within 50 ms to the maximum which can be almost 10-fold greater than the basal levels. For low odor concentration, the increase in cAMP is transient and may last only 100 ms; while for higher concentration cAMP levels settle after a initial peak to a lower level around half the maximal value (Boekhoff *et al.*, 1990; Breer *et al.*, 1990)

Lowe *et al.* (1989) reported that the odor-induced cyclase activity by different odors is strictly correlated with the EOG response. This gave a strong support to the role of adenylyl cyclase in olfactory transduction. Wong *et al*., (2000) reported that knock out mice for AC III are completly anosmic, further supporting that cAMP signaling is the unique system by which OSNs transduce odorant stimulation.

The production of cAMP in the cilia of newt OSNs has been measured directly by Takeuchi & Kurahashi (2005) during prolonged odor stimulation. During the rising phase of the response, the rate of cAMP production was found to increase linearly with time. At most, all neuronal cilia combined generated ~ 200 000 molecules of cAMP per second per cell. Given the high surface-to-volume ratio of the cilium cAMP concentrations were as high as 129 μM, which was 6 times the half-maximally effective concentration of cAMP ($K_{1/2}$).

1.9 Ion channels:

1.9.1 The CNG channel

In 1987 Nakamura & Gold discovered how the odor-induced production of cAMP is linked to neuronal excitability. As previously described in photoreceptors (rod, Fesenko *et al.*, 1985; cone, Haynes & Yau, 1985) they discovered a cAMP-gated current in excised patches from olfactory cilia of toad OSNs. The channel was then described in many another species including salamander, frog, newt, rat and mouse (Firestein *et al.*, 1991b; Kleene *et al.*, 1994; Kurahashi & Kaneko, 1991; Munger *et al.*, 2001; Frings *et al.*, 1992) Kaupp *et al*. (1989) first cloned the gene encoding for the CNG channel in bovine retinal rods beginning investigations at the molecular level of the physiological and biophysical properties of these ion channels. At present, six CNG channel genes have been identified in mammalian genomes. These genes code for four types of A subunits and two types of B subunits (Hofmann *et al.*, 2005). CNG channels are composed of four subunits forming a tetramer with a central pore. The topology of each subunit is similar to that of the cationic voltage-activated channels with six transmembrane-spanning domains, a pore-loop domain between the fifth and sixth transmembrane domain, and intracellular N- and C-terminal regions. CNG channels are activated by the direct binding of cyclic nucleotides to a large C-terminal cyclic nucleotide-binding domain and are only weakly sensitive to membrane voltage (Fig 1.7 A).

Native retinal rod channels are composed of two types of subunits: CNGA1 and CNGB1 (Chen *et al.*, 1993; Kaupp *et al.*, 1989) with a stoichiometry of three CNGA1 and one CNGB1a (a B1 splice variant) subunits (Weitz *et al.*, 2002; Bonigk *et al.*, 1993). Retinal cone channels are also composed of two types of subunits: CNGA3 and CNGB3 (Bonigk *et al.*, 1993; Gerstner *et al.*, 2000) with a stoichiometry of two CNGA3 and two CNGB3

subunits (Peng *et al.*, 2004). Native channels of olfactory sensory neurons are instead composed of three types of subunits: CNGA2, CNGA4 and CNGB1 (Dhallan *et al.*, 1990; Ludwig *et al.*, 1990; Bradley *et al.*, 1994; Liman & Buck, 1994; Sautter *et al.*, 1998) with a stoichiometry of two CNGA2, one CNGA4 and one CNGB1b (a B1 splice variant) (see Fig 1.7, Zheng & Zagotta, 2004). Ultrastructural data show that CNGA2 is localized at a higher density in the cilia of OSN as other components of olfactory transduction (Matsuzaki *et al.*, 1999).

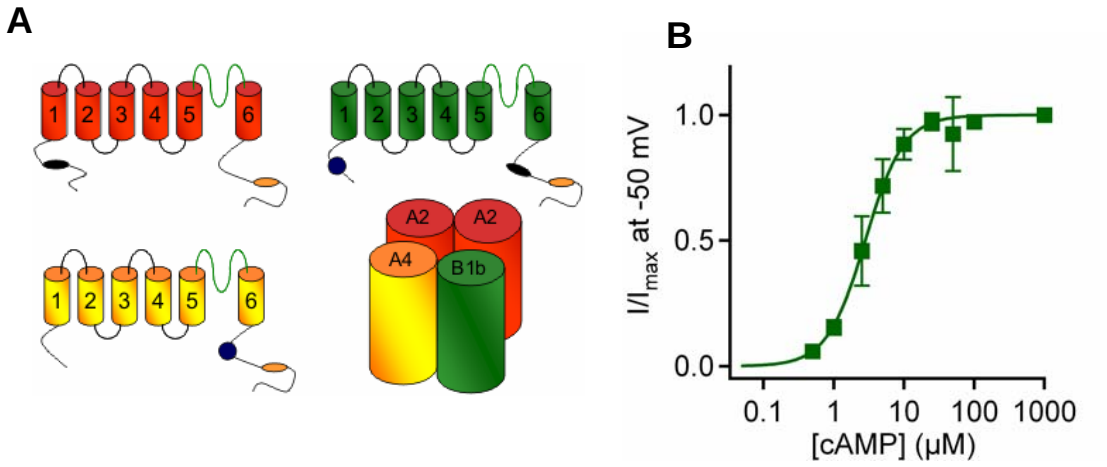

Figure 1.7 Olfactory CNG Channels.
Topological model and assembly of subunits of the olfactory CNG channel. Each transmembrane domain is indicated by a number, the pore loop is located between 5 and 6. The cyclic nucleotide binding site (brown) is located in the C-terminal domain. Calmodulin binding sites of the calcium-dependent 'Baa type' are represented in black, whereas the calcium-independent 'IQ-type' are in blue (A). Dose-responses from membrane patches excised from dendritic knob/cilia of OSNs containing olfactory channels activated by cAMP. The continuous line is the best fit of the Hill equation to the data with $K_{1/2}$ = 2.7 µM, n=1.5. (B, from (Pifferi *et al*., 2006a)

The channel density in the cilium has been estimated by electrophysiological methods with widely differing results: 1750 channels/µm^2 in toad (Kurahashi & Kaneko, 1993), 67–202 channels/µm^2 in frog (Kleene *et al.*, 1994; Larsson *et al.*, 1997), and 8 channels/µm^2 in rat (Reisert *et al.*, 2003). Flannery *et al.*, (2006) combining both mathematical modeling and experimental data reported that the proximal segment of frog olfactory cilia, the first 20% of the cilium, appears to express a small fraction of the CNG channels, whereas the distal segment contains the majority, mostly clustered in one region. However, this conclusion was partially challenged by Takeuki & Kurahashi (2008) who,

using local uncaging of cAMP, found that the sensitivity to cyclic nucleotides along newt olfactory cilia is uniform. The soma and dendrite also express CNG channels but at much lower densities (Lowe & Gold, 1993a; Kurahashi & Kaneko, 1993).

Recently, knock out mice for each gene coding for the CNG channel subunits expressed in OSN have been developed. The analysis of the phenotype of each knock out line clarified the fundamental role of CNG in olfactory transduction and how the modulation of this channel participates in shaping the odor-induced response in OSNs (Brunet *et al.*, 1996; Munger *et al.*, 2001; Michalakis *et al.*, 2006).

Knock out mice missing the CNG channel subunit CNGA2 lacked EOG responses to most odorants tested (Brunet *et al.*, 1996). However other studies, showed that residual responses to some odorants are present in mice lacking CNGA2 (Zhao & Reed, 2001; Lin *et al.*, 2004). Knock out mice for CNGA4 or B1 showed alteration in odor adaptation (see later, 1.9.1.1, Munger *et al.*, 2001; Bradley *et al.*, 2001; Michalakis *et al.*, 2006) but also a defective trafficking to the cilia of other CNG subunits. These latter results points out that OSNs have mechanisms that ensure the targeting to the cilia of CNG channel only composed by the three types of subunits. Jenkins *et al.* (2006) reported that, in MDCK cell line and in mouse OSNs ciliary targeting of olfactory CNG channels requires the CNGB1b subunit and the interaction with kinesin-2 motor protein KIF17.

The properties of CNG channels are strongly affected by the presence of divalent ions both intracellularly and extracellularly; first, I will discuss the properties in absence of divalent cations.

The olfactory CNG channels are permeant to all monovalent alkali cation with permeability ratios of Na^+ (1): K^+ (0.81): Li^+ (1): Rb^+ (0.6): Cs^+ (0.52) in rat (Frings *et al.*, 1992) and Na^+ (1): K^+ (0.93): Li^+ (0.93): Rb^+ (0.91): Cs^+ (0.72) in newt (Kurahashi, 1990). Using organic cations Balasubramanian *et al*. (1995) estimated that the channel pore in rat CNG must measure at least 6.5x6.5Å. The current-voltage relation is almost linear with a slight outward rectification (Frings *et al.*, 1992; Kurahashi, 1990; Bonigk *et al.*, 1999). Once activated, the CNG channel current does not spontaneously inactivate (Zufall *et al.*, 1991a; Kramer & Siegelbaum, 1992; Kurahashi & Kaneko, 1993). The single channel conductance varies from 8 to 46 pS between species (Zufall *et al.*, 1991a; Frings *et al.*, 1992; Zufall & Firestein, 1993; Larsson *et al.*, 1997; Kurahashi & Kaneko, 1993) with a maximum open probability of 0.7-0.8 (Kurahashi & Kaneko, 1993; Larsson *et al.*, 1997; Kleene, 1997;

Reisert *et al.*, 2003). The relation between concentration of cAMP and CNG current is well fitted with a Hill equation (eq 1.1, Fig 1.7 B). Half-maximal activation ($K_{1/2}$) is in the micromolar range and varies in different species: about 3 μM in mouse (Song *et al.*, 2008; Michalakis *et al.*, 2006; Pifferi *et al.*, 2006a), 4.1 μM in rat (Bonigk *et al.*, 1999), 2 μM in frog (Kleene, 1999), 19 μM in toad (Kurahashi & Kaneko, 1993). The Hill coefficient ranges from 1.3 and 2.3 suggesting that at least 2 molecules of cAMP must bind before the channel gating. Recently, Nache *et al*. (2005) and Biskup *et al*. (2007) demonstrated that in homomeric CNGA2 channel the binding of the second cAMP molecule brings the channel almost to its maximum open probability of about 0.7–0.8 (Kurahashi & Kaneko, 1993; Larsson *et al.*, 1997; Reisert *et al.*, 2003; Kleene, 1997).

CNG channels are modulated by divalent cations on both sides of the ciliary membrane. Ca^{2+} and Mg^{2+} acting directly and indirectly play a fundamental role in shaping the odor induced response in OSNs.

Modulation by extracellular divalent cations will be described first. Zufall & Firestein (1993) reported that Ca^{2+} and Mg^{2+} entry at negative potential produces an open channel block causing an increase in flickering activity of the channel. This temporary block reduces the current carried by all cations producing a very small single channel conductance (~ 1.5 pS, Zufall & Firestein, 1993, 0.56 pS, Kleene, 1997). It has been demonstrated that the block of Ca^{2+} and Mg^{2+} is voltage-dependent with a smaller effect at positive voltages. In salamander the IC_{50} at saturating concentration of cAMP and at -50 mV is 30 μM for Ca^{2+} and 200 μM Mg^{2+} (Zufall & Firestein, 1993), while in frog is 180 μM for Ca^{2+} and 280 μM Mg^{2+} (Kleene, 1995). Moreover, the block of extracellular divalents is more effective at lower concentration of cAMP causing a reduction in the sensitivity of the channel to cyclic nucleotide (in frog the $K_{1/2}$ at -50 mV is 1.3 μM in absence of extracellular Ca^{2+} and became 10.6 μM in the presence of 3 mM extracellular Ca^{2+} (Kleene, 1999). The block of CNG channels by divalents plays a relevant physiological role. Indeed at a resting membrane potential lower than -50 mV, 1 mM external Ca^{2+} blocks most of the channels. Without this Ca^{2+} block, the opening of a single CNG channel would be enough to produce a considerable depolarization of the cell given that OSNs have a high input resistance. In the absence of divalent current block an increase in intracellular cAMP concentration could trigger the generation of action potentials in the absence of odor stimulation. The detection of odor would therefore be unreliable.

Ca^{2+} is also able to permeate through the CNG channels. Dzeja *et al.* (1999) reported that the fraction of current carried by Ca^{2+} is 0.4 in heterologously expressed rat CNG channels with 2 mM of extracellular Ca^{2+} at -70 mV. There is not yet a measurement of this parameter in OSNs but using Ca^{2+} sensitive dye it has been reported that during odor stimulation there is an increase in intracellular Ca^{2+} concentration in cilia through the activation of CNG channel (Leinders-Zufall *et al.*, 1998; Leinders-Zufall *et al.*, 1997).

The modulation by intracellular Ca^{2+} has been shown to play a pivotal role in adaptation and it will be discussed in the following paragraph.

1.9.1.1 Modulation of CNG and adaptation

With prolonged or repeated odor stimulation, the OSN shows a property variously described as adaptation, desensitization, or inactivation. Two experimental approaches have been used to demonstrate this process.

In the first, a prolonged odor stimulus is applied. Despite the continued presence of the stimulus, the receptor current decreases with time (Kurahashi & Shibuya, 1990; Firestein *et al.*, 1990; Zufall *et al.*, 1991b; Reisert & Matthews, 1999). A similar result was obtained if cAMP is allowed to diffuse into the cell through the patch pipette (Kurahashi, 1990; Lagostena & Menini, 2003). In both cases, the decrease in current can be largely eliminated by removing of Ca^{2+} from the extracellular bath (see Fig 1.8 A; Kurahashi & Shibuya, 1990; Zufall *et al.*, 1991b; Kurahashi, 1990).

In another protocol two brief odor pulses are delivered with a short interval. If the interval between the pulses is sufficiently short, the amplitude of the response to the second pulse is reduced (Kurahashi & Shibuya, 1990; Kurahashi & Menini, 1997). At that point, the cell is in an adapted state, the first (conditioning) pulse having desensitized the neuron to subsequent stimuli. The desensitization is greater with shorter interstimulus intervals (see Fig 1.8 B; Kurahashi & Shibuya, 1990; Kurahashi & Menini, 1997; Takeuchi *et al.*, 2003). The desensitization disappears gradually and the OSN recovers from adaptation if the interval between pulses is sufficiently long. Adaptation both shifts and broadens the dynamic range of the neuron (Kurahashi & Menini, 1997; Reisert & Matthews, 1999; Boccaccio *et al.*, 2006). In the adapted state, a stronger stimulus is required to produce a half maximal response. The slope of the dose–response curve is also reduced, indicating that the

neuronal response is graded with stimulus strength over a greater range of concentrations. During a prolonged exposure to an odorant, adaptation is expected to continuously reset the neuron to discriminate higher odorant concentrations without saturating the transduction process. Many studies have clearly shown that adaptation is mediated via modulation of olfactory CNG channels by intracellular Ca^{2+}.

For native CNG channels it has been demonstrated that the addition of micromolar concentrations of intracellular Ca^{2+} is able to decrease the channel sensitivity to cAMP, probably by activating a Ca^{2+}-responsive endogenous factor already pre-associated with the channel (Kramer & Siegelbaum, 1992; Lynch & Lindemann, 1994; Balasubramanian *et al.*, 1996; Bradley *et al.*, 2004). Bradley *et al*. (2004) have shown that Ca^{2+}-free calmodulin, called apocalmodulin, is able to bind to the heterologously-expressed heteromeric olfactory CNG channels even in the absence of Ca^{2+}. Moreover, when Ca^{2+} concentration rises above 100 nM, Ca^{2+} can rapidly modulate the CNG channel sensitivity by binding directly to the pre-associated calmodulin. Furthermore, it was suggested (Bradley *et al.*, 2004) that also in native channels the pre-associated endogenous factor could be apocalmodulin, although a demonstration is still missing. Since Ca^{2+} enters into the olfactory cilia through the CNG channel itself, the pre-associated Ca^{2+}-responsive factor could provide a very fast feedback modulation at the channel level.

Early works (Chen & Yau, 1994; Liu *et al.*, 1994; Varnum & Zagotta, 1997; Grunwald *et al.*, 1999; Zheng *et al.*, 2003) identified in the N-terminus of CNGA2 a classic basic amphiphilic α-helix (Baa) motif with high affinity for Ca^{2+}–calmodulin and showed that the sensitivity to cAMP of heterologously-expressed homomeric CNGA2 channels was decreased by the binding of Ca^{2+}–calmodulin to the Baa motif (Fig 1.7 A). However, in recent years, there has been considerable progress in elucidating the molecular events producing modulation of the native channels and it has been shown that the Baa motif of CNGA2 does not play any role in Ca^{2+}–calmodulin modulation of heteromeric channels. Instead, by comparing properties of native channels with heterologously-expressed heteromeric channels, the modulatory subunits CNGA4 and CNGB1b have been shown to be responsible for the physiological modulation of Ca^{2+}–calmodulin (see Fig 1.7 B, Bradley *et al.*, 2004; Bradley *et al.*, 2001). Munger *et al*. (2001) measured, in excised patches containing native heteromeric olfactory CNG channels, a fast current inhibition upon addition of Ca^{2+}–calmodulin that persisted for several seconds also after calmodulin was

removed in Ca^{2+}-free solution. In contrast, homomeric CNGA2 showed a slower onset of inhibition by Ca^{2+}–calmodulin and a faster recovery suggesting that CNGB1 and A4 mediated the physiological relevant modulation of the channel (Bradley *et al.*, 2001).

Indeed, the modulatory subunits also have calmodulin binding sites: CNGA4 has an IQ-type calmodulin binding site located at the C-terminal region, while CNGB1b has a similar IQ-type site located at the N-terminal region and a Baa motif in the C-terminal region. It has been shown that the IQ-type sites are necessary and sufficient for Ca^{2+}–calmodulin channel inhibition, whereas the Baa-type site is not necessary (Bradley *et al.*, 2004; Bradley *et al.*, 2001). Moreover OSNs from knock out mice for CNGA4 showed a reduced adaptation both after prolonged odor stimulation and with double pulse protocol (Munger *et al.*, 2001). However these data have partially been challenged by a subsequent report showing that the lack of the CNGA4 or B1 greatly reduced the sensitivity of the channel to cAMP but also impaired the trafficking of subunits to olfactory cilia (Michalakis *et al.*, 2006). Indeed Song *et al*. (2008) reported that in mice with CNG channels lacking the IQ-type calmodulin binding site in the B1 subunit, so that they are insensitive to calmodulin modulation, but with normal trafficking and cAMP sensitiviy the adaptation to double stimulation is not affected suggesting that calmodulin did not play a pivotal role in this process. However in this mouse line the response to odors shows a longer termination both after brief and long lasting odor stimulation pointing out the role of Ca^{2+}- calmodulin modulation in shaping the termination of the odor response (Song *et al.*, 2008).

These results can also suggest that calmodulin is not the Ca^{2+}-responsive factor that is coassembled with the CNG channel (Bradley *et al.*, 2004). Other experimental evidences argue against this hypothesis, in particular the endogenous factor appears to bind the CNG

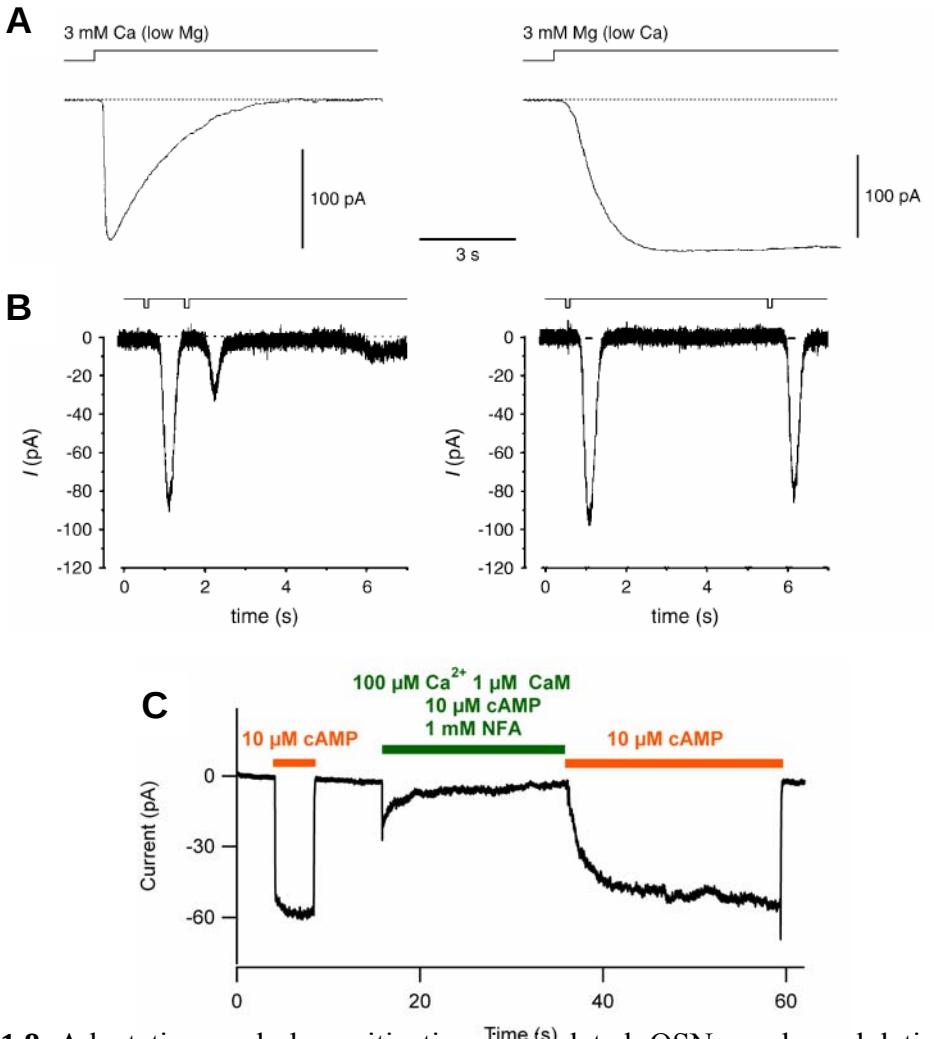

Figure 1.8 Adaptation and desensitization in isolated OSNs and modulation of CNG channels.

Desensitization during prolonged odor stimulation. In each recording, the bar at the top represents a prolonged stimulation with 10 mM n-amyl acetate. The left recording was made in the presence of 3 mM extracellular Ca^{2+}; the response was transient. When the Ca^{2+} was removed (replaced with 3 mM Mg^{2+} to maintain the divalent block of CNG channel), the response did not appreciably decay. Holding potential -34 mV. (A, from Kurahashi & Shibuya, 1990), Desensitization during repeated odor stimulation. In each recording, the top trace indicates 2 identical 100-ms pulses of the odorant lilial (1 mM) delivered with an interval in between. When the interval was 1 s (recording at the left), the response to the second pulse was reduced by 67%. With a 5-s interval (recording at the right), the response was reduced by just 15%. Holding potential -54 mV. (B, from Takeuchi & Kurahashi, 2003). Native olfactory CNG channels are inhibited by Ca^{2+}-calmodulin in excised inside-out patches. A patch was exposed to 10 µM cAMP in a solution containing nominally 0 Ca^{2+}. Then the same patch was exposed to a solution containing, in addition to 10 µM cAMP, 1 µM calmodulin and 67 µM Ca2+ (in the presence of 1 mM NFA to block native Ca^{2+}-activated Cl^- current). The addition of Ca^{2+}-calmodulin quickly inhibited the cAMP-gated current that slowly recovered to its initial value after removal of Ca^{2+}-calmodulin (C, from Pifferi *et al*., 2006a).

channels in a very stable manner, being washed away only after intense rinsing in Ca^{2+}-free solution (Kramer & Siegelbaum, 1992; Kleene, 1999; Bradley *et al.*, 2004). However, it is also possible to speculate that the binding of ‘‘native’’ calmodulin is more stable because the channel or the calmodulin itself undergoes post-transductional modifications that change the properties of the interaction. On the other hand, it cannot be excluded that also other proteins, in addition to calmodulin, contribute to the Ca^{2+}-mediated modulation of olfactory CNG channels.

1.9.2 The Calcium-activated Chloride Channel

The first report of the presence of Calcium-activated chloride channel (CaCC) in OSN was made by Kleene and Gestand in 1991 using excised cilia of frog OSN. After this first report, CaCC has been described in ORNs of amphibia (Kleene & Gesteland, 1991; Kurahashi & Yau, 1994), mammals (Lowe & Gold, 1993b; Reisert *et al.*, 2003; Reisert *et al.*, 2005), and fish (Sato & Suzuki, 2000). In frog, the channels are present in virtually all the olfactory cilia (Kleene *et al.*, 1994). The channel density in the cilium is estimated to be 62–78/μm^2 (Larsson *et al.*, 1997; Reisert *et al.*, 2003). In frog, the densities of the CNG and Cl^- channels are similar (Larsson *et al.*, 1997). In rat, though, Cl^- channels are in excess by a factor of about 8 (Reisert *et al.*, 2003). The current conducted by a single olfactory Cl^- channel is so small that single-channel studies have not been possible. By noise analysis of macroscopic currents, the unit conductance was estimated to be just 0.8 pS in frog (Larsson *et al.*, 1997). Low-pass filtering below 100 Hz reduces the measured conductance to 0.5 pS (Kleene, 1997). In a neuron, which is expected to cut off frequencies below ~16 Hz (Schild & Restrepo, 1998), it is likely that the effective conductance is smaller still. The unit conductance is ~1.5 pS in rat (Reisert *et al.*, 2003). These values are similar to the unit conductance of the CNG channel in physiological solutions (1.5 pS, Zufall & Firestein, 1993; 0.56 pS, Kleene, 1997). Not surprisingly, then, the ratio of maximum CNG and Cl^- currents in physiological solutions primarily reflects the relative abundances of the 2 types of channel. In frog, the maximum currents are almost equal (Kleene, 1997; Kleene, 1993). In rat, where the Cl^- channels are more numerous, the maximum Cl^- current is greater than the maximum CNG current by a factor of 33 (Reisert *et al.*, 2003). Indeed, under voltage clamp conditions, the fraction of odor-induced current carried by Cl^- channel ranges from 36% in

newt and salamander (Kurahashi & Yau, 1993) 60 % in *Xenopus laevis* (Zhainazarov & Ache, 1995) and 85% in rat (Lowe & Gold, 1993b) and up to 90% in mice (Reisert *et al.*, 2005; Boccaccio & Menini, 2007).

The relation between $[Ca^{2+}]_i$ and Cl^- current is well-fitted by the Hill equation. Studies in frog (Kleene & Gesteland, 1991), rat (Reisert *et al.*, 2003), and mouse (Reisert *et al.*, 2005; Pifferi *et al.*, 2006b) have shown that half maximal activation ($K_{1/2}$) occurs from 2.2 to 4.7 μM Ca^{2+}. In one other study, $K_{1/2}$ was much higher, 26 μM; (Hallani *et al.*, 1998); the reason can be related to the unbuffered Ca^{2+} solution used in that study. Gating of the channel is probably cooperative; the Hill slope parameter n ranges from 2.0 to 2.8. The channel's maximum open probability is 0.97. The very small single channel conductance with high maximum open probability allows a high amplification without an increase of noise giving OSNs the ability to improve their signal to noise ratio (Kleene, 1997). In frog OSNs the shape of the current-voltage relation varies with concentration of the gating ligand. At 2–3 μM Ca^{2+}, significant outward rectification is apparent. At saturating Ca^{2+} levels, though, inward rectification is seen (Kleene & Gesteland, 1991). In neither case is the mechanism of rectification known. One cannot yet exclude the possibility that 2 Cl^- channels, one with each type of rectification, contribute to the current.

In amphibian OSN the CaCCs did not show spontaneous inactivation after exposure to Ca^{2+} (Kleene, 1993; Kleene & Gesteland, 1991). In contrast in inside-out patches excised from dendritic knob/cilia of rodent (mouse and rat) OSNs it was reported that CaCC undergoes a Ca^{2+}-dependent inactivation which is reversible after removal of Ca^{2+} for some seconds (Reisert *et al.*, 2003; Reisert *et al.*, 2005). In contrast in rat OSN, Hallani *et al.* (1998) did not find this type of inactivation. Moreover, in rodents an irreversible run-down of current mediated by CaCC was also observed suggesting that some modulatory component of the channel is lost after the excision of the membrane (Reisert *et al.*, 2003; Reisert *et al.*, 2005).

The ionic selectivity of olfactory CaCCs was studied in two different studies with different results (Reisert *et al.*, 2003; Hallani *et al.*, 1998). In the first report the permeability sequence was $Cl^->F^->I^->Br^-$ with (Hallani *et al.*, 1998), whereas Reisert *et al.* (2003) reported the sequence $I^->Br^->Cl^->F^-$. The reason of this discrepancy is not clear. In general most of the CaCCs show the permeability sequence reported by Reisert *et al.* (2003). This sequence indicates that the permeability is primarily determined by the hydration

energy of the ion. The theory of ion selectivity (reviewed in (Wright & Diamond, 1977; Eisenman & Horn, 1983) shows that a binding site with a low electrical field strength (where the interaction of ions with the channel is weaker than ion-water inter-actions) generates the permeability sequence $I^->Br^->Cl^->F^-$, as observed in CaCCs channels. The selectivity pattern of such a weak site is mainly determined by differences between the hydration energies of the individual ion species, while differences in binding energy play a minor role. In contrast, a binding site with high field strength generates a permeability sequence with the reverse order $F^->Cl^->Br^->I^-$.

1.10 Mechanisms of response termination

Even as the receptor current is generated, processes commence that inactivate it. As noted before there is abundant evidence that normal inactivation requires an influx of Ca^{2+}. The falling phase of the odor response is slowed or eliminated at positive potentials (Kurahashi & Shibuya, 1990; Takeuchi & Kurahashi, 2003; Lowe & Gold, 1993a) in the absence of extracellular Ca^{2+} (Kurahashi, 1990; Kurahashi & Shibuya, 1990; Zufall *et al.*, 1991b) or on addition of an intracellular Ca^{2+} chelator (Kurahashi & Shibuya, 1990). Each of these conditions inhibits the accumulation of cytoplasmic free Ca^{2+}. Adaptation to repeated brief stimuli is also greatly reduced at positive potentials (Kurahashi & Menini, 1997; Takeuchi & Kurahashi, 2003; Boccaccio *et al.*, 2006). Finally, the receptor current begins to decline just as the Ca^{2+} concentration peaks (Leinders-Zufall *et al.*, 1998; Reisert & Matthews, 2001b). The current generated by photorelease of cAMP also shows Ca^{2+}-dependent adaptation (Boccaccio *et al.*, 2006; Kurahashi & Menini, 1997). Thus, at least, part of the inactivation occurs at steps in the cascade following the activation of the cyclase. However, the inactivation during a prolonged odor stimulus is faster than that seen during prolonged release of caged cAMP (Takeuchi & Kurahashi, 2002). This indicates that other mechanisms of inactivation exist upstream of the channels. Many mechanisms may contribute to termination of odor-induced currents even if we still lacks a general knowledge of the relative importance of different processes. For brief stimulation the termination can be determined by:

(i) $G_{\alpha olf}$ is inactivated by its intrinsic GTPase function; as noted before the adding of non-hydrolysable GTP-γ-S via the patch pipette produced a prolonged odor-induced response (Firestein *et al.*, 1991a).

(ii) cAMP and Ca^{2+} should diffuse away from the channels.

(iii) Phosphodiesterases hydrolyze cAMP. PDE1C2 is localized to OSNs cilia and it is activated by Ca^{2+}-calmodulin via CaMKII (Borisy *et al.*, 1992; Yan *et al.*, 1995). However the PDE is not involved in adaptation during a double pulse protocol since the photorelease of non-hydrolysable 8Br-cAMP showed a Ca^{2+}-dependent adaptation (Boccaccio *et al.*, 2006).

(iv) Ca^{2+} is expelled from the cilia through a Na^{+}/Ca^{2+} exchanger (Reisert *et al.*, 2003; Reisert & Matthews, 1998; Pyrski *et al.*, 2007). Indeed, blocking of the Na^{+}/Ca^{2+} exchanger by bathing the OSN with Li^{+} or $Choline^{+}$ prolonged the odor-induced response due to longer activation of the Ca^{2+}-activated Cl^{-} channel (Reisert & Matthews, 1998). Moreover, Castillo *et al*. (2007) reported that also a Ca^{2+}ATPase, PMCA, contributes to clearance of intracellular Ca^{2+} during odor stimulation.

(v) Ca^{2+}-calmodulin modulation of CNG channel: Song *et al*. (2008) reported that in mouse with CNG channels insensitive to calmodulin the response to odor shows a longer termination both after brief and long lasting odor stimulation.

Other mechanisms contribute to termination of responses to prolonged or intense stimulation:

(i) G-protein–coupled receptor kinase 3 (GRK3) and β-arrestin-2 can inactivate the odorant receptor protein through internalization and degradation in lysosomal compartments (Dawson *et al.*, 1993; Schleicher *et al.*, 1993; Mashukova *et al.*, 2006; Peppel *et al.*, 1997).

(ii) Ca^{2+}–CaM activates CaMKII, which in turn phosphorylates the type III adenylyl cyclase (Boekhoff *et al.*, 1996; Wei *et al.*, 1996; Leinders-Zufall *et al.*, 1999). Early results (reviewed by Boekhoff *et al.*, 1996) were complex, but it is now believed that this inhibits the cyclase, thus reducing the production of cAMP. The cyclase is also inhibited by RGS2, but the role of this in transduction is uncertain (Sinnarajah *et al.*, 2001).

(iii) Intraciliary Cl^- should be depleted during a prolonged response (Lindemann, 2001), and this would limit or prevent further Cl^- efflux. Such depletion does not occur during brief stimulation (Boccaccio *et al.*, 2006).

1.11 Calcium-activated chloride channels in other cell types

Many cell types express Cl^- channels that are activated by intracellular [Ca^{2+}] in the micromolar range. This type of conductance was first described in *Xenopus* oocyte (Miledi, 1982; Barish, 1983) and subsequently characterized in taste receptors cells, in photoreceptors, in different neuronal cell types, in smooth muscle cells, in airway and intestinal epithelial cells, in exocrine gland, in kidney, in cardiac muscle cells and in endothelial cells (for review see Hartzell et al., 2005a). CaCC plays different physiological roles in various cell types.

In *Xenopus* oocyte, CaCC play a fundamental role in blocking polyspermy by generating the so-called fertilization potential (Webb & Nuccitelli, 1985) Upon fertilization, the membrane potential increases from the resting potential of ~ - 40 mV to ~ + 20 mV for several minutes. This depolarization is dependent on the activation of CaCCs. The initial activation of CaCCs is due to the release of Ca^{2+} from internal stores through the production of IP_3 that is triggered by egg activation after fertilization (Hartzell *et al*., 2005a). In the following phase the activation of CaCCs is maintained by the entry of Ca^{2+} through the store-operated Ca^{2+} channels (Hartzell, 1996; Kumura & Hartzell, 2000).

CaCCs are also present in both mammalian and amphibian taste receptors (McBride, Jr. & Roper, 1991; Herness & Sun, 1999). Taste stimuli produce a depolarizing current in taste receptor cells that may result in a discharge of action potentials (Lindemann, 1996). In *Necturus*, action potentials in the taste receptors are followed by an outward current that is mediated by CaCCs, which open in response to Ca^{2+} influx during the action potentials (McBride, Jr. & Roper, 1991; Taylor & Roper, 1994). The CaCCs produce a hyperpolarization in these cells because E_{Cl} is between −60 mV and −80 mV. This hyperpolarization could play a role in taste adaptation (Taylor & Roper, 1994).

In photoreceptor (both cones and rods) CaCCs are localized in inner segment (Barnes & Hille, 1989; Barnes, 1994; Maricq & Korenbrot, 1988; Bader *et al.*, 1982). The depolarization produced by the dark current opens voltage-gated Ca^{2+}-channels located at

the synaptic terminal causing a Ca^{2+} influx that activates a large Cl^- conductance. Upon illumination, the dark current turns off, the cell membrane hyperpolarizes, and transmitter release stops (Yau, 1994). The role of CaCCs in rods is not known, but it has been suggested that in cones they play a role in modulating lateral inhibition (Barnes & Hille, 1989; Maricq & Korenbrot, 1988; Thoreson & Burkhardt, 1991). Cones in the dark center of an illuminated annulus often exhibit action potentials whose repolarization is afforded by CaCCs. However, the precise role of CaCCs in photoreceptors remains ambiguous because of uncertainties about $[Cl^-]_i$.

CaCCs are expressed in a variety of different neurons, including dorsal root ganglion (DRG) neurons, spinal cord neurons, and neurons of the autonomic nervous system. Generally, CaCCs are not expressed in all neurons of a group, but rather in a subset, suggesting that these channels perform a specific function for this subset of neurons. The functions of CaCCs in neurons remain poorly established, but it has been suggested that they are involved in action potential repolarization, generation of after-polarizations, and membrane oscillatory behavior. About 45–90% of the somatosensory neurons from the DRG that sense skin temperature, touch, muscle tension, and pain express CaCCs (Bader *et al.*, 1987; Scott *et al.*, 1988; Stapleton *et al.*, 1994; Currie *et al.*, 1995). In the mouse DRG, CaCCs are expressed selectively in a subset of medium diameter (30– 40 μm diameter) sensory neurons (Andre *et al.*, 2003), suggesting that signaling in these neurons is somehow different from the rest of the population. It has been proposed that CaCCs in DRG are responsible for after-depolarizations following action potentials (Mayer, 1985; De Castro *et al.*, 1997). The estimated $[Cl^-]_i$ in DRG neurons is 30 mM (Gilbert *et al.*, 2007), which produces an E_{Cl} of −35 mV. Thus opening CaCCs by Ca^{2+} entry or Ca^{2+} release from stores would depolarize the cell membrane or produce after-depolarizations (Deschenes *et al.*, 1976; Duchen, 1990; Crain, 1956).

In smooth muscle cells CaCCs are involved in regulation of myogenic tone and contraction activated by various agonists (Davis & Hill, 1999; Large & Wang, 1996). Because in these cells E_{Cl} is more positive than the resting potential, opening CaCCs will produce a depolarization (Chipperfield & Harper, 2000). The activation of CaCCs is mediate by Ca^{2+} entry through the voltage-gated Ca^{2+}-channels or through the Ca^{2+} released from intracellular stores by inositol 1,4,5-trisphosphate (IP_3) generated through the PLC pathway (Large & Wang, 1996; Davis & Hill, 1999). For example norepinephrine, released by

sympathetic stimulation, induces smooth muscle contraction by activation of G_q-coupled α-adrenergic receptors (Wahlstrom, 1973; Bolton, 1979; Byrne & Large, 1985; Byrne & Large, 1988).

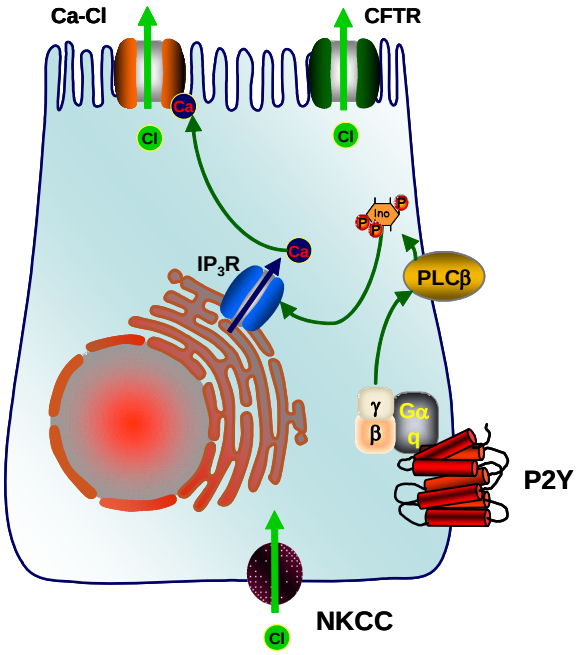

Figure 1.9 Ca^{2+}-activated Cl^- channels in epithelial cells.
Ca^{2+}-activated Cl^- channels are involved in regulation of secretion in many types of epithelial cells. Schematic diagram showing the mechanisms involved in secretion activation in airway epithelium. ATP activates P2Y receptors, that through $G_{\alpha q}$, stimulates the production of IP_3 by PLCβ. Ca^{2+} is released by intracellular stores and gates Ca^{2+}-activated Cl^- channel causing an increase of fluid secretion.

In airway epithelia CaCCs control the level of airway surface liquid, which is important for mucous hydration and protection against infection. Secretion of fluids is accomplished by basally located transporters that accumulate Cl^- in the cell against the Cl^- electrochemical gradient and by apical Cl^- channels that permit Cl^- to flow into the extracellular space down its electrochemical gradient. Airway epithelial cells coexpress CaCCs and cystic fibrosis transmembrane regulator (CFTR) in their apical membrane (Boucher *et al.*, 1989; Kartner *et al.*, 1991). The stimulation of secretion by ATP or UTP is dependent on the activation of CaCCs (Knowles *et al.*, 1991; Tarran *et al.*, 2002). UTP/ATP stimulates G_q-coupled P2Y purinergic receptors to increase IP_3 production and subsequently Ca^{2+} release from internal stores that actives CaCCs causing, in turn, the increase of secretion of fluids (Fig 1.9, Gabriel *et al.*, 2000; Donaldson *et al.*, 1989).

CaCCs are also expressed in various types of exocrine glands such as lachrymal, parotid, submandibular, sublingual and pancreas. Also in these cell types CaCCs are involved in regulation of fluid secretion. The parasympathetic neurotransmitter acetylcoline stimulates fluid secretion through the activation of muscarinic receptor-induced production of IP_3 that releases Ca^{2+} from internal stores (Botelho & Dartt, 1980; Hunter *et al.*, 1983; Melvin *et al.*, 1991; Douglas & Poisner, 1963).

1.12 Bestrophin and Best Disease

Best Vitelliform Macular Dystrophy (BVMD, also known as Best Disease, ONIM no. 153700) is an autosomal-dominant, progressive, juvenile-onset retinal macular degeneration that is due to an alteration in retinal pigment epithelium (RPE) function (Fig 1.10; Best, 1905; Gass, 1987; Mohler & Fine, 1981; Pianta *et al.*, 2003). RPE is a monolayer of cells in direct contact with photoreceptors and it plays a central role in controlling the communication between the retina and the choroidal blood vessels (Fig 1.10 A-B). Best Disease is associated with large deposits of a yellow pigmented material in the subretinal and sub-retinal pigment epithelium (RPE) spaces. The deposits initially resemble an egg yolk (vitelliform). The lesion then often passes through a pseudohypopyon stage that is often accompanied by detachment of the neural retina from the RPE (Jaffe & Schatz, 1988; Men *et al.*, 2004; Pianta *et al.*, 2003; Pierro *et al.*, 2002; Vedantham & Ramasamy, 2005). With age, the deposits become disorganized (the vitelleruptive stage) and the RPE/choroid layer becomes thickened partly as a consequence of pigment accumulation in the RPE layer (Pianta *et al.*, 2003; Pierro *et al.*, 2002). The retinal layer above the thickened area becomes thinner, the photoreceptors degenerate, and deterioration of central vision follows (Fig 1.10 A). There is a considerable variability in the age of onset and the expressivity of vitelliform lesions. The nature of the yellow pigment in BVMD is not known, but from its histological appearance, it is often assumed to be lipofuscin.

Lipofuscin is a yellow pigment that normally accumulates with age in granules in the lysosomal compartment of RPE cells (Sparrow & Boulton, 2005). Lipofuscin originates at least partly from photoreceptor outer segments that are phagocytosed by the RPE and is composed partly of oxidized proteins and lipids as well as fluorescent compounds. The major fluorophores include a diretinal conjugate, *N*-retinylidene-*N*-retinylethanolamine

(A2E), and its photooxidation products (Eldred & Lasky, 1993; Bui *et al.*, 2006). A2E may disrupt membrane integrity by a detergent-like effect (Eldred & Lasky, 1993), and its photooxidation products may activate complement (Zhou *et al.*, 2006) and promote apoptosis (Sparrow & Cai, 2001). It has been shown that A2E mediates blue-light-induced damage in the retina (Sparrow & Cai, 2001) and is believed to be an important causal factor in macular dystrophy.

The gene responsible for Best disease was positionally cloned in 1998 from families exhibiting macular degeneration with a juvenile age of onset (Marquardt *et al.*, 1998; Petrukhin *et al.*, 1998). The gene was named bestrophin-1, Best1 (or VDM2). The expression of human Best1 (hBest1) is highly restricted. The levels in retina and RPE are much higher than in any other tissue, although some expression is noted in brain, spinal cord, kidney, and testis. Protein expression for hBest1 has been reported only in RPE. In mouse, mBest1 protein expression has been reported in colon, kidney, and trachea in addition to RPE (Bakall *et al.*, 2003; Barro *et al.*, 2006). In particular, Best1 is localized in baso-lateral membrane of RPE (Bakall *et al.*, 2003; Marmorstein *et al.*, 2000).

Although it was initially hypothesized that hBest1 might be a transporter of lipid components of lipofuscin (Petrukhin *et al.*, 1998), there is now considerable evidence that bestrophins function as Ca^{2+}-activated Cl^- channels (Sun *et al.*, 2002; Tsunenari *et al.*, 2003; Qu *et al.*, 2003; Hartzell *et al.*, 2008). The suggestion that bestrophins are Cl^- channels is particularly intriguing because the hallmark diagnostic feature of Best disease is a decreased slow light peak in the electrooculogram that is correlated with permeability of baso-lateral membrane of RPE (Fig 1.11 A). To measure electrooculogram electrodes are placed on either side of the eye at the canthus and the subject is instructed to look alternately left and right. At the extremes of the saccades, the voltage recorded by the external electrodes is different because of the different orientation of the dipole set up by the RPE transepithelial potential. Typically, the recorded voltage is on the order of 20–150 μV in the dark-adapted eye. The voltage increases about twofold within 5–15 min after turning on the lights. The dark-adapted value is called the dark trough, and the maximum voltage in the light is termed the light peak (LP). Because the voltages can depend on many factors including placement of the electrodes, the ratio of the dark trough to the LP, the Arden ratio (Arden *et al.*, 1962), is usually used as the relevant comparative parameter. The Arden ratio in normal individuals is usually >2 and is considered pathologic if it is <1.5. Still, there is considerable variability

in the Arden ratio, at least partly as a consequence of variability in eye movements (Fig 1.11 A; Riemslag et al., 1989).

There is considerable evidence that the LP is generated by a Cl^- channel in the basolateral membrane of the RPE (Gallemore *et al.*, 1988; Gallemore & Steinberg, 1993). When the basolateral Cl^- conductance increases, the basolateral membrane depolarizes, which thus increases the transepithelial potential. Because hBest1 immunoreactivity is located basolaterally in RPE cells (Bakall *et al.*, 2003; Marmorstein *et al.*, 2000; Mullins *et al.*, 2007), it has reasonably been assumed that BVMD is caused by a defect in the basolateral RPE hBest1 (Hartzell & Qu, 2003; Sun *et al.*, 2002). The mechanisms that turn on the basolateral Cl^- conductance in the light remain obscure. There is evidence that the LP, although generated by the RPE, requires intact photoreceptors. This has led to the suggestion that photoreceptors in light produce a diffusible signal ("the light peak substance") that binds to receptors on the RPE to activate the Cl^- conductance (Fig. 1.11 B; (Gallemore *et al.*, 1988; Gallemore & Steinberg, 1993; Linsenmeier & Steinberg, 1982). A second messenger cascade is implied by the very slow time course of the LP (~10 min). The identity of the diffusible signal and the second messenger pathway remains unknown. Although several candidates have been proposed for the LP substance, ATP is favored because ATP mimics the LP (Peterson *et al.*, 1997; Strauss, 2005). It has been suggested that ATP released by photoreceptors acts on G protein-coupled purinergic receptors (P2Y) in the RPE to elevate cytosolic Ca^{2+}, which in turn activates the Cl^- conductance (Fig. 1.11 B).

Although bestrophins function as Cl^- channels, the question remains whether BVMD is caused by a defect in plasma membrane bestrophin Cl^- channel function. A strong argument supporting the idea that hBest1 mutations produce macular dystrophy by altering hBest1 Cl^- channel function is the finding that of the 31 disease-causing mutations that have been studied, all of them except 3 alter the Cl^- channel function of hBest1 expressed in HEK-293 cells (Marchant *et al.*, 2007; Sun *et al.*, 2002; Yu *et al.*, 2007; Yu *et al.*, 2006; Hartzell *et al.*, 2008). Of the mutants that affect Cl^- channel function, the current amplitudes of the mutants are almost zero or much smaller than wild type. Often the mutants suppress the current produced by coexpression of wild-type channels. This is consistent with the dominant mechanism of inheritance, but data regarding the mechanisms of the dominant negative effects are lacking.

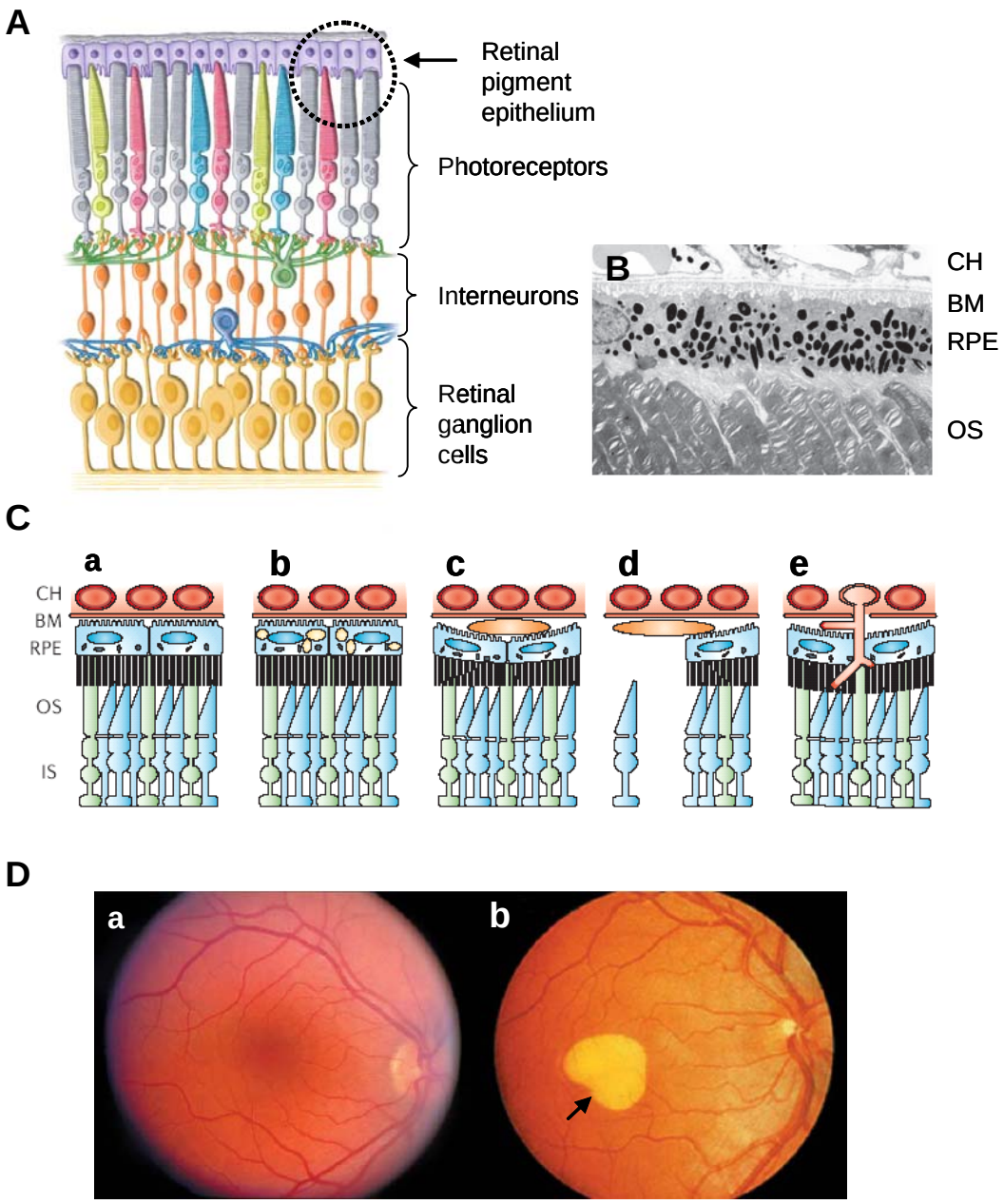

Figure 1.10 Best Vitelliform Macular Dystrophy

Schematic organization of the mammalian retina (A, from Hartzell *et al*., 2005b). Outer segments of photoreceptors are in contact with the retinal pigment epithelium (RPE), a monolayer of cells that are specialized to service the adjacent photoreceptors (A-B, from Rattner & Nathans, 2006). Schematic illustration of the RPE and Bruch's membrane (BM) histopathology associated with Best disease (C): normal retina and RPE. (a); accumulation of lipofuscin in RPE cells (b); a druse (deposits composed of a complex mixture of lipids) sandwiched between the RPE and Bruch's membrane (c); a druse with adjacent geographic RPE atrophy and loss of overlying photoreceptors (d); choroidal neovascularization (e) (CH, choroid, OS, outer segment, IS, inner segments). Typical fundus images of normal (D-a) and of Best vitelliform macular dystrophy affected retina at vitelliform stage (D-B). Accumulation of large yellow-pigmented material (arrow) is a typical hallmark of Best disease (from Hartzell *et al*., 2005b).

The hypothesis that BVMD is caused by Cl^- channel dysfunction has recently been challenged by Marmostein's lab (Marmorstein & Marmorstein, 2007; Marmorstein & Kinnick, 2007; Marmorstein *et al.*, 2004; Rosenthal *et al.*, 2006). The most compelling evidence is that mice with the mBest1 gene disrupted ($mBest1^{-/-}$ null) have no retinal pathology. A surprising and important finding is that the LP is not generated solely by Best1, at least in mice. Furthermore, RPE CaCC currents are not obviously affected by knockout of mBest1 (Marmorstein *et al.*, 2006). Although the amplitude of the LP in response to maximum light intensity was unchanged in $mBest1^{-/-}$ mice, the luminance-response curve (the sensitivity of the LP to light intensity) was altered. At low illumination intensities, the LP was enhanced in the knockout. This suggests that mBest1 expression reduces the sensitivity of the LP to light and that knockout relieves this inhibition. Marmorstein and co-workers (Marmorstein *et al.*, 2006; Wu *et al.*, 2007) have shown that voltage-gated Ca^{2+} (Ca_v) channels play an important role. The LP is reduced by the Ca^{2+} channel blocker nimodipine (Marmorstein *et al.*, 2006) and is also reduced in mice lacking the α 1.3 Ca_v channel subunit (Wu *et al.*, 2007) or the Ca_v channel β4 subunit (Marmostein et al., 2006). In addition, Rosenthal *et al.* (2006) have shown that hBest1 expression in RPE-J cells affects the function of endogenous Ca_v channels in these cells. Overexpression of wild-type hBest1 shifts the voltage dependence of Ca^{2+} channel activation to the left and accelerates activation (Rosenthal *et al*. 2006). Moreover Yu *et al*. (2008) reported that hBest1, expressed in HEK-293 can inhibit Ca_v channel by direct interaction between the SH3 domain in C-terminus of bestrophin and β subunit of Ca_v 1.3. Interestingly this inhibition was not seen with mBest1 suggesting a possible species-specific function of Best1. Moreover, it could partially explain the lack of a retinal alteration observed in $mBest1^{-/-}$ mice.

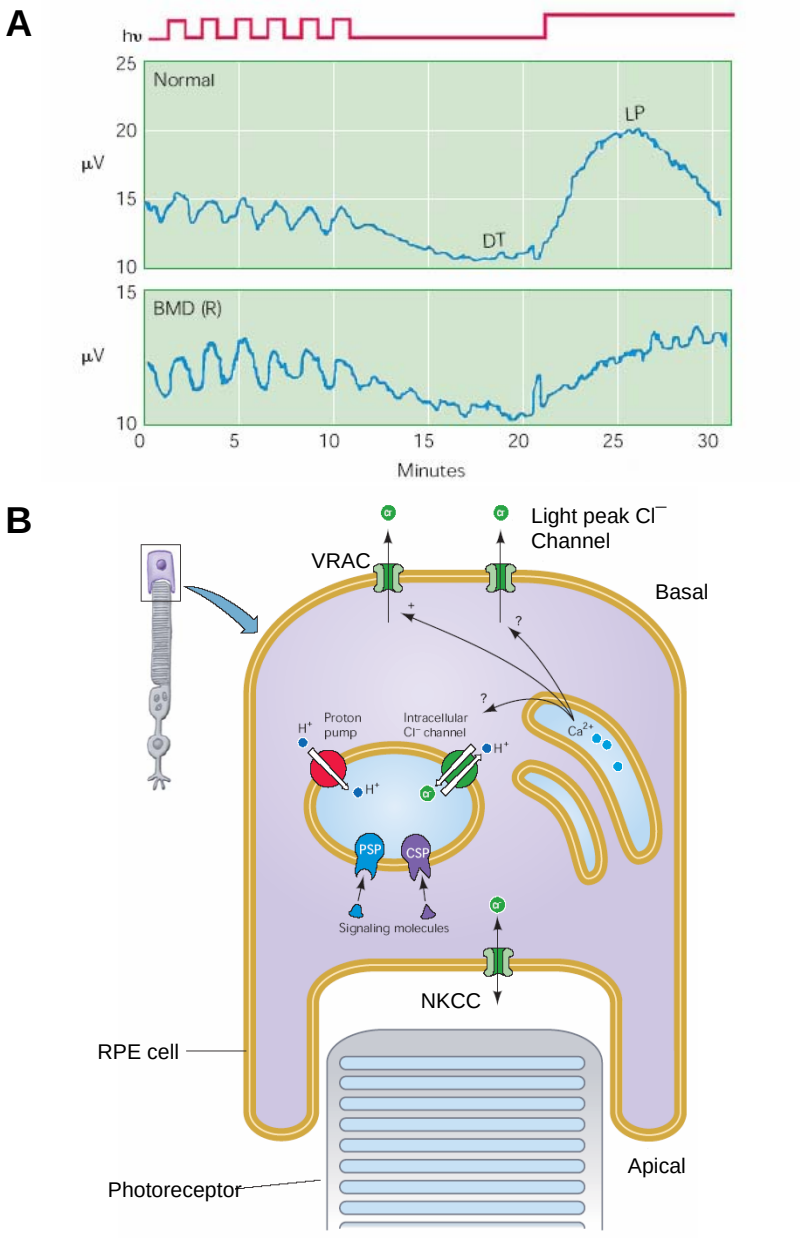

Figure 1.11 Ca^{2+}-activated Cl^- channels in RPE.
Typical electrooculogram recording in a normal subject (upper panel in A) or in a Best disease-affected subject (lower panel in A). The light peak shows a big reduction. Schematic mechanism of generation of the light peak in RPE cells (B, from Hartzell *et al.,* 2005b). Cl^- is accumulated in RPE at the apical level by NKCC activity. The activation of photoreceptors by light stimulates the release of a unidentified "light peak substance" that via a second messenger cascade induces the activation of Ca^{2+}-activated Cl^- channels in the basolateral membrane.

1.13 Bestrophins: a new family chloride channel

After the first identification of hBest1 as the gene responsible for BVMD bestrophins have been unambiguously identified in mammals, birds, bony fish, amphibians, echinoderms, insects, nematodes, and flat worms (reviewed in Hartzell *et al.*, 2008). All of the vertebrate bestrophins fall into one of four paralogous branches. The human genome contains four bestrophin paralogs (hBest1, hBest2, hBest3, and hBest4; Tsunenari *et al.*, 2003; Stohr *et al.*, 2002). All other mammals have either three or four bestrophin paralogs. Mice, for example, have three paralogs and one pseudogene (Kramer *et al.*, 2004). Bestrophins in all of these species have a conserved N-terminal domain that includes the putative transmembrane regions, and a C-terminal domain that is highly variable in both length and sequence.

The first clear evidence that bestrophins are Cl^- channels was presented by Sun *et al*. (2002) who showed that expression of hBest1 and several other bestrophins in HEK-293 cells induced Cl^- currents. Now several different arguments support the idea that bestrophins are Cl^- channels.

(i) Bestrophins from different species expressed in HEK-293 cells produce a novel Ca^{2+}-activated Cl^- current (Qu *et al.*, 2004; Qu *et al.*, 2003; Sun *et al.*, 2002). The type of current induced by mouse Bestrophin 2 (mBest2) is the same in different cell lines (Qu *et al.*, 2004). Because one would not necessarily expect upregulation of the same kind of Cl^- channel in different cell types, the appearance of similar currents in different cells minimizes (but does not eliminate) the concern over upregulation of endogenous channels (Qu *et al.*, 2004).

(ii) Different bestrophins produce currents with different current-voltage relations and kinetics of activation (Sun *et al.*, 2002;T sunenari *et al.*, 2003). For example, hBest1 currents have linear current-voltage relationships and are essentially time independent, whereas hBest3 currents strongly inwardly rectify and activate slowly with time (Tsunenari *et al.*, 2003). These different characteristics provide some confidence that the currents are specific to the type of bestrophin expressed.

(iii) hBest1 and mBest2 currents are inhibited by the modification of sulfhydryl groups with membrane impermeant $MTSET^+$ (Tsunenari *et al.*, 2003; Qu *et al.*, 2004; Qu & Hartzell, 2004). Modification of ionic currents by $MTSET^+$ is a common approach

used to identify amino acids that line the permeation pathway (Karlin & Akabas, 1998).

(iv) Expression of mutant bestrophins can act as dominant-negative on wild-type channels. Notably G299E and W93C inhibit the current induced by expression of the wild-type bestrophin (Sun *et al.*, 2002; Qu *et al.*, 2003), suggesting that the channels are multimers. Semiquantitative coimmunoprecipitation shows that bestrophins form multimeric complexes composed of four or five subunits, as one would expect for a channel protein (Sun *et al.*, 2002).

(v) Point mutations in both hBest1 and mBest2 produce changes in Cl^- channel properties such as the permeability of various anion and/or change of channel gating. Because it is generally agreed that the selectivity of a channel is determined by the channel pore, the ability to change the selectivity by a mutation provides strong evidence that bestrophin is responsible for forming the channel (Qu *et al.*, 2004; Pusch, 2004).

(vi) Endogenous Ca^{2+} activated Cl^- currents in Drosophila S2 cells can be specifically abolished by several RNAi constructs for dBest1 and dBest2, suggesting the involvement of these protein in CaCCs (Chien *et al.*, 2006).

The properties of bestrophins were generally investigated after transient heterologously expression in HEK-293 cells. Ca^{2+} sensitivity has been investigated for some bestrophins. hBest1 is activated by increase of $[Ca^{2+}]_i$ with an EC_{50} ~ 150 nM (Fischmeister & Hartzell, 2005). Sun et al. (2002) reported that hBest1 current can be rapidly activated by release of Ca^{2+} from caged Ca^{2+}, suggesting a direct activation by Ca^{2+} without the involvement of phosphorylation or other enzymatic processes. Xenopus best2 and mBest2 has an EC_{50} ~ 200 nM (Qu *et al.*, 2004; Qu *et al.*, 2003). Tsunenari et al. (2006) reported the activation by Ca^{2+} of hBest4 in excised inside-out patches with EC_{50} ~ 200 nM further suggesting a direct activation by Ca^{2+}. They also suggest that the Ca^{2+} binding site might be located in the C-terminus immediately after the last transmembrane domain because this region contains a high density of acidic amino acids that could coordinate positively charged Ca^{2+}. This region exhibits some similarity to the Ca^{2+} bowl of BK potassium channels. Finally endogenous Drosophila bestrophins in S2 cells can be activated in excised patches by Ca^{2+}, suggesting that Ca^{2+} acts on the channel directly (Chien *et al.*, 2006). However, addition of ATP accelerates the activation (Chien *et al.*, 2006).

The only data available on single channel properties derives from Drosophila bestrophins. Indeed, Chien et al. (2006) reported that in inside-out patches dBest1 has a single channel conductance of ~ 2 pS. This small single channel conductance is a common feature of many CaCCs expressed in many cell types (Hartzell *et al.*, 2005a; Frings *et al.*, 2000).

The ionic selectivity of bestrophins was investigated with some details for mBest2 and xBest2 (Qu *et al.*, 2004; Qu *et al.*, 2003). In both cases the channel showed a weak selectivity among various anions, as reported for many CaCC (Hartzell *et al.*, 2005a; Frings *et al.*, 2000) with the following permeability sequence: $SCN^- > I^- > Br^- > Cl^- > F^-$ (Qu *et al.*, 2004; Qu *et al.*, 2003).

Two different topology models have been proposed for hBest1 (Fig 1.12, Tsunenari *et al.*, 2003; Milenkovic *et al.*, 2007). Tsunenari *et al.* (2003) performed a very detailed analysis of hBest1 topology and suggested that of the six hydrophobic domains predicted by hydropathy, TM1, TM2, TM3, TM4, and TM6 traversed the membrane and that TM5 might be a reentrant loop (Fig. 1.12 A). This prediction was based on data from three different methods. (*i*) Substitution of cysteine residues for selected amino acids in hBest1 and examination of the effect of extracellular $MTSET^+$ (a membrane impermeant sulfhydryl reagent) on heterologously expressed Cl^- currents. (*ii*) Tsunenari *et al.* (2003) also examined the ability of inserted N-glycosylation sites to be glycosylated, that occurs in a topologically extracellular compartment (Fig. 1.12 A, glycosylated, solid red residues; not glycosylated, red letter). (*iii*) Finally, TEV protease sites were inserted and their ability to be cleaved by protease added to the topologically cytoplasmic compartment were examined (Fig. 1.12 A, TEV protease sites cleaved, solid cyan residues; not cleaved, cyan letter). In contrast, Milenkovic *et al* (2007) tested the topology of hBest1 by examining the ability of various hBest1 fragments consisting of predicted transmembrane domains or groups of predicted transmembrane domains to be incorporated into the membrane in the presence of a Lep H1 membrane targeting domain. They found that TM1, -2, -4, -5, and -6 were capable of being incorporated into the membrane when they were alone. TMD4 was able to incorporate into the membrane when it was presented alone or with TMD3; however, it was not able to incorporate when it was presented with TM5, TM2 + TM3, TM3 + TM5, or TM5 + TM6. These results suggested that only TM1, -2, -5, and -6 cross the membrane (Fig. 1.12 B). These two models are directly contradictory. The Tsunenari model places amino acids

~200–231 in an extracellular loop, whereas in the Milenkovic model, this domain is included in a large cytoplasmic loop (aminoacids 106–230). It is possible to speculate that the differences derived from the different experimental approaches used in these studies. Although experimental data for bestrophin transmembrane topology exist mainly for hBest1, the high conservation of the N-terminal 350 amino acids, which includes all the predicted transmembrane domains, suggests that the topology will be similar for each vertebrate bestrophins.

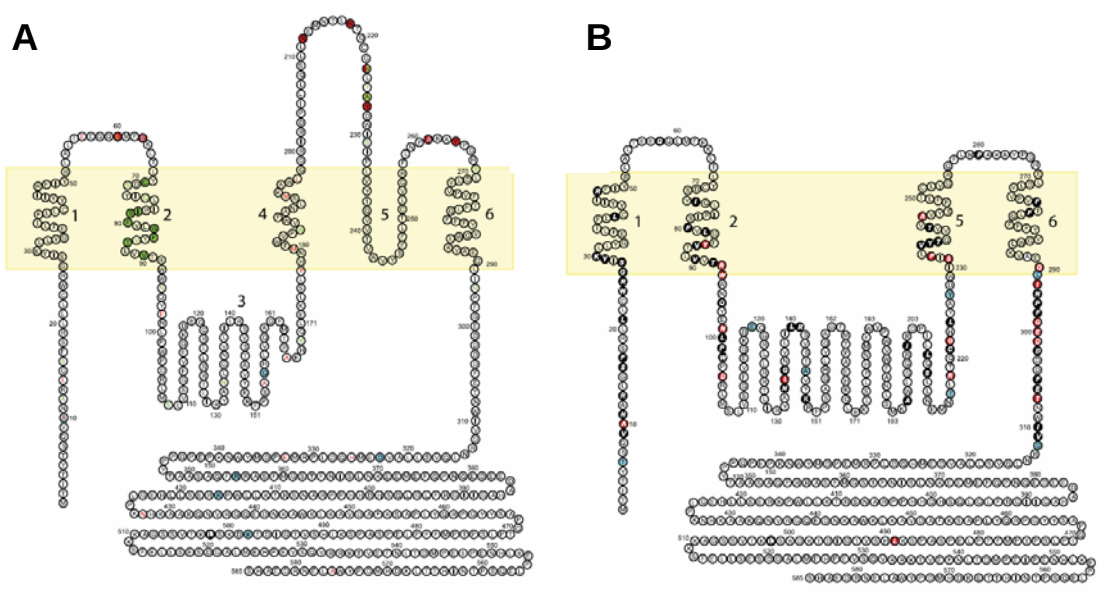

Figure 1.12 hBest1 topology models.
A: Model proposed by Tsunenari *et al.* (2003). Hydrophobic domains determined by hydropathy analysis are labeled 1–6. The amino acids are colored according to the evidence supporting their topological location. Green background: modified by MTSET; green letter: not modified by MTSET; red background; inserted N-glycosylation site is glycosylated in an in vitro translation system with microsomes (extracellular); red letter: not glycosylated; cyan background: inserted TEV protease site is cleaved in an in vitro translation system without detergent (cytosolic); cyan letter: cleaved by TEV protease in presence of detergent. B: Model proposed by Milenkovic *et al.* (2007). Topology was determined by examining the ability of fragments of hBest1 to insert into the membrane in an in vitro translation assay with microsomes (from Hartzell *et al*., 2008)

2. Materials and Methods

2.1 Immunohistochemistry

The mice (P15 and adult) were sacrificed by cervical dislocation and decapitated. These procedures are in accordance with the Italian Guidelines for the Use of Laboratory Animals (Decreto Legislativo 27/01/1992, no. 116). The turbinates were exposed by hemisection of the head sagittal along the septum and the olfactory epithelium was dissected. After fixation in 4% formaldehyde, 15% aqueous saturated picric acid, 150 mM sodium phosphate pH 7.4 for 1 hour at 4 ºC, the olfactory epithelia were washed in phosphate-buffered saline (PBS), equilibrated in 30% sucrose overnight (for OE from adult mice, tissues were previously decalcified by overnight incubation in 0.2 M EDTA) and 30 µm coronal sections were cut on a cryostat. Sections were air-dried overnight, treated for 15 minutes with 0.5 % sodium dodecyl sulphate in PBS for antigen retrieval, incubated in blocking solution (2% normal goat serum, 0.2% Triton X-100 in PBS) for 90 minutes and incubated overnight at 4 ºC in primary antibodies diluted in blocking solution (anti-mBest2 was diluted 1:50). After rinses in 0.1 % Triton X-100 in PBS, sections were incubated with fluorophore-conjugated secondary antibodies in blocking solution for 2 hours at room temperature, washed and mounted with Vectashield (Vector Laboratories). The staining was analyzed with an Olympus Fluoview 300 confocal microscope (BX51WI). Primary antibodies were: mouse monoclonal anti-CNGA2 (provided by F. Müller and U. B. Kaupp, Forschungszentrum Jülich, Jülich, Germany) and goat anti-OMP (provided by F. Margolis, University of Maryland, Baltimore, MD, USA), used respectively at 1:200 and 1:500. Secondary antibodies were: Alexa 488-conjugated donkey anti-goat, Alexa-594 conjugated chicken anti-rabbit, Alexa 488-conjugated goat anti-rabbit, Alexa 594-conjugated goat anti-mouse diluted 1:200 (Molecular Probes). For competition experiments anti mBest2 antibody

was incubated with antigen for 2.5 hours at 37 ºC (2 µl of antibody for each antigen in 50 µl of PBS). After centrifugation at 13,000 g the supernatant was used for staining OE sections.

To generate the anti-mBest2 the C-terminal 431-bp fragment of mBest2 was amplified by PCR and ligated to GST sequence in the isopropyl-β-D-thiogalactoside (IPTG)-inducible pGEX vector (Amersham Pharmacia Biosciences, Piscataway, NJ) to generate a GST-mBest2 344-Cend fusion. Protein production was achieved in BL21 bacteria after a 0.5-mM IPTG induction for 2 h at 30 °C. GST-mBest2 was affinity-purified on GSH-Sepharose resin (Amersham Pharmacia Biosciences), following the manufacturer's protocols. Purified protein was used to immunize rabbits (the production of anti mBest2 antibody was performed by Giovanni Pascarella and Silvia Zucchelli in the lab of Prof. Stefano Gustincich at the Neurobiology Sector, SISSA, Trieste, Italy).

3.4 Cell culture and transfection

HEK-293 cells were grown in DMEM (Gibco, Italy) supplemented with 10% fetal bovine serum (Sigma, Italy), 100 IU/ml penicillin and 100 µg/ml streptomycin (Sigma) at 37°C in a humidified CO_2 incubator. Transfection of HEK-293 cells with mBest2 construct in pCMV-Sport6 (obtained by RZPD, Germany, GenBank accession no. BC019528) was performed by using FuGENE 6 reagent (Roche Diagnostics, Germany) according to the manufacturer's protocol. Cotransfection with EFGP in pGFP (Clontech, USA), at 1:5 ratio was used as reporter and only green fluorescent cells were used for experiments. After 36-48 hours after transfection the cells were plated on Petri dishes treated with poly-L-lysine (Sigma, Italy) to improve the adhesion and used for electrophysiological recording in the following 24-48 hours.

2.3 Dissociation of mouse olfactory sensory neurons

Olfactory sensory neurons were dissociated enzymatically from the olfactory epithelium of 1-2-months-old mice. The mice were sacrificed as described in 2.1 and then the turbinates were exposed by hemisection of the head along the septum. The olfactory epithelium was removed and transferred in 1 ml of zero-divalent mammalian Ringer's

solution (for composition of all solution, see 2.7.1). The tissue was incubated in 1 mM cystein and 1 U/ml papain (Sigma, Italy) for 20 minutes at room temperature. The reaction was stopped by adding 1 ml of Ringer's solution with 0.1 mg/ml BSA (bovine serum albumin), 200 µg/ ml leupeptin, and 0.025 mg/ml of DNaseI (all from Sigma, Italy). The olfactory epithelium was loosened by trituration with a flame polished pipette. After centrifugation (300 g for 5-7 min) the cells were resuspended in 1 ml of Ringer's solution and plated on Petri dishes (Nunc, USA) coated with poly-L-lysine and concanavalin A (Type V, Sigma, Italy).

2.4 The experimental setup for patch-clamp recording

Both experiments with HEK-293 cells and olfactory sensory neurons were performed on the same experimental setup. The preparation was visualized with an Olympus IX70 inverted microscope (Olympus, Japan) placed on an antivibration table (TMC, USA). A homemade Faraday cage provided adequate electrical shielding. All recordings were performed using an Axopatch 1-D amplifier controlled by Clampex 9.2 via a Digidata 1322A (all from Axon Instruments, USA). Data were sampled at 10 kHz and low- pass filtered at 4 kHz with a variable Filter VBF/8 (Kemo, UK). Patch-pipettes were made from borosilicate glass (outer diameter, OD, 1.65 mm; inner diameter, ID, 1.1 mm, WPI, USA) with a PP-830 puller (Narishige, Japan). They had a resistance of 2-4 MΩ, for HEK-293, and 7-10 MΩ for olfactory sensory neurons, when filled with standard intracellular solution. Pipettes were mounted in a pipette holder with an Ag/AgCl electrode for electrical recording. The holder movements were controlled by a mechanical micromanipulator for bigger displacements (MC-35A, Narishige, Japan) and by a hydraulic micromanipulator for smaller movements to approach the cells (MWO-3 Narishige, Japan). In experiments in which the bath concentration of Cl^- was changed, the bath was grounded through a 3 M KCl agar bridge connected with a Ag/AgCl reference electrode. Experiments were done at room temperature (20-24 ºC).

In inside-out recordings from excised patches from dendritic knob/cilia of OSNs leak currents in the respective Ca^{2+}-free solution were subtracted. Dose–response relations for the Ca^{2+}-activated Cl^- conductance were constructed by normalizing individual patches to their

maximal current in order to average data across patches. For whole-cell recordings from HEK-293 cells leak currents were not subtracted.

2.5 The perfusion system for patch-clamp recording

The perfusion system was based on that described by Hodgkin *et al.* (1985). Rapid exchange of the solution was achieved by translating the boundary between two flowing streams of solution in front of the cell attached to the patch pipette (or the excised patch in inside-out experiment). Streams of solution emerged from up to four glass tubes with ID of 0.90 mm (Vitro Dynamics, USA). Changes between these four streams were performed by Perfusion Fast-Step SF-77B (Warner Instrument Corp., USA) under control of Digidata 1322A (Axon Instruments, USA). Solution exchange was complete within less than 20 ms. The perfusion system was entirely gravity driven; the solutions were stored in 25-50 ml syringes and polyethylene tubes (ID 1.14 mm) were used for connection with the recording chamber. The flow of solution was controlled by solenoid valves that could be manually controlled (see Fig 2.1). The recording chamber was continuously bathed with mammalian Ringer solution while an aspiration tube, placed at the opposite site and connected with a trap bottle, controlled the level of solution in the recording chamber.

2.6 The experimental setup for eletroolfactogram recording (EOG)

The mouse was sacrificed as described in 2.1. The head was cut sagittaly to expose the medial surface of the olfactory turbinates. The method used to perform EOG recordings was very similar to that described by Zhao *et al.* (1998). The recording electrode was made with borosilicate glass (OD, 1.65 mm; ID, 1.1 mm, WPI, USA) pulled with a PP-830 puller (Narishige, Japan) to obtain a tip with 10-20 μm in diameter after fire polishing. The tip of the pipette was filled with Ringer's solution with 0.6 % agar and finally back filled with Ringer's solution. The pipette was mounted in a pipette holder with an Ag/AgCl for electrical recording and placed on the surface of the olfactory epithelium. The data were collected with an Axopatch 200B amplifier controlled by Clampex 9.2 via a Digidata 1322A (all from Axon Instruments, USA). The signals were recorded at a sampling rate of 1 kHz

and low-pass filtered at 25 Hz with a variable Filter VBF/8 (Kemo, UK). The ground electrode was located directly in the brain of the mouse.

Vapor-phase odorant stimuli were generated by placing 0.9 ml of odorant solution in a 10 ml glass test tube and capped with a rubber stopper. Two 20-gauge needles provided the input and output ports for the odorant-containing vapor above the solution. For stimulation, a 100-ms pulse of the odorant vapor at 8 psi was injected into the continuous stream of humidified air. The pulse was controlled by a Picospritzer solenoid-controlled valve (Intracel, UK). The odorant stimulus pathway was cleaned by air between each stimulus presentation. The minimum interval between two adjacent stimuli was at least one minute (see Fig 2.2).

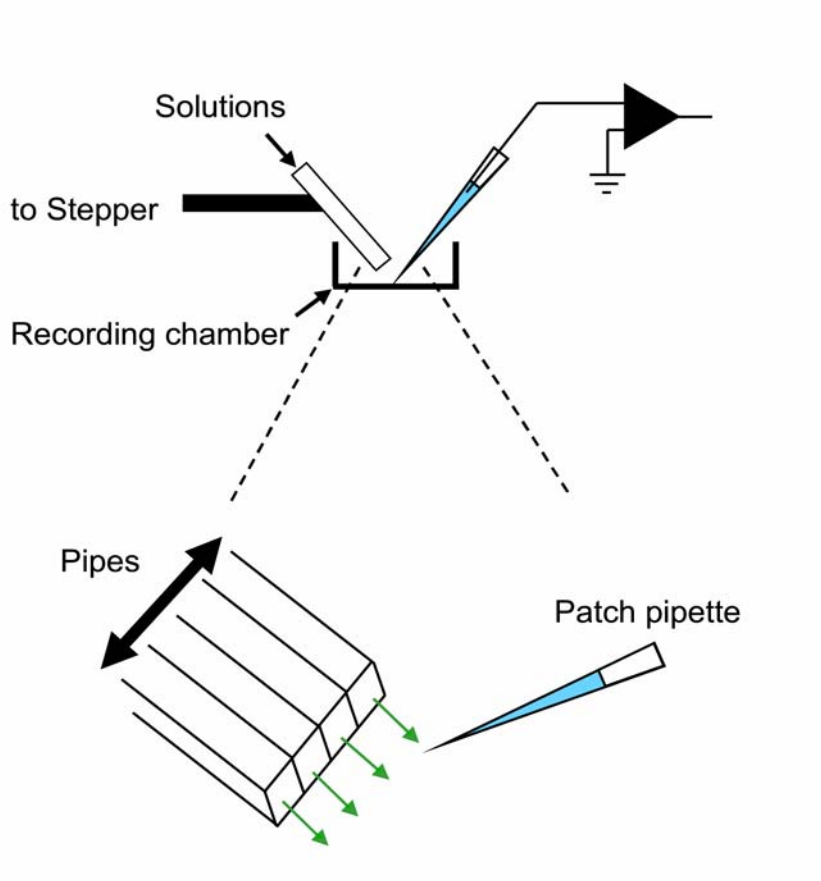

Figure 2.1 Perfusion system used for patch clamp recordings.
Four parallel streams of solutions, emerging from glass pipes, were delivered in front of the patch pipette. Stepping the pipes sideway, it was possible to change rapidly (less than 20 ms) the solution bathing the cells (or the excised patches) attached to the patch pipette.

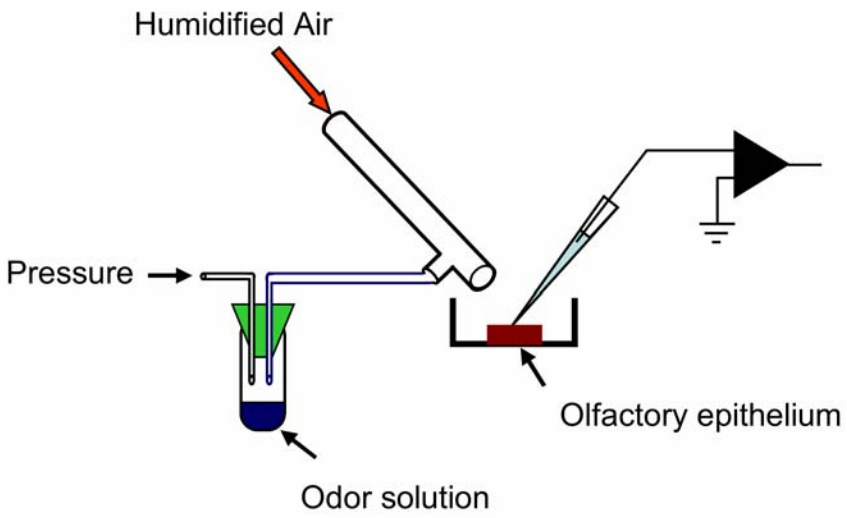

Figure 2.2 Setup for EOG recording.
Odorant solutions in the vapor phase were delivered to a semi-intact preparation of mouse olfactory epithelium in a continuous stream of humidified air.

2.7 Solutions

2.7.1 Ionic composition

Solutions with different ionic compositions were used for experiments. The compositions of solutions used for recording from olfactory sensory neurons are listed in the following table:

	NaCl (mM)	**KCl** (mM)	**LiCl** (mM)	**$CaCl_2$** (mM)	**$MgCl_2$** (mM)	**HEDTA** (mM)	**EDTA** (mM)
Ringer	140	5		1	1		
Zero-divalent Ringer	140	5					1
Li sol.			140			10	
Na sol.	140					10	
0.5 µM Ca^{2+}			140	1.242		10	
1.5 µM Ca^{2+}			140	3.209		10	
3.8 µM Ca^{2+}			140	5.866		10	
13 µM Ca^{2+}			140	8.263		10	
100 µM Ca^{2+}			140	9.98		10	

All solutions contained also 10 mM HEPES as pH buffer and all were adjusted to pH 7.2 with NMDG or HCl as appropriate. The Ringer solution contained also 10 mM D-

glucose and 1 mM sodium pyruvate. For permeability experiment the NaCl in "Na sol" was completely replaced with Na^+ salt of different anions. The program WinMAXC (C. Patton, Stanford University, Palo Alto, CA USA) was used to calculate free divalent concentrations in buffered solutions. The free Ca^{2+} concentrations in the HEDTA-buffered Ca solutions were determined by Fura-4F (Molecular Probes-Invitrogen, Italy) measurements by using an LS-50B luminescence spectrophotometer (PerkinElmer, USA).

The composition of solutions used for recording from HEK-293 are listed in the following table:

	NaCl (mM)	**KCl** (mM)	**CsCl** (mM)	**$CaCl_2$** (mM)	**$MgCl_2$** (mM)	**HEDTA** (mM)	**EGTA** (mM)
Ringer	140	5		2	1		
0 Ca^{2+} intra			140			5	
5 µM Ca^{2+} intra			140	2.5		5	
0.05 µM Ca^{2+}			140				1.25
0.1 µM Ca^{2+}			140	0.309			1.25
0.14 µM Ca^{2+}			140	1.1805			1.25
0.2 µM Ca^{2+}			140	1.41			1.25
0.25 µM Ca^{2+}			140	1.622			1.25
0.4 µM Ca^{2+}			140	1.968			1.25
4.5 µM Ca^{2+}			140	2.444			1.25

All solutions contained also 10 mM HEPES as pH buffer. The Ringer solution was adjusted to pH 7.4 or 7.2 with NaOH or HCl as appropriated. For permeability experiment the NaCl in Ringer was completely replaced with Na^+ salt of different anions. For solution with F^- all divalents were omitted to avoid precipitation of insoluble salts. All salts used were purchased from Sigma (Italy).

2.7.2 Odorant solutions

Odor solution for EOG experiments were made daily by dilution from 2.5 M stock solution in DMSO (dimethyl sulfoxide). The odors used were amylacetate, cineole and acetophenone (all purchased by Sigma, Italy).

2.7.3 Other solutions

Various blockers for mBest2 and native Ca^{2+}-activated Cl^- were used. Niflumic acid (NFA, Sigma, Italy) was dissolved in DMSO at 200 mM, stored at + 4 ºC and diluted in saline solution to the final concentration. 4-acetamido-4'-isothiocyanato-stilben-2,2'-disulfonate (SITS, Sigma, Italy) was directly dissolved in saline solution up to 5 mM. 4,4'-diisothiocyanatostilbene-2,2'-disulfonic acid (DIDS, Sigma or Molecular Probes) was directly dissolved in saline solution up to 200 µM. 5-Nitro-2-(3-phenylpropylamino)benzoic acid (NPPB, Tocris, UK) was dissolved in DMSO at 83 mM , stored at -20 ºC and diluted in Ringer's solution to 100 µM. To activate the CNG channel in inside-out excised patches from olfactory sensory neurons 100 µM of cAMP or cGMP were directly added to "Li sol" or "Na sol".

2.8 Data analysis

Data analysis and figures were made with Igor software (Wavemetrics, USA). Data are given as mean ± SEM.

2.9 mBest2$^{-/-}$ null mouse line

The mBest2 null mouse line was purchased from Deltagen (USA). The targeting vector was constructed using 0.8-kb (5') and 2.9-kb (3') mouse Best2 genomic DNA fragments as homology arms. The two arms flanked a promoterless lacZ and a neomycin-resistant gene cassette (lacZ-neo). Homologous recombination in mouse embryonic stem cells resulted in the insertion of the lacZ-neo cassette, replacing a region spanning exon 1 through a part of exon 3 of the mouse Best2 locus. Germ-line–transmitting chimeric mice generated from the targeted embryonic stem cells were bred with C57BL/6 mice to produce mBest2$^{+/-}$ mice. Intercrossing of heterozygous mice generated Best2$^{-/-}$ mice.

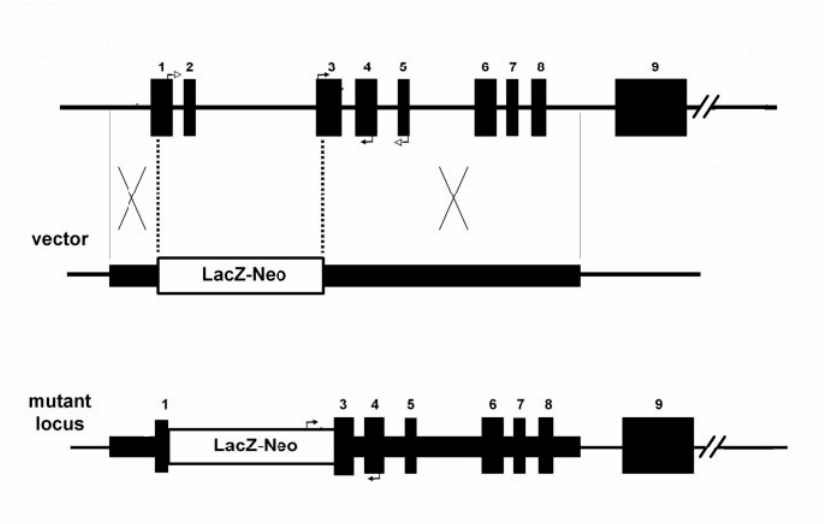

Figure 2.3 Targeted disruption of the mouse Best2 gene.
Schematic representation of wild-type locus, targeting vector, and mutant locus. Thick lines: fragments used for constructing the targeting vector 5' and 3' arms. Thin lines: genomic DNA or vector backbone sequence. Numbered solid boxes: Best2 exons. Labeled boxes: the LacZ and neor expression cassette.

3. Results

3.1 Localization of mBest2

The olfactory sensory transduction occurs in specialized cilia extended from the knobs of OSNs on the surface of the olfactory epithelium (OE). To examine the subcellular localization of mBest2 in OSNs we performed immunohistochemistry experiments on OE cryosection from adult and P15 mice using the anti-mBest2 polyclonal antibody. We found a homogenous staining on the surface of OE (Fig. 3.1 A-C) without any remarkable difference among zones of OE both in adult and in P15 mice (not shown). The staining was abolished when the antibody was pre-incubated with the recombinant protein proving signal specificity (Fig. 3.2). Specific antibodies against OMP, a typical marker of mature OSNs (Keller & Margolis, 1975), and the olfactory CNG channel subunit CNGA2 (Meyer *et al*., 2000), known to be present in the cilia, were used as cellular or subcellular markers. Double-staining for mBest2 and OMP showed that mBest2 is expressed in mature OSNs (Fig. 3.1 D-F). Double-staining experiments for mBest2 and CNGA2 proved that mBest2 was present on the luminal surface of the OE (Fig. 3.3 A-C) restricted to the cilia of OSNs, where it colocalized with CNGA2 (higher magnification, Fig. 3.3 D-F). Therefore, mBest2 appears to be expressed at the site of olfactory transduction.

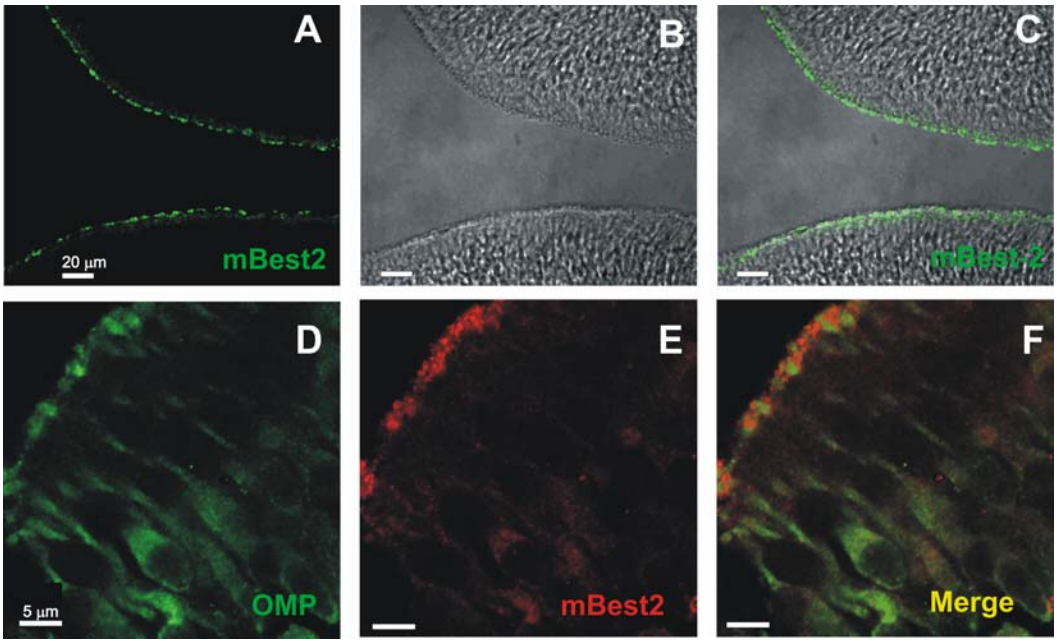

Figure 3.1 Localization of mBest2 on the sensory cilia of OSNs.
Olfactory epithelium (bright field in B) labeled with affinity-purified anti-mBest2 polyclonal antibody (green) is shown as the fluorescence signal (A) or a digital addition of the fluorescence and bright-field images (C). mBest2 is located at the luminal surface of the sensory epithelium. Double staining for mBest2 (red) and OMP (green). mBest2 was located at the end of dendrites of mature OSNs (D-F).

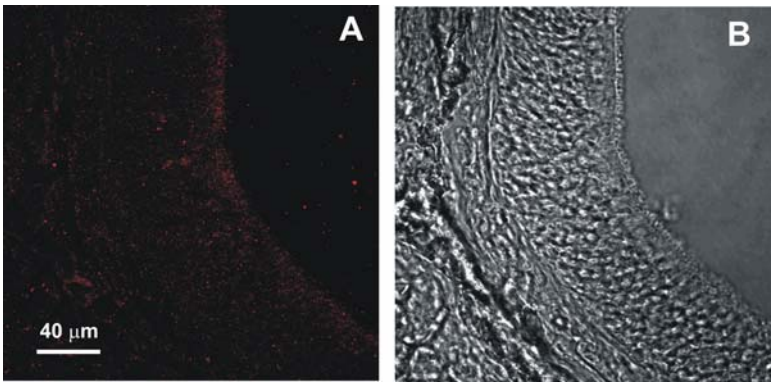

Figure 3.2 Control of specificity of anti-mBest2 antibody.
Olfactory epithelium was stained with anti-mBest2 antibody previously incubated with C-terminus of mBest2 protein used for antibody production. The absence of the staining suggests the specificity of anti-mBest2 antibody.

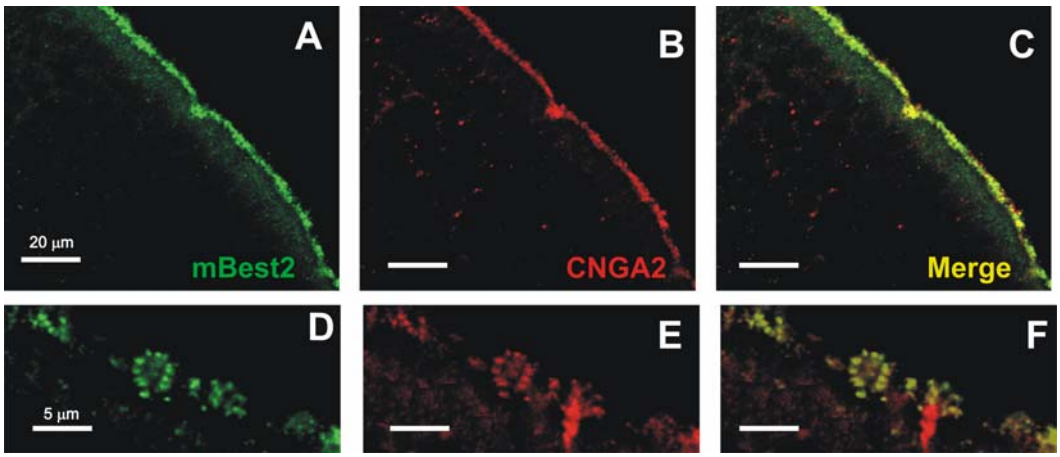

Figure 3.3 Localization of mBest2 on the sensory cilia of OSNs.
Double staining for mBest2 (A) and CNGA2 (B). Label is shown as the red fluorescence channel digitally combined with the green channel. mBest2 and CNGA2 colocalized at the luminal surface of OE (C). In D-F higher magnification of the OE as in A-C. mBest2 was expressed on cilia of OSNs and colocalized with CNGA2.

3.2 Properties of mBest2

The localization of mBest2 strongly suggests that it could be involved in olfactory transduction. Therefore electrophysiological properties of mBest2 after heterologous expression in HEK-293 cells were measured and compared with those of native Ca^{2+}-activated Cl^- channels of OSNs. Many attempts have been done to record mBest2 current in inside-out configuration but no detectable Ca^{2+}-activated Cl^- currents were measured in mBest2-transfected cells. Tsunenari *et al*. (2006) reported that Ca^{2+}-activated Cl^- currents induced by heterologous expression of hBest4 could be detected in excised inside-out patches. They suggest, though, that measurements in excised patches could be obtained only because of the particularly large Cl^- current induced by heterologous expression of hBest4 when compared with the other bestrophins. Therefore the functional properties of mBest2 have been determined in the whole-cell configuration.

mBest2 was expressed in HEK-293 cells by transient transfection. Cells were subjected to whole-cell patch clamp using solutions that either eliminated cation currents (intracellular solution contained Cs^+ to block endogenous K^+ currents) or set the Nernst potentials of cation currents and Cl^- currents at very different values. The calculated

reversal potential for Cl^- (E_{Cl}) was -1 mV. Free $[Ca^{2+}]_i$ was buffered to various values using EGTA or HEDTA. The holding potential was 0 mV and for most experiments the voltage was stepped from -100 mV to +100 mV with 20 mV increments for 200 ms (Fig 3.4 A upper panel).

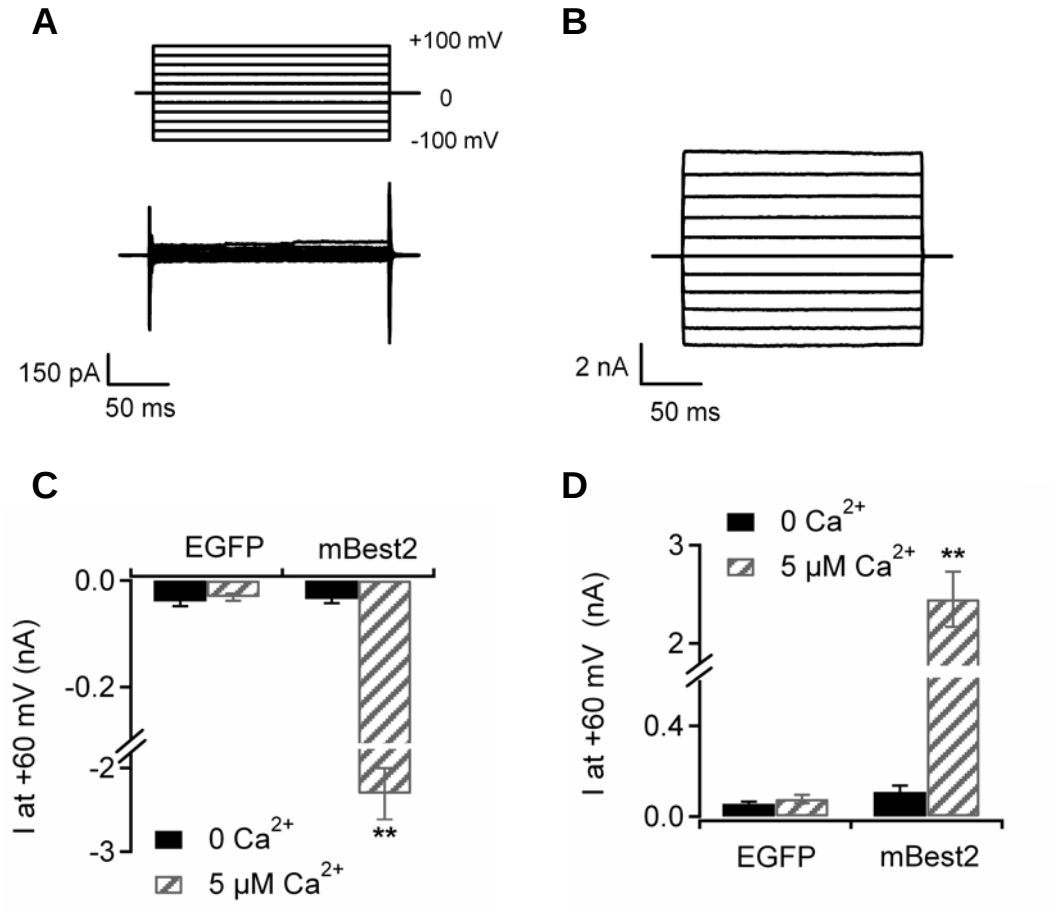

Figure 3.4 mBest2 generates a Ca^{2+}-dependent current in HEK-293 cells.
HEK-293 cells transfected with mBest2 and EGFP. Recordings in whole-cell voltage clamp were made with a pipette solution containing nominally 0 free $[Ca^{2+}]_i$ (< 10 nM, A) or 5 µM of $[Ca^{2+}]_i$ (B). The voltage protocol is shown above A. Mean steady-state current amplitudes measured at -60 mV (C) and at +60 mV (D) in cell transfected with EGFP alone or with mBest2 and EGFP with pipette solution containing either 0 or 5 µM of free $[Ca^{2+}]_i$ (n=8-26).

3.2.1 Calcium sensitivity

Fig 3.4 A/B shows representative current recordings obtained in cells transfected with mBest2 with nominally 0 $[Ca^{2+}]_i$ (< 10 nM) or with a solution containing 5 µM of $[Ca^{2+}]_i$ showing a robust induction of current after adding of intracellular Ca^{2+}. The analysis of different cells shows that in HEK-293 cells transfected only with EGFP currents were consistently small regardless of free $[Ca^{2+}]_i$. Currents at -60 mV were -39 ± 8 pA (n=8) with nominally 0 $[Ca^{2+}]_i$ and -31 ± 7 pA with 5 µM of $[Ca^{2+}]_i$ (n=8); at +60 mV the currents were 57 ± 10 pA (n=8) with nominally 0 $[Ca^{2+}]_i$ and 78 ± 19 pA with 5 µM of $[Ca^{2+}]_i$ (n=8). In contrast, the cells transfected with mBest2 showed a big Ca^{2+}-activated current. Indeed, the currents at -60 mV were -35 ± 8 pA (n=12) with nominally 0 $[Ca^{2+}]_i$ but -2308 ± 309 pA with 5 µM of $[Ca^{2+}]_i$ (n=26); at +60 mV the currents were 108 ± 28 pA (n=8) with nominally 0 $[Ca^{2+}]_i$ and 2444 ± 19 pA with 5 µM of $[Ca^{2+}]_i$ (n=8, Fig 3.4 C-D).

The Ca^{2+}-activated current was voltage and time independent and its amplitude remained stable for long time after that whole cell was obtained (until 10 min). The measured reversal potential was, after correction for liquid junction potential, -2.4 ± 0.4 mV, a value in good accordance with the calculated E_{Cl} of -1 mV. The I-V relation is almost linear with a slight outward rectification: the ratio of the current at +50 mV and at -50 mV was 1.24 ± 0.04 (n=45).

Dose response relations were obtained activating the current with intracellular EGTA buffered solutions with various free $[Ca^{2+}]_i$. Currents from different cells were normalized to the cell capacitance measured with the method described by Lindau & Neher (1988) and dose response relations were fitted with the Hill equation (eq 1.1). At -50 mV the $K_{1/2}$ was 0.4 µM and *n* was 6.6, in good accordance with previous data available on mBest2 (Qu *et al.*, 2004), see Fig 3.5).

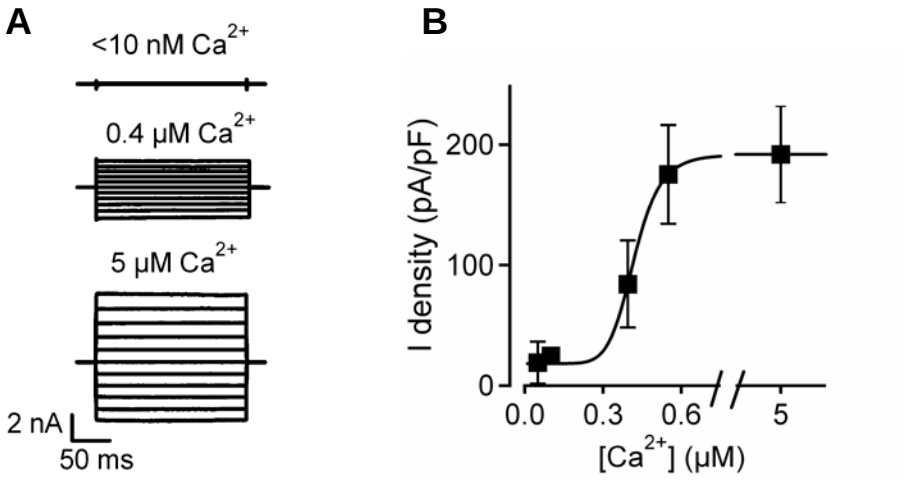

Figure 3.5 Dependence of mBest2 on $[Ca^{2+}]_i$.
Representative whole-cell recording traces from mBest2 transfected cells with various intracellular free $[Ca^{2+}]_i$ (A). The amplitude of average density currents at -50 mV is plotted versus $[Ca^{2+}]_i$ and fitted with the Hill equation with $K_{1/2}$= 0.4 µM and n= 6.6 (n=5-12 cells, B).

3.2.2 Anion selectivity

To confirm that Ca^{2+}-induced current in mBest2-transfected cells was carried by Cl^-, all NaCl in the extracellular solution was replaced with sodium gluconate, an anion that is impermeable in most Cl^- channels ($[Cl^-]_o$= 11 mM, Frings *et al*., 2000). Fig 3.6 A-C shows that this ionic substitution caused a big shift in reversal potential toward a more positive value in accordance with Nernst equation. The average of reversal potential with gluconate as the main extracellular anion was 53 ± 10 mV (n=11) slightly smaller than the calculated E_{Cl} (~65 mV). The not perfect Nernstian behavior could be due to a slight permeation of gluconate or to the presence in HEK-293 of a small endogenous non-selective cation current that interfered with the measurement of mBest2 currents.

The ability to select among various ions is a key feature of ion channels and different channels exhibit very different kinds of selectivity. Therefore anion substitutions were used to investigate the selectivity of mBest2 current. Chloride ions outside the cells were replaced

and the permeability ratios relative to chloride were calculated using the Goldman-Hodgkin-Katz equation with the following relation:

$$P_X / P_{Cl} = \frac{[Cl^-]_i}{[X]_o \exp(\Delta E_{rev} F / RT)} - \frac{[Cl^-]_o}{[X]_o}$$

where $[Cl^-]_i$ is the concentration of chloride in the pipette, $[Cl^-]_o$, $[X^-]_o$ are the concentrations of anions after ionic substitution, ΔE_{rev} is the shift in reversal potential, T is the absolute temperature, F is the Faraday constant (~96,4685 C mol^{-1}) and R is the gas constant (~ 8.31 J K^{-1} mol^{-1}).

mBest2 current exhibited the following permeability sequence:

$SCN^- > I^- > NO_3^- > Br^- > Cl^- > F^- > MeS^-$ (Methylsulfate)

and the permeability ratios were:

2.62: 1.79: 1.4: 1.15: 1: 0.56: 0.32

showing that mBest2 are relatively non-selective anion channels as reported for many native Ca^{2+}-activated Cl^- currents (Hartzell et al., 2005a). A difference to voltage-gated K^+ channels (that exhibit >100-fold selectivity between ions having radii that differ by less than 0.5 Å) is that mBest2 channels change their ion selectivity only ~3-fold between ions that differ in radius by ~1.2 Å (Fig. 3.7). Furthermore, mBest2 differs from K^+ channels in that there is no peak in the relationship between ionic radius and permeability. Rather, the relationship is monotonic with larger anions being more permeable than smaller anions.

Permeability ratios provide an estimate of the difference between the hydration energy in water and the solvation energy provided by the channel. Because there is no current at the reversal potential, this measurement is an indication of the ability of the ion to enter the channel. The process of moving from the aqueous environment to the channel pore involves exchanging the energy of stabilization of the ion in bulk water for the energy of stabilization of the ion by its interaction with the channel. Because ions are stabilized in bulk water by shells of water molecules surrounding the ion, stabilization of the ion in water can be characterized by its hydration energy (G_{hyd}). Stabilization of the ion by interaction with the pore can involve solvation of the ion by part of the channel protein, as in the case of the KcsA channel or other mechanisms (Dawson *et al.*, 1999; Smith *et al.*, 1999). The ease of ion permeation is determined by the difference between G_{hyd} in bulk water and the energy of stabilization (or solvation) by the channel. The smaller the difference, the more easily an ion enters the channel. Generally, larger ions, that have a lower effective charge density (if the

charge is uniformly distributed in the ion) have lower hydration energies. Thus larger ions are relatively more permeant than smaller ions. Permeability ratios, however, do not measure the ability of the ion to traverse the channel, which is measured by the conductance or the slope of the current-voltage relationship. To some extent, the conductance of an ion through the channel reflects how rapidly it dissociates from the ligands that stabilize the permeant ion in the channel. Figure 3.8 shows the relative conductance of anions through mBest2 channel. As reported for other Ca^{2+}-activated Cl^- channel (Hartzell *et al.*, 2005a; Qu & Hartzell, 2000) the relative permeability and conductance sequences may be different. The ease with which an ion enters the pore (permeability) depends on the ease with which the anion loses its bound water. However, the ease with which an ion passes through the channel (conductance) exhibits a bell-shaped relationship to hydration energy. These relationships suggest that anions with large hydration energies are poorly conductive because they do not enter the channel well (as shown by the P_X/P_{Cl} versus ΔG_{hyd} plots), whereas ions that have small hydration energies are poorly conductive (as shown by the G_X/G_{Cl} versus ΔG_{hyd} plots) because they become lodged in the pore, even though they enter the channel easily.

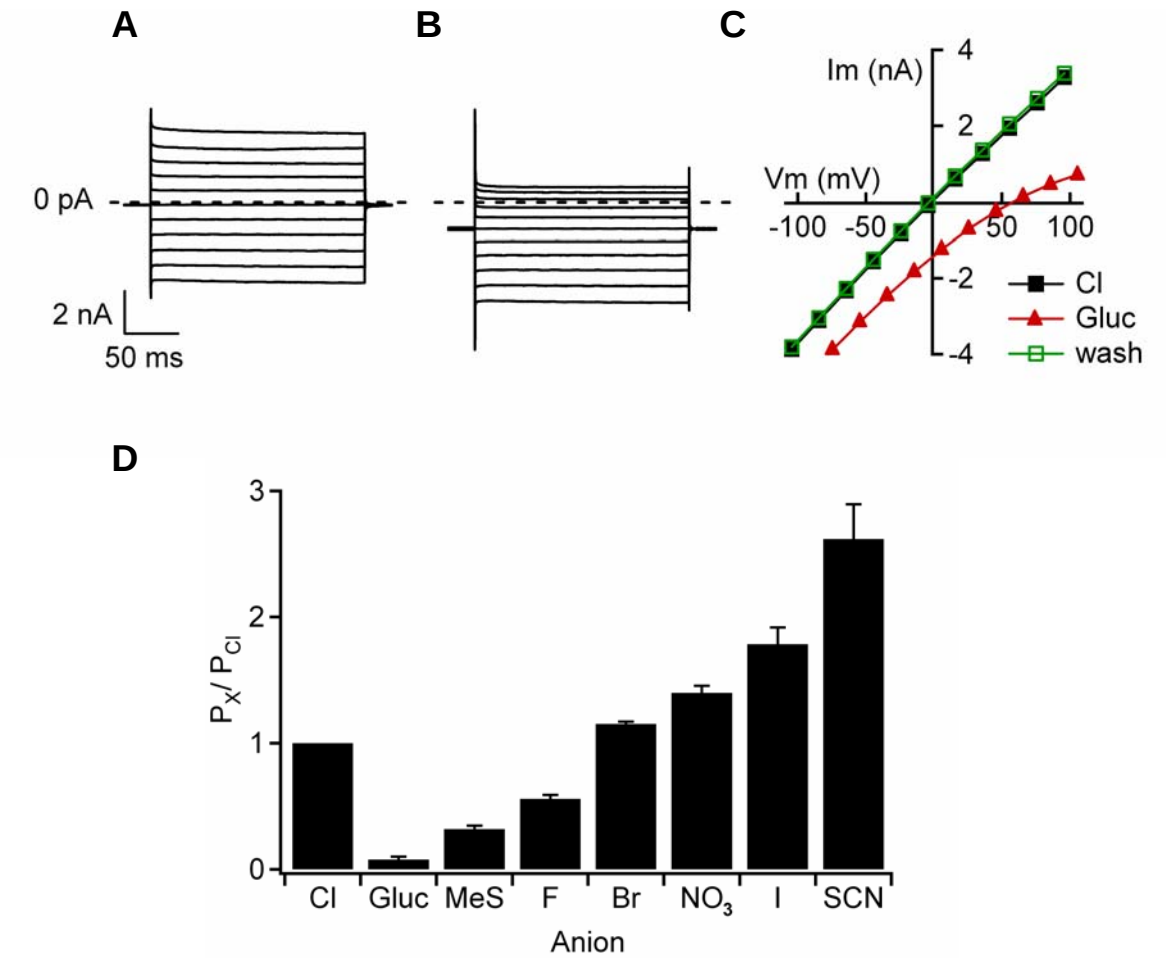

Figure 3.6 Ionic selectivity of mBest2 currents.
Currents in mBest2-transfected HEK-293 cells were activated by 5 µM of free $[Ca^{2+}]_i$. Typical recording with symmetrical Cl^- solution in (A) or after replacing extracellular NaCl with Na-gluconate in (B). The IV relationship from the experiment in (A-B) show the shift in E_{rev} (C) indicating that mBest2 current is carried by Cl^-. Relative permeability ratios (P_X/P_{Cl}) of mBest2 were calculated with the Goldman-Hodgkin-Katz equation from measured shifts of E_{rev} (D).

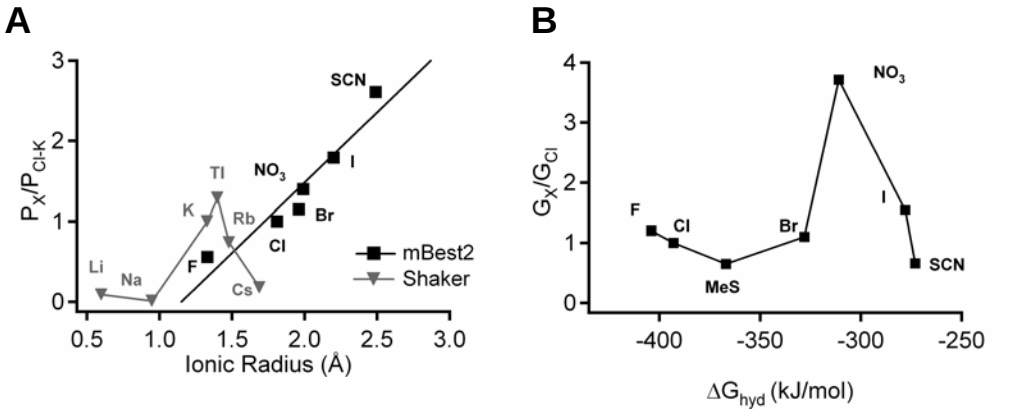

Figure 3.7 Selectivity and permeation through mBest2 channel.
Relative permeability of anions through mBest2 as function of ionic radius compared with the permeability of cations through the Shaker K^+ channel.

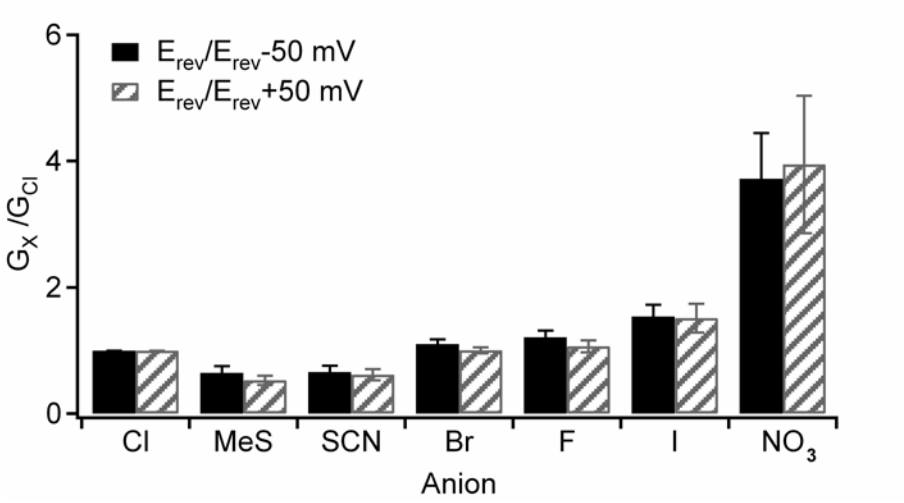

Figure 3.8 Relative conductance of anions through mBest2 channel.
Conductance was measured as the slope of the current-voltage relationship calculated between E_{rev} and E_{rev} +50 mV (or E_{rev} -50 mV) in symmetrical Cl^- solution or in bionic conditions after substitution of extracellular NaCl with solutions containing other anions as sodium salts.

3.2.3 Pharmacological properties

Specific blockers for calcium-activated chloride channels with high binding affinity are not available. Most blockers require high concentrations to completely block Cl^- currents and may have undesirable side effects. Several compounds have been used to characterize the pharmacological profile of mBest2 current. First I will describe the results of application of the drugs to the extracellular side.

The most common blocker for native Ca^{2+}-activated Cl^- currents is niflumic acid (NFA). It blocks Ca^{2+}-activated Cl^- currents in Xenopus oocyte in the 10 μM range (Qu & Hartzell, 2001) and at 300-500 μM the Ca^{2+}-activated Cl^- currents of OSNs (Lowe & Gold, 1993b; Reisert & Matthews, 1998; Reisert *et al.*, 2005; Boccaccio & Menini, 2007; Kleene, 1993).

Figure 3.9 A shows the effect of application of 1 mM of NFA on mBest2 current. NFA rapidly blocked the Ca^{2+}-induced current measured at -50 mV and, after NFA removal, the current slowly returned toward its initial value. The block by NFA did not show a voltage-dependence and, on average, the extracellular application of 1 mM NFA blocked 75 ± 5 % of the Ca^{2+}-activated current at -50 mV and 77 ± 4 %.at +50 mV (n=15; Fig. 3.9 B).

The study of the dose-dependence of the extracellular blocking effect of NFA in the range from 10 μM to 1 mM revealed a more complex phenomenon. Current blockage by NFA developed with time and reached almost the same steady-state blockage level at every tested concentration, whereas the time necessary to reach steady state was longer as the NFA concentration was decreased. This behavior has been observed both at -50 mV and +50 mV (Fig 3.9 C-E). This particular behavior could suggest that NFA, after crossing the plasma membrane, blocks mBest2 by interaction with an intracellular binding site. However the precise mechanism of NFA blockage is not clarified at the molecular level yet.

Two other structurally-related blockers were tested: 4-acetamido-4'-isothiocyanato-stilben-2,2'-disulfonate (SITS) and 4,4'-diisothiocyanatostilbene-2,2'- disulfonic acid (DIDS). SITS is a well characterized blocker of Ca^{2+}-activated Cl^- current involved in olfactory transduction at 2-5 mM concentration (Lowe & Gold, 1993b; Kurahashi & Yau, 1993 ;Kurahashi & Menini, 1997). DIDS is able to block the Ca^{2+}-activated Cl^- currents in Xenopus oocytes with a $K_{1/2}$ of 48 μM at +100 mV and previous report showed that it also blocks mBest2-induced currents (Qu *et al.*, 2004; Qu & Hartzell, 2001). Figure 3.10 A

shows the effect of application of 2 mM of SITS on mBest2 currents. SITS rapidly blocked the Ca^{2+}-induced current measured at -50 mV and, after its removal, the current rapidly returned toward its initial value. The extracellular SITS blockage was measured in the range from 10 µM to 5 mM and it was rapid and reversible. A fit of the data with the Hill equation gave a $K_{1/2}$ of 0.4 mM and a Hill coefficient of 0.7 (Fig. 3.10 B). Similar results were obtained with DIDS. mBest2 showed a higher sensitivity to DIDS with a $K_{1/2}$ of 44 µM and a Hill's coefficient of 0.7.

Finally, 5-Nitro-2-(3-phenylpropylamino)benzoic acid (NPPB) was tested. NPPB is reported to block the Ca^{2+}-activated Cl^- currents in Xenopus oocyte with a $K_{1/2}$ of 22-68 µM (Wu & Hanill, 1992). The application of 100 µM was able to rapidly blocked the mBest2-induced current both at -50 mV and +50 mV (Fig 3.12). After the removing of the drug the current took a long time to recover to the initial value (up to 5 min). On average the extracellular application of 100 µM NPPB blocked 87 ± 13 % of the Ca^{2+}-activated current at -50 mV and 86 ± 13 % at +50 mV (n= 5, Fig. 3.12 B).

The intracellular blocking action of some compounds has been also tested by adding them in the patch pipette. Figure 3.13 A shows representative current recordings of mBest2 activated with 5 µM $[Ca^{2+}]_i$ in control condition, with 2 mM SITS or with 300 µM NFA in pipette. Amplitude of currents recorded with SITS in the pipette did not shown a significant reduction in comparison with recordings in control condition, whereas the addition of NFA caused a big reduction of mBest2-mediated currents. Indeed at -50 mV the mean current was -2499 ± 362 pA in control solution, -2314 ± 251 pA but only -168 ± 30 pA with NFA (n=6-7, Fig 3.13 D/E). The same effect was observed also at +50 mV.

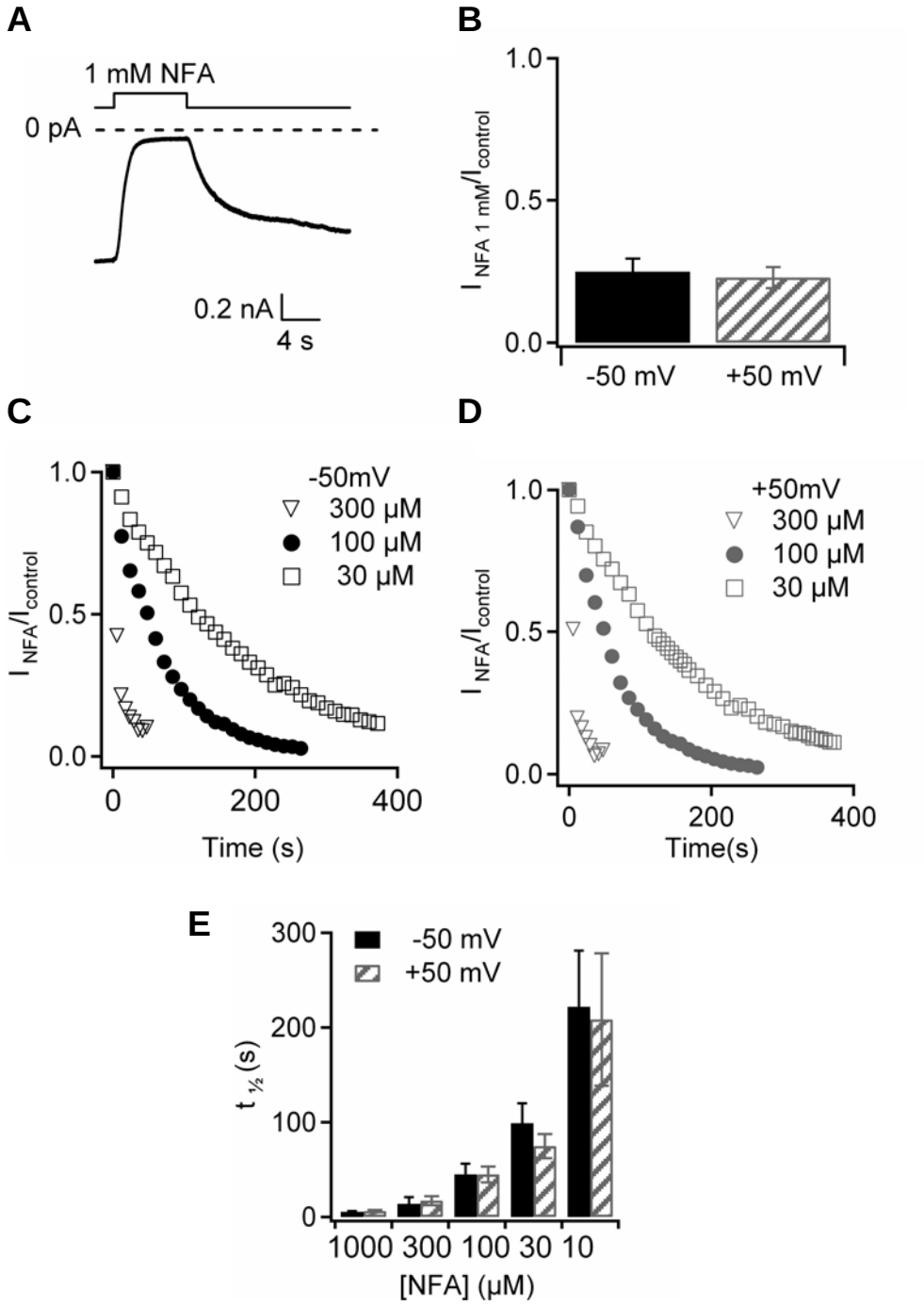

Figure 3.9 Extracellular blockage by NFA on mBest2 currents.
Current in mBest2-transfected HEK-293 cells were activated by 5 µM of free $[Ca^{2+}]_i$.1 mM of NFA was bath-applied for the time indicated (A). Mean ratios between the amplitude of the currents in control condition and after application of 1 mM of NFA at -50 mV and +50 mV (n= 15, B). Time course of blockage of mBest2 currents by various NFA concentrations at -50 mV (C) and at +50 mV (D). Time necessary to block half of the current ($t_{½}$) at various NFA concentration (n=2-5, E).

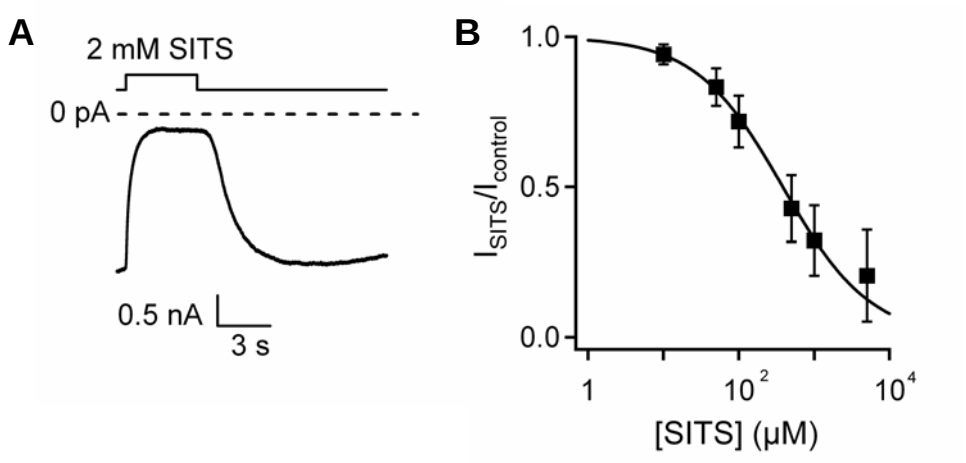

Figure 3.10 Extracellular blockage by SITS on mBest2 currents.
mBest2-expressing HEK-293 cells were voltage clamped at -50 mV with 5 µM of free $[Ca^{2+}]_i$. 2 mM of SITS were bath-applied for the time indicated (A). Sensitivity of mBest2 currents to extracellular SITS. Amplitude of the currents in the presence of various SITS concentrations normalized to control currents was plotted versus SITS concentration and fitted with the Hill equation with $K_{1/2}$= 380 µM and n= 0.7 (n= 5-9 cells).

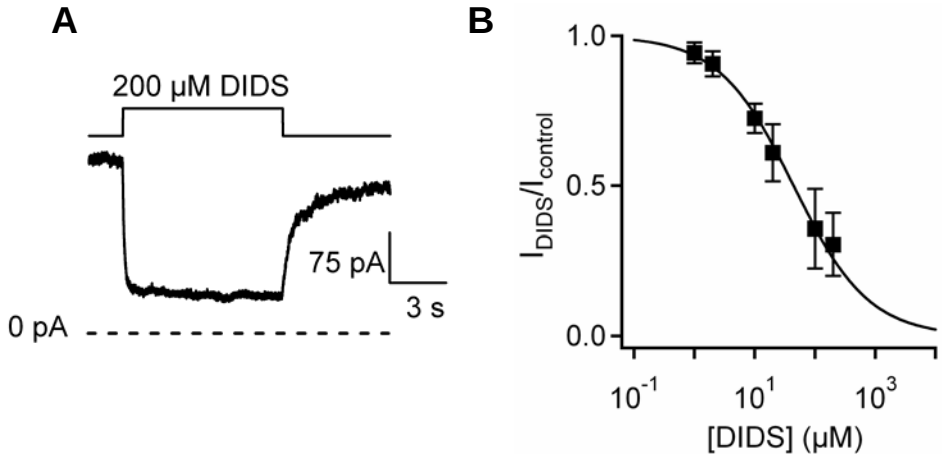

Figure 3.11 Extracellular blockage by DIDS on mBest2 currents.
mBest2-expressing HEK-293 cells were voltage clamped at -50 mV with 5 µM of free $[Ca^{2+}]_i$. 200 µM of DIDS were bath-applied for the time indicated (A). Sensitivity of mBest2 currents to extracellular DIDS. Amplitude of the currents in the presence of various DIDS concentrations normalized to control currents was plotted versus DIDS concentration and fitted with the Hill equation with $K_{1/2}$= 44 µM and n= 0.7 (n= 5-9 cells).

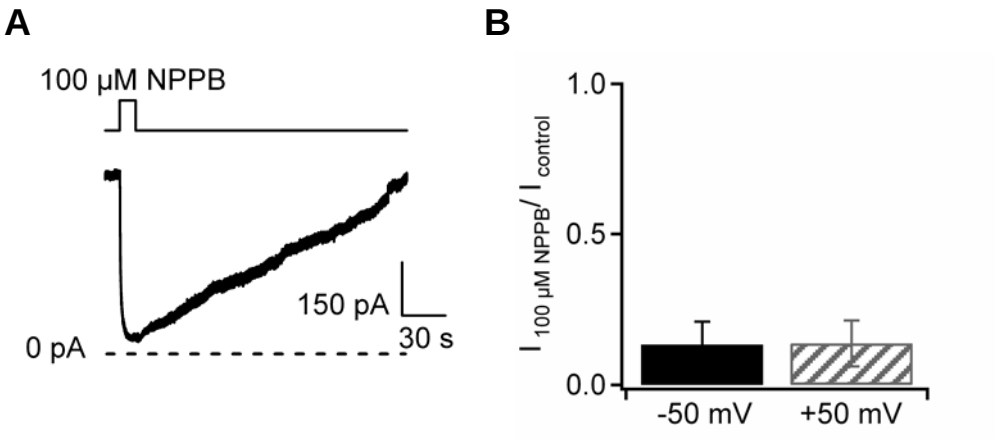

Figure 3.12 Extracellular blockage by NPPB on mBest2 currents.
mBest2-expressing HEK-293 cells were voltage clamped at -50 mV with 5 µM of free $[Ca^{2+}]_i$.1 mM of NPPB was bath-applied for the time indicated (A). Mean ratios between the amplitude of the currents in control condition and after application of 1 mM of NPPB at -50 mV and +50 mV (n= 5, B).

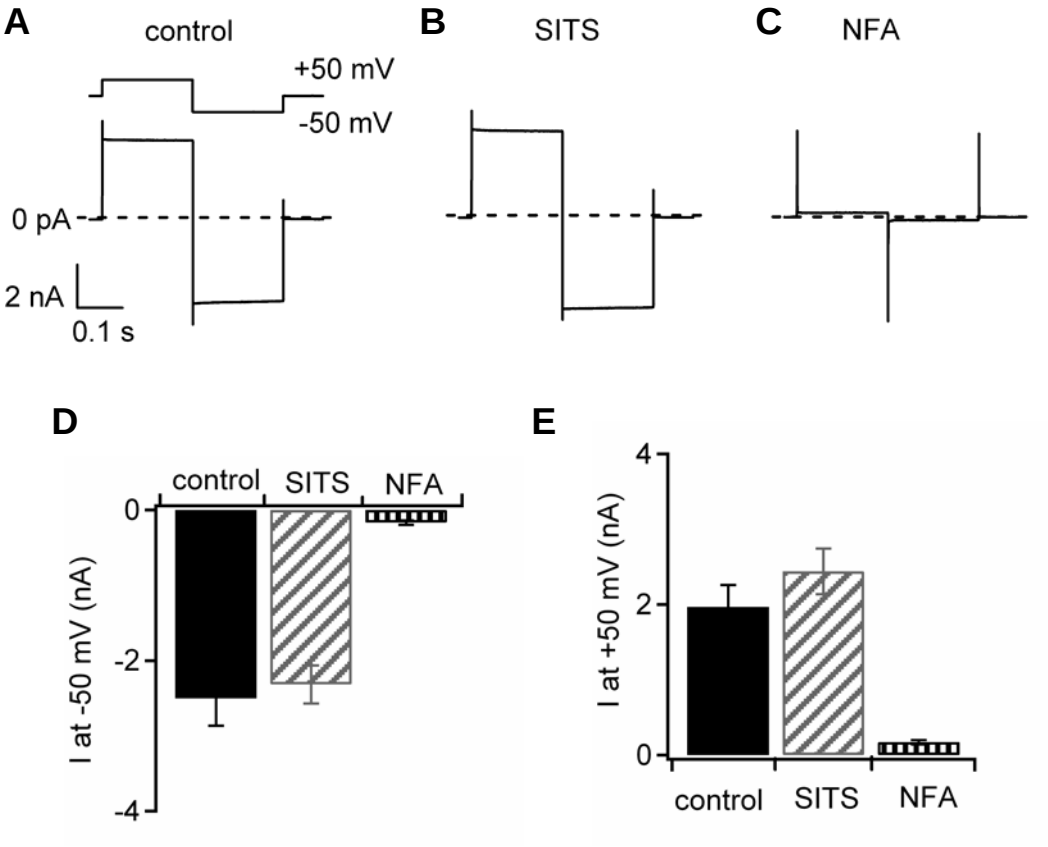

Figure 3.13 Intracellular blockage by NFA and SITS on mBest2 currents.
Representative mBest2 current traces activated by 5 μM of free $[Ca^{2+}]_i$ in control condition (A), with 2 mM SITS in pipette (B) or 300 μM NFA (C). Mean steady state current amplitudes measured at -50 mV (D) and at +50 mV (E) in control condition and with blockers in the pipette solution (n=6-7).

3.3 Properties of the native calcium-activated chloride channel

The electrophysiological properties of Ca^{2+}-activated Cl^- channels involved in olfactory transduction were studied in acutely dissociated mouse OSNs using inside-out patches excised from dendritic knob /cilia. By this method it is possible to isolate the channels responsible for odorant-induced currents and selectively activate them by bath application of Ca^{2+} and cyclic nucleotide.

Figure 3.14 D shows the typical recordings obtained from an inside-out patch using symmetrical NaCl, divalent-free solution at holding potentials of -50 mV and +50 mV. The bath application of cAMP rapidly activated the CNG channel generating an inward non-

inactivating current at -50 mV and an outward current at +50 mV. Similarly the bath application of a solution containing 100 µM of free Ca^{2+} activated the Cl^- channel. In this recording condition the CNG and Ca^{2+}-activated Cl^- currents had similar amplitude. Indeed, at -50 mV the CNG current was -71 ± 28 pA (n=19) and the Cl^- current was -52 ± 15 pA (n=29, Fig 3.14 E).

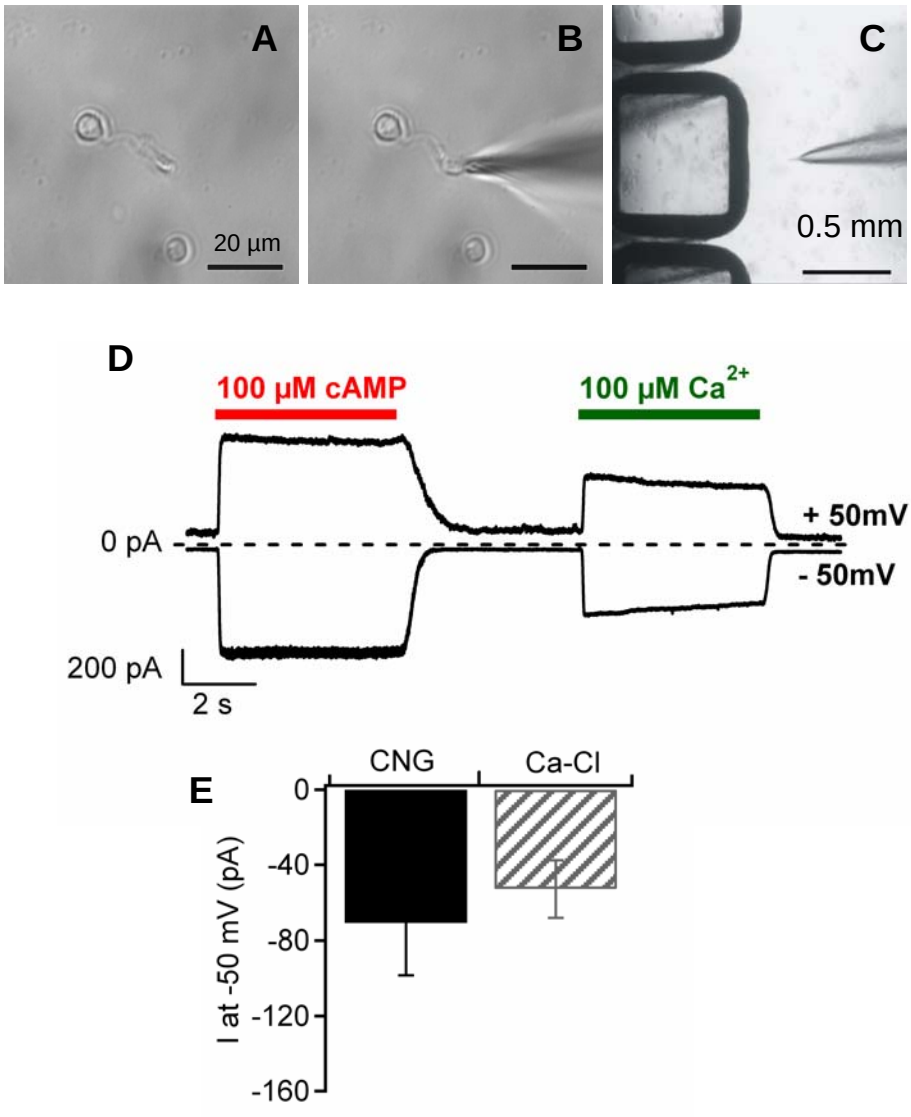

Figure 3.14 Recordings of ion channels involved in olfactory transduction.
Acutely dissociated mouse OSNs were used to record ion channels responsible for odorant-induced receptor current using inside-out patches excised from dendritic knob and cilia (A-C). Representative recording of channel activity: cAMP activated the CNG channel whereas Ca^{2+} gated the Cl^- channel (D). Mean amplitude of peak currents mediated by transduction ion channels (n=19-29, E).

3.3.1 Calcium sensitivity

The Cl^- channel in excised inside-out patches from OSNs showed a reversible reduction of the current with a time course of some seconds after activation by Ca^{2+}. This reduction was present at every [Ca^{2+}] tested and it can be rescued by removing of Ca^{2+} for at least 1 minute. This effect was observed in previous studies in rat (Reisert *et al*., 2003) and in mouse (Reisert *et al*., 2005) whereas another report in rat by Hallani *et al*. (1998) did not found any inactivation. In contrast, recordings from amphibian OSNs with the excised cilium technique did not show any Cl^- current inactivation (Kleene, 1993; Kleene & Gesteland, 1991). These differences could be due to species-specific properties of the channel or to the loss of some component in inside out patches from rodent OSNs that is preserved in the frog excised cilium.

The dose response to $[Ca^{2+}]_i$ was determined by application on the same patch of different solutions with various free $[Ca^{2+}]_i$ for 3 s at a holding potential of -50 mV or + 50 mV using symmetrical LiCl solutions (Fig 3.15 A-B). Li^+ was used to disable the Na^+/Ca^{2+} exchanger present in cilia of OSN (Reisert *et al.*, 2003; Reisert & Matthews, 1998), so that the Ca^{2+} concentration near the membrane patch could be properly controlled by the bath solution. The peak normalized currents were plotted versus [Ca^{2+}] and fitted with the Hill equation (Fig 3.15 C-D). At -50 mV the $K_{1/2}$ was 4.7 μM and *n* was 2.5, whereas at +50 mV $K_{1/2}$ was 2.6 μM and *n* was 3.2.

The slight decrease in $K_{1/2}$ at positive voltages could in principle reflect a voltage sensitivity in the Ca^{2+} binding step or the gating step, while the Hill coefficient suggest that at least 3 Ca^{2+} ions are necessary to gate the channel.

The IV relationship was measured using a ramp protocol from -100 mV to +100 mV and back with a frequency of 1 mV/ms. To avoid possible bias due to Ca^{2+}-dependent inactivation the ramp protocol was always delivered after 500 ms from application of the Ca^{2+} containing solution. In symmetrical Cl^- solutions the channel showed a slight inward rectification, indeed the ratio of the current at +50 mV and at -50 mV was 0.61 ± 0.08 (n=9, Fig 3.16).

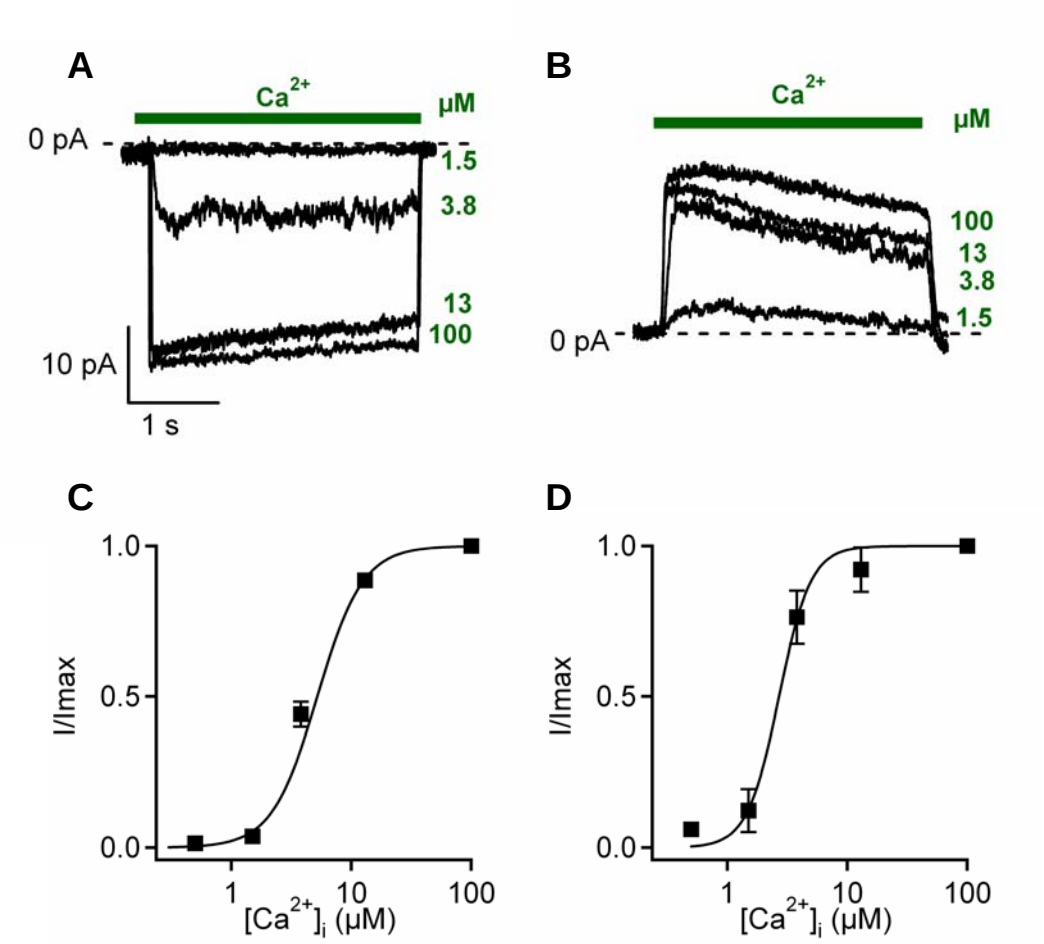

Figure 3.15 Dependence of olfactory Cl^- channels on $[Ca^{2+}]_i$.
A membrane patch was excised from the dendritic knob/cilia of an OSN, and the cytoplasmatic side was exposed to the indicated free $[Ca^{2+}]$ at -50 mV (A) or at +50 mV (B). Normalized current was plotted versus $[Ca^{2+}]_i$ and fitted to Hill equation. At -50 mV $K_{1/2}$ was 4.7 µM and *n* was 2.5 (C), whereas at +50 mV $K_{1/2}$ was 2.6 µM and *n* was 3.2 (D).

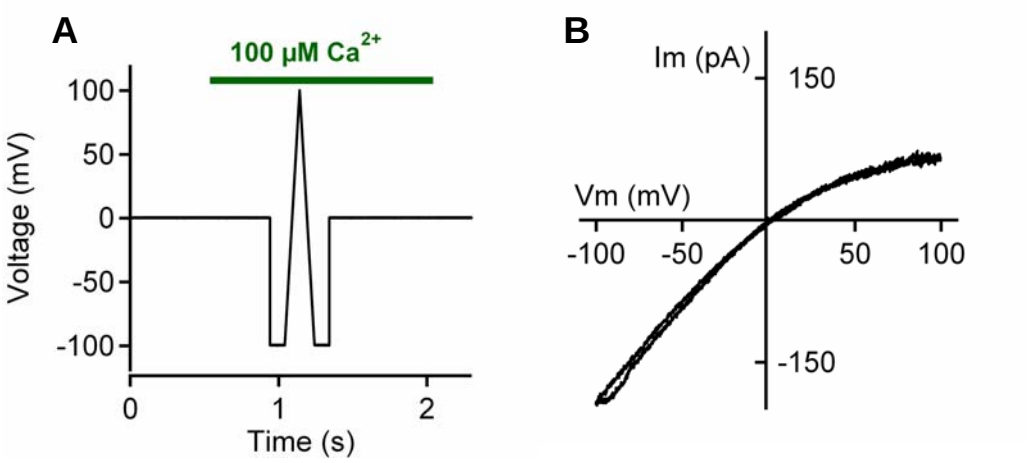

Figure 3.16 IV relationship of olfactory Cl^- channel.
The IV relation was measured using a ramp protocol delivered after 500 ms from activation by Ca^{2+} application (A). The Cl^- channel exhibited a slight inward rectification.

3.3.2 Single channel conductance

Single-channel measurements are not feasible because the unitary current is too small. Therefore stationary noise analysis was performed using Cl^- current recorded at various $[Ca^{2+}]_i$. Each trace was subdivided in 100 ms intervals to minimize the effect of Ca^{2+}-dependent inactivation and the mean and the variance was calculated. The data were fitted with the following equation:

$$\sigma^2 = i\bar{I} - \frac{\bar{I}^2}{N}$$

where σ^2 is the variance of the current, *i* is the single channel current, N is the number of the channels in the patch and $\bar{I}$ is the mean current (Fig. 3.17 A). The single channel conductance of the olfactory Cl^- channel at -50 mV was 1.6 ± 0.3 pS (n=3). The maximum open probability was calculated with the relation:

$$P_{open\,\max} = \frac{\bar{I}_{\max}}{iN}$$

and it results 0.81 ± 0.13 (n=3).

The same procedure was applied to CNG channels with symmetrical LiCl solution and the single channel conductance at-50 mV was 14 ± 1 pS (n=13) and the maximum open probability was 0.84 ± 0.05 (n=13, Fig 3.17 B).

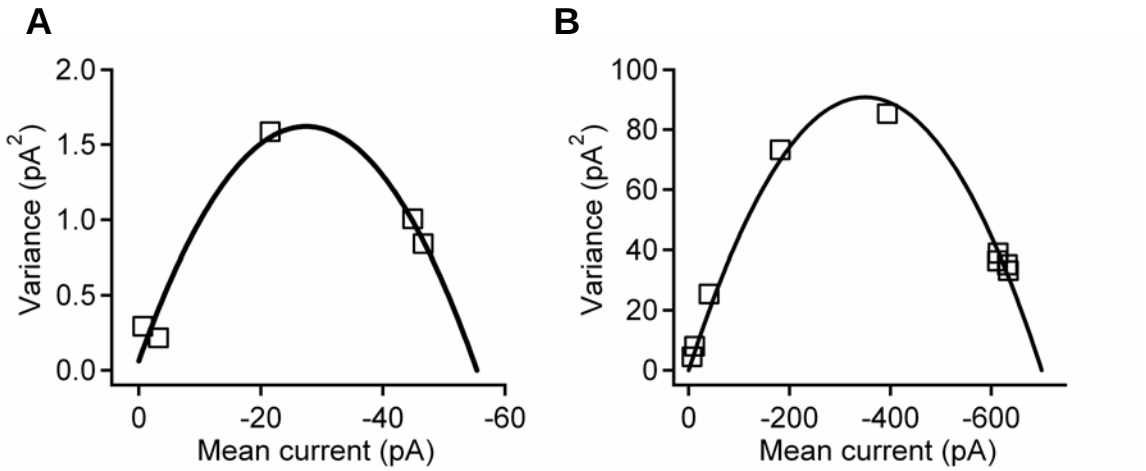

Figure 3.17 Single-channel properties of olfactory transduction channels.
The single-channel conductances of Cl^- channel (A) and CNG channel (B) were estimated by stationary noise analysis.

3.3.3 Anion selectivity

As for mBest2, the anionic selectivity of the Ca^{2+}-activated Cl^- channel of OSNs was measured. The Cl^- channels were activated previously in each patch first with Ca^{2+} in a solution containing 140 mM of NaCl (as in the pipette) and in a solution in which NaCl was replaced by the Na^+ salt of other anions. The IV relation was measured as reported in Fig 3.18 A and the shift in reversal potential was used to calculate the permeability ratio between a given anion and chloride using the Goldman-Hodgkin-Katz equation with the following relation:

$$P_X / P_{Cl} = \frac{[Cl^-]_i}{[X]_o \exp(-\Delta E_{rev} F / RT)} - \frac{[Cl^-]_o}{[X]_o}$$

mBest2 current exhibited the following permeability sequence:

$$SCN^- > I^- > NO_3^- > Br^- > Cl^- > MeS^- \text{ (Methylsulfate)}$$

and the permeability ratios were:

14.58: 4.69: 3.44: 2.20: 1: 0.12

Also for the olfactory Cl^- channel the selectivity for different anions is relatively low. Moreover, as reported for mBest2 the bigger anions, with lower hydratation energy, are more permeable indicating that the permeation mechanism is the same in both channels.

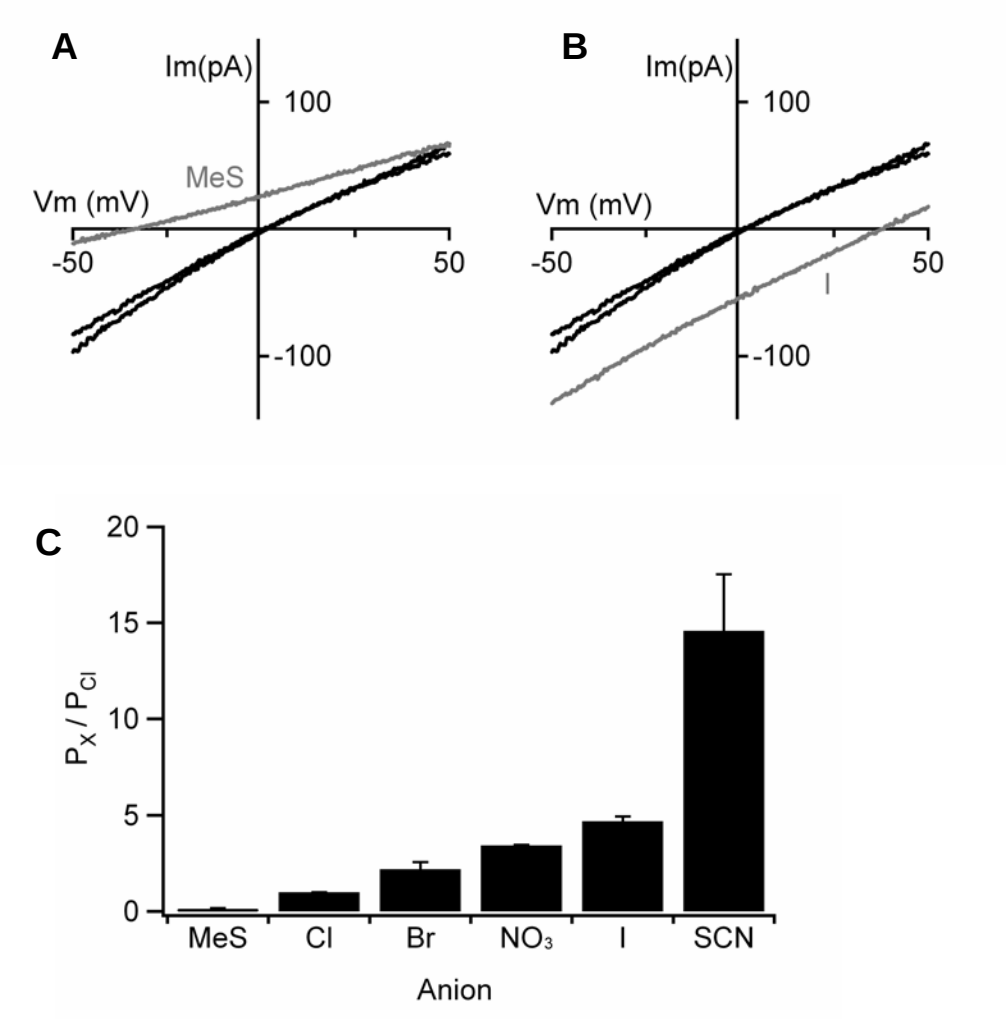

Figure 3.18 Ionic permeabiliy of olfactory Cl^- channels.
(A-B) A membrane patch was excised from the dendritic knob/cilia of an OSN and the Cl^- channel was activated by bath application of Ca^{2+} with symmetrical Cl^- solution (black traces) or with solution in which most Cl^- was replaced with MeS (A) or with I^- (B). Relative permeability ratios (P_X/P_{Cl}) were calculated with the Goldman-Hodgkin-Katz equation from measured shifts of E_{rev} (C, n=5-8).

3.3.4 Pharmacological properties

Previous studies have shown that the Cl^- component of the olfactory transduction current is blocked by 300 µM-1 mM of NFA or 2-5 mM of SITS (Reisert *et al.*, 2005; Lowe & Gold, 1993b; Kurahashi & Yau, 1993; Kurahashi & Menini, 1997). Here, these compounds were applied at the intracellular side of patches in the inside-out configuration. The application of 1 mM of NFA within the Ca^{2+} solution was able to completely block the

Ca^{2+}-activated Cl^- current (Fig 3.19 A). Ramp protocol demonstrated that the blockage is not voltage-dependent (Fig 3.19 C). In contrast, as reported for mBest2, intracellular application of 2 mM SITS was not able to significantly block the Cl^- channel at any potential tested (Fig 3.19 B-D).

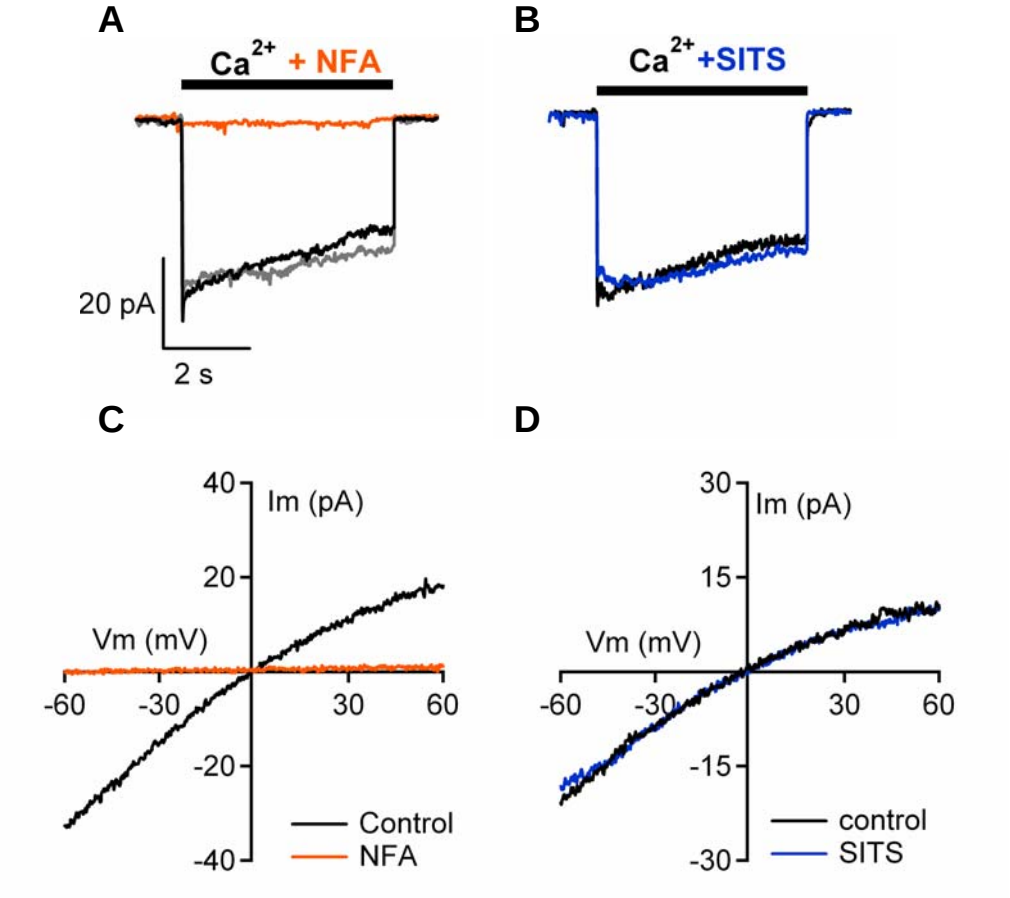

Figure 3.19 Pharmacology of olfactory Cl^- channels.
Olfactory Cl^- channels were activated by 100 µM of Ca^{2+} at -50 mV. In the same patch bath application of 1 mM of NFA with Ca^{2+} failed to activate the channel (A). The block was completely reversible (wash, gray trace in A) and voltage-independent as measured with voltage ramp protocol (C). On the contrary the bath application of 2 mM of SITS did not cause the block of olfactory Cl^- channels.

3.4 Odorant-induced responses in mBest2-null mice

To investigate the role of mBest2 in olfactory transduction, a mose line in which mBest2 is genetically inactivated was used. The odorant sensitivity of OSNs has been measured by recording the response to brief odorants pulses (100 ms) using elecetroolfactogram (EOG) recordings (Scott & Scott-Johnson, 2002). Odorants were delivered in the vapor phase to the surface of olfactory epithelium. Each of three commonly used odorants, amylacetate, acephonenone and cineole gave very similar results. Figure 3.20 shows EOG amplitude responses to 2.5 M amylacetate (a saturating concentration, see below) from 13 locations across the turbinates. The EOG amplitude varied at different recording locations, but there was no difference between the wild-type and the mBest2$^{-/-}$ mice in comparable locations.

Dose responses to odorant stimulation were obtained by delivering the vapor phase of odor solutions at concentrations raging from 2.5x10^{-5} M to 2.5 M to the olfactory epithelium. Figure 3.21 A shows the representative recordings obtained in wild type and mBest2$^{-/-}$ mice with amylacetate. The maximum EOG amplitudes were similar in wild type, 0.74 ± 0.13 mV (n=14) and mBest2$^{-/-}$, 1.16 ± 0.33 mV (n=13). Also the dose response relations were very similar with an EC_{50} of ~ 10^{-3} M both for wild type and mBest2$^{-/-}$ (Fig 3.21 B).

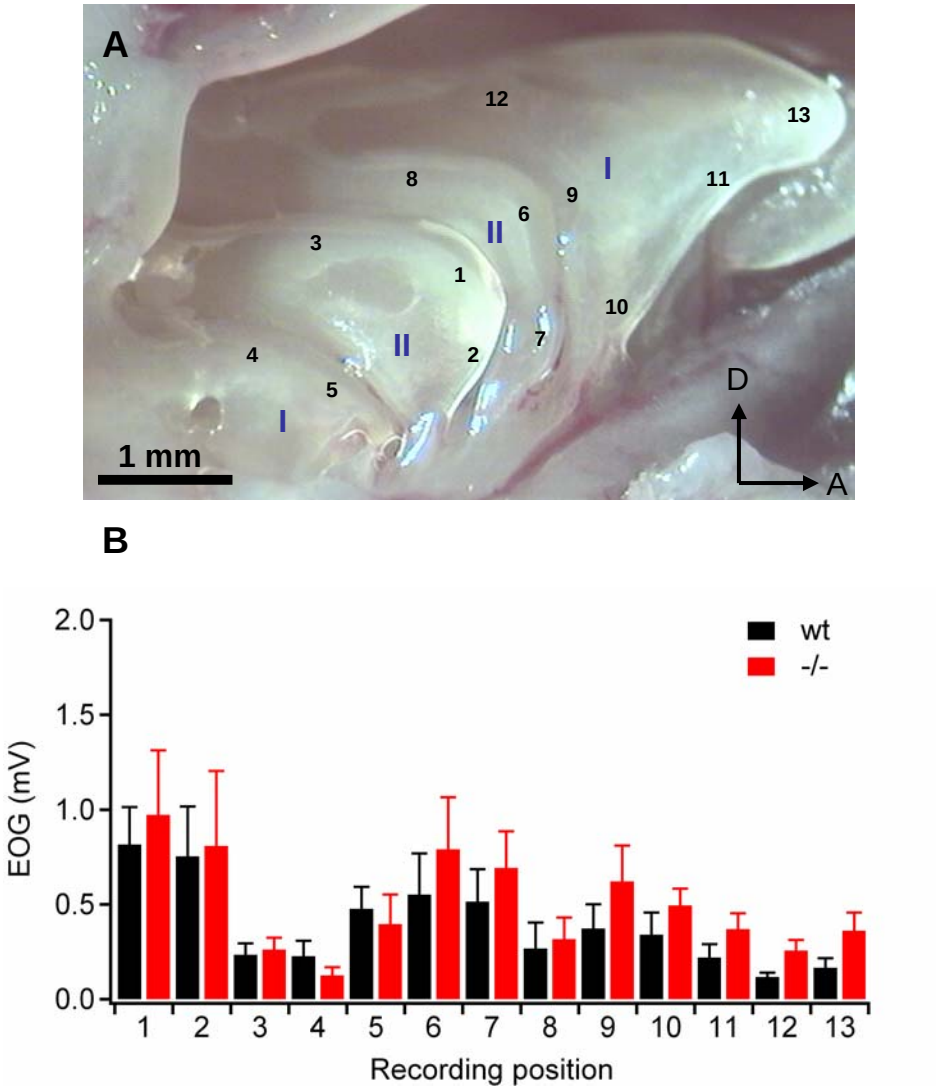

Figure 3.20 Sensitivity to odorant stimulation in mBest2-null mice
Averaged EOG amplitudes to a 100 ms pulse of odorant vapor from a solution containing 2.5 M amylacetate solution measured at 13 different locations along turbinate (B). These locations are indicated in the photograph in (A). D, dorsal; A, anterior.

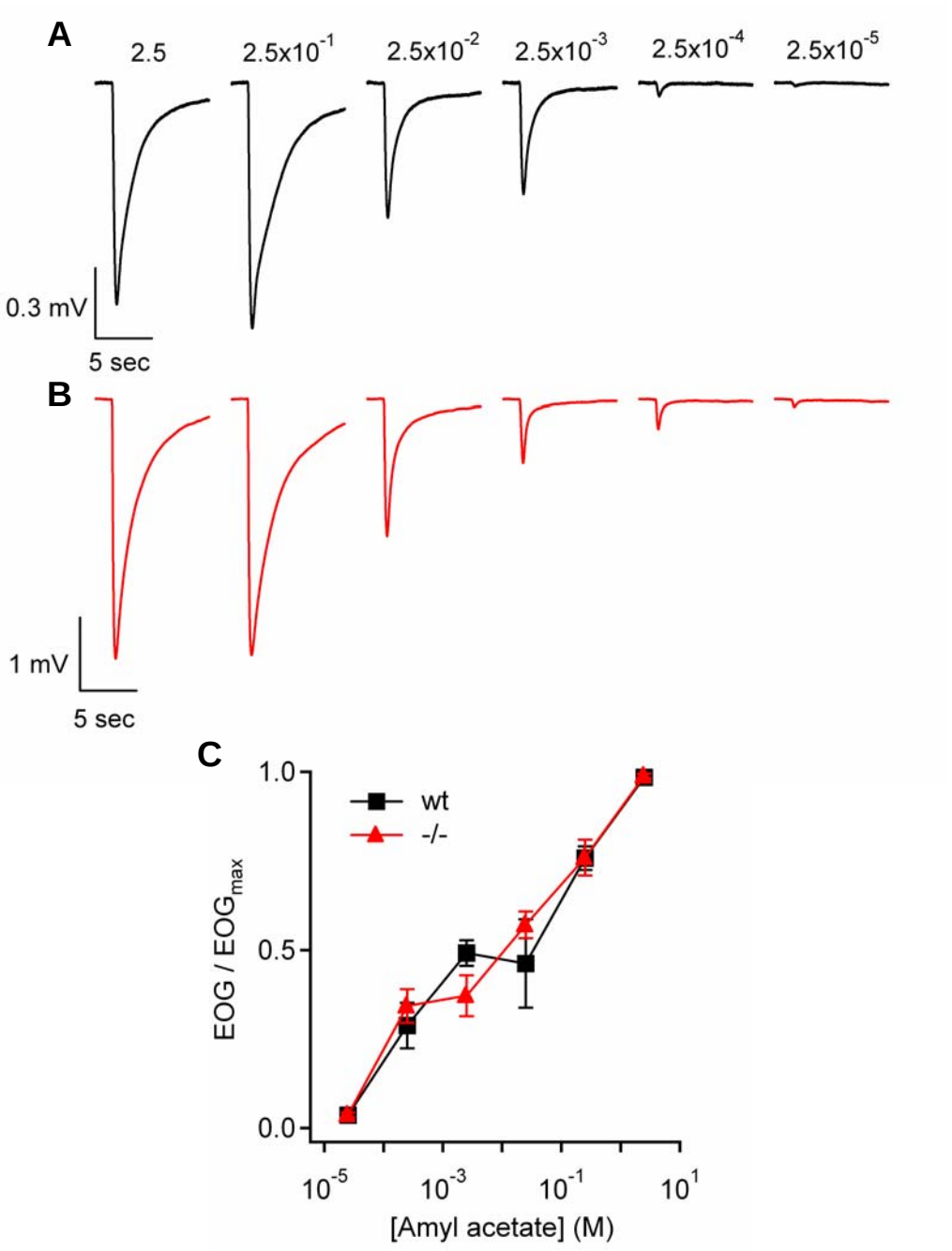

Figure 3.21 Dose-response of EOG responses in mBest2 null mice.
The epithelium was exposed to 100 ms pulses of odorant vapor of increasing concentrations of amyl acetate solutions. Representative EOG recordings from wild type (A, in black) and mBest2$^{-/-}$ (A, in red) mice. Normalized EOG responses were plotted versus the odorant concentration (B). Wild type and mBest2$^{-/-}$ had a similar dose-response.

4. Discussion

The olfactory transduction is the molecular cascade, occurring in the cilia of OSNs, that transforms the binding of odorant molecules to a specific odorant receptor into a graded changing of membrane potential through the activation of two different ion channels: the CNG channel and the Ca^{2+}-activated Cl^- channel (Schild & Restrepo, 1998; Menini *et al.*, 2004; Kleene, 2008). While the CNG channel has been characterized at molecular level (Kaupp & Seifert, 2002; Pifferi *et al.*, 2006a), the molecular identity of the Ca^{2+}-activated Cl^- channel remains elusive. The data presented in this Thesis reveal the mBest2 could be a component of the Ca^{2+}-activated Cl^- channel involved in olfactory transduction.

mBest2 is expressed in mature OSN and it is targeted to the cilia of OSNs, where it colocalizes with CNGA2, the principal subunit of the CNG olfactory channel responsible for the primary transduction current. Electrophysiological properties of Ca^{2+}-activated Cl^- currents of native channels in dendritic knob/cilia of OSNs and of mBest2 expressed in HEK-293 cells are remarkably similar. In fact, both currents have the same anion permeability sequence, current–voltage relations quite close to linearity, voltage-independent and side-specific blockage by NFA and SITS but a Ca^{2+} sensitivity difference of one order of magnitude. The data of odorant sensitivity obtained by EOG recordings from mBest2$^{-/-}$ mice do not show significant differences from wild-type mice indicating that the lack of mBest2 does not produce a big impairment of olfactory transduction. It is possible to speculate that mBest2 is a modulatory subunit of Ca^{2+}-activated Cl^- channel of OSNs and its absence does not cause an effect detectable by EOG recording.

Comparison of functional properties between Ca^{2+}-activated Cl^- currents from OSNs and mBest2-mediated currents

To functionally compare native of Ca^{2+}-activated Cl^- channels of OSNs and heterologously expressed mBest2 channles, we performed an electrophysiological analysis of the two currents. A side-by-side comparison in excised inside-out patches for both types of Ca^{2+}-activated Cl^- channels was not possible, because we did not detect any measurable current in inside-out excised patches from HEK-293 cells expressing mBest2. Therefore, we determined mBest2 functional properties with the whole-cell voltage–clamp technique. Although several properties between native and mBest2 currents were very similar, the non-perfect match could be due to several reasons. First, the use of different recording configurations could produce different results. Second, there could be a lack of posttranslational modification of mBest2 in heterologous systems, such as phosphorylation or sumoylation, that can modulate ion channels (Muller *et al.*, 2001; Rajan *et al.*, 2005). Third, ion channels are often composed of more than one type of subunit and/or have additional regulatory proteins that modify the functional properties.

The most significant difference between the two currents was found to be their sensitivity to intracellular Ca^{2+}. In fact, currents were half-maximal at a Ca^{2+} concentration of 0.4 μM for mBest2, similar to previous results (Qu *et al.*, 2004; Qu *et al.*, 2003), whereas native currents required a higher Ca^{2+} concentration, 4.7 μM, in general agreement with micromolar values measured in rat (Reisert *et al*., 2003) and mouse (Reisert *et al*., 2005). Dose–response relations obtained from isolated frog olfactory cilia also showed a similar $K_{1/2}$ of 4.8 μM (Kleene & Gesteland, 1991). Moreover native Ca^{2+}-activated Cl^- channels showed a higher Ca^{2+} sensitivity at positive voltage (4.7 μM at -50 mV vs 2.6 μM at +50 mV) in accordance with previous results both in frog and rodents OSNs (Kleene & Gesteland, 1991; Reisert *et al.*, 2003; Reisert *et al.*, 2005). In contrast, mBest2 shows almost the same Ca^{2+} sensitivity at each tested voltage (Qu *et al.*, 2004). Another study by Hallani *et al.* (1998) measured electrophysiological properties of a Ca^{2+}-activated Cl^- current from rat excised patches that did not show similar characteristics to those reported here and by Reisert et al., (2003;2005). Finally as previously reported (Reisert *et al.*, 2003; Reisert *et al.*, 2005) the native Ca^{2+}-activated Cl^- current slowly inactivated in the presence of a constant Ca^{2+} concentration when measured in excised patches, whereas mBest2 currents in whole-cell recordings did not show any time-dependent change in the presence of any given Ca^{2+}

concentration, as described before (Qu *et al.*, 2004; Qu *et al.*, 2003; Qu & Hartzell, 2004; Qu *et al.*, 2006). However, in isolated frog olfactory cilia, Kleene and Gesteland (1991) did not find any current inactivation during prolonged exposure to Ca^{2+}. The difference in inactivation properties may reflect specific differences between amphibian and mammalian channels or may indicate that some factor remains inside the isolated cilia, whereas it is lost upon excision of the membrane patch. It also unknown if this inactivation occurs also in intact OSNs, however it is possible to speculate that also this phenomenon could be involved in desensitization after long-lasting odor stimulation. In contrast, in fast adaptation it seems that Ca^{2+}-activated Cl^- channels are not involved (Boccaccio *et al.*, 2006; Kurahashi & Menini, 1997).

The current–voltage relations activated by high Ca^{2+} concentrations in symmetrical Cl^- solutions were quite close to linearity, with only a moderate inward rectification in native channels, as reported by Kleene & Gesteland (1991) and Reisert *et al.* (2005), and a slight outward rectification in mBest2 currents. Previous reports found a more linear current-voltage relation for mBest2 currents (Qu *et al.*, 2004; Qu & Hartzell, 2004).

Single-channel events have not been directly measured because of small unit conductances. The single-channel conductance has been estimated by noise analysis to be 1.6 pS for native channels, in good agreement with previous estimates of 0.5–1.7 pS (Reisert *et al.*, 2003; Larsson *et al.*, 1997). Data from endogenous Drosophila bestrophin in S2 cells and heterologous expression of dBest1give show a single channel conductance of about 2 pS (Chien *et al*., 2006), very similar to those of native olfactory Ca^{2+}-activated Cl^- channel.

Both native olfactory and mBest2 currents exhibited the same anion permeability sequence $SCN^->I^->NO_3^->Br^->Cl^->>MeS^-$, although the calculated permeability ratios were not identical showing that native Ca^{2+}-activated Cl^- channel is more selective than mBest2. This permeability sequence corresponds to the Eisenman ‘‘weak field strength’’ lyotropic series (Eisenmann & Horn, 1973), indicating that in both channels, the interaction between the permeant ion and the channel is weak, since permeability is related to the ease with which the permeant ion leaves the bulk solution and enters the channel. These data are in general agreement with previous measurements from mBest2 current and from rat OSNs (Qu *et al.*, 2004; Qu & Hartzell, 2004; Bakall *et al.*, 2008).

The blocking properties of NFA and SITS were revealed to be similar in native olfactory and mBest2 currents. From the extracellular side, both NFA and SITS block the

mBest2 current in the same range of concentration in which the native current is blocked (Kurahashi & Yau, 1993; Kurahashi & Menini, 1997; Lowe & Gold, 1993b; Reisert & Matthews, 1998; Reisert *et al.*, 2005) From the intracellular side, only NFA blocks both native Ca^{2+}-activated Cl^- channel and mBest2, whereas SITS does not have a significant effect, in agreement with previous measurements in frog olfactory cilia (Frings *et al.*, 2000; Kleene, 1993).

Mechanism of Ca^{2+} activation.

Native olfactory channels appear to be rapidly activated by Ca^{2+} in inside-out patches (Reisert *et al.*, 2003; Reisert *et al.*, 2005) and in isolated olfactory cilia (Kleene, 1993; Kleene & Gesteland, 1991), whereas similar experiments for Ca^{2+} activation of mBest2 are missing. In a recent study Tsunenari *et al.* (2006) have shown that hBest4 can be activated by Ca^{2+} in excised inside-out patches, indicating that diffusible messengers or protein phosphorylation are not implicated in Ca^{2+} activation. However, because the current activates and deactivates very slowly in response to Ca^{2+} (time constant of 10–20 seconds), indirect Ca^{2+} activation through a membrane-associated messenger cannot be excluded. Moreover data from endogenous Drosophila bestrophin in S2 cells and heterologous expression of dBest1 showed that it is possible to activate the channel in inside-out configuration (Chien *et al*., 2006).Also in these cases the time course of activation is quite slow (half time ~ 1 min) but it can be faster, at least two-fold, by addition of ATP to Ca^{2+} solution, suggesting the involvement of some ATP-dependent enzymatic process (Chien *et al*., 2006). However Kranjc *et al*. (unpublished results) found that specific mutation (D301A, D304A) in a stretch of negative charged aminoacids, located in the C-terminus immediately after the last transmembrane domain, completely abolished the Ca^{2+} sensitivity of mBest2, suggesting that a direct binding of Ca^{2+} is necessary to gate mBest2.

Odorant response and mBest2

The odorant-induced response was analyzed in mBest2$^{-/-}$ mice by EOG recording. The overall responses were not significantly different in comparison with wild-type mice suggesting that the absence of mBest2 does not cause a big impairment of olfactory transduction. However it is not possible to exclude that the differences are too weak to be detectable by EOG or that some compensatory mechanisms occur in mBest2$^{-/-}$ mice. Single-

cell recording will be necessary to better clarify the role of mBest2 in odorant-induced response in mouse OSNs.

Conclusions

The colocalization of mBest2 with CNGA2 on the cilia of OSNs, together with the functional data, strongly indicates that mBest2 is a component of Ca^{2+}-activated Cl^- channel involved in olfactory transduction. Future studies should examine the involvement of additional components in forming and/or modulating the native olfactory channel. Recently is has been found a novel protein, TMEM16A, that is able to mediate Ca^{2+}-activated Cl^- current in different types of epithelial cells and in Xenopus oocyte has been found (Caputo *et al.*, 2008; Schroeder *et al*., 2008; Yang *et al.*, 2008). Very interestingly a homolog of this protein, TMEM16B, has been reported to be expressed in olfactory epithelium (Sammeta *et al.*, 2007). It is possible to speculate possible that interactions of mBest2 with this protein could be important to generate the Ca^{2+}-activated Cl^- current of OSNs. Indeed, recently it has been found that hBest1 can also bind voltage-gated Ca^{2+} channel Ca_v 1.3 and modulate its biophysical properties, suggesting that bestrophins could act a multifunctional regulator of membrane permeability as previously reported for CFTR (Hartzell *et al.*, 2008; Yu *et al.*, 2008; Mehta, 2005; Schwiebert *et al.*, 1999).

5. References

Andre, S., Boukhaddaoui, H., Campo, B., Al Jumaily, M., Mayeux, V., Greuet, D., Valmier, J., & Scamps, F. (2003). Axotomy-induced expression of calcium-activated chloride current in subpopulations of mouse dorsal root ganglion neurons. *J.Neurophysiol.* **90**, 3764-3773.

Arden, G. B., Barrada, A., & Kelsey, J. H. (1962). New clinical test of retinal function based upon the stranding potential of the eye. *Br.J.Ophthalmol.* **46**, 449-467.

Bader, C. R., Bertrand, D., & Schlichter, R. (1987). Calcium-activated chloride current in cultured sensory and parasympathetic quail neurones. *J.Physiol* **394**, 125-148.

Bader, C. R., Bertrand, D., & Schwartz, E. A. (1982). Voltage-activated and calcium-activated currents studied in solitary rod inner segments from the salamander retina. *J.Physiol* **331**, 253-284.

Bakall, B., Marmorstein, L. Y., Hoppe, G., Peachey, N. S., Wadelius, C., & Marmorstein, A. D. (2003). Expression and localization of bestrophin during normal mouse development. *Invest Ophthalmol.Vis.Sci.* **44**, 3622-3628.

Bakall, B., McLaughlin, P., Stanton, J. B., Zhang, Y., Hartzell, H. C., Marmorstein, L. Y., & Marmorstein, A. D. (2008). Bestrophin-2 is involved in the generation of intraocular pressure. *Invest Ophthalmol.Vis.Sci.* **49**, 1563-1570.

Bakalyar, H. A. & Reed, R. R. (1990). Identification of a specialized adenylyl cyclase that may mediate odorant detection. *Science* **250**, 1403-1406.

Balasubramanian, S., Lynch, J. W., & Barry, P. H. (1995). The permeation of organic cations through cAMP-gated channels in mammalian olfactory receptor neurons. *J.Membr.Biol.* **146**, 177-191.

Balasubramanian, S., Lynch, J. W., & Barry, P. H. (1996). Calcium-dependent modulation of the agonist affinity of the mammalian olfactory cyclic nucleotide-gated channel by calmodulin and a novel endogenous factor. *J.Membr.Biol.* **152**, 13-23.

Barish, M. E. (1983). A transient calcium-dependent chloride current in the immature Xenopus oocyte. *J.Physiol* **342**, 309-325.

Barnes, S. (1994). After transduction: response shaping and control of transmission by ion channels of the photoreceptor inner segments. *Neuroscience* **58**, 447-459.

Barnes, S. & Hille, B. (1989). Ionic channels of the inner segment of tiger salamander cone photoreceptors. *J.Gen.Physiol* **94**, 719-743.

Barro, S. R., Spitzner, M., Schreiber, R., & Kunzelmann, K. (2006). Bestrophin 1 enables Ca2+ activated Cl- conductance in epithelia. *J.Biol.Chem.*

Belluscio, L., Gold, G. H., Nemes, A., & Axel, R. (1998). Mice deficient in G(olf) are anosmic. *Neuron* **20**, 69-81.

Berkhout, T. A., Blaney, F. E., Bridges, A. M., Cooper, D. G., Forbes, I. T., Gribble, A. D., Groot, P. H., Hardy, A., Ife, R. J., Kaur, R., Moores, K. E., Shillito, H., Willetts, J., & Witherington, J. (2003). CCR2: characterization of the antagonist binding site from a combined receptor modeling/mutagenesis approach. *J.Med.Chem.* **46**, 4070-4086.

Best, F. (1905). Über eine heretitäre Maculaffektion: Beiträge zur Vererbungslehere. *Z Augenheilkd.* **13**, 199-212.

Biskup, C., Kusch, J., Schulz, E., Nache, V., Schwede, F., Lehmann, F., Hagen, V., & Benndorf, K. (2007). Relating ligand binding to activation gating in CNGA2 channels. *Nature* **446**, 440-443.

Boccaccio, A., Lagostena, L., Hagen, V., & Menini, A. (2006). Fast adaptation in mouse olfactory sensory neurons does not require the activity of phosphodiesterase. *J.Gen.Physiol* **128**, 171-184.

Boccaccio, A. & Menini, A. (2007). Temporal development of cyclic nucleotide-gated and Ca2+ -activated Cl- currents in isolated mouse olfactory sensory neurons. *J.Neurophysiol.* **98**, 153-160.

Boekhoff, I., Kroner, C., & Breer, H. (1996). Calcium controls second-messenger signalling in olfactory cilia. *Cell Signal.* **8**, 167-171.

Boekhoff, I., Tareilus, E., Strotmann, J., & Breer, H. (1990). Rapid activation of alternative second messenger pathways in olfactory cilia from rats by different odorants. *EMBO J.* **9**, 2453-2458.

Bolton, T. B. (1979). Mechanisms of action of transmitters and other substances on smooth muscle. *Physiol Rev.* **59**, 606-718.

Bonigk, W., Altenhofen, W., Muller, F., Dose, A., Illing, M., Molday, R. S., & Kaupp, U. B. (1993). Rod and cone photoreceptor cells express distinct genes for cGMP-gated channels. *Neuron* **10**, 865-877.

Bonigk, W., Bradley, J., Muller, F., Sesti, F., Boekhoff, I., Ronnett, G. V., Kaupp, U. B., & Frings, S. (1999). The native rat olfactory cyclic nucleotide-gated channel is composed of three distinct subunits. *J.Neurosci.* **19**, 5332-5347.

Borisy, F. F., Ronnett, G. V., Cunningham, A. M., Juilfs, D., Beavo, J., & Snyder, S. H. (1992). Calcium/calmodulin-activated phosphodiesterase expressed in olfactory receptor neurons. *J.Neurosci.* **12**, 915-923.

Botelho, S. Y. & Dartt, D. A. (1980). Effect of calcium antagonism or chelation on rabbit lacrimal gland secretion and membrane potentials. *J.Physiol* **304**, 397-403.

Boucher, R. C., Cheng, E. H., Paradiso, A. M., Stutts, M. J., Knowles, M. R., & Earp, H. S. (1989). Chloride secretory response of cystic fibrosis human airway epithelia. Preservation of calcium but not protein kinase C- and A-dependent mechanisms. *J.Clin.Invest* **84**, 1424-1431.

Bradley, J., Bonigk, W., Yau, K. W., & Frings, S. (2004). Calmodulin permanently associates with rat olfactory CNG channels under native conditions. *Nat.Neurosci.* **7**, 705-710.

Bradley, J., Li, J., Davidson, N., Lester, H. A., & Zinn, K. (1994). Heteromeric olfactory cyclic nucleotide-gated channels: a subunit that confers increased sensitivity to cAMP. *Proc.Natl.Acad.Sci.U.S.A* **91**, 8890-8894.

Bradley, J., Reuter, D., & Frings, S. (2001). Facilitation of calmodulin-mediated odor adaptation by cAMP-gated channel subunits. *Science* **294**, 2176-2178.

Breer, H., Boekhoff, I., & Tareilus, E. (1990). Rapid kinetics of second messenger formation in olfactory transduction. *Nature* **345**, 65-68.

Bruch, R. C., Medler, K. F., Tran, H. N., & Hamlin, J. A. (1997). G-protein beta gamma subunit genes expressed in olfactory receptor neurons. *Chem.Senses* **22**, 587-592.

Brunet, L. J., Gold, G. H., & Ngai, J. (1996). General anosmia caused by a targeted disruption of the mouse olfactory cyclic nucleotide-gated cation channel. *Neuron* **17**, 681-693.

Buck, L. & Axel, R. (1991). A novel multigene family may encode odorant receptors: a molecular basis for odor recognition. *Cell* **65**, 175-187.

Buck, L. B. (2000). The molecular architecture of odor and pheromone sensing in mammals. *Cell* **100**, 611-618.

Bui, T. V., Han, Y., Radu, R. A., Travis, G. H., & Mata, N. L. (2006). Characterization of native retinal fluorophores involved in biosynthesis of A2E and lipofuscin-associated retinopathies. *J.Biol.Chem.* **281**, 18112-18119.

Byrne, N. G. & Large, W. A. (1985). Evidence for two mechanisms of depolarization associated with alpha 1-adrenoceptor activation in the rat anococcygeus muscle. *Br.J.Pharmacol.* **86**, 711-721.

Byrne, N. G. & Large, W. A. (1988). Membrane ionic mechanisms activated by noradrenaline in cells isolated from the rabbit portal vein. *J.Physiol* **404**, 557-573.

Caputo, A., Caci, E., Ferrera, L., Pedemonte, N., Barsanti, C., Sondo, E., Pfeffer, U., Ravazzolo, R., Zegarra-Moran, O., & Galietta, L. J. (2008). TMEM16A, A Membrane Protein Associated With Calcium-Dependent Chloride Channel Activity. *Science*.

Castillo, K., Delgado, R., & Bacigalupo, J. (2007). Plasma membrane Ca(2+)-ATPase in the cilia of olfactory receptor neurons: possible role in Ca(2+) clearance. *Eur.J.Neurosci.* **26**, 2524-2531.

Chen, T. Y., Peng, Y. W., Dhallan, R. S., Ahamed, B., Reed, R. R., & Yau, K. W. (1993). A new subunit of the cyclic nucleotide-gated cation channel in retinal rods. *Nature* **362**, 764-767.

Chen, T. Y. & Yau, K. W. (1994). Direct modulation by Ca(2+)-calmodulin of cyclic nucleotide-activated channel of rat olfactory receptor neurons. *Nature* **368**, 545-548.

Chess, A., Simon, I., Cedar, H., & Axel, R. (1994). Allelic inactivation regulates olfactory receptor gene expression. *Cell* **78**, 823-834.

Chien, L. T., Zhang, Z. R., & Hartzell, H. C. (2006). Single Cl- channels activated by Ca2+ in Drosophila S2 cells are mediated by bestrophins. *J.Gen.Physiol* **128**, 247-259.

Chipperfield, A. R. & Harper, A. A. (2000). Chloride in smooth muscle. *Prog.Biophys.Mol.Biol.* **74**, 175-221.

Church, W. B., Jones, K. A., Kuiper, D. A., Shine, J., & Iismaa, T. P. (2002). Molecular modelling and site-directed mutagenesis of human GALR1 galanin receptor defines determinants of receptor subtype specificity. *Protein Eng* **15**, 313-323.

Corotto, F. S., Piper, D. R., Chen, N., & Michel, W. C. (1996). Voltage- and Ca(2+)-gated currents in zebrafish olfactory receptor neurons. *J.Exp.Biol.* **199**, 1115-1126.

Crain, S. M. (1956). Resting and action potentials of cultured chick embryo spinal ganglion cells. *J.Comp Neurol.* **104**, 285-329.

Crumling, M. A. & Gold, G. H. (1998). Ion concentrations in the mucus covering the olfactory epithelium in rodents. *Soc Neurosci Abstr* **24**, 2099.

Currie, K. P., Wootton, J. F., & Scott, R. H. (1995). Activation of Ca(2+)-dependent Cl- currents in cultured rat sensory neurones by flash photolysis of DM-nitrophen. *J.Physiol* **482 (Pt 2)**, 291-307.

Davis, M. J. & Hill, M. A. (1999). Signaling mechanisms underlying the vascular myogenic response. *Physiol Rev.* **79**, 387-423.

Dawson, D. C., Smith, S. S., & Mansoura, M. K. (1999). CFTR: mechanism of anion conduction. *Physiol Rev.* **79**, S47-S75.

Dawson, T. M., Arriza, J. L., Jaworsky, D. E., Borisy, F. F., Attramadal, H., Lefkowitz, R. J., & Ronnett, G. V. (1993). Beta-adrenergic receptor kinase-2 and beta-arrestin-2 as mediators of odorant-induced desensitization. *Science* **259**, 825-829.

De Castro, F., Geijo-Barrientos, E., & Gallego, R. (1997). Calcium-activated chloride current in normal mouse sympathetic ganglion cells. *J.Physiol* **498 (Pt 2)**, 397-408.

Del Punta, K., Leinders-Zufall, T., Rodriguez, I., Jukam, D., Wysocki, C. J., Ogawa, S., Zufall, F., & Mombaerts, P. (2002). Deficient pheromone responses in mice lacking a cluster of vomeronasal receptor genes. *Nature* **419**, 70-74.

Deschenes, M., Feltz, P., & Lamour, Y. (1976). A model for an estimate in vivo of the ionic basis of presynaptic inhibition: an intracellular analysis of the GABA-induced depolarization in rat dorsal root ganglia. *Brain Res.* **118**, 486-493.

Dhallan, R. S., Yau, K. W., Schrader, K. A., & Reed, R. R. (1990). Primary structure and functional expression of a cyclic nucleotide-activated channel from olfactory neurons. *Nature* **347**, 184-187.

Donaldson, J., Brown, A. M., & Hill, S. J. (1989). Temporal changes in the calcium-dependence of the histamine H1-receptor-stimulation of cyclic AMP accumulation in guinea-pig cerebral cortex. *Br.J.Pharmacol.* **98**, 1365-1375.

Douglas, W. W. & Poisner, A. M. (1963). The influence of calcium on the secretory response of the submaxillary gland to acetylcholine or to noradrenaline. *J.Physiol* **165**, 528-541.

Duchamp-Viret, P., Duchamp, A., & Chaput, M. A. (2000). Peripheral odor coding in the rat and frog: quality and intensity specification. *J.Neurosci.* **20**, 2383-2390.

Duchen, M. R. (1990). Effects of metabolic inhibition on the membrane properties of isolated mouse primary sensory neurones. *J.Physiol* **424**, 387-409.

Dulac, C. & Wagner, S. (2006). Genetic analysis of brain circuits underlying pheromone signaling. *Annu.Rev.Genet.* **40**, 449-467.

Dzeja, C., Hagen, V., Kaupp, U. B., & Frings, S. (1999). Ca2+ permeation in cyclic nucleotide-gated channels. *EMBO J.* **18**, 131-144.

Eggan, K., Baldwin, K., Tackett, M., Osborne, J., Gogos, J., Chess, A., Axel, R., & Jaenisch, R. (2004). Mice cloned from olfactory sensory neurons. *Nature* **428**, 44-49.

Eisenman, G. & Horn, R. (1983). Ionic selectivity revisited: the role of kinetic and equilibrium processes in ion permeation through channels. *J.Membr.Biol.* **76**, 197-225.

Eldred, G. E. & Lasky, M. R. (1993). Retinal age pigments generated by self-assembling lysosomotropic detergents. *Nature* **361**, 724-726.

Feinstein, P. & Mombaerts, P. (2004). A contextual model for axonal sorting into glomeruli in the mouse olfactory system. *Cell* **117**, 817-831.

Fesenko, E. E., Kolesnikov, S. S., & Lyubarsky, A. L. (1985). Induction by cyclic GMP of cationic conductance in plasma membrane of retinal rod outer segment. *Nature* **313**, 310-313.

Firestein, S., Darrow, B., & Shepherd, G. M. (1991a). Activation of the sensory current in salamander olfactory receptor neurons depends on a G protein-mediated cAMP second messenger system. *Neuron* **6**, 825-835.

Firestein, S., Picco, C., & Menini, A. (1993). The relation between stimulus and response in olfactory receptor cells of the tiger salamander. *J.Physiol* **468**, 1-10.

Firestein, S., Shepherd, G. M., & Werblin, F. S. (1990). Time course of the membrane current underlying sensory transduction in salamander olfactory receptor neurones. *J.Physiol* **430**, 135-158.

Firestein, S. & Werblin, F. S. (1987). Gated currents in isolated olfactory receptor neurons of the larval tiger salamander. *Proc.Natl.Acad.Sci.U.S.A* **84**, 6292-6296.

Firestein, S., Zufall, F., & Shepherd, G. M. (1991b). Single odor-sensitive channels in olfactory receptor neurons are also gated by cyclic nucleotides
FIRESTEIN1991. *J.Neurosci.* **11**, 3565-3572.

Fischmeister, R. & Hartzell, H. C. (2005). Volume sensitivity of the bestrophin family of chloride channels. *J.Physiol* **562**, 477-491.

Flannery, R. J., French, D. A., & Kleene, S. J. (2006). Clustering of cyclic-nucleotide-gated channels in olfactory cilia. *Biophys.J.* **91**, 179-188.

Frings, S. & Lindemann, B. (1990). Single unit recording from olfactory cilia. *Biophys.J.* **57**, 1091-1094.

Frings, S., Lynch, J. W., & Lindemann, B. (1992). Properties of cyclic nucleotide-gated channels mediating olfactory transduction. Activation, selectivity, and blockage. *J.Gen.Physiol* **100**, 45-67.

Frings, S., Reuter, D., & Kleene, S. J. (2000). Neuronal Ca2+ -activated Cl- channels--homing in on an elusive channel species. *Prog.Neurobiol.* **60**, 247-289.

Gabriel, S. E., Makhlina, M., Martsen, E., Thomas, E. J., Lethem, M. I., & Boucher, R. C. (2000). Permeabilization via the P2X7 purinoreceptor reveals the presence of a Ca2+-activated Cl- conductance in the apical membrane of murine tracheal epithelial cells. *J.Biol.Chem.* **275**, 35028-35033.

Gallemore, R. P., Griff, E. R., & Steinberg, R. H. (1988). Evidence in support of a photoreceptoral origin for the "light-peak substance". *Invest Ophthalmol.Vis.Sci.* **29**, 566-571.

Gallemore, R. P. & Steinberg, R. H. (1993). Light-evoked modulation of basolateral membrane Cl- conductance in chick retinal pigment epithelium: the light peak and fast oscillation. *J.Neurophysiol.* **70**, 1669-1680.

Gass, J. D. M. (1987) *Stereoscopic Atlas of Macular Disease: Diagnosis and Treatement*. St. Louis, MO: Mosby.

Gerstner, A., Zong, X., Hofmann, F., & Biel, M. (2000). Molecular cloning and functional characterization of a new modulatory cyclic nucleotide-gated channel subunit from mouse retina. *J.Neurosci.* **20**, 1324-1332.

Gilad, Y., Man, O., Paabo, S., & Lancet, D. (2003). Human specific loss of olfactory receptor genes. *Proc.Natl.Acad.Sci.U.S.A* **100**, 3324-3327.

Gilad, Y., Przeworski, M., & Lancet, D. (2004). Loss of olfactory receptor genes coincides with the acquisition of full trichromatic vision in primates. *PLoS.Biol.* **2**, E5.

Gilbert, D., Franjic-Wurtz, C., Funk, K., Gensch, T., Frings, S., & Mohrlen, F. (2007). Differential maturation of chloride homeostasis in primary afferent neurons of the somatosensory system. *Int.J.Dev.Neurosci.* **25**, 479-489.

Gimelbrant, A. A., Haley, S. L., & McClintock, T. S. (2001). Olfactory receptor trafficking involves conserved regulatory steps. *J.Biol.Chem.* **276**, 7285-7290.

Godfrey, P. A., Malnic, B., & Buck, L. B. (2004). The mouse olfactory receptor gene family. *Proc.Natl.Acad.Sci.U.S.A* **101**, 2156-2161.

Gold, G. H. (1999). Controversial issues in vertebrate olfactory transduction. *Annu.Rev.Physiol* **61**, 857-871.

Graziadei, P. & Bannister, L. H. (1967). Some observations on the fine structure of the olfactory epithelium in the domestic duck. *Z.Zellforsch.Mikrosk.Anat.* **80**, 220-228.

Graziadei, P. P., Levine, R. R., & Graziadei, G. A. (1978). Regeneration of olfactory axons and synapse formation in the forebrain after bulbectomy in neonatal mice. *Proc.Natl.Acad.Sci.U.S.A* **75**, 5230-5234.

Grosmaitre, X., Vassalli, A., Mombaerts, P., Shepherd, G. M., & Ma, M. (2006). Odorant responses of olfactory sensory neurons expressing the odorant receptor MOR23: a patch clamp analysis in gene-targeted mice. *Proc.Natl.Acad.Sci.U.S.A* **103**, 1970-1975.

Grunwald, M. E., Zhong, H., Lai, J., & Yau, K. W. (1999). Molecular determinants of the modulation of cyclic nucleotide-activated channels by calmodulin. *Proc.Natl.Acad.Sci.U.S.A* **96**, 13444-13449.

Hallani, M., Lynch, J. W., & Barry, P. H. (1998). Characterization of calcium-activated chloride channels in patches excised from the dendritic knob of mammalian olfactory receptor neurons. *J.Membr.Biol.* **161**, 163-171.

Hartzell, C., Putzier, I., & Arreola, J. (2005a). Calcium-activated chloride channels. *Annu.Rev.Physiol* **67**, 719-758.

Hartzell, C., Qu, Z., Putzier, I., Artinian, L., Chien, L. T., & Cui, Y. (2005b). Looking chloride channels straight in the eye: bestrophins, lipofuscinosis, and retinal degeneration. *Physiology (Bethesda.)* **20**, 292-302.

Hartzell, H. C. & Qu, Z. (2003). Chloride currents in acutely isolated Xenopus retinal pigment epithelial cells. *J.Physiol* **549**, 453-469.

Hartzell, H. C., Qu, Z., Yu, K., Xiao, Q., & Chien, L. T. (2008). Molecular physiology of bestrophins: multifunctional membrane proteins linked to best disease and other retinopathies. *Physiol Rev.* **88**, 639-672.

Haynes, L. & Yau, K. W. (1985). Cyclic GMP-sensitive conductance in outer segment membrane of catfish cones. *Nature* **317**, 61-64.

Herness, M. S. & Sun, X. D. (1999). Characterization of chloride currents and their noradrenergic modulation in rat taste receptor cells. *J.Neurophysiol.* **82**, 260-271.

Hirono, J., Sato, T., Tonoike, M., & Takebayashi, M. (1992). Simultaneous recording of [Ca2+]i increases in isolated olfactory receptor neurons retaining their original spatial relationship in intact tissue. *J.Neurosci.Methods* **42**, 185-194.

Hodgkin, A. L., McNaughton, P. A., & Nunn, B. J. (1985). The ionic selectivity and calcium dependence of the light-sensitive pathway in toad rods. *J.Physiol* **358**, 447-468.

Hofmann, F., Biel, M., & Kaupp, U. B. (2005). International Union of Pharmacology. LI. Nomenclature and structure-function relationships of cyclic nucleotide-regulated channels. *Pharmacol.Rev.* **57**, 455-462.

Hoppe, R., Breer, H., & Strotmann, J. (2006). Promoter motifs of olfactory receptor genes expressed in distinct topographic patterns. *Genomics* **87**, 711-723.

Hoppe, R., Frank, H., Breer, H., & Strotmann, J. (2003). The clustered olfactory receptor gene family 262: genomic organization, promotor elements, and interacting transcription factors. *Genome Res.* **13**, 2674-2685.

Hunter, M., Smith, P. A., & Case, R. M. (1983). The dependence of fluid secretion by mandibular salivary gland and pancreas on extracellular calcium. *Cell Calcium* **4**, 307-317.

Jaffe, G. J. & Schatz, H. (1988). Histopathologic features of adult-onset foveomacular pigment epithelial dystrophy. *Arch.Ophthalmol.* **106**, 958-960.

Jaworsky, D. E., Matsuzaki, O., Borisy, F. F., & Ronnett, G. V. (1995). Calcium modulates the rapid kinetics of the odorant-induced cyclic AMP signal in rat olfactory cilia. *J.Neurosci.* **15**, 310-318.

Jenkins, P. M., Hurd, T. W., Zhang, L., McEwen, D. P., Brown, R. L., Margolis, B., Verhey, K. J., & Martens, J. R. (2006). Ciliary targeting of olfactory CNG channels requires the CNGB1b subunit and the kinesin-2 motor protein, KIF17. *Curr.Biol.* **16**, 1211-1216.

Jones, D. T. & Reed, R. R. (1987). Molecular cloning of five GTP-binding protein cDNA species from rat olfactory neuroepithelium. *J.Biol.Chem.* **262**, 14241-14249.

Jones, D. T. & Reed, R. R. (1989). Golf: an olfactory neuron specific-G protein involved in odorant signal transduction. *Science* **244**, 790-795.

Kaneko, H., Nakamura, T., & Lindemann, B. (2001). Noninvasive measurement of chloride concentration in rat olfactory receptor cells with use of a fluorescent dye. *Am.J.Physiol Cell Physiol* **280**, C1387-C1393.

Kaneko, H., Putzier, I., Frings, S., Kaupp, U. B., & Gensch, T. (2004). Chloride accumulation in mammalian olfactory sensory neurons. *J.Neurosci.* **24**, 7931-7938.

Kang, J. & Caprio, J. (1995). In vivo responses of single olfactory receptor neurons in the channel catfish, Ictalurus punctatus. *J.Neurophysiol.* **73**, 172-177.

Karlin, A. & Akabas, M. H. (1998). Substituted-cysteine accessibility method. *Methods Enzymol.* **293**, 123-145.

Karlson, P. & Luscher, M. (1959). Pheromones': a new term for a class of biologically active substances. *Nature* **183**, 55-56.

Kartner, N., Hanrahan, J. W., Jensen, T. J., Naismith, A. L., Sun, S. Z., Ackerley, C. A., Reyes, E. F., Tsui, L. C., Rommens, J. M., Bear, C. E., & . (1991). Expression of the cystic fibrosis gene in non-epithelial invertebrate cells produces a regulated anion conductance. *Cell* **64**, 681-691.

Katada, S., Hirokawa, T., Oka, Y., Suwa, M., & Touhara, K. (2005). Structural basis for a broad but selective ligand spectrum of a mouse olfactory receptor: mapping the odorant-binding site. *J.Neurosci.* **25**, 1806-1815.

Kaupp, U. B., Niidome, T., Tanabe, T., Terada, S., Bonigk, W., Stuhmer, W., Cook, N. J., Kangawa, K., Matsuo, H., Hirose, T., & . (1989). Primary structure and functional expression from complementary DNA of the rod photoreceptor cyclic GMP-gated channel. *Nature* **342**, 762-766.

Kaupp, U. B. & Seifert, R. (2002). Cyclic nucleotide-gated ion channels. *Physiol Rev.* **82**, 769-824.

Kawai, F., Kurahashi, T., & Kaneko, A. (1996). T-type Ca2+ channel lowers the threshold of spike generation in the newt olfactory receptor cell. *J.Gen.Physiol* **108**, 525-535.

Keller, A. & Margolis, F. L. (1975). Immunological studies of the rat olfactory marker protein. *J.Neurochem.* **24**, 1101-1106.

Klabunde, T. & Hessler, G. (2002). Drug design strategies for targeting G-protein-coupled receptors. *Chembiochem.* **3**, 928-944.

Kleene, S. J. (1993). Origin of the chloride current in olfactory transduction. *Neuron* **11**, 123-132.

Kleene, S. J. (1995). Block by external calcium and magnesium of the cyclic-nucleotide-activated current in olfactory cilia. *Neuroscience* **66**, 1001-1008.

Kleene, S. J. (1997). High-gain, low-noise amplification in olfactory transduction. *Biophys.J.* **73**, 1110-1117.

Kleene, S. J. (1999). Both external and internal calcium reduce the sensitivity of the olfactory cyclic-nucleotide-gated channel to CAMP. *J.Neurophysiol.* **81**, 2675-2682.

Kleene, S. J. (2008). The Electrochemical Basis of Odor Transduction in Vertebrate Olfactory Cilia. *Chem.Senses*.

Kleene, S. J. & Gesteland, R. C. (1981). Dissociation of frog olfactory epithelium with N-ethylmaleimide. *Brain Res.* **229**, 536-540.

Kleene, S. J. & Gesteland, R. C. (1991). Calcium-activated chloride conductance in frog olfactory cilia. *J.Neurosci.* **11**, 3624-3629.

Kleene, S. J., Gesteland, R. C., & Bryant, S. H. (1994). An electrophysiological survey of frog olfactory cilia. *J.Exp.Biol.* **195**, 307-328.

Knowles, M. R., Clarke, L. L., & Boucher, R. C. (1991). Activation by extracellular nucleotides of chloride secretion in the airway epithelia of patients with cystic fibrosis. *N.Engl.J.Med.* **325**, 533-538.

Kramer, F., Stohr, H., & Weber, B. H. (2004). Cloning and characterization of the murine Vmd2 RFP-TM gene family. *Cytogenet.Genome Res.* **105**, 107-114.

Kramer, R. H. & Siegelbaum, S. A. (1992). Intracellular Ca2+ regulates the sensitivity of cyclic nucleotide-gated channels in olfactory receptor neurons. *Neuron* **9**, 897-906.

Kuluga, H. R., Leitch, C. C., Eichers, E. R., Badano, J. L., Lesemann, A., Hoskins, B. E., Lupski, J. R., Beales, P. L., Reed, R. R., & Katsanis, N. (2004). Loss of BBS proteins causes anosmia in humans and defects in olfactory cilia structure and function in the mouse. *Nature Genet.* **36**, 994-998.

Kumura, A. & Hartzell, H. C. (2000) Bimodal control of Ca^{2+}-activated Cl^{-} channel by different Ca^{2+} signala. *J Gen Physiol* **115**, 59-80.

Kurahashi, T. (1989). Activation by odorants of cation-selective conductance in the olfactory receptor cell isolated from the newt. *J.Physiol* **419**, 177-192.

Kurahashi, T. (1990). The response induced by intracellular cyclic AMP in isolated olfactory receptor cells of the newt. *J.Physiol* **430**, 355-371.

Kurahashi, T. & Kaneko, A. (1991). High density cAMP-gated channels at the ciliary membrane in the olfactory receptor cell. *Neuroreport* **2**, 5-8.

Kurahashi, T. & Kaneko, A. (1993). Gating properties of the cAMP-gated channel in toad olfactory receptor cells. *J.Physiol* **466**, 287-302.

Kurahashi, T. & Menini, A. (1997). Mechanism of odorant adaptation in the olfactory receptor cell. *Nature* **385**, 725-729.

Kurahashi, T. & Shibuya, T. (1990). Ca2(+)-dependent adaptive properties in the solitary olfactory receptor cell of the newt. *Brain Res.* **515**, 261-268.

Kurahashi, T. & Yau, K. W. (1993). Co-existence of cationic and chloride components in odorant-induced current of vertebrate olfactory receptor cells. *Nature* **363**, 71-74.

Kurahashi, T. & Yau, K. W. (1994). Olfactory transduction. Tale of an unusual chloride current. *Curr.Biol.* **4**, 256-258.

Lagostena, L. & Menini, A. (2003). Whole-cell recordings and photolysis of caged compounds in olfactory sensory neurons isolated from the mouse. *Chem.Senses* **28**, 705-716.

Large, W. A. & Wang, Q. (1996). Characteristics and physiological role of the Ca(2+)-activated Cl- conductance in smooth muscle. *Am.J.Physiol* **271**, C435-C454.

Larsson, H. P., Kleene, S. J., & Lecar, H. (1997). Noise analysis of ion channels in non-space-clamped cables: estimates of channel parameters in olfactory cilia. *Biophys.J.* **72**, 1193-1203.

Leinders-Zufall, T., Greer, C. A., Shepherd, G. M., & Zufall, F. (1998). Imaging odor-induced calcium transients in single olfactory cilia: specificity of activation and role in transduction. *J.Neurosci.* **18**, 5630-5639.

Leinders-Zufall, T., Ma, M., & Zufall, F. (1999). Impaired odor adaptation in olfactory receptor neurons after inhibition of Ca2+/calmodulin kinase II. *J.Neurosci.* **19**, RC19.

Leinders-Zufall, T., Rand, M. N., Shepherd, G. M., Greer, C. A., & Zufall, F. (1997). Calcium entry through cyclic nucleotide-gated channels in individual cilia of olfactory receptor cells: spatiotemporal dynamics. *J.Neurosci.* **17**, 4136-4148.

Lewcock, J. W. & Reed, R. R. (2004). A feedback mechanism regulates monoallelic odorant receptor expression. *Proc.Natl.Acad.Sci.U.S.A* **101**, 1069-1074.

Li, J., Ishii, T., Feinstein, P., & Mombaerts, P. (2004). Odorant receptor gene choice is reset by nuclear transfer from mouse olfactory sensory neurons. *Nature* **428**, 393-399.

Lidow, M. S. & Menco, B. P. (1984). Observations on axonemes and membranes of olfactory and respiratory cilia in frogs and rats using tannic acid-supplemented fixation and photographic rotation. *J.Ultrastruct.Res.* **86**, 18-30.

Liman, E. R. & Buck, L. B. (1994). A second subunit of the olfactory cyclic nucleotide-gated channel confers high sensitivity to cAMP. *Neuron* **13**, 611-621.

Liman, E. R. & Corey, D. P. (1996). Electrophysiological characterization of chemosensory neurons from the mouse vomeronasal organ. *J.Neurosci.* **16**, 4625-4637.

Lin, W., Arellano, J., Slotnick, B., & Restrepo, D. (2004). Odors detected by mice deficient in cyclic nucleotide-gated channel subunit A2 stimulate the main olfactory system. *J.Neurosci.* **24**, 3703-3710.

Lindau, M. & Neher, E. (1988). Patch-clamp techniques for time-resolved capacitance measurements in single cells. *Pflugers Arch.* **411**, 137-146.

Lindemann, B. (1996). Taste reception. *Physiol Rev.* **76**, 718-766.

Lindemann, B. (2001). Predicted profiles of ion concentrations in olfactory cilia in the steady state. *Biophys.J.* **80**, 1712-1721.

Linsenmeier, R. A. & Steinberg, R. H. (1982). Origin and sensitivity of the light peak in the intact cat eye. *J.Physiol* **331**, 653-673.

Liu, A. H., Zhang, X., Stolovitzky, G. A., Califano, A., & Firestein, S. J. (2003). Motif-based construction of a functional map for mammalian olfactory receptors. *Genomics* **81**, 443-456.

Liu, M., Chen, T. Y., Ahamed, B., Li, J., & Yau, K. W. (1994). Calcium-calmodulin modulation of the olfactory cyclic nucleotide-gated cation channel. *Science* **266**, 1348-1354.

Lowe, G. (2003). Electrical signaling in the olfactory bulb. *Curr.Opin.Neurobiol.* **13**, 476-481.

Lowe, G. & Gold, G. H. (1993a). Contribution of the ciliary cyclic nucleotide-gated conductance to olfactory transduction in the salamander. *J.Physiol* **462**, 175-196.

Lowe, G. & Gold, G. H. (1991). The spatial distributions of odorant sensitivity and odorant-induced currents in salamander olfactory receptor cells. *J.Physiol* **442**, 147-168.

Lowe, G. & Gold, G. H. (1993b). Nonlinear amplification by calcium-dependent chloride channels in olfactory receptor cells. *Nature* **366**, 283-286.

Lowe, G., Nakamura, T., & Gold, G. H. (1989). Adenylate cyclase mediates olfactory transduction for a wide variety of odorants. *Proc.Natl.Acad.Sci.U.S.A* **86**, 5641-5645.

Ludwig, J., Margalit, T., Eismann, E., Lancet, D., & Kaupp, U. B. (1990). Primary structure of cAMP-gated channel from bovine olfactory epithelium. *FEBS Lett.* **270**, 24-29.

Lynch, J. W. & Barry, P. H. (1989). Action potentials initiated by single channels opening in a small neuron (rat olfactory receptor). *Biophys.J.* **55**, 755-768.

Lynch, J. W. & Barry, P. H. (1991). Inward rectification in rat olfactory receptor neurons. *Proc.R.Soc.Lond B Biol.Sci.* **243**, 149-153.

Lynch, J. W. & Lindemann, B. (1994). Cyclic nucleotide-gated channels of rat olfactory receptor cells: divalent cations control the sensitivity to cAMP. *J.Gen.Physiol* **103**, 87-106.

Ma, M., Chen, W. R., & Shepherd, G. M. (1999). Electrophysiological characterization of rat and mouse olfactory receptor neurons from an intact epithelial preparation. *J.Neurosci.Methods* **92**, 31-40.

Malnic, B., Hirono, J., Sato, T., & Buck, L. B. (1999). Combinatorial receptor codes for odors. *Cell* **96**, 713-723.

Manivet, P., Schneider, B., Smith, J. C., Choi, D. S., Maroteaux, L., Kellermann, O., & Launay, J. M. (2002). The serotonin binding site of human and murine 5-HT2B receptors: molecular modeling and site-directed mutagenesis. *J.Biol.Chem.* **277**, 17170-17178.

Marchant, D., Yu, K., Bigot, K., Roche, O., Germain, A., Bonneau, D., Drouin-Garraud, V., Schorderet, D. F., Munier, F., Schmidt, D., Le Neindre, P., Marsac, C., Menasche, M., Dufier, J. L., Fischmeister, R., Hartzell, C., & Abitbol, M. (2007). New VMD2 gene mutations identified in patients affected by Best vitelliform macular dystrophy. *J.Med.Genet.* **44**, e70.

Maricq, A. V. & Korenbrot, J. I. (1988). Calcium and calcium-dependent chloride currents generate action potentials in solitary cone photoreceptors. *Neuron* **1**, 503-515.

Marmorstein, A. D. & Kinnick, T. R. (2007). Focus on molecules: bestrophin (best-1). *Exp.Eye Res.* **85**, 423-424.

Marmorstein, A. D. & Marmorstein, L. Y. (2007). The challenge of modeling macular degeneration in mice. *Trends Genet.* **23**, 225-231.

Marmorstein, A. D., Marmorstein, L. Y., Rayborn, M., Wang, X., Hollyfield, J. G., & Petrukhin, K. (2000). Bestrophin, the product of the Best vitelliform macular dystrophy gene (VMD2), localizes to the basolateral plasma membrane of the retinal pigment epithelium. *Proc.Natl.Acad.Sci.U.S.A* **97**, 12758-12763.

Marmorstein, A. D., Stanton, J. B., Yocom, J., Bakall, B., Schiavone, M. T., Wadelius, C., Marmorstein, L. Y., & Peachey, N. S. (2004). A model of best vitelliform macular dystrophy in rats. *Invest Ophthalmol.Vis.Sci.* **45**, 3733-3739.

Marmorstein, L. Y., Wu, J., McLaughlin, P., Yocom, J., Karl, M. O., Neussert, R., Wimmers, S., Stanton, J. B., Gregg, R. G., Strauss, O., Peachey, N. S., & Marmorstein, A. D. (2006). The light peak of the electroretinogram is dependent on voltage-gated calcium channels and antagonized by bestrophin (best-1). *J.Gen.Physiol* **127**, 577-589.

Marquardt, A., Stohr, H., Passmore, L. A., Kramer, F., Rivera, A., & Weber, B. H. (1998). Mutations in a novel gene, VMD2, encoding a protein of unknown properties cause juvenile-onset vitelliform macular dystrophy (Best's disease). *Hum.Mol.Genet.* **7**, 1517-1525.

Martensson, I. L., Keenan, R. A., & Licence, S. (2007). The pre-B-cell receptor. *Curr.Opin.Immunol.* **19**, 137-142.

Mashukova, A., Spehr, M., Hatt, H., & Neuhaus, E. M. (2006). Beta-arrestin2-mediated internalization of mammalian odorant receptors. *J.Neurosci.* **26**, 9902-9912.

Matsuzaki, O., Bakin, R. E., Cai, X., Menco, B. P., & Ronnett, G. V. (1999). Localization of the olfactory cyclic nucleotide-gated channel subunit 1 in normal, embryonic and regenerating olfactory epithelium. *Neuroscience* **94**, 131-140.

Maue, R. A. & Dionne, V. E. (1987). Patch-clamp studies of isolated mouse olfactory receptor neurons. *J.Gen.Physiol* **90**, 95-125.

Mayer, M. L. (1985). A calcium-activated chloride current generates the after-depolarization of rat sensory neurones in culture. *J.Physiol* **364**, 217-239.

McBride, D. W., Jr. & Roper, S. D. (1991). Ca(2+)-dependent chloride conductance in Necturus taste cells. *J.Membr.Biol.* **124**, 85-93.

Mehta, A. (2005). CFTR: more than just a chloride channel. *Pediatr.Pulmonol.* **39**, 292-298.

Melvin, J. E., Koek, L., & Zhang, G. H. (1991). A capacitative Ca2+ influx is required for sustained fluid secretion in sublingual mucous acini. *Am.J.Physiol* **261**, G1043-G1050.

Men, G., Batioglu, F., Ozkan, S. S., Atilla, H., Ozdamar, Y., & Aslan, O. (2004). Best's vitelliform macular dystrophy with pseudohypopyon: an optical coherence tomography study. *Am.J.Ophthalmol.* **137**, 963-965.

Menco, B. P. (1980). Qualitative and quantitative freeze-fracture studies on olfactory and nasal respiratory epithelial surfaces of frog, ox, rat, and dog. III. Tight-junctions. *Cell Tissue Res.* **211**, 361-373.

Menco, B. P. (1997). Ultrastructural aspects of olfactory signaling. *Chem.Senses* **22**, 295-311.

Menco, B. P., Bruch, R. C., Dau, B., & Danho, W. (1992). Ultrastructural localization of olfactory transduction components: the G protein subunit Golf alpha and type III adenylyl cyclase. *Neuron* **8**, 441-453.

Menini, A., Lagostena, L., & Boccaccio, A. (2004). Olfaction: from odorant molecules to the olfactory cortex. *News Physiol Sci.* **19**, 101-104.

Meyer, M. R., Angele, A., Kremmer, E., Kaupp, U. B., & Muller, F. (2000). A cGMP-signaling pathway in a subset of olfactory sensory neurons. *Proc.Natl.Acad.Sci.U.S.A* **97**, 10595-10600.

Michalakis, S., Reisert, J., Geiger, H., Wetzel, C., Zong, X., Bradley, J., Spehr, M., Huttl, S., Gerstner, A., Pfeifer, A., Hatt, H., Yau, K. W., & Biel, M. (2006). Loss of CNGB1 protein leads to olfactory dysfunction and subciliary cyclic nucleotide-gated channel trapping. *J.Biol.Chem.* **281**, 35156-35166.

Michaloski, J. S., Galante, P. A., & Malnic, B. (2006). Identification of potential regulatory motifs in odorant receptor genes by analysis of promoter sequences. *Genome Res.* **16**, 1091-1098.

Miledi, R. (1982). A calcium-dependent transient outward current in Xenopus laevis oocytes. *Proc.R.Soc.Lond B Biol.Sci.* **215**, 491-497.

Milenkovic, V. M., Rivera, A., Horling, F., & Weber, B. H. (2007). Insertion and topology of normal and mutant bestrophin-1 in the endoplasmic reticulum membrane. *J.Biol.Chem.* **282**, 1313-1321.

Mohler, C. W. & Fine, S. L. (1981). Long-term evaluation of patients with Best's vitelliform dystrophy. *Ophthalmology* **88**, 688-692.

Mombaerts, P. (1999). Seven-transmembrane proteins as odorant and chemosensory receptors. *Science* **286**, 707-711.

Mombaerts, P. (2001). The human repertoire of odorant receptor genes and pseudogenes. *Annu.Rev.Genomics Hum.Genet.* **2**, 493-510.

Mombaerts, P. (2004b). Genes and ligands for odorant, vomeronasal and taste receptors. *Nat.Rev.Neurosci.* **5**, 263-278.

Mombaerts, P. (2004a). Genes and ligands for odorant, vomeronasal and taste receptors. *Nat.Rev.Neurosci.* **5**, 263-278.

Mombaerts, P., Wang, F., Dulac, C., Chao, S. K., Nemes, A., Mendelsohn, M., Edmondson, J., & Axel, R. (1996a). Visualizing an olfactory sensory map. *Cell* **87**, 675-686.

Mombaerts, P., Wang, F., Dulac, C., Chao, S. K., Nemes, A., Mendelsohn, M., Edmondson, J., & Axel, R. (1996b). Visualizing an olfactory sensory map. *Cell* **87**, 675-686.

Morrison, E. E. & Costanzo, R. M. (1990). Morphology of the human olfactory epithelium. *J.Comp Neurol.* **297**, 1-13.

Muller, F., Vantler, M., Weitz, D., Eismann, E., Zoche, M., Koch, K. W., & Kaupp, U. B. (2001). Ligand sensitivity of the 2 subunit from the bovine cone cGMP-gated channel is modulated by protein kinase C but not by calmodulin. *J.Physiol* **532**, 399-409.

Mullins, R. F., Kuehn, M. H., Faidley, E. A., Syed, N. A., & Stone, E. M. (2007). Differential macular and peripheral expression of bestrophin in human eyes and its implication for best disease. *Invest Ophthalmol.Vis.Sci.* **48**, 3372-3380.

Munger, S. D., Lane, A. P., Zhong, H., Leinders-Zufall, T., Yau, K. W., Zufall, F., & Reed, R. R. (2001). Central role of the CNGA4 channel subunit in Ca2+-calmodulin-dependent odor adaptation. *Science* **294**, 2172-2175.

Nache, V., Schulz, E., Zimmer, T., Kusch, J., Biskup, C., Koopmann, R., Hagen, V., & Benndorf, K. (2005). Activation of olfactory-type cyclic nucleotide-gated channels is highly cooperative. *J.Physiol* **569**, 91-102.

Nakamura, T. & Gold, G. H. (1987). A cyclic nucleotide-gated conductance in olfactory receptor cilia. *Nature* **325**, 442-444.

Nakamura, T., Kaneko, H., & Nishida, N. (1997). Direct measurement of the chloride concentration in newt olfactory receptors with the fluorescent probe. *Neurosci.Lett.* **237**, 5-8.

Nickell, W. T., Kleene, N. K., Gesteland, R. C., & Kleene, S. J. (2006). Neuronal chloride accumulation in olfactory epithelium of mice lacking NKCC1. *J.Neurophysiol.* **95**, 2003-2006.

Nickell, W. T., Kleene, N. K., & Kleene, S. J. (2007). Mechanisms of neuronal chloride accumulation in intact mouse olfactory epithelium. *J.Physiol* **583**, 1005-1020.

Niimura, Y. & Nei, M. (2003). Evolution of olfactory receptor genes in the human genome. *Proc.Natl.Acad.Sci.U.S.A* **100**, 12235-12240.

Oka, Y., Omura, M., Kataoka, H., & Touhara, K. (2004). Olfactory receptor antagonism between odorants. *EMBO J.* **23**, 120-126.

Okada, Y., Teeter, J. H., & Restrepo, D. (1994). Inositol 1,4,5-trisphosphate-gated conductance in isolated rat olfactory neurons. *J.Neurophysiol.* **71**, 595-602.

Omura, M., Sekine, H., Shimizu, T., Kataoka, H., & Touhara, K. (2003). In situ Ca2+ imaging of odor responses in a coronal olfactory epithelium slice. *Neuroreport* **14**, 1123-1127.

Pace, U., Hanski, E., Salomon, Y., & Lancet, D. (1985). Odorant-sensitive adenylate cyclase may mediate olfactory reception. *Nature* **316**, 255-258.

Peng, C., Rich, E. D., & Varnum, M. D. (2004). Subunit configuration of heteromeric cone cyclic nucleotide-gated channels. *Neuron* **42**, 401-410.

Peppel, K., Boekhoff, I., McDonald, P., Breer, H., Caron, M. G., & Lefkowitz, R. J. (1997). G protein-coupled receptor kinase 3 (GRK3) gene disruption leads to loss of odorant receptor desensitization. *J.Biol.Chem.* **272**, 25425-25428.

Peterson, W. M., Meggyesy, C., Yu, K., & Miller, S. S. (1997). Extracellular ATP activates calcium signaling, ion, and fluid transport in retinal pigment epithelium. *J.Neurosci.* **17**, 2324-2337.

Petrukhin, K., Koisti, M. J., Bakall, B., Li, W., Xie, G., Marknell, T., Sandgren, O., Forsman, K., Holmgren, G., Andreasson, S., Vujic, M., Bergen, A. A., McGarty-Dugan, V., Figueroa, D., Austin, C. P., Metzker, M. L., Caskey, C. T., & Wadelius, C. (1998). Identification of the gene responsible for Best macular dystrophy. *Nat.Genet.* **19**, 241-247.

Pianta, M. J., Aleman, T. S., Cideciyan, A. V., Sunness, J. S., Li, Y., Campochiaro, B. A., Campochiaro, P. A., Zack, D. J., Stone, E. M., & Jacobson, S. G. (2003). In vivo micropathology of Best macular dystrophy with optical coherence tomography. *Exp.Eye Res.* **76**, 203-211.

Pierro, L., Tremolada, G., Introini, U., Calori, G., & Brancato, R. (2002). Optical coherence tomography findings in adult-onset foveomacular vitelliform dystrophy. *Am.J.Ophthalmol.* **134**, 675-680.

Pifferi, S., Boccaccio, A., & Menini, A. (2006a). Cyclic nucleotide-gated ion channels in sensory transduction. *FEBS Lett.* **580**, 2853-2859.

Pifferi, S., Pascarella, G., Boccaccio, A., Mazzatenta, A., Gustincich, S., Menini, A., & Zucchelli, S. (2006b). Bestrophin-2 is a candidate calcium-activated chloride channel involved in olfactory transduction. *Proc.Natl.Acad.Sci.U.S.A* **103**, 12929-12934.

Pun, R. Y. & Kleene, S. J. (2004). An estimate of the resting membrane resistance of frog olfactory receptor neurones. *J.Physiol* **559**, 535-542.

Pusch, M. (2004). Ca(2+)-activated chloride channels go molecular. *J.Gen.Physiol* **123**, 323-325.

Pyrski, M., Koo, J. H., Polumuri, S. K., Ruknudin, A. M., Margolis, J. W., Schulze, D. H., & Margolis, F. L. (2007). Sodium/calcium exchanger expression in the mouse and rat olfactory systems. *J.Comp Neurol.* **501**, 944-958.

Qu, Z., Chien, L. T., Cui, Y., & Hartzell, H. C. (2006). The anion-selective pore of the bestrophins, a family of chloride channels associated with retinal degeneration. *J.Neurosci.* **26**, 5411-5419.

Qu, Z., Fischmeister, R., & Hartzell, C. (2004). Mouse bestrophin-2 is a bona fide Cl(-) channel: identification of a residue important in anion binding and conduction. *J.Gen.Physiol* **123**, 327-340.

Qu, Z. & Hartzell, C. (2004). Determinants of anion permeation in the second transmembrane domain of the mouse bestrophin-2 chloride channel. *J.Gen.Physiol* **124**, 371-382.

Qu, Z. & Hartzell, H. C. (2000). Anion permeation in Ca(2+)-activated Cl(-) channels. *J.Gen.Physiol* **116**, 825-844.

Qu, Z. & Hartzell, H. C. (2001). Functional geometry of the permeation pathway of Ca2+-activated Cl-channels inferred from analysis of voltage-dependent block. *J.Biol.Chem.* **276**, 18423-18429.

Qu, Z., Wei, R. W., Mann, W., & Hartzell, H. C. (2003). Two bestrophins cloned from Xenopus laevis oocytes express Ca(2+)-activated Cl(-) currents. *J.Biol.Chem.* **278**, 49563-49572.

Rajan, S., Plant, L. D., Rabin, M. L., Butler, M. H., & Goldstein, S. A. (2005). Sumoylation silences the plasma membrane leak K+ channel K2P1. *Cell* **121**, 37-47.

Rattner, A. & Nathans, J. (2006). Macular degeneration: recent advances and therapeutic opportunities. *Nat.Rev.Neurosci.* **7**, 860-872.

Reisert, J., Bauer, P. J., Yau, K. W., & Frings, S. (2003). The Ca-activated Cl channel and its control in rat olfactory receptor neurons. *J.Gen.Physiol.* **122**, 349-363.

Reisert, J., Lai, J., Yau, K. W., & Bradley, J. (2005). Mechanism of the excitatory Cl-response in mouse olfactory receptor neurons. *Neuron* **45**, 553-561.

Reisert, J. & Matthews, H. R. (1998). Na+-dependent Ca2+ extrusion governs response recovery in frog olfactory receptor cells. *J.Gen.Physiol.* **112**, 529-535.

Reisert, J. & Matthews, H. R. (1999). Adaptation of the odour-induced response in frog olfactory receptor cells. *J.Physiol.* **519 Pt 3**, 801-813.

Reisert, J. & Matthews, H. R. (2001a). Response properties of isolated mouse olfactory receptor cells. *J.Physiol.* **530**, 113-122.

Reisert, J. & Matthews, H. R. (2001b). Simultaneous recording of receptor current and intraciliary Ca2+ concentration in salamander olfactory receptor cells. *J.Physiol.* **535**, 637-645.

Reisert, J., Yau, K. W., & Margolis, F. L. (2007). Olfactory marker protein modulates the cAMP kinetics of the odour-induced response in cilia of mouse olfactory receptor neurons. *J.Physiol* **585**, 731-740.

Ressler, K. J., Sullivan, S. L., & Buck, L. B. (1993). A zonal organization of odorant receptor gene expression in the olfactory epithelium. *Cell* **73**, 597-609.

Restrepo, D., Miyamoto, T., Bryant, B. P., & Teeter, J. H. (1990). Odor stimuli trigger influx of calcium into olfactory neurons of the channel catfish. *Science* **249**, 1166-1168.

Reuter, D., Zierold, K., Schroder, W. H., & Frings, S. (1998). A depolarizing chloride current contributes to chemoelectrical transduction in olfactory sensory neurons in situ. *J.Neurosci.* **18**, 6623-6630.

Rivkees, S. A., Barbhaiya, H., & IJzerman, A. P. (1999). Identification of the adenine binding site of the human A1 adenosine receptor. *J.Biol.Chem.* **274**, 3617-3621.

Rodriguez, I. (2007). Odorant and pheromone receptor gene regulation in vertebrates. *Curr.Opin.Genet.Dev.* **17**, 465-470.

Rosenthal, R., Bakall, B., Kinnick, T., Peachey, N., Wimmers, S., Wadelius, C., Marmorstein, A., & Strauss, O. (2006). Expression of bestrophin-1, the product of the VMD2 gene, modulates voltage-dependent Ca2+ channels in retinal pigment epithelial cells. *FASEB J.* **20**, 178-180.

Rothman, A., Feinstein, P., Hirota, J., & Mombaerts, P. (2005). The promoter of the mouse odorant receptor gene M71. *Mol.Cell Neurosci.* **28**, 535-546.

Saito, H., Kubota, M., Roberts, R. W., Chi, Q., & Matsunami, H. (2004). RTP family members induce functional expression of mammalian odorant receptors. *Cell* **119**, 679-691.

Sammeta, N., Yu, T. T., Bose, S. C., & McClintock, T. S. (2007). Mouse olfactory sensory neurons express 10,000 genes. *J.Comp Neurol.* **502**, 1138-1156.

Sato, K. & Suzuki, N. (2000). The contribution of a Ca(2+)-activated Cl(-) conductance to amino-acid-induced inward current responses of ciliated olfactory neurons of the rainbow trout. *J.Exp.Biol.* **203**, 253-262.

Sato, Y., Miyasaka, N., & Yoshihara, Y. (2007). Hierarchical regulation of odorant receptor gene choice and subsequent axonal projection of olfactory sensory neurons in zebrafish. *J.Neurosci.* **27**, 1606-1615.

Sautter, A., Zong, X., Hofmann, F., & Biel, M. (1998). An isoform of the rod photoreceptor cyclic nucleotide-gated channel beta subunit expressed in olfactory neurons. *Proc.Natl.Acad.Sci.U.S.A* **95**, 4696-4701.

Schild, D. (1989). Whole-cell currents in olfactory receptor cells of Xenopus laevis. *Exp.Brain Res.* **78**, 223-232.

Schild, D. & Restrepo, D. (1998). Transduction mechanisms in vertebrate olfactory receptor cells. *Physiol Rev.* **78**, 429-466.

Schleicher, S., Boekhoff, I., Arriza, J., Lefkowitz, R. J., & Breer, H. (1993). A beta-adrenergic receptor kinase-like enzyme is involved in olfactory signal termination. *Proc.Natl.Acad.Sci.U.S.A* **90**, 1420-1424.

Schoppa, N. E. & Urban, N. N. (2003). Dendritic processing within olfactory bulb circuits. *Trends Neurosci.* **26**, 501-506. Schroeder, B. C., Chen, T., Jan, Y. N., & Jan, J. Y. (2008). Expression clonig of TMEM16a as Calcium-activated Chloride channel subunit. *Cell* **134**, 1019-1929

Schwiebert, E. M., Benos, D. J., Egan, M. E., Stutts, M. J., & Guggino, W. B. (1999). CFTR is a conductance regulator as well as a chloride channel. *Physiol Rev.* **79**, S145-S166.

Scott, J. W. & Scott-Johnson, P. E. (2002). The electroolfactogram: a review of its history and uses. *Microsc.Res.Tech.* **58**, 152-160.

Scott, R. H., McGuirk, S. M., & Dolphin, A. C. (1988). Modulation of divalent cation-activated chloride ion currents. *Br.J.Pharmacol.* **94**, 653-662.

Serizawa, S., Miyamichi, K., Nakatani, H., Suzuki, M., Saito, M., Yoshihara, Y., & Sakano, H. (2003). Negative feedback regulation ensures the one receptor-one olfactory neuron rule in mouse. *Science* **302**, 2088-2094.

Serizawa, S., Miyamichi, K., & Sakano, H. (2004). One neuron-one receptor rule in the mouse olfactory system. *Trends Genet.* **20**, 648-653.

Shirley, S. G., Robinson, C. J., Dickinson, K., Aujla, R., & Dodd, G. H. (1986). Olfactory adenylate cyclase of the rat. Stimulation by odorants and inhibition by Ca2+. *Biochem.J.* **240**, 605-607.

Shykind, B. M. (2005). Regulation of odorant receptors: one allele at a time. *Hum.Mol.Genet.* **14 Spec No 1**, R33-R39.

Sicard, G. & Holley, A. (1984). Receptor cell responses to odorants: similarities and differences among odorants. *Brain Res.* **292**, 283-296.

Sinnarajah, S., Dessauer, C. W., Srikumar, D., Chen, J., Yuen, J., Yilma, S., Dennis, J. C., Morrison, E. E., Vodyanoy, V., & Kehrl, J. H. (2001). RGS2 regulates signal transduction in olfactory neurons by attenuating activation of adenylyl cyclase III. *Nature* **409**, 1051-1055.

Sklar, P. B., Anholt, R. R., & Snyder, S. H. (1986). The odorant-sensitive adenylate cyclase of olfactory receptor cells. Differential stimulation by distinct classes of odorants. *J.Biol.Chem.* **261**, 15538-15543.

Smith, S. S., Steinle, E. D., Meyerhoff, M. E., & Dawson, D. C. (1999). Cystic fibrosis transmembrane conductance regulator. Physical basis for lyotropic anion selectivity patterns. *J.Gen.Physiol* **114**, 799-818.

Song, Y., Cygnar, K. D., Sagdullaev, B., Valley, M., Hirsh, S., Stephan, A., Reisert, J., & Zhao, H. (2008). Olfactory CNG channel desensitization by Ca2+/CaM via the B1b subunit affects response termination but not sensitivity to recurring stimulation. *Neuron* **58**, 374-386.

Sparrow, J. R. & Boulton, M. (2005). RPE lipofuscin and its role in retinal pathobiology. *Exp.Eye Res.* **80**, 595-606.

Sparrow, J. R. & Cai, B. (2001). Blue light-induced apoptosis of A2E-containing RPE: involvement of caspase-3 and protection by Bcl-2. *Invest Ophthalmol.Vis.Sci.* **42**, 1356-1362.

Stapleton, S. R., Scott, R. H., & Bell, B. A. (1994). Effects of metabolic blockers on Ca(2+)-dependent currents in cultured sensory neurones from neonatal rats. *Br.J.Pharmacol.* **111**, 57-64.

Stohr, H., Marquardt, A., Nanda, I., Schmid, M., & Weber, B. H. (2002). Three novel human VMD2-like genes are members of the evolutionary highly conserved RFP-TM family. *Eur.J.Hum.Genet.* **10**, 281-284.

Strauss, O. (2005). The retinal pigment epithelium in visual function. *Physiol Rev.* **85**, 845-881.

Strotmann, J., Wanner, I., Krieger, J., Raming, K., & Breer, H. (1992). Expression of odorant receptors in spatially restricted subsets of chemosensory neurones. *Neuroreport* **3**, 1053-1056.

Sullivan, S. L., Ressler, K. J., & Buck, L. B. (1994). Odorant receptor diversity and patterned gene expression in the mammalian olfactory epithelium. *Prog.Clin.Biol.Res.* **390**, 75-84.

Sun, H., Tsunenari, T., Yau, K. W., & Nathans, J. (2002). The vitelliform macular dystrophy protein defines a new family of chloride channels. *Proc.Natl.Acad.Sci.U.S.A* **99**, 4008-4013.

Takeuchi, H., Imanaka, Y., Hirono, J., & Kurahashi, T. (2003). Cross-adaptation between olfactory responses induced by two subgroups of odorant molecules. *J.Gen.Physiol* **122**, 255-264.

Takeuchi, H. & Kurahashi, T. (2002). Photolysis of caged cyclic AMP in the ciliary cytoplasm of the newt olfactory receptor cell. *J.Physiol* **541**, 825-833.

Takeuchi, H. & Kurahashi, T. (2003). Identification of second messenger mediating signal transduction in the olfactory receptor cell. *J.Gen.Physiol* **122**, 557-567.

Takeuchi, H. & Kurahashi, T. (2005). Mechanism of signal amplification in the olfactory sensory cilia. *J.Neurosci.* **25**, 11084-11091.

Takeuchi, H. & Kurahashi, T. (2008). Distribution, amplification, and summation of cyclic nucleotide sensitivities within single olfactory sensory cilia. *J.Neurosci.* **28**, 766-775.

Tarran, R., Loewen, M. E., Paradiso, A. M., Olsen, J. C., Gray, M. A., Argent, B. E., Boucher, R. C., & Gabriel, S. E. (2002). Regulation of murine airway surface liquid volume by CFTR and Ca2+-activated Cl- conductances. *J.Gen.Physiol* **120**, 407-418.

Taylor, R. & Roper, S. (1994). Ca(2+)-dependent Cl- conductance in taste cells from Necturus. *J.Neurophysiol.* **72**, 475-478.

Thoreson, W. B. & Burkhardt, D. A. (1991). Ionic influences on the prolonged depolarization of turtle cones in situ. *J.Neurophysiol.* **65**, 96-110.

Tirindelli, R. & Ryba, N. J. (1996). The G-protein gamma-subunit G gamma 8 is expressed in the developing axons of olfactory and vomeronasal neurons. *Eur.J.Neurosci.* **8**, 2388-2398.

Tomaru, A. & Kurahashi, T. (2005). Mechanisms determining the dynamic range of the bullfrog olfactory receptor cell. *J.Neurophysiol.* **93**, 1880-1888.

Trotier, D. (1986). A patch-clamp analysis of membrane currents in salamander olfactory receptor cells. *Pflugers Arch.* **407**, 589-595.

Trotier, D. & Doving, K. B. (1996). Direct influence of the sodium pump on the membrane potential of vomeronasal chemoreceptor neurones in frog. *J.Physiol* **490 (Pt 3)**, 611-621.

Tsunenari, T., Nathans, J., & Yau, K. W. (2006). Ca2+-activated Cl- Current from Human Bestrophin-4 in Excised Membrane Patches. *J.Gen.Physiol*.

Tsunenari, T., Sun, H., Williams, J., Cahill, H., Smallwood, P., Yau, K. W., & Nathans, J. (2003). Structure-function analysis of the bestrophin family of anion channels. *J.Biol.Chem.* **278**, 41114-41125.

Varnum, M. D. & Zagotta, W. N. (1997). Interdomain interactions underlying activation of cyclic nucleotide-gated channels. *Science* **278**, 110-113.

Vassalli, A., Rothman, A., Feinstein, P., Zapotocky, M., & Mombaerts, P. (2002). Minigenes impart odorant receptor-specific axon guidance in the olfactory bulb. *Neuron* **35**, 681-696.

Vassar, R., Ngai, J., & Axel, R. (1993). Spatial segregation of odorant receptor expression in the mammalian olfactory epithelium. *Cell* **74**, 309-318.

Vedantham, V. & Ramasamy, K. (2005). Optical coherence tomography in Best's disease: an observational case report. *Am.J.Ophthalmol.* **139**, 351-353.

Von Dannecker, L. E., Mercadante, A. F., & Malnic, B. (2005). Ric-8B, an olfactory putative GTP exchange factor, amplifies signal transduction through the olfactory-specific G-protein Galphaolf. *J.Neurosci.* **25**, 3793-3800.

Von Dannecker, L. E., Mercadante, A. F., & Malnic, B. (2006). Ric-8B promotes functional expression of odorant receptors. *Proc.Natl.Acad.Sci.U.S.A* **103**, 9310-9314.

Wahlstrom, B. A. (1973). A study on the action of noradrenaline on ionic content and sodium, potassium and chloride effluxes in the rat portal vein. *Acta Physiol Scand.* **89**, 522-530.

Webb, D. J. & Nuccitelli, R. (1985). Fertilization potential and electrical properties of the Xenopus laevis egg. *Dev.Biol.* **107**, 395-406.

Wei, J., Wayman, G., & Storm, D. R. (1996). Phosphorylation and inhibition of type III adenylyl cyclase by calmodulin-dependent protein kinase II in vivo. *J.Biol.Chem.* **271**, 24231-24235.

Weitz, D., Ficek, N., Kremmer, E., Bauer, P. J., & Kaupp, U. B. (2002). Subunit stoichiometry of the CNG channel of rod photoreceptors. *Neuron* **36**, 881-889.

Wong, S. T., Trinh, K., Hacker, B., Chan, G. C., Lowe, G., Gaggar, A., Xia, Z., Gold, G. H., & Storm, D. R. (2000). Disruption of the type III adenylyl cyclase gene leads to peripheral and behavioral anosmia in transgenic mice. *Neuron* **27**, 487-497.

Wright, E. M. & Diamond, J. M. (1977). Anion selectivity in biological systems. *Physiol Rev.* **57**, 109-156.

Wu, J., Marmorstein, A. D., Striessnig, J., & Peachey, N. S. (2007). Voltage-dependent calcium channel CaV1.3 subunits regulate the light peak of the electroretinogram. *J.Neurophysiol.* **97**, 3731-3735.

Yan, C., Zhao, A. Z., Bentley, J. K., Loughney, K., Ferguson, K., & Beavo, J. A. (1995). Molecular cloning and characterization of a calmodulin-dependent phosphodiesterase enriched in olfactory sensory neurons. *Proc.Natl.Acad.Sci.U.S.A* **92**, 9677-9681.

Yang, Y. D., Cho, H., Koo, J. Y., Tak, M. H., Cho, Y., Shim, W. S., Park, S. P., Lee, J., Lee, B., Kim, B. M., Raouf, R., Shin, Y. K., & Oh, U. (2008). TMEM16A confers receptor-activated calcium-dependent chloride conductance. *Nature*.

Yau, K. W. (1994). Phototransduction mechanism in retinal rods and cones. The Friedenwald Lecture. *Invest Ophthalmol.Vis.Sci.* **35**, 9-32.

Young, J. M., Friedman, C., Williams, E. M., Ross, J. A., Tonnes-Priddy, L., & Trask, B. J. (2002). Different evolutionary processes shaped the mouse and human olfactory receptor gene families. *Hum.Mol.Genet.* **11**, 535-546.

Young, J. M., Shykind, B. M., Lane, R. P., Tonnes-Priddy, L., Ross, J. A., Walker, M., Williams, E. M., & Trask, B. J. (2003). Odorant receptor expressed sequence tags demonstrate olfactory expression of over 400 genes, extensive alternate splicing and unequal expression levels. *Genome Biol.* **4**, R71.

Yu, K., Cui, Y., & Hartzell, H. C. (2006). The bestrophin mutation A243V, linked to adult-onset vitelliform macular dystrophy, impairs its chloride channel function. *Invest Ophthalmol.Vis.Sci.* **47**, 4956-4961.

Yu, K., Qu, Z., Cui, Y., & Hartzell, H. C. (2007). Chloride channel activity of bestrophin mutants associated with mild or late-onset macular degeneration. *Invest Ophthalmol.Vis.Sci.* **48**, 4694-4705.

Yu, K., Xiao, Q., Cui, G., Lee, A., & Hartzell, H. C. (2008). The best disease-linked Cl-channel hBest1 regulates Ca V 1 (L-type) Ca2+ channels via src-homology-binding domains. *J.Neurosci.* **28**, 5660-5670.

Zhainazarov, A. B. & Ache, B. W. (1995). Odor-induced currents in Xenopus olfactory receptor cells measured with perforated-patch recording. *J.Neurophysiol.* **74**, 479-483.

Zhang, X. & Firestein, S. (2002). The olfactory receptor gene superfamily of the mouse. *Nat.Neurosci.* **5**, 124-133.

Zhao, H. & Firestein, S. (1999). Vertebrate odorant receptors. *Cell Mol.Life Sci.* **56**, 647-659.

Zhao, H., Ivic, L., Otaki, J. M., Hashimoto, M., Mikoshiba, K., & Firestein, S. (1998). Functional expression of a mammalian odorant receptor. *Science* **279**, 237-242.

Zhao, H. & Reed, R. R. (2001). X inactivation of the OCNC1 channel gene reveals a role for activity-dependent competition in the olfactory system. *Cell* **104**, 651-660.

Zheng, J., Varnum, M. D., & Zagotta, W. N. (2003). Disruption of an intersubunit interaction underlies Ca2+-calmodulin modulation of cyclic nucleotide-gated channels. *J.Neurosci.* **23**, 8167-8175.

Zheng, J. & Zagotta, W. N. (2004). Stoichiometry and assembly of olfactory cyclic nucleotide-gated channels. *Neuron* **42**, 411-421.

Zhou, J., Jang, Y. P., Kim, S. R., & Sparrow, J. R. (2006). Complement activation by photooxidation products of A2E, a lipofuscin constituent of the retinal pigment epithelium. *Proc.Natl.Acad.Sci.U.S.A* **103**, 16182-16187.

Zhuang, H. & Matsunami, H. (2007). Synergism of accessory factors in functional expression of mammalian odorant receptors. *J.Biol.Chem.* **282**, 15284-15293.

Zozulya, S., Echeverri, F., & Nguyen, T. (2001). The human olfactory receptor repertoire. *Genome Biol.* **2**, RESEARCH0018.

Zufall, F. & Firestein, S. (1993). Divalent cations block the cyclic nucleotide-gated channel of olfactory receptor neurons. *J.Neurophysiol.* **69**, 1758-1768.

Zufall, F., Firestein, S., & Shepherd, G. M. (1991a). Analysis of single cyclic nucleotide-gated channels in olfactory receptor cells
ZUFALL1991A. *J.Neurosci.* **11**, 3573-3580.

Zufall, F., Shepherd, G. M., & Firestein, S. (1991b). Inhibition of the olfactory cyclic nucleotide gated ion channel by intracellular calcium
ZUFALL1991. *Proc.R.Soc.Lond B Biol.Sci.* **246**, 225-230.

FEBS Letters 580 (2006) 2853–2859

Minireview

Cyclic nucleotide-gated ion channels in sensory transduction

Simone Pifferi, Anna Boccaccio, Anna Menini*

International School for Advanced Studies, S.I.S.S.A., Sector of Neurobiology, Via Beirut 2-4, 34014 Trieste, Italy

Received 26 March 2006; accepted 31 March 2006

Available online 12 April 2006

Edited by Horst Feldmann

Abstract Cyclic nucleotide-gated (CNG) channels, directly activated by the binding of cyclic nucleotides, were first discovered in retinal rods, cones and olfactory sensory neurons. In the visual and olfactory systems, CNG channels mediate sensory transduction by conducting cationic currents carried primarily by sodium and calcium ions. In olfactory transduction, calcium in combination with calmodulin exerts a negative feedback on CNG channels that is the main molecular mechanism responsible for fast adaptation in olfactory sensory neurons. Six mammalian CNG channel genes are known and some human visual disorders are caused by mutations in retinal rod or cone CNG genes.

Keywords: Transduction; Sensory; Adaptation; Olfaction; cAMP; Channelopathy

1. Introduction

Ion channels directly gated by cGMP in retinal rods were first discovered 21 years ago [1]. Fesenko and collaborators [1] showed that cGMP directly activates a current in isolated patches of outer segment membrane of retinal rods. The current was activated by cGMP alone, without the presence of other factors such as ATP or kinases. Moreover, the cGMP-gated current could not be activated by AMP, GMP, ATP or GTP. The cGMP-gated current was shown to be cationic, and the dependence of current activation from cGMP concentration was well described by a Hill function with a coefficient of 1.8 [1]. The discovery of ion channels directly gated by cGMP occurred while studying the molecular mechanisms of phototransduction. Both Ca^{2+} and cGMP were considered as possible second messengers mediating the electrical response to light. However, the action of cGMP was at first believed to be indirect, because in those years the dogma that cyclic nucleotides acted on proteins only by phosphorylation mediated by a cyclic nucleotide-dependent kinase was still standing. Fesenko et al. [1] contributed to unravelling the molecular mechanisms of phototransduction showing that cGMP can directly activate ion channels. Similar channels were also found in cone photoreceptors [2]. Indeed in photoreceptors cGMP keeps ion channels open in the dark, allowing a continuous influx of Na^+ and Ca^{2+} (dark current), and Ca^{2+} is in turn extruded by a Na^+–Ca^{2+}–K^+ exchanger. Light absorption by rhodopsin triggers an enzymatic cascade that leads to the activation of a phosphodiesterase that hydrolyses cGMP to GMP and therefore produces a decrease in the cGMP-gated current. As a consequence photoreceptors hyperpolarize in response to light with a subsequent decrease in glutamate synaptic release (reviewed in [3,4]).

In 1987, Nakamura and Gold [5] detected a similar ionic current directly activated by cGMP or cAMP in the cilia of olfactory sensory neurons. Odorant molecules bind to odorant receptors and activate an enzymatic cascade that leads to an increase in the concentration of cAMP in the cilia, as will be described later in more detail (Fig. 1). Cyclic nucleotide-gated (CNG) channels have also been described in other neuronal and non-neuronal cells (reviewed in [6]).

2. CNG channel subunits

Kaupp et al. [7] first cloned the gene encoding for the CNG channel in bovine retinal rods beginning investigations at the molecular level of the physiological and biophysical properties of these ion channels. At present, six CNG channel genes have been identified in mammalian genomes. These genes code for four types of "A" subunits and two types of "B" subunits [8]. CNG channels are composed of four subunits forming a tetramer with a central pore. The topology of each subunit is similar to that of the cationic voltage-activated channels with six transmembrane spanning domains, a pore-loop domain between the fifth and sixth transmembrane domain, and intracellular N- and C-terminal regions. CNG channels are activated by the direct binding of cyclic nucleotides to a large C-terminal cyclic nucleotide-binding domain and are only weakly sensitive to membrane voltage (Fig. 3E).

Unfortunately, different nomenclatures for the CNG subunits have been used for several years in different laboratories, and therefore the reading of most of the previous papers may result confusing. We will use the most recent commonly agreed nomenclature for CNG channels [8] and indicate previous names in parenthesis.

Native retinal rod channels are composed of two types of subunits: CNGA1 (α1, CNG1, RCNC1) and CNGB1 (β1, CNG4, RCNC2) [7,9] with a stoichiometry of three CNGA1 and one CNGB1a (a B1 splice variant) subunits [10,11]. Retinal cone channels are also composed of two types of subunits: CNGA3

*Corresponding author. Fax: +39 040 2240470.
E-mail address: menini@sissa.it (A. Menini).

Abbreviation: CNG, cyclic nucleotide-gated

0014-5793/$32.00
doi:10.1016/j.febslet.2006.03.086

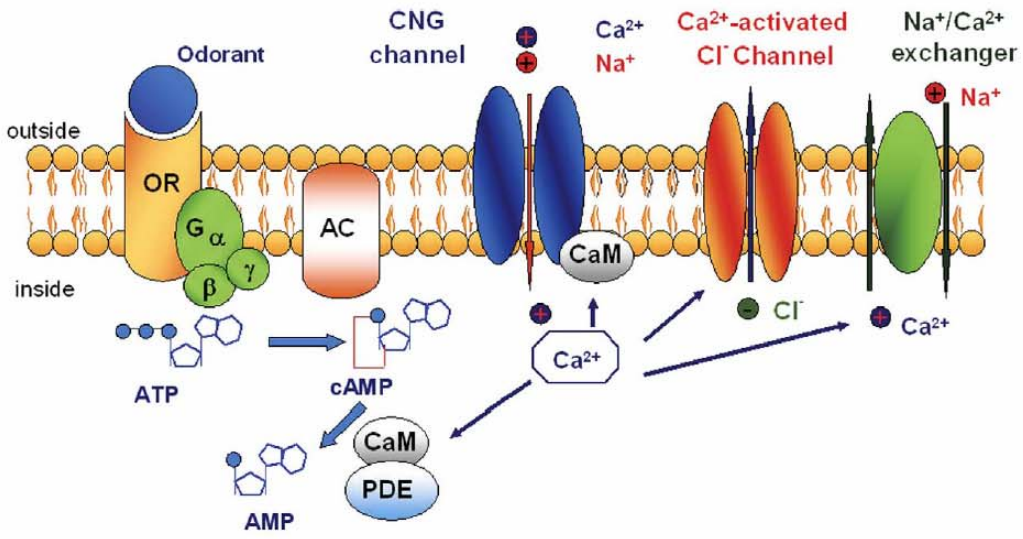

Fig. 1. Olfactory transduction in the cilia of olfactory sensory neurons. Odorant molecules bind to odorant receptors (OR) in the ciliary membrane activating a G-protein (G) that, in turn, stimulates an adenylate cyclase (AC). cAMP directly gates CNG channels causing an odorant-induced inward current carried by Na^+ and Ca^{2+} ions. The increased Ca^{2+} concentration in the cilia causes the opening of Ca^{2+}-activated Cl^- channels and the subsequent Cl^- efflux which further depolarizes the cell. Intracellular Ca^{2+} also binds to calmodulin (CaM) lowering the ligand sensitivity of the cAMP-gated channels. Ca^{2+}–calmodulin also stimulates the activity of a phosphodiesterase (PDE). Ca^{2+} is extruded by a Na^+/Ca^{2+} exchanger.

(α2, CNG3, CCNC1) and CNGB3 (β2, CNG6, CCNC2) [12,13] with a stoichiometry of two CNGA3 and two CNGB3 subunits [14]. Native channels of olfactory sensory neurons are instead composed of three types of subunits: CNGA2 (α3, CNG2, OCNC1), CNGA4 (α4, CNG5, OCNC2, CNGB2) and CNGB1 (β1, CNG4, RCNC2) [15–19] with a stoichiometry of two CNGA2, one CNGA4 and one CNGB1b (a B1 splice variant) [20] (Fig. 3E). The subunits CNGA1, CNGA2, and CNGA3 when expressed alone in heterologous systems can form a functional channel activated by cyclic nucleotides, whereas the other subunits cannot form functional channels but have a physiologically relevant modulatory role. Indeed, electrophysiological studies measuring the functional properties of the heterologously expressed principal subunits showed several differences with the respective native channels such as activation by cyclic nucleotides, ion permeation, sensitivity to blockers, and regulation by the complex Ca^{2+}–calmodulin, suggesting that additional subunits and/or modulatory components were still to be discovered [6,21,22]. Cloning of the genes of additional subunits allowed the study of the influence of the subunit composition on the channel properties [6,23–25]. As an example, Fig. 3C shows the comparison between currents activated by cAMP in homomeric CNGA2 channels expressed in HEK293 cells and native olfactory channels. The concentration of cAMP necessary to obtain 50% of the maximal current activation of homomeric CNGA2 channels was about 30 μM, while in heteromeric native channels was about 3 μM, corresponding to a 10-fold higher sensitivity for cAMP of native channels compared with homomeric CNGA2 channels.

The CNG subunit composition of retinal rods, cones or olfactory sensory neurons is tuned to a specific physiological role in sensory transduction. In this review, we will primarily focus on the olfactory CNG channel.

3. Olfactory transduction and adaptation

In vertebrates, volatile odorant molecules reach the olfactory epithelium in the nasal cavity and interact with odorant receptors located in the cilia of olfactory sensory neurons, where olfactory transduction occurs. Olfactory sensory neurons are bipolar neurons with a single dendrite that reaches the surface of the epithelium and terminates with a knob from which several cilia protrude. The binding of odorant molecules to odorant receptors [26] in the cilia triggers an enzymatic cascade that leads to an increase in the intraciliary concentration of cAMP (Fig. 1). cAMP causes the opening of the ciliary CNG channels that allow an influx of Na^+ and Ca^{2+} inside the cilia. Ca^{2+}-activated Cl^- channels are then activated in turn and, due to the unusually high intracellular Cl^- concentration, produce the outflow of Cl^-, contributing to the inward current [27]. As a result of the odorant binding the olfactory sensory neuron depolarizes. The depolarization spreads passively to the dendrite and soma of the neuron, triggering action potentials that are conducted along the axon to the olfactory bulb [28–30]. The olfactory CNG channel allows Ca^{2+} entry not only for excitatory but also for inhibitory effects [31]. The complex Ca^{2+}–calmodulin activates a phosphodiesterase (PDE1C2) that hydrolyzes cAMP [32,33], and also produces a negative feedback effect on the CNG channel itself, that has been shown to mediate olfactory adaptation [34]. Indeed, during short repetitive exposures to odorants, olfactory sensory neurons rapidly adapt to the stimulus by decreasing their responsiveness in a Ca^{2+}-dependent manner [35]. Kurahashi and Menini [36] investigated the localization of the principal molecular mechanism for adaptation in the olfactory transduction process. To determine whether the response reduction in the adapted state was attributable to a reduction in the cAMP

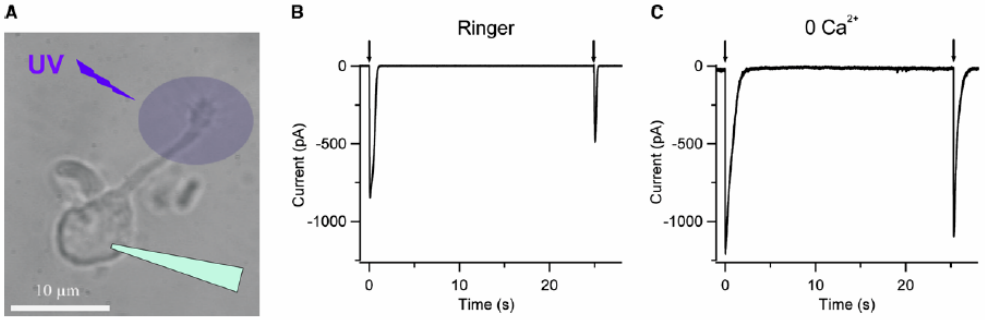

Fig. 2. Odorant adaptation in an isolated mouse olfactory sensory neuron. (A) Patch-clamp in the voltage-clamp whole-cell configuration was used to record currents from isolated mouse olfactory sensory neurons. Caged cAMP was included in the intracellular solution filling the patch pipette. Within a few minutes after rupture of the patch to establish the whole-cell configuration, the caged cAMP diffused into the cilia. Ultraviolet light flashes were applied to release the physiologically active cAMP into the ciliary region. (B) and (C) Responses at −50 mV to two identical ultraviolet light flashes releasing the same concentration of cAMP were recorded in the same neuron in a Ringer or in a nominally 0 Ca^{2+} solution (10 mM EGTA) in the same neuron. In Ringer (B), adaptation was observed, as the peak amplitude of the response to the second flash (−489 pA) was about 58% of the response to the first flash (−842 pA). In a nominally 0 Ca^{2+} solution (C) adaptation was abolished (unpublished results from Boccaccio et al. [38]).

production or was instead due to other processes occurring after the production of cAMP, CNG channels in intact neurons were directly activated by flash photolysis of caged cAMP (Fig. 2). The ciliary cytoplasm was loaded with caged cAMP through diffusion from a patch pipette. Application of ultraviolet light flashes to the ciliary region caused the photolysis of caged cAMP, thereby producing rapid and repeatable increments in cAMP concentration. Therefore, cAMP-gated channels could be directly activated, bypassing the early stages of odorant transduction (i.e. odorant receptor activation and G-protein and adenylate cyclase signalling, Fig. 1). Fig. 2 shows the results of an experiment illustrating that adaptation was measured with repetitive caged cAMP photolysis and that extracellular Ca^{2+} was necessary for adaptation. In physiological Ringer solution the peak of the current response to the second flash was reduced to about 58% of the control response (Fig. 2B), whereas in a nominally 0 Ca^{2+} solution the current responses to repetitive flashes were almost identical. Kurahashi and Menini [36] showed that cAMP- and odorant-induced responses had similar adaptation properties, indicating that the entire adaptation process takes place after the production of cAMP and might be mediated by Ca^{2+}–calmodulin-dependent inhibition of the olfactory CNG channel. Experiments on olfactory adaptation performed in knock-out mice of the CNGA4 subunit confirmed that the molecular mechanism for adaptation is localized at the channel level, most likely through CNG channel inhibition by Ca^{2+}–calmodulin [37].

Recent experiments were also performed to investigate if the Ca^{2+}–calmodulin-induced activity of the PDE (Fig. 1) is required for olfactory adaptation. Using the poorly hydrolysable caged 8-Br-cAMP and the PDE inhibitor IBMX it has been shown that an increase in PDE activity is not necessary for adaptation [38], furtherly supporting the notion that the Ca^{2+}-mediated negative feedback on the olfactory CNG channel is the main molecular mechanism responsible for fast adaptation. At present the overall molecular picture of how Ca^{2+} causes adaptation is the following: Ca^{2+} enters the cilia through the CNG channels and the channel sensitivity to cAMP is significantly reduced by Ca^{2+}–calmodulin modulation. As a consequence, CNG channel open probability could be significantly reduced. Thus, in the adapted state, the same cyclic nucleotide concentration as in the control state produces a lower CNG channel open probability and therefore a smaller current (Fig. 2). A recent mathematical model of adaptation based on direct negative regulation of CNG channels by Ca^{2+}–calmodulin in olfactory cilia well reproduces the experimental data [39].

4. Modulation of CNG channels by Ca^{2+}–calmodulin

Studies of native CNG channels have shown that the addition of micromolar concentrations of intracellular Ca^{2+} was able to decrease the channel sensitivity to cGMP or cAMP, probably by activating a Ca^{2+}-responsive endogenous factor already pre-associated with the channel [40–46]. Bradley et al. [44] have recently shown that Ca^{2+}-free calmodulin, called apocalmodulin, is able to bind to the heterologously expressed heteromeric olfactory CNG channels even in the absence of Ca^{2+}. Moreover, when Ca^{2+} concentration rises above 100 nM, Ca^{2+} can rapidly modulate the CNG channel sensitivity by directly binding to the pre-associated calmodulin. Furthermore, it was suggested [44] that also in native channels the pre-associated endogenous factor could be apocalmodulin, although a demonstration is still missing. Since Ca^{2+} enters into the olfactory cilia through the CNG channel itself, the pre-associated Ca^{2+}-responsive factor could provide a very fast feedback modulation at the channel level.

Early works [47–51] have identified in the N-terminus of CNGA2 a classic basic amphiphilic α-helix (Baa) motif with high affinity for Ca^{2+}–calmodulin and have shown that the sensitivity to cAMP of heterologously expressed homomeric CNGA2 channels was decreased by the binding of Ca^{2+}–calmodulin to the Baa motif. However, in recent years, there has been a considerable progress in elucidating the molecular events producing modulation of the native channels and it has been shown that the Baa motif of CNGA2 does not play any role in Ca^{2+}–calmodulin modulation of heteromeric channels. Instead, by comparing properties of native channels with heterologously expressed heteromeric channels, the

modulatory subunits CNGA4 and CNGB1b have been shown to be responsible for the physiological modulation of Ca^{2+}–calmodulin. Bradley et al. [44,52] and Munger et al. [37] measured, in excised patches containing native heteromeric olfactory CNG channels, a fast current inhibition upon addition of Ca^{2+}–calmodulin that persisted for several seconds also after calmodulin was removed in Ca^{2+}-free solution. Fig. 3D illustrates the rapid Ca^{2+}–calmodulin inhibition and slower recovery when native olfactory CNG channels were activated by 10 μM cAMP in an excised inside-out patch from the knob/cilia of a mouse olfactory sensory neuron.

The modulatory subunits CNGA4 and CNGB1b are necessary for the rapid inhibitory effect of Ca^{2+}–calmodulin and for maintaining the inhibitory action for several seconds, even after Ca^{2+}–calmodulin removal [37,44,52]. Instead, modulation of the rod and cone channels by Ca^{2+}–calmodulin requires only the CNGB1a and CNGB3 subunits, respectively [53,54]. In rods, the mechanism of Ca^{2+}–calmodulin inhibition of the CNG channel seems to be quite well understood: Ca^{2+}–calmodulin binds to a IQ-type calmodulin binding site in the N-terminal region of the CNGB1a subunit that is also necessary for the interaction with the CNGA1 subunit, thus preventing the direct interaction between the C-terminal region of CNGA1 with the N-terminal region of CNGB1a. Since the interaction between these intracellular channel domains is responsible for a higher ligand sensitivity of the rod channel, the binding of Ca^{2+}–calmodulin decreases the ligand sensitivity causing an inhibitory effect on the rod channel [53,54]. Also the olfactory modulatory subunits have calmodulin binding sites: CNGA4 has a IQ-type calmodulin binding site located at the C-terminal region, while CNGB1b has a similar IQ-type site located at the N-terminal region and a Baa motif in the C-terminal region. It has been shown that the IQ-type sites are necessary and sufficient for Ca^{2+}–calmodulin channel inhibition, whereas the Baa-type site is not necessary [44,55]. However, at present, the molecular mechanism by which the binding of

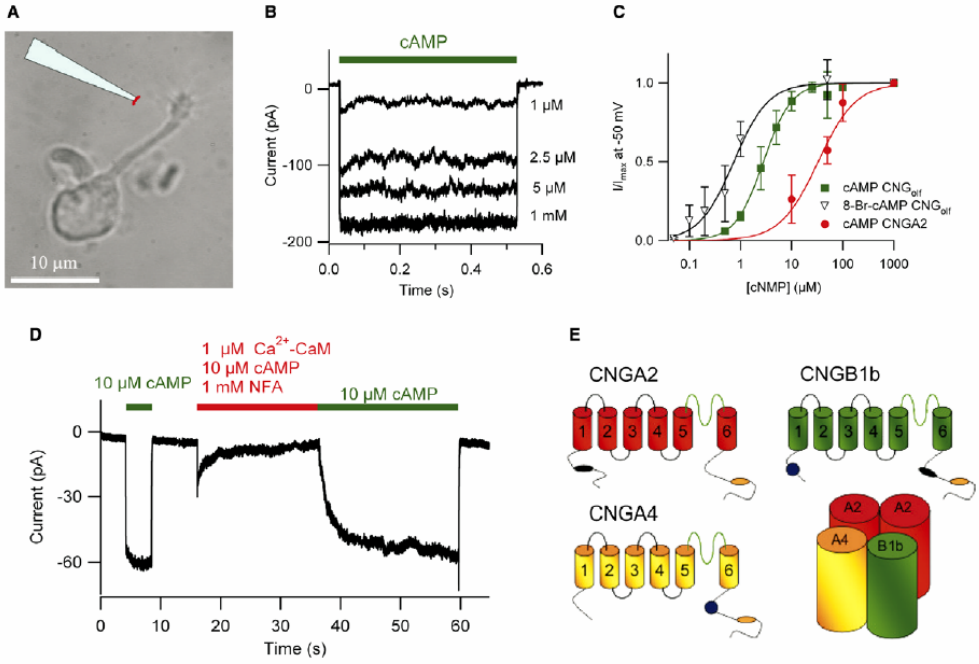

Fig. 3. CNG channels in olfactory sensory neurons. (A) A membrane patch was excised in the inside-out configuration from the dendritic knob/cilia of an isolated mouse olfactory sensory neuron and exposed to different solutions containing cyclic nucleotides to activate the CNG channel. (B) Native olfactory CNG channels were activated in the same patch by the indicated concentrations of cAMP in the absence of Ca^{2+} and Mg^{2+}, in an inside-out excised patch from the knob/cilia. Holding potential was −50 mV. (C) Dose–responses from membrane patches containing native channels activated by cAMP (□) or by the hydrolysis resistant analogue 8-Br-cAMP (△). Dose–response from patches excised from the membrane of HEK293 cells expressing homomeric CNGA2 channels activated by cAMP (○). The continuous lines are the best fit of the Hill equation: $I/I_{max} = c^n/(c^n + K_{1/2}^n)$ to the data with the following values at −50 mV for the native channel: $K_{1/2}$(cAMP) = 2.7 μM, n(cAMP) = 1.5, $K_{1/2}$(8-Br-cAMP) = 0.7 μM, n(8-Br-cAMP) = 1.6. For homomeric CNGA2 channels (○) $K_{1/2}$(cAMP) = 33 μM, n(cAMP) = 1.2. Fits of the Hill equation to data for native channels at +50 mV gave: $K_{1/2}$(cAMP) = 1.6 μM, n(cAMP) = 1.4, $K_{1/2}$(8-Br-cAMP) = 0.4 μM, n(8-Br-cAMP) = 1.5. (D) Native olfactory CNG channels are inhibited by Ca^{2+}–calmodulin in excised inside-out patches. A patch was exposed to 10 μM cAMP in a solution containing nominally 0 Ca^{2+}. Then the same patch was exposed to a solution containing, in addition to 10 μM cAMP, 1 μM calmodulin and 67 μM Ca^{2+} (in the presence of 1 mM NFA to block native Ca^{2+}-activated Cl current). The addition of Ca^{2+}–calmodulin quickly inhibited the cAMP-gated current that slowly recovered to its initial value after removal of Ca^{2+}–calmodulin (Pifferi, unpublished data). (E) Topological model and assembly of subunits of the olfactory CNG channel. Each transmembrane domain is indicated by a number, the pore loop is located between 5 and 6. The cyclic nucleotide binding site (brown) is located in the C-terminal domain. Calmodulin binding sites of the calcium-dependent 'Baa type' are represented in black, whereas the calcium independent 'IQ-type' are in blue.

Ca^{2+}–calmodulin decreases the ligand sensitivity of the olfactory channel is not yet understood.

5. Channelopathies

Some mutations in the genes encoding CNG subunits have been shown to produce visual disorders in human patients. Some forms of retinitis pigmentosa, an eye disease characterized by a progressive degeneration of the retina which affects night vision and peripheral vision, possibly leading to blindness, are caused by mutations in the CNGA1 or CNGB1 genes of the rod photoreceptors [56]. Achromatopsia, a retinal disorder characterized by the loss of color discrimination and by photophobia, is caused by mutations in the CNGA3 and CNGB3 genes of the cone photoreceptors [57,58]. More than 40 mutations in the CNGA3 channel gene, giving rise to various forms of achromatopsia, have been identified [59]. Peng et al. [60] functionally characterized some mutations in the human CNGB3 subunit and reported alterations in cyclic nucleotide sensitivity, ion selectivity, single channel properties, and plasma membrane targeting of the heteromeric CNG cone channel.

The function of CNG channel subunits has been also investigated by targeted disruption of genes encoding the CNGA2, A3, A4 or B1 subunits [37,60–64]. Deletion of the CNGA3 subunit produced mice lacking cone responses to light, whereas the rod pathway was completely intact [63]. Knock-out of the CNGB1 gene in mice caused the alteration in targeting of the CNGA1 subunit in rod outer segment, abolished the response to light and caused retinal degeneration, similarly to human retinitis pigmentosa [61]. Knock-out of the olfactory CNGA2 gene caused the absence of any detectable response to odorants in mice, that therefore had a general anosmia, and demonstrated that the cAMP-mediated pathway is the only trasduction mechanism that mediates odorant detection [64]. Knock-out of the olfactory CNGA4 gene caused alterations in odorant adaptation, furtherly demonstrating the fundamental role of modulatory subunits in the physiological function of CNG channels [37].

6. Conclusions

The recent progress in our knowledge of the biophysical and physiological properties of CNG channels allows a better understanding of sensory transduction. However, up to today, a few questions are still open. It has been shown that the Ca^{2+}-dependent regulation of CNG channels in olfactory sensory is responsible for adaptation and that the ligand sensitivity is reduced when Ca^{2+}–calmodulin interacts with both modulatory subunits [37,44,52,55], but the nature of this interaction is not yet understood.

On the contrary, in the retinal rod channel, it has been shown that the binding of Ca^{2+}–calmodulin to the CNGB1a N-terminus decreases the ligand sensitivity by interfering with the direct interaction with the CNGA1 C-terminus, an interdomain interaction, essential to have high ligand sensitivity [51]. However, the physiological role of Ca^{2+}–calmodulin regulation in retinal rods is unclear and it does not seem to be involved in adaptation [65,66].

It has been proposed that the endogenous factor co-assembled with the native olfactory channel is calmodulin, although a conclusive demonstration is still lacking. Moreover, some experimental evidence argues against this hypothesis, in particular the endogenous factor appears to bind the CNG channels in a very stable manner, being washed away only after intense rinsing in Ca^{2+}-free solution [40,43,44]. However, it is also possible to speculate that the binding of ''native'' calmodulin is more stable because the channel or the calmodulin itself undergoes post-transductional modifications that change the properties of the interaction. On the other hand, it cannot be excluded that also other proteins, in addition to calmodulin, contribute to the Ca^{2+}-mediated modulation of olfactory CNG channels.

Acknowledgments: The authors' work is supported by Grants: NFG 503221 from the European Community, and COFIN 2004 from the Italian Ministry of Education, Research and University.

References

[1] Fesenko, E.E., Kolesnikov, S.S. and Lyubarsky, A.L. (1985) Induction by cyclic GMP of cationic conductance in plasma membrane of retinal rod outer segment. Nature 313, 310–313.
[2] Haynes, L. and Yau, K.W. (1985) Cyclic GMP-sensitive conductance in outer segment membrane of catfish cones. Nature 317, 61–64.
[3] Burns, M.E. and Baylor, D.A. (2001) Activation, deactivation, and adaptation in vertebrate photoreceptor cells. Annu. Rev. Neurosci. 24, 779–805.
[4] Burns, M.E. and Arshavsky, V.Y. (2005) Beyond counting photons: trials and trends in vertebrate visual transduction. Neuron 48, 387–401.
[5] Nakamura, T. and Gold, G.H. (1987) A cyclic nucleotide-gated conductance in olfactory receptor cilia. Nature 325, 442–444.
[6] Kaupp, U.B. and Seifert, R. (2002) Cyclic nucleotide-gated ion channels. Physiol. Rev. 82, 769–824.
[7] Kaupp, U.B., Niidome, T., Tanabe, T., Terada, S., Bonigk, W., Stuhmer, W., Cook, N.J., Kangawa, K., Matsuo, H. and Hirose, T. (1989) Primary structure and functional expression from complementary DNA of the rod photoreceptor cyclic GMP-gated channel. Nature 342, 762–766.
[8] Hofmann, F., Biel, M. and Kaupp, U.B. (2005) International Union of Pharmacology. LI. Nomenclature and structure–function relationships of cyclic nucleotide-regulated channels. Pharmacol. Rev. 57, 455–462.
[9] Chen, T.Y., Peng, Y.W., Dhallan, R.S., Ahamed, B., Reed, R.R. and Yau, K.W. (1993) A new subunit of the cyclic nucleotide-gated cation channel in retinal rods. Nature 362, 764–767.
[10] Zhong, H., Molday, L.L., Molday, R.S. and Yau, K.W. (2002) The heteromeric cyclic nucleotide-gated channel adopts a 3A:1B stoichiometry. Nature 420, 193–198.
[11] Weitz, D., Ficek, N., Kremmer, E., Bauer, P.J. and Kaupp, U.B. (2002) Subunit stoichiometry of the CNG channel of rod photoreceptors. Neuron 36, 881–889.
[12] Bonigk, W., Altenhofen, W., Muller, F., Dose, A., Illing, M., Molday, R.S. and Kaupp, U.B. (1993) Rod and cone photoreceptor cells express distinct genes for cGMP-gated channels. Neuron 10, 865–877.
[13] Gerstner, A., Zong, X., Hofmann, F. and Biel, M. (2000) Molecular cloning and functional characterization of a new modulatory cyclic nucleotide-gated channel subunit from mouse retina. J. Neurosci. 20, 1324–1332.
[14] Peng, C., Rich, E.D. and Varnum, M.D. (2004) Subunit configuration of heteromeric cone cyclic nucleotide-gated channels. Neuron 42, 401–410.
[15] Dhallan, R.S., Yau, K.W., Schrader, K.A. and Reed, R.R. (1990) Primary structure and functional expression of a cyclic nucleotide-activated channel from olfactory neurons. Nature 347, 184–187.
[16] Ludwig, J., Margalit, T., Eismann, E., Lancet, D. and Kaupp, U.B. (1990) Primary structure of cAMP-gated channel from bovine olfactory epithelium. FEBS Lett. 270, 24–29.
[17] Bradley, J., Li, J., Davidson, N., Lester, H.A. and Zinn, K. (1994) Heteromeric olfactory cyclic nucleotide-gated channels: a subunit

that confers increased sensitivity to cAMP. Proc. Natl. Acad. Sci. USA 91, 8890–8894.
[18] Liman, E.R. and Buck, L.B. (1994) A second subunit of the olfactory cyclic nucleotide-gated channel confers high sensitivity to cAMP. Neuron 13, 611–621.
[19] Sautter, A., Zong, X., Hofmann, F. and Biel, M. (1998) An isoform of the rod photoreceptor cyclic nucleotide-gated channel beta subunit expressed in olfactory neurons. Proc. Natl. Acad. Sci. USA 95, 4696–4701.
[20] Zheng, J. and Zagotta, W.N. (2004) Stoichiometry and assembly of olfactory cyclic nucleotide-gated channels. Neuron 42, 411–421.
[21] Menini, A. (1995) Cyclic nucleotide-gated channels in visual and olfactory transduction. Biophys. Chem. 55, 185–196.
[22] Gavazzo, P., Picco, C., Maxia, L. and Menini, A. (1996) Properties of native and cloned cyclic nucleotide-gated channels from bovine in: Neurobiology (Torre and Conti, Eds.), pp. 75–83, Plenum Press, New York.
[23] Dzeja, C., Hagen, V., Kaupp, U.B. and Frings, S. (1999) Ca^{2+} permeation in cyclic nucleotide-gated channels. EMBO J. 18, 131–144.
[24] Bonigk, W., Bradley, J., Muller, F., Sesti, F., Boekhoff, I., Ronnett, G.V., Kaupp, U.B. and Frings, S. (1999) The native rat olfactory cyclic nucleotide-gated channel is composed of three distinct subunits. J. Neurosci. 19, 5332–5347.
[25] Matulef, K. and Zagotta, W.N. (2003) Cyclic nucleotide-gated ion channels. Annu. Rev. Cell Dev. Biol. 19, 23–44.
[26] Buck, L. and Axel, R. (1991) A novel multigene family may encode odorant receptors: a molecular basis for odor recognition. Cell 65, 175–187.
[27] Frings, S., Reuter, D. and Kleene, S.J. (2000) Neuronal Ca^{2+}-activated Cl-channels – homing in on an elusive channel species. Prog. Neurobiol. 60, 247–289.
[28] Schild, D. and Restrepo, D. (1998) Transduction mechanisms in vertebrate olfactory receptor cells. Physiol. Rev. 78, 429–466.
[29] Firestein, S. (2001) How the olfactory system makes sense of scents. Nature 413, 211–218.
[30] Menini, A., Lagostena, L. and Boccaccio, A. (2004) Olfaction: from odorant molecules to the olfactory cortex. News Physiol. Sci. 19, 101–104.
[31] Matthews, H.R. and Reisert, J. (2003) Calcium, the two-faced messenger of olfactory transduction and adaptation. Curr. Opin. Neurobiol. 13, 469–475.
[32] Borisy, F.F., Ronnett, G.V., Cunningham, A.M., Juilfs, D., Beavo, J. and Snyder, S.H. (1992) Calcium/calmodulin-activated phosphodiesterase expressed in olfactory receptor neurons. J. Neurosci. 12, 915–923.
[33] Yan, C., Zhao, A.Z., Bentley, J.K., Loughney, K., Ferguson, K. and Beavo, J.A. (1995) Molecular cloning and characterization of a calmodulin-dependent phosphodiesterase enriched in olfactory sensory neurons. Proc. Natl. Acad. Sci. USA 92, 9677–9681.
[34] Menini, A. (1999) Calcium signalling and regulation in olfactory neurons. Curr. Opin. Neurobiol. 9, 419–426.
[35] Kurahashi, T. and Shibuya, T. (1990) Ca2(+)-dependent adaptive properties in the solitary olfactory receptor cell of the newt. Brain Res. 515, 261–268.
[36] Kurahashi, T. and Menini, A. (1997) Mechanism of odorant adaptation in the olfactory receptor cell. Nature 385, 725–729.
[37] Munger, S.D., Lane, A.P., Zhong, H., Leinders-Zufall, T., Yau, K.W., Zufall, F. and Reed, R.R. (2001) Central role of the CNGA4 channel subunit in Ca^{2+}–calmodulin-dependent odor adaptation. Science 294, 2172–2175.
[38] Boccaccio A., Lagostena L., Hagen V., and Menini A. (2004). Currents induced by photolysis of caged 8Br-cAMP in mouse olfactory sensory neurons. Program No. 178.10. Abstract Society of Neuroscience.
[39] Reidl, J., Borowski, P., Sensse, A., Starke, J., Zapotocky, M. and Eiswirth, M. (2006) Model of calcium oscillations due to negative feedback in olfactory cilia. Biophys. J. 90, 1147–1155.
[40] Kramer, R.H. and Siegelbaum, S.A. (1992) Intracellular Ca^{2+} regulates the sensitivity of cyclic nucleotide-gated channels in olfactory receptor neurons. Neuron 9, 897–906.
[41] Lynch, J.W. and Lindemann, B. (1994) Cyclic nucleotide-gated channels of rat olfactory receptor cells: divalent cations control the sensitivity to cAMP. J. Gen. Physiol 103, 87–106.
[42] Balasubramanian, S., Lynch, J.W. and Barry, P.H. (1996) Calcium-dependent modulation of the agonist affinity of the mammalian olfactory cyclic nucleotide-gated channel by calmodulin and a novel endogenous factor. J. Membr. Biol. 152, 13–23.
[43] Kleene, S.J. (1999) Both external and internal calcium reduce the sensitivity of the olfactory cyclic-nucleotide-gated channel to CAMP. J. Neurophysiol. 81, 2675–2682.
[44] Bradley, J., Bonigk, W., Yau, K.W. and Frings, S. (2004) Calmodulin permanently associates with rat olfactory CNG channels under native conditions. Nat. Neurosci. 7, 705–710.
[45] Gordon, S.E., Downing-Park, J. and Zimmerman, A.L. (1995) Modulation of the cGMP-gated ion channel in frog rods by calmodulin and an endogenous inhibitory factor. J. Physiol. 486 (Pt. 3), 533–546.
[46] Rebrik, T.I. and Korenbrot, J.I. (1998) In intact cone photoreceptors, a Ca^{2+}-dependent, diffusible factor modulates the cGMP-gated ion channels differently than in rods. J. Gen. Physiol. 112, 537–548.
[47] Chen, T.Y. and Yau, K.W. (1994) Direct modulation by Ca(2+)-calmodulin of cyclic nucleotide-activated channel of rat olfactory receptor neurons. Nature 368, 545–548.
[48] Liu, M., Chen, T.Y., Ahamed, B., Li, J. and Yau, K.W. (1994) Calcium–calmodulin modulation of the olfactory cyclic nucleotide-gated cation channel. Science 266, 1348–1354.
[49] Varnum, M.D. and Zagotta, W.N. (1997) Interdomain interactions underlying activation of cyclic nucleotide-gated channels. Science 278, 110–113.
[50] Grunwald, M.E., Zhong, H., Lai, J. and Yau, K.W. (1999) Molecular determinants of the modulation of cyclic nucleotide-activated channels by calmodulin. Proc. Natl. Acad. Sci. USA 96, 13444–13449.
[51] Zheng, J., Varnum, M.D. and Zagotta, W.N. (2003) Disruption of an intersubunit interaction underlies Ca^{2+}–calmodulin modulation of cyclic nucleotide-gated channels. J. Neurosci. 23, 8167–8175.
[52] Bradley, J., Reuter, D. and Frings, S. (2001) Facilitation of calmodulin-mediated odor adaptation by cAMP-gated channel subunits. Science 294, 2176–2178.
[53] Weitz, D., Zoche, M., Muller, F., Beyermann, M., Korschen, H.G., Kaupp, U.B. and Koch, K.W. (1998) Calmodulin controls the rod photoreceptor CNG channel through an unconventional binding site in the N-terminus of the beta-subunit. EMBO J. 17, 2273–2284.
[54] Trudeau, M.C. and Zagotta, W.N. (2002) Mechanism of calcium/calmodulin inhibition of rod cyclic nucleotide-gated channels. Proc. Natl. Acad. Sci. USA 99, 8424–8429.
[55] Bradley, J., Reisert, J. and Frings, S. (2005) Regulation of cyclic nucleotide-gated channels. Curr. Opin. Neurobiol. 15, 343–349.
[56] Trudeau, M.C. and Zagotta, W.N. (2002) An intersubunit interaction regulates trafficking of rod cyclic nucleotide-gated channels and is disrupted in an inherited form of blindness. Neuron 34, 197–207.
[57] Kohl, S., Baumann, B., Broghammer, M., Jagle, H., Sieving, P., Kellner, U., Spegal, R., Anastasi, M., Zrenner, E., Sharpe, L.T. and Wissinger, B. (2000) Mutations in the CNGB3 gene encoding the beta-subunit of the cone photoreceptor cGMP-gated channel are responsible for achromatopsia (ACHM3) linked to chromosome 8q21. Hum. Mol. Genet. 9, 2107–2116.
[58] Kohl, S., Marx, T., Giddings, I., Jagle, H., Jacobson, S.G., Apfelstedt-Sylla, E., Zrenner, E., Sharpe, L.T. and Wissinger, B. (1998) Total colourblindness is caused by mutations in the gene encoding the alpha-subunit of the cone photoreceptor cGMP-gated cation channel. Nat. Genet. 19, 257–259.
[59] Wissinger, B., Gamer, D., Jagle, H., Giorda, R., Marx, T., Mayer, S., Tippmann, S., Broghammer, M., Jurklies, B., Rosenberg, T., Jacobson, S.G., Sener, E.C., Tatlipinar, S., Hoyng, C.B., Castellan, C., Bitoun, P., Andreasson, S., Rudolph, G., Kellner, U., Lorenz, B., Wolff, G., Verellen-Dumoulin, C., Schwartz, M., Cremers, F.P., Apfelstedt-Sylla, E., Zrenner, E., Salati, R., Sharpe, L.T. and Kohl, S. (2000) CNGA3 mutations in hereditary cone photoreceptor disorders. Am. J. Hum. Genet. 69, 722–737.
[60] Peng, C., Rich, E.D. and Varnum, M.D. (2003) Achromatopsia-associated mutation in the human cone photoreceptor cyclic nucleotide-gated channel CNGB3 subunit alters the ligand sensitivity and pore properties of heteromeric channels. J. Biol. Chem. 278, 34533–34540.

[61] Huttl, S., Michalakis, S., Seeliger, M., Luo, D.G., Acar, N., Geiger, H., Hudl, K., Mader, R., Haverkamp, S., Moser, M., Pfeifer, A., Gerstner, A., Yau, K.W. and Biel, M. (2005) Impaired channel targeting and retinal degeneration in mice lacking the cyclic nucleotide-gated channel subunit CNGB1. J. Neurosci. 25, 130–138.
[62] Baker, H., Cummings, D.M., Munger, S.D., Margolis, J.W., Franzen, L., Reed, R.R. and Margolis, F.L. (1999) Targeted deletion of a cyclic nucleotide-gated channel subunit (OCNC1): biochemical and morphological consequences in adult mice. J. Neurosci. 19, 9313–9321.
[63] Biel, M., Seeliger, M., Pfeifer, A., Kohler, K., Gerstner, A., Ludwig, A., Jaissle, G., Fauser, S., Zrenner, E. and Hofmann, F. (1999) Selective loss of cone function in mice lacking the cyclic nucleotide-gated channel CNG3. Proc. Natl. Acad. Sci. USA 96, 7553–7557.
[64] Brunet, L.J., Gold, G.H. and Ngai, J. (1996) General anosmia caused by a targeted disruption of the mouse olfactory cyclic nucleotide-gated cation channel. Neuron 17, 681–693.
[65] Pugh Jr., E.N., Nikonov, S. and Lamb, T.D. (1999) Molecular mechanisms of vertebrate photoreceptor light adaptation. Curr. Opin. Neurobiol. 9, 410–418.
[66] Fain, G.L., Matthews, H.R., Cornwall, M.C. and Koutalos, Y. (2001) Adaptation in vertebrate photoreceptors. Physiol Rev. 81, 117–151.

Bestrophin-2 is a candidate calcium-activated chloride channel involved in olfactory transduction

Simone Pifferi*†, Giovanni Pascarella†‡, Anna Boccaccio*, Andrea Mazzatenta*, Stefano Gustincich‡, Anna Menini*§, and Silvia Zucchelli‡

*Sector of Neurobiology, International School for Advanced Studies (SISSA), Via Beirut 2-4, 34014 Trieste, Italy; and ‡Giovanni Armenise–Harvard Foundation Laboratory, Sector of Neurobiology, International School for Advanced Studies (SISSA), AREA Science Park, S.S. 14, Km 163.5, Basovizza, 34012 Trieste, Italy

Edited by Joseph A. Beavo, University of Washington School of Medicine, Seattle, WA, and approved July 5, 2006 (received for review June 2, 2006)

Ca-activated Cl channels are an important component of olfactory transduction. Odor binding to olfactory receptors in the cilia of olfactory sensory neurons (OSNs) leads to an increase of intraciliary Ca concentration by Ca entry through cyclic nucleotide-gated (CNG) channels. Ca activates a Cl channel that leads to an efflux of Cl from the cilia, contributing to the amplification of the OSN depolarization. The molecular identity of this Cl channel remains elusive. Recent evidence has indicated that bestrophins are able to form Ca-activated Cl channels in heterologous systems. Here we have analyzed the expression of bestrophins in the mouse olfactory epithelium and demonstrated that only mouse bestrophin-2 (mBest2) was expressed. Single-cell RT-PCR showed that mBest2 was expressed in OSNs but not in supporting cells. Immunohistochemistry revealed that mBest2 was expressed on the cilia of OSNs, the site of olfactory transduction, and colocalized with the main CNGA2 channel subunit. Electrophysiological properties of Ca-activated Cl currents from native channels in dendritic knob/cilia of mouse OSNs were compared with those induced by the expression of mBest2 in HEK-293 cells. We found the same anion permeability sequence, small estimated single-channel conductances, a Ca sensitivity difference of one order of magnitude, and the same side-specific blockage of the two Cl channel blockers commonly used to inhibit the odorant-induced Ca-activated Cl current in OSNs, niflumic acid, and 4-acetamido-4′-isothiocyanato-stilben-2,2′-disulfonate (SITS). Therefore, our data suggest that mBest2 is a good candidate for being a molecular component of the olfactory Ca-activated Cl channel.

ion channel | olfaction | olfactory sensory neurons | patch–clamp | sensory coding

The initial steps of olfaction occur in olfactory sensory neurons (OSNs), located in the olfactory epithelium (OE) of the nasal cavity. OSNs are responsible for the detection of odorant molecules present in the environment and the generation of the neural signal that is transmitted to the brain (for reviews, see refs. 1–3). OSNs are bipolar neurons with a single dendrite that terminates with a knob, from which protrude several tiny cilia, where the transduction of the olfactory signal takes place. Odorant molecules bind to olfactory receptor proteins, and this interaction triggers an increase in the ciliary concentration of cAMP through the activation of receptor-coupled G protein and adenylate cyclase. Cyclic nucleotide-gated (CNG) channels located in the ciliary membrane are directly activated by cAMP, causing a depolarizing influx of Na and Ca ions. It is well known that Ca-activated Cl channels are present in the ciliary membrane (4, 5), and that the increase in Ca concentration inside the cilia activates a Cl current (4–7). OSNs maintain an unusually high internal concentration of Cl that is in the same range of the Cl concentration present in the mucus at the external side of the cilia (8–11). In physiological conditions, the opening of Ca-activated Cl channels in the ciliary membrane causes an efflux of Cl ions from the cilia, corresponding to an inward current that further contributes to the depolarization of OSNs (4–7). During olfactory transduction, the secondary Ca-activated Cl current plays the important role of a high-gain and low-noise amplifier of the primary CNG current (ref. 12; for reviews, see refs. 13–15), contributing between 50% and 85% of the total odorant-induced current (6, 7, 11). Nevertheless, the molecular players of Cl homeostasis in OSNs are still elusive. Only recently, it has been shown that NKCC1, a Na-K-2Cl cotransporter, is implicated in the maintenance of a high Cl concentration inside OSNs (16, 17), although another study indicates the possibility that NKCC1 is not the only component involved in this process (18).

The molecular identity of the Ca-activated Cl channel involved in olfactory transduction is still obscure. Bestrophins from several species produce Ca-activated Cl currents when expressed heterologously (refs. 19–26; for review, see ref. 27). In the mouse, this gene family comprises three genes (mBest1, -2, and -4) and a pseudogene (mBest3; ref. 28). In humans, several different mutations in bestrophin-1 cause bestrophin vitelliform macular dystrophy (refs. 29 and 30; for review, see refs. 20 and 31).

The biophysical properties of mBest2 have been recently investigated with the patch–clamp technique, showing that mBest2 by itself forms Ca-activated Cl channels in heterologous systems and is a structural component of the ion-conducting pore. Bestrophin-2 can thus be considered a bona fide Cl channel (21, 22, 26, 32).

We demonstrate here that mBest2 mRNA is expressed in OSNs, and that the mBest2 protein is located on the cilia, where olfactory transduction occurs. On the cilia, mBest2 colocalizes with CNGA2, the main subunit of the olfactory CNG channel (for review, see ref. 33). We measured, with the patch–clamp technique, the functional properties of the current induced by heterologous expression of mBest2 and those of the native Ca-activated Cl current from dendritic knob/cilia of mouse OSNs. The colocalization of mBest2 with CNGA2 on the cilia and the similarities of some functional properties of mBest2 currents with those of the native olfactory Ca-activated Cl channels indicate mBest2 is a good candidate for being a molecular component of the olfactory Ca-activated Cl channel.

Results

Bestrophin-2 Is Expressed in OSNs. Bestrophins have been proposed to constitute a new family of Ca-activated Cl channels (for review, see ref. 27). In the mouse, the bestrophin family is composed of three coding genes (mBest1, -2, and -4) and one pseudogene (mBest3; see ref. 28). We screened the expression of mBest1, -2, and -4 in the OE by RT-PCR (Fig. 1*a*). In this tissue, we detected the expression of mRNA of mBest2 but not of

Conflict of interest statement: No conflicts declared.

This paper was submitted directly (Track II) to the PNAS office.

Abbreviations: OSN, olfactory sensory neuron; OE, olfactory epithelium; CNG, cyclic nucleotide-gated; mBest2, mouse bestrophin-2; NFA, niflumic acid; SITS, 4-acetamido-4′-isothiocyanato-stilben-2,2′-disulfonate; MeS, methanesulfonate.

†S.P. and G.P. contributed equally to this work.

§To whom correspondence should be addressed. E-mail: menini@sissa.it.

PHYSIOLOGY

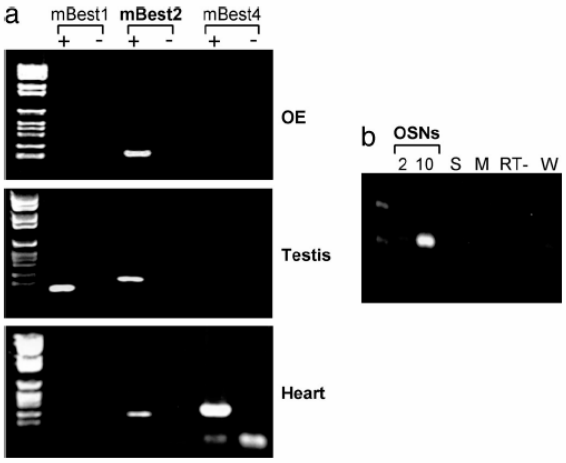

Fig. 1. mBest2 is expressed in mouse OSNs. (*a*) Primers specific for mBest1, -2, and -4 were used to amplify cDNA obtained from RNA of OE, testis, and heart. (*b*) Primers specific for mBest2 were used to amplify cDNA made from RNA of 2 OSNs, 10 OSNs, and 10 supporting cells (S). Other negative controls are resuspension media for OSNs (M), retrotranscriptase free sample (RT−) and water-only sample (W).

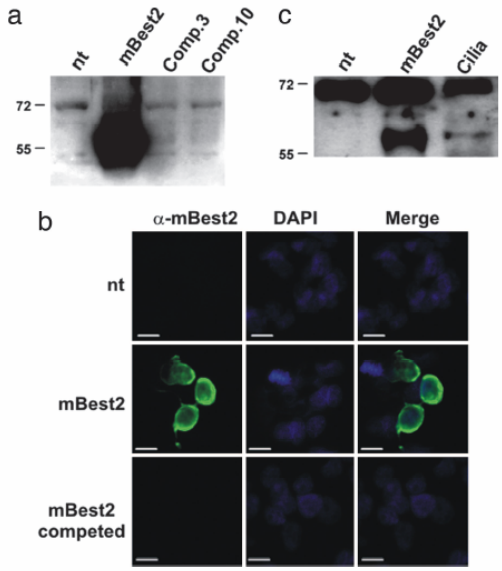

Fig. 2. Expression of mBest2 in transfected HEK-293 cells, anti-mBest2 antibody specificity, and expression of mBest2 in olfactory cilia preparation. HEK-293 cells were transiently transfected with mBest2, and the specificity of α-mBest2 antibody was demonstrated by competing the specific mBest2 signal with incubation of 3 or 10 μg of purified GST-mBest2 in Western blot (*a*) or with 30 μg of purified mBest2 in immunofluorescence (*b*). (Scale bar, 10 μm.) (*c*) Expression of mBest2 in olfactory cilia was detected by Western blot analysis using a cilia-enriched preparation.

mBest1 and -4. As controls, we identified mRNAs of mBest1 and -2 in the testis and of mBest2 and -4 in the heart (28). As expected, we also observed in the OE the expression of the CNGA2 subunit of the olfactory CNG channel (data not shown). The identity of mBest2 PCR-amplified fragments was verified by cloning and sequencing. To assess whether splicing or edited variants of mBest2 were expressed in the OE, we cloned the ORF of mBest2 from this tissue by RT-PCR using a DNA polymerase with high proofreading activity. Three independent clones showed 100% identity to BC019528, proving that no OE-specific posttranscriptional modifications occurred.

We examined the cell-type-specific expression of mBest2 by carrying out RT-PCR experiments on a small number of solitary cells from the OE. After enzymatic digestion and mechanical trituration of the adult mouse OE, we harvested single OSNs and supporting cells, purified their RNAs, and performed RT-PCR experiments. By analyzing 2–10 individual OSNs or supporting cells from the OE, we observed that the expression of mBest2 was restricted to OSNs (Fig. 1*b*).

Production of Anti-mBest2 Antibody and Western Blot. To study the expression of the mBest2 protein, we generated a specific polyclonal antibody raised against the C-terminal 144-aa residues of mBest2 (mBest2 344-C-end), a region that is not conserved across bestrophin family members. After transfection of mBest2 cDNA cloned in an expression vector, mBest2 protein was detected in Western blot by the polyclonal antibody as a 57-kDa protein, as expected (Fig. 2*a*). The mBest2-specific band completely disappeared by competition with recombinant GST-mBest2, proving the specificity of the antibody. To assess whether this polyclonal antibody recognizes mBest2 in immunofluorescence experiments, we successfully immunolabeled HEK-293 cells at the cell membrane when transfected with mBest2 cDNA. The staining was abolished when the antibody was preincubated with the recombinant protein (Fig. 2*b*). We tested by Western blot the expression of mBest2 protein in the OE by using a preparation enriched in olfactory cilia. As shown in Fig. 2*c*, mBest2 protein was detected at the expected molecular weight. The signal was completely abolished by preincubation with recombinant GST-mBest2 (data not shown).

Localization of mBest2 on the Cilia of OSNs. The olfactory sensory transduction occurs in specialized cilia extended from the knobs of OSNs on the surface of the OE. To examine the subcellular localization of mBest2 in OSNs, we performed immunohistochemistry experiments on OE cryosection from adult and postnatal day 15 (P15) mice by using the anti-mBest2 polyclonal antibody. We found a homogenous staining on the surface of OE (Fig. 3 *a–c*) without any remarkable difference among the zones of OE in both adult and P15 mice (not shown). The staining was abolished when the antibody was preincubated with the recombinant protein proving signal specificity (data not shown). Specific antibodies against olfactory marker protein (OMP), a typical marker of mature OSNs (34), and the olfactory CNG channel subunit CNGA2 (35), known to be present in the cilia, were used as cellular or subcellular markers. Double staining for mBest2 and OMP showed that mBest2 is expressed in mature OSNs (Fig. 3 *d–f*). Double-staining experiments for mBest2 and CNGA2 proved that mBest2 was present on the luminal surface of the OE (Fig. 3 *e–g*) restricted to the cilia of OSNs, where it colocalized with CNGA2 (higher magnification; Fig. 3 *j–l*). Therefore, mBest2 appears to be expressed at the site of olfactory transduction.

Functional Properties of Ca-Activated Cl Currents from OSNs and mBest2-Transfected HEK-293 Cells. Functional properties of native olfactory Ca-activated Cl currents were measured with the patch–clamp technique from excised inside-out patches from dendritic knob/cilia of mouse OSNs (Figs. 4 , 5, and 7). To compare the functional properties of native olfactory Ca-activated Cl currents with those of heterologously expressed mBest2 currents, we aimed at carrying out a side-by-side comparison in inside-out membrane patches. However, of 78 excised inside-out patches from mBest2- transfected HEK-293 cells, we did not detect any measurable Cl current activated by Ca. A recent report (25) has

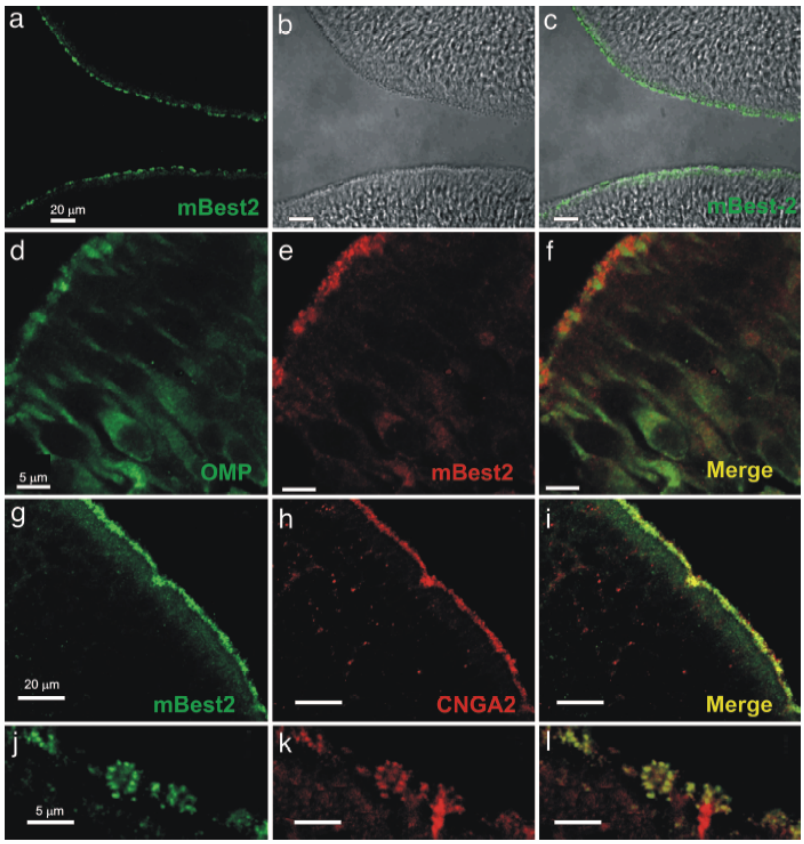

Fig. 3. Localization of mBest2 on the sensory cilia of OSNs. (*a* and *c*) OE (bright field in *b*) labeled with affinity-purified anti-mBest2 polyclonal antibody (green) is shown as the fluorescence signal (*a*) or a digital addition of the fluorescence and bright-field images (*c*). mBest2 is located at the luminal surface of the sensory epithelium. (*d–f*) Double staining for mBest2 (red) and OMP (green). mBest2 was located at the end of dendrites of mature OSNs. (*g–i*) Double staining for mBest2 (green) and CNGA2 (red). Label is shown as the red fluorescence channel digitally combined with the green channel. mBest2 and CNGA2 colocalized at the luminal surface of OE. (*j–l*) Higher magnification of the OE as in *g–i*. mBest2 was expressed on cilia of OSNs and colocalized with CNGA2.

shown that Ca-activated Cl currents induced by heterologous expression of hBest4 could be detected in excised inside-out patches. They suggested, though, that measurements in excised patches could be obtained only because of the particularly large Cl current induced by heterologous expression of hBest4 (24) when compared with the other bestrophins. Here, in the absence of a detectable mBest2-induced current in inside-out patches, we determined the functional properties of mBest2 currents in the whole-cell configuration and those of native Ca-activated Cl currents in the inside-out configuration (Figs. 4–7).

Ca Sensitivity and Single-Channel Conductance. To compare the Ca sensitivity of native olfactory currents with those of mBest2 currents, dose–response relations were obtained by activating currents with various Ca concentrations (Fig. 4). Normalized currents were plotted versus Ca concentration and fitted by the Hill equation. At −50 mV for mBest2 currents, $K_{1/2}$ was 0.4 μM, and n_H was 2.5, whereas for native currents $K_{1/2}$ was 4.7 μM, and n_H was 6.6. mBest2 current amplitudes did not significantly change up to a few minutes of continuous exposure to Ca, whereas the native Ca-activated Cl currents in excised patches displayed a slight inactivation (Fig. 4 *b*, *c*, and *f*). Single-channel events could not be detected even at low Ca concentrations, and therefore we performed stationary noise analysis to estimate the single-channel conductance. By calculating the ratio between variance and mean current at low Ca concentrations, we estimated a single-channel conductance of 0.26 ± 0.06 pS (n = 4) for mBest2 and 1.6 ± 0.5 pS (n = 3) for native olfactory channels.

Anion Selectivity and Rectification. We replaced NaCl in the bathing solution with NaI, NaBr, $NaNO_3$, or NaMethanesulfonate (NaMeS); measured the shift in reversal potential; and calculated the relative permeability ratios (Fig. 5 *a–c*). Replacement of Cl with MeS shifted the reversal potential from near zero in symmetrical Cl to more positive values for mBest2 (Fig. 5*a*) or to more negative values for native currents (Fig. 5*b*). The measured direction of the shift in reversal potentials was as expected for Cl-selective channels in our experimental conditions, showing that Ca-activated currents were Cl-selective both for mBest2 and for native currents. Fig. 5*c* shows a comparison between the calculated permeability ratios. The same permeability sequence $I>NO_3>Br>Cl\gg MeS$ was obtained both in native and in mBest2 channels, although the calculated permeability ratios for the various anions were not identical. The current–voltage relations in symmetrical Cl solutions were almost linear (Fig. 5 *a* and *b*), with a slight rectification in opposite directions for native (I_{+50}/I_{-50} = 0.61 ± 0.08) and mBest2 currents (I_{+50}/I_{-50} = 1.24 ± 0.04; Fig. 5*d*).

PHYSIOLOGY

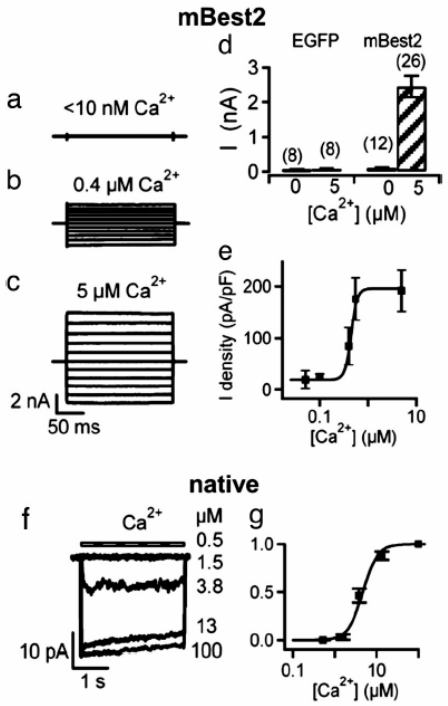

Fig. 4. Calcium sensitivity. (*a–e*) mBest2 and EGFP were transfected in HEK-293 cells. Recordings were made 2–3 days after transfection. Whole-cell voltage-clamp recordings were performed with pipette solutions containing <10 nM free Ca (nominally 0 Ca) (*a*), 0.4 μM (*b*), or 5 μM free Ca (*c*). Voltage steps of 200-ms duration were given from a holding potential of 0 mV to voltages between −100 and +100 mV in 20-mV steps. (*d*) Mean steady-state current amplitudes measured at +60 mV in cells transfected with EGFP alone or with mBest2 and EGFP with pipette solutions containing either 0 or 5 μM free Ca. (*e*) Dependence of mBest2 current on intracellular Ca concentration at −50 mV. The amplitude of the average density currents was plotted versus Ca and fitted to the Hill equation with $K_{1/2}$ = 0.4 μM (5–12 cells; solid line). (*f*) A membrane patch was excised from the dendritic knob/cilia of an OSN, and the cytoplasmic side was exposed to the indicated free Ca concentrations at −50 mV. (*g*) Dependence of native current on intracellular Ca concentration fitted to the Hill equation $K_{1/2}$ = 4.7 μM (four patches).

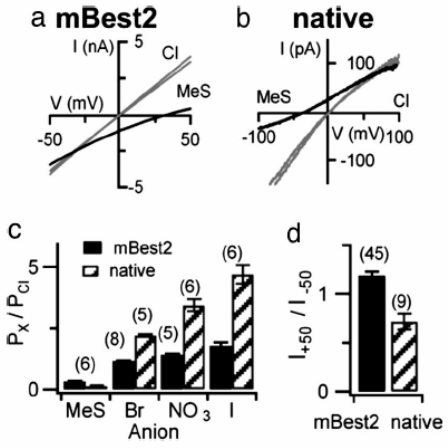

Fig. 5. Anion selectivity. Current-voltage relationships from a ramp protocol measured with bath solutions containing 140 mM NaCl or NaMeS, as indicated for whole-cell mBest2 currents activated by 5 μM Ca (*a*) or native currents activated by 100 μM Ca in an inside-out membrane patch from the dendritic knob/cilia of an OSN (*b*). The two almost-identical traces in symmetrical Cl were measured before and after anion substitution both in *a* and *b*. (*c*) Relative permeability ratios (P_X/P_{Cl}) calculated with the Goldman–Hodgkin–Katz relation from measured reversal potentials were I:NO_3:Br:Cl:MeS = 1.8:1.4:1.2:1:0.3 for mBest2 currents and 4.7:3.4:2.2:1:0.13 for native olfactory currents. (*d*) Rectification of Ca-activated Cl currents calculated as the ratio of currents measured at +50 and −50 mV from experiments as in *a* and *b* in symmetrical Cl.

Extracellular Blockers. Specific blockers for Ca-activated Cl channels with high binding affinity are not available. The most commonly used extracellular blockers of the Ca-activated Cl component of the odorant-induced current in OSNs are 300–500 μM niflumic acid (NFA) and 2–5 mM 4-acetamido-4′-isothiocyanato-stilben-2,2′-disulfonate (SITS; refs. 6, 7, 17, and 36). Here, we investigate the extracellular blockage properties of NFA and SITS on mBest2 currents (Fig. 6). Two millimolar SITS rapidly blocked the Ca-induced current measured at −50 mV and, after SITS removal, the current returned to its initial level (Fig. 6*a*). The blockage by 1 mM NFA was also rapid, and the current slowly recovered toward its original level (Fig. 6*b*). In mBest2-expressing cells, the extracellular application of 1 mM NFA blocked 77 ± 3%, whereas 2 mM SITS blocked 85% ± 4% of the Ca-activated current at −50 mV (Fig. 6*c*). We measured the extracellular SITS blockage in the range from 10 μM to 5 mM and found that it was rapid, reversible, and dose-dependent with a $K_{1/2}$ of 0.4 mM (Fig. 6*d*). The study of the dose dependence of the extracellular blocking effect of NFA in the range from 10 μM to 1 mM revealed a more complex phenomenon. Current blockage by NFA developed with time and reached almost the same steady-state blockage level at every tested concentration, whereas the time necessary to reach steady state was longer as the NFA concentration was decreased (Fig. 6 *e* and *f*). Similar results were obtained at −50 and +50 mV for both NFA and SITS, indicating that their blockage properties on mBest2 current were not voltage-dependent.

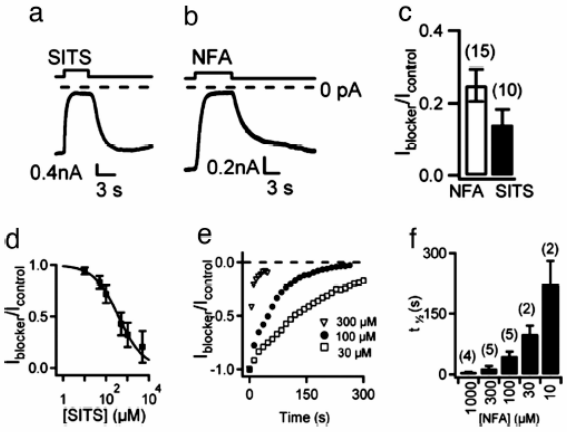

Fig. 6. Extracellular blockage by SITS and NFA on mBest2 currents. HEK-293 cells expressing mBest2 were voltage-clamped at −50 mV with 5 μM intracellular free Ca. Two millimolar SITS (*a*) or 1 mM NFA (*b*) were bath-applied for the time indicated. (*c*) Mean ratios between the amplitudes of the current in the presence and absence of the blocker. (*d*) Sensitivity of mBest2 currents to extracellular SITS. Amplitude of the currents in the presence of various SITS concentrations normalized to control currents was plotted versus SITS concentration and fitted to the Hill equation (five to nine cells). (*e*) Time course of blockage of mBest2 current by various NFA concentrations. (*f*) Time necessary to block half of the current ($t_{1/2}$) at various NFA concentrations.

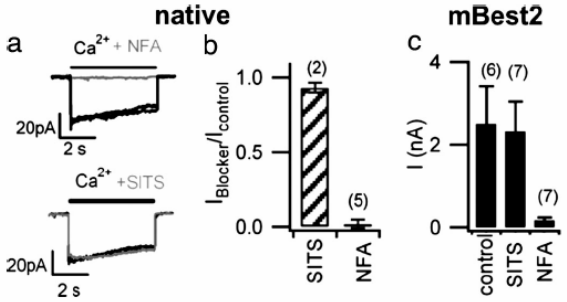

Fig. 7. Intracellular blockage by NFA and SITS. (*a*) Native currents were activated in inside-out patches from dendritic/knob cilia of an OSN by 100 μM Ca at −50 mV. In the same patch, bath application of 1 mM NFA (gray trace, *Upper*) rapidly and reversibly blocked the current, whereas 2 mM SITS (gray trace, *Lower*) did not significantly block the current. Black traces in each image are Ca-activated Cl currents recorded before and after application of each blocker and show the stability of the recordings. (*b*) Ratios between native olfactory Ca-activated Cl currents measured in the presence and absence of SITS or NFA. (*c*) Comparison of average currents measured in mBest2-transfected HEK-293 cells activated by 5 μM intracellular free Ca^{2+} in control and with the intracellular addition of 300 μM NFA or 2 mM SITS.

Intracellular Blockers. We investigated the intracellular blockage properties of NFA and SITS on native olfactory Ca-activated Cl channels in excised inside-out patches. Ca-activated Cl currents were rapidly blocked by the application of 1 mM NFA to the intracellular side (Fig. 7 *a* and *b*), whereas currents were not affected by the addition of 2 mM SITS (Fig. 7 *a* and *b*). The intracellular blockage of NFA or SITS was measured in mBest2 currents by calculating the average whole-cell current activated by 5 μM Ca in the patch pipette in the absence of blockers (control) or in the presence of 300 μM NFA or 2 mM SITS. Intracellular application of 2 mM SITS did not significantly affect Ca-activated mBest2 current, whereas 300 μM NFA blocked most of the current (Fig. 7*c*), similarly to the effects measured on native olfactory Ca-activated Cl currents (Fig. 7*b*).

Discussion

The data presented in this study reveal that mBest2 is expressed in the cilia of OSNs, where it colocalizes with CNGA2, the principal subunit of the CNG olfactory channel responsible for the primary transduction current. Electrophysiological properties of Ca-activated Cl currents of native channels in dendritic/knob cilia of OSNs and of mBest2 expressed in HEK-293 cells are remarkably similar. In fact, both currents have the same anion permeability sequence, small estimated single-channel conductances, current–voltage relations quite close to linearity, and voltage-independent side-specific blockage by NFA and SITS but a Ca sensitivity difference of one order of magnitude. Therefore, the colocalization of mBest2 with CNGA2 on the cilia and the functional data suggest that mBest2 plays a role in olfactory transduction as a molecular component of the ciliary Ca-activated Cl channel. If functional properties of native Ca-activated Cl currents and mBest2 currents are similar, nonetheless they are not identical, and the existing differences indicate the possibility that, as in the case of olfactory CNG channels (reviewed in ref. 33), native channels may be composed of additional proteins.

Comparison of Functional Properties Between Ca-Activated Cl Currents from Knob/Cilia of OSNs and mBest2-Dependent Currents. To functionally compare native Ca-activated Cl currents of OSNs and heterologously expressed mBest2, we performed an electrophysiological analysis of the two currents. A side-by-side comparison in excised inside-out patches for both Ca-dependent currents was not possible, because we did not detect any measurable current in inside-out excised patches from HEK-293 cells expressing mBest2. Therefore, we determined mBest2 functional properties with the whole-cell voltage–clamp technique. Although several properties between native and mBest2 currents were very similar, the nonperfect match could be due to several reasons. First, the use of different recording configurations could produce different results. Second, there could be a lack of posttranslational modification of mBest2 in heterologous systems, such as phosphorylation or sumoylation, that can modulate ion channels (37, 38). Third, ion channels are often composed of more than one type of subunit and/or have additional regulatory proteins that modify the functional properties.

The most significant difference between the two currents was found to be their sensitivity to intracellular Ca. In fact, currents were half-maximal at a Ca concentration of 0.4 μM for mBest2, similar to previous results (19, 21), whereas native currents required a higher Ca concentration, 4.7 μM, in general agreement with micromolar values measured in rat (39) and mouse (17). Dose–response relations obtained from isolated frog olfactory cilia also showed a similar $K_{1/2}$ of 4.8 μM (4). In all cases, there was no significant voltage dependence of Ca activation. Another study (40) measured electrophysiological properties of a Ca-activated Cl current from rat excised patches that did not show similar characteristics to those reported here and by refs. 17 and 39.

The native Ca-activated Cl current slowly inactivated in the presence of a constant Ca concentration when measured in excised patches, as shown by refs. 17 and 39, whereas mBest2 currents in whole-cell recordings did not show any time-dependent change in the presence of any given Ca concentration, as described in refs. 21–23 and 26. However, in isolated frog olfactory cilia, Kleene and Gesteland (4) did not find any current inactivation during prolonged exposure to Ca. The difference in inactivation properties may reflect specific differences between amphibian and mammalian channels or may indicate that some factor remains inside the isolated cilia, whereas it is lost upon excision of the membrane patch.

The current–voltage relations activated by high Ca concentrations in symmetrical Cl solutions were quite close to linearity, with only a moderate inward rectification in native channels, as reported by refs. 4 and 39, and a slight outward rectification in mBest2 currents. Previous reports found a more linear current-voltage relation for mBest2 currents (21, 22).

Single-channel events have not been directly measured because of small unit conductances. The single-channel conductance has been estimated by noise analysis to be 1.6 pS for native channels, in good agreement with previous estimates of 0.5–1.7 pS (39, 41) and 0.3 pS for mBest2 channels. The quite large numerical difference could originate from a different single level of conductance and also from the existence of multiple conductance levels and gating properties in the two channels.

Both native olfactory and mBest2 currents exhibited the same anion permeability sequence $I>NO_3>Br>Cl\gg MeS$, although the calculated permeability ratios were not identical. This permeability sequence corresponds to the Eisenman "weak field strength" lyotropic series (42), indicating that in both channels, the interaction between the permeant ion and the channel is weak, and permeability is related to the ease with which the permeant ion leaves the bulk solution and enters the channel. Our data are in general agreement with previous measurements (21, 22, 39).

The blocking properties of NFA and SITS were revealed to be similar in native olfactory and mBest2 currents. From the extracellular side, both NFA and SITS block the mBest2 current in the same range of concentration in which the native current is blocked (6, 7, 36). From the intracellular side, only NFA blocks both Ca-activated Cl currents, whereas SITS does not have a

significant effect, in agreement with previous measurements in frog olfactory cilia (5, 15).

Mechanism of Ca Activation. Native olfactory channels appear to be rapidly activated by Ca in inside-out patches (see also refs. 17 and 39) and in isolated olfactory cilia (4, 5), whereas similar experiments for Ca activation of mBest2 are missing. A recent study (25) has shown that hBest4 can be activated by Ca in excised inside-out patches, indicating that diffusible messengers or protein phosphorylation are not implicated in Ca activation. However, because the current activates and deactivates very slowly in response to Ca (time constant of 10–20 seconds), indirect Ca activation through a membrane-associated messenger cannot be excluded. Tsunenari *et al.* (25) also suggest that, alternatively, Ca could directly bind to hBest4, but that the binding controls the channel through another entity. Because bestrophin homologues have different channel kinetics and voltage dependencies (23, 24), we cannot exclude that each bestrophin has a different gating mechanism, as in the case of the TRP family of ion channels (43). We have found that mBest2 is the only bestrophin expressed in the OE. Site-directed mutagenesis experiments have demonstrated (21, 22, 26) that the putative second transmembrane domain of mBest2 participates in forming the channel pore, and therefore mBest2 appears to be at least part of the pore. However, it might also be possible that mBest2 forms a heteromultimer with other channel subunits, or that it has associated proteins that may, for example, modify Ca sensitivity and inactivation properties. It is likely that future studies will identify additional molecular components and/or modulators of the native olfactory Ca-activated Cl channel.

Conclusions

The colocalization of mBest2 with CNGA2 on the cilia of OSNs, together with the functional data, strongly indicates that mBest2 mediates the Ca-activated Cl current involved in olfactory transduction. Future studies should examine the involvement of additional components in forming and/or modulating the native olfactory channel. Our results contribute to the elucidation of the molecular mechanisms underlying olfactory transduction and provide further information about the physiological role of bestrophins. Indeed, our data indicate that olfactory transduction is a good experimental system to study the physiological function of mBest2.

Materials and Methods

RT-PCR and Single-Cell RT-PCR. Tissue and single neurons were obtained from adult C57Black/6 mice. A description of the method is given in *Supporting Text*, which is published as supporting information on the PNAS web site.

Production of an Anti-mBest2 Polyclonal Antibody. Antibody was raised by immunization of rabbit using GST-C-terminal 431-bp mBest2 fusion protein (for details, see *Supporting Text*).

Cell Culture, Transfections, and Immunoblot. HEK-293 cells were transfected with mBest2 construct in pCMV-Sport6 by using FuGENE 6 reagent (Roche Diagnostics, Indianapolis, IN). For Western blot, membrane fractions enriched in olfactory cilia from OSNs were obtained with the calcium-shock method according to ref. 44 (see *Supporting Text*).

Immunofluorescence. Immunolabeling was performed by standard protocols for tissue fixation and processing (see *Supporting Text*). The staining was analyzed by confocal microscopy.

Electrophysiology. mBest2 currents were recorded in the whole-cell patch–clamp configuration from HEK-293 transfected cells. Native olfactory currents were recorded in inside-out patches excised from the dendritic knob/cilia of OSNs, obtained by enzymatic dissociation of the OE of 4- to 8-week-old C57Black/6 and BALB/c mice, as described (45, 46). For details, see *Supporting Text*. Averaged values are mean ± SEM. In the figures, the number of recorded cells or patches is indicated in parentheses; error bars indicate SEM.

We thank L. Buck, M. Pusch, R. Tirindelli, P. Pelosi, E. Cherubini, A. Nistri, and V. Torre for interesting discussions; F. Margolis (University of Maryland, Baltimore, MD) for the gift of the OMP antibody; F. Müller and U. B. Kaupp (Forschungszentrum Julich, Julich, Germany) for the gift of the CNGA2 monoclonal antibody; M. Stebel for mBest2 polyclonal antibody production; L. Masten for OE and ciliary membrane preparations; C. Patton for discussion on Ca buffering; B. Cataletto, M. Celussi, and G. Adami for help with calcium measurements; L. De Maso for technical help; and M. Schipizza-Lough for checking the English. This work was supported by European Union Grant NFG 503221, the Giovanni Armenise–Harvard Foundation, and the Istituto Italiano di Tecnologia.

1. Schild, D. & Restrepo, D. (1998) *Physiol. Rev.* **78,** 429–466.
2. Buck, L. B. (2000) *Cell* **100,** 611–618.
3. Menini, A., Lagostena, L. & Boccaccio, A. (2004) *News Physiol. Sci.* **19,** 101–104.
4. Kleene, S. J. & Gesteland, R. C. (1991) *J. Neurosci.* **11,** 3624–3629.
5. Kleene, S. J. (1993) *Neuron* **11,** 123–132.
6. Lowe, G. & Gold, G. H. (1993) *Nature* **366,** 283–286.
7. Kurahashi, T. & Yau, K. W. (1993) *Nature* **363,** 71–74.
8. Kaneko, H., Nakamura, T. & Lindemann, B. (2001) *Am. J. Physiol.* **280,** C1387–C1393.
9. Reuter, D., Zierold, K., Schroder, W. H. & Frings, S. (1998) *J. Neurosci.* **18,** 6623–6630.
10. Nakamura, T., Kaneko, H. & Nishida, N. (1997) *Neurosci. Lett.* **237,** 5–8.
11. Zhainazarov, A. B. & Ache, B. W. (1995) *J. Neurophysiol.* **74,** 479–483.
12. Kleene, S. J. (1997) *Biophys. J.* **73,** 1110–1117.
13. Matthews, H. R. & Reisert, J. (2003) *Curr. Opin. Neurobiol.* **13,** 469–475.
14. Menini, A. (1999) *Curr. Opin. Neurobiol.* **9,** 419–426.
15. Frings, S., Reuter, D. & Kleene, S. J. (2000) *Prog. Neurobiol.* **60,** 247–289.
16. Kaneko, H., Putzier, I., Frings, S., Kaupp, U. B. & Gensch, T. (2004) *J. Neurosci.* **24,** 7931–7938.
17. Reisert, J., Lai, J., Yau, K. W. & Bradley, J. (2005) *Neuron* **45,** 553–561.
18. Nickell, W. T., Kleene, N. K., Gesteland, R. C. & Kleene, S. J. (2006) *J. Neurophysiol.* **95,** 2003–2006.
19. Qu, Z., Wei, R. W., Mann, W. & Hartzell, H. C. (2003) *J. Biol. Chem.* **278,** 49563–49572.
20. Hartzell, C., Qu, Z., Putzier, I., Artinian, L., Chien, L. T. & Cui, Y. (2005) *Physiology (Bethesda)* **20,** 292–302.
21. Qu, Z., Fischmeister, R. & Hartzell, C. (2004) *J. Gen. Physiol.* **123,** 327–340.
22. Qu, Z. & Hartzell, C. (2004) *J. Gen. Physiol.* **124,** 371–382.
23. Sun, H., Tsunenari, T., Yau, K. W. & Nathans, J. (2002) *Proc. Natl. Acad. Sci. USA* **99,** 4008–4013.
24. Tsunenari, T., Sun, H., Williams, J., Cahill, H., Smallwood, P., Yau, K. W. & Nathans, J. (2003) *J. Biol. Chem.* **278,** 41114–41125.
25. Tsunenari, T., Nathans, J. & Yau, K. W. (2006) *J. Gen. Physiol.* **127,** 749–754.
26. Qu, Z., Chien, L. T., Cui, Y. & Hartzell, H. C. (2006) *J. Neurosci.* **26,** 5411–5419.
27. Hartzell, C., Putzier, I. & Arreola, J. (2005) *Annu. Rev. Physiol* **67,** 719–758.
28. Kramer, F., Stohr, H. & Weber, B. H. (2004) *Cytogenet. Genome Res.* **105,** 107–114.
29. Petrukhin, K., Koisti, M. J., Bakall, B., Li, W., Xie, G., Marknell, T., Sandgren, O., Forsman, K., Holmgren, G., Andreasson, S., *et al.* (1998) *Nat. Genet.* **19,** 241–247.
30. Marquardt, A., Stohr, H., Passmore, L. A., Kramer, F., Rivera, A. & Weber, B. H. (1998) *Hum. Mol. Genet.* **7,** 1517–1525.
31. White, K., Marquardt, A. & Weber, B. H. (2000) *Hum. Mutat.* **15,** 301–308.
32. Pusch, M. (2004) *J. Gen. Physiol.* **123,** 323–325.
33. Kaupp, U. B. & Seifert, R. (2002) *Physiol. Rev.* **82,** 769–824.
34. Keller, A. & Margolis, F. L. (1975) *J. Neurochem.* **24,** 1101–1106.
35. Meyer, M. R., Angele, A., Kremmer, E., Kaupp, U. B. & Muller, F. (2000) *Proc. Natl. Acad. Sci. USA* **97,** 10595–10600.
36. Kurahashi, T. & Menini, A. (1997) *Nature* **385,** 725–729.
37. Muller, F., Vantler, M., Weitz, D., Eismann, E., Zoche, M., Koch, K. W. & Kaupp, U. B. (2001) *J. Physiol.* **532,** 399–409.
38. Rajan, S., Plant, L. D., Rabin, M. L., Butler, M. H. & Goldstein, S. A. (2005) *Cell* **121,** 37–47.
39. Reisert, J., Bauer, P. J., Yau, K. W. & Frings, S. (2003) *J. Gen. Physiol.* **122,** 349–363.
40. Hallani, M., Lynch, J. W. & Barry, P. H. (1998) *J. Membr. Biol.* **161,** 163–171.
41. Larsson, H. P., Kleene, S. J. & Lecar, H. (1997) *Biophys. J.* **72,** 1193–1203.
42. Eisenman, G. & Horn, R. (1983) *J. Membr. Biol.* **76,** 197–225.
43. Clapham, D. E. (2003) *Nature* **426,** 517–524.
44. Pace, U., Hanski, E., Salomon, Y. & Lancet, D. (1985) *Nature* **316,** 255–258.
45. Lagostena, L. & Menini, A. (2003) *Chem. Senses* **28,** 705–716.
46. Boccaccio, A., Lagostena, L., Hagen, V. & Menini, A. (2006) *J. Gen. Physiol.* **128,** 171–184.

Chem. Senses 33: 397–404, 2008

doi:10.1093/chemse/bjn007
Advance Access publication February 25, 2008

Electroolfactogram Responses from Organotypic Cultures of the Olfactory Epithelium from Postnatal Mice

Giulietta Pinato, Juraj Rievaj, Simone Pifferi, Michele Dibattista, Lara Masten and Anna Menini

Neurobiology Sector, International School for Advanced Studies, SISSA, Italian Institute of Technology, SS 14 Km 163.5, 34012 Basovizza, Trieste, Italy

Correspondence to be sent to: Anna Menini, Neurobiology Sector, International School for Advanced Studies, SISSA, SS 14 Km 163.5, 34012 Basovizza, Trieste, Italy. e-mail: menini@sissa.it

Abstract

Organotypic cultures of the mouse olfactory epithelium connected to the olfactory bulb were obtained with the roller tube technique from postnatal mice aged between 13 and 66 days. To test the functionality of the cultures, we measured electro-olfactograms (EOGs) at different days in vitro (DIV), up to 7 DIV, and we compared them with EOGs from identical acute preparations (0 DIV). Average amplitudes of EOG responses to 2 mixtures of various odorants at concentrations of 1 mM or 100 μM decreased in cultures between 2 and 5 DIV compared with 0 DIV. The percentage of responsive cultures was 57%. We also used the phosphodiesterase inhibitor 3-isobutyl-1-methylxanthine (IBMX) to trigger the olfactory transduction cascade bypassing odorant receptor activation. Average amplitudes of EOG responses to 500 μM IBMX were not significantly different in cultures up to 6 DIV or 0 DIV, and the average percentage of responsive cultures between 2 and 5 DIV was 72%. The dose–response curve to IBMX measured in cultures up to 7 DIV was similar to that at 0 DIV. Moreover, the percentage of EOG response to IBMX blocked by niflumic acid, a blocker of Ca-activated Cl channels, was not significantly different in cultured or acute preparations.

Key words: electroolfactogram, IBMX, olfaction, organotypic culture, transduction

Introduction

The olfactory system allows the detection and perception of a large number of odorant molecules. The initial events in olfaction occur in the olfactory epithelium (OE), in the nasal cavity, where the olfactory sensory neurons (OSNs) are located. OSNs are bipolar neurons with a dendritic process ending with several cilia and an axon projecting to the olfactory bulb (OB). Odorant molecules bind to odorant receptors in the ciliary membrane of OSNs, initiating the olfactory transduction cascade. The binding of odorant molecules to odorant receptors activates a G protein, which stimulates adenylate cyclase to produce cyclic adenosine 3′,5′monophosphate (cAMP). The increased concentration of cAMP opens cyclic nucleotide–gated (CNG) channels allowing a depolarizing influx of Na and Ca ions into the cilia. The increase in intraciliary Ca concentration opens Ca-activated Cl channels that further contribute to depolarization. Action potentials evoked by odor-induced depolarization propagate through the axons of OSNs to the OB, where odorant information is further processed (for reviews, see Schild and Restrepo 1998; Menini 1999; Firestein 2001; Buck 2004; Menini et al. 2004; Lledo et al. 2005).

Several experimental models have been used to study olfactory transduction, coding, and regeneration, from invertebrates to mammals (Ache and Young 2005), including in vivo as well as in vitro preparations. For in vitro experiments, acute preparations are usually employed: dissociated OSNs (Kleene and Gesteland 1983; Boccaccio et al. 2006), slices of the OE (Hegg et al. 2003) or of the OB (Nickell et al. 1996; Pinato and Midtgaard 2005), and semi-intact preparations of the OE and of the OB (Ma et al. 1999; Lin et al. 2007). Several types of culture methods for OSNs have also been developed from embryonic, newborn, or adult rats (Noble et al. 1984; Pixley and Pun 1990; Chuah et al. 1991; Ronnett et al. 1991; Trombley and Westbrook 1991; Vargas and Lucero 1999). Organotypic cultures of the mammalian OE, where OSNs are cultivated in their native environment, have been developed not only by using fetal tissue (Farbman 1977; Gonzales et al. 1985; Gong et al. 1996; Goetze et al. 2002) but also postnatal tissue (Michel et al. 1999; Josephson et al. 2004). Organotypic cultures have several advantages over acute preparations or living animals: whereas cells are maintained in their native environment,

organotypic cultures allow easier visualization, long-lasting monitor of the activity, delivery of substances such as gene constructs or small interfering RNAs (siRNA), and measurement of the induced functional modifications.

The organotypic culture preparations of OE from postnatal mice developed by Michel et al. (1999) or by Josephson et al. (2004) were rather different. Josephson et al. cultured pieces of OE and OB explanted from 1- to 4-day-old mice. Using cell-specific markers, they identified various long-lived cell types, including the presence of mature OSNs marked by the olfactory marker protein (OMP) up to 28 days in vitro (DIV). They also tested the functionality of the cultures by measuring the electroolfactograms (EOGs) in response to puffs of vapor from an odorant mixture solution and measured EOG responses from 13 of 30 cultures tested corresponding to a percentage of about 43% (13/30) responsive cultures (Josephson et al. 2004). The organotypic culture model from postnatal mice developed by Michel et al. (1999) consisted of the explanted half olfactory cavities including the turbinates and the epithelium connected to the corresponding OB. Michel et al. showed that those explants after several DIV had a structural morphology similar to that observed in situ: the OE structure and all the bulbar layers were preserved, and anti-OMP immunoserum specifically labeled the sensory neurons up to at least 10 DIV. However, electrophysiological experiments that would allow verifying the functional integrity of the OSNs maintained in vitro have not been investigated yet.

The purpose of our study was to obtain organotypic cultures of the OE connected to OB and test their functionality by measuring the EOGs in response to odorants or to 3-isobutyl-1-methylxanthine (IBMX), an inhibitor of phosphodiesterase. We compared these measurements with controls obtained from acute preparations of OEs connected to OB. These measurements are of primary importance to contribute to the assessment of whether, and to which extent, these cultures can be used as a chronic model to address questions related, for example, to proteins involved in the signal transduction cascade or in the coding process, employing gene or siRNA delivery (Li et al. 2006).

Materials and methods

Preparation of organotypic cultures

Olfactory organotypic cultures were prepared from BALB/c mice aged between 13 and 66 days. Mice were anesthetized with CO_2 inhalation and decapitated, in accordance with the regulations of the Italian Animal Welfare Act and the local authority veterinary service. The cultures were prepared with a technique similar to that developed by Michel et al. (1999) and based on the Gähwiler's roller tube technique (Gahwiler 1981), with some modifications as described in the following. The head was split midsagittally and placed in mammalian Ringer's solution containing (in millimoles): 140 NaCl, 5 KCl, 1 $CaCl_2$, 1 $MgCl_2$, 10 HEPES, 10 D-Glucose, 1 sodium pyruvate, and pH 7.4 with NaOH. The cranial bones and the septum were removed, and each brain hemisphere was detached, leaving the OB intact. The turbinates with the OE connected to the OB were placed on a glass cover slip of 12 × 24 mm in a 20-µl drop of chicken plasma reconstituted according to the manufacturer's instructions from filtered and lyophilized plasma (30-0390L Cocalico Biologicals, Reamstown, PA, or P3266 Sigma, St Louis, MO). The plasma was then coagulated by carefully adding 30 µl bovine thrombin (activity 200 U/ml, 2374 Merck). Cover slips with the explants were kept under the hood at room temperature in a covered petri dish to prevent the tissue from drying out. After waiting about 40 min for a complete coagulation, the cover slips with the olfactory explants were inserted into 15-mm culture tubes containing 2 ml of growth medium. Tubes were capped and placed in a roller drum rotating at 20 turns/h inside an incubator at 37 °C. (The glass cover slips were previously cleaned by immersion in a 0.5 M HCl solution for 24 h, washed with deionized water, placed in ethanol for 30 min, washed again, and dried at 150 °C.) The growth medium was changed every 2 days and contained: MEM with Glutamax (Gibco, 41090), 25 mM HEPES, 25 mM D-glucose, 2.5 mM $MgCl_2$, 0.5 mM ascorbic acid sodium salt, 0.5 mg/l insulin, penicillin (100 U/ml), streptomycin (100 µg/ml) (Gibco), 20% horse serum (Gibco, Grand Island, NY), and pH 7.4.

Electroolfactograms

Cultures at different DIV, or acute preparations, were transferred to the recording chamber, completely immersed and perfused with mammalian Ringer's solution, at room temperature (20–22 °C). EOGs were measured at the surface of the OE (Ottoson 1955; Scott and Scott-Johnson 2002). The recording electrodes were made from glass capillaries pulled with a Narishige PP83 puller (Narishige, Tokyo, Japan), gently broken at the tip, fire polished, and filled with mammalian Ringer's solution (electrical resistance of about 1 MΩ). The electrode was connected via an Ag/AgCl wire to the head stage of a MultiClamp 700B patch-clamp amplifier (Axon Instruments, Union City, CA). The bath electrode consisted in an Ag/AgCl pellet placed in the recording chamber. Stimuli, consisting of a mixture of odorants (Sigma) or of IBMX (Sigma), were delivered by a multipipe system placed close to the epithelium. The recording pipette was placed close to the surface of the OE with a micromanipulator (Luigs and Neumann, Retingen, Germany). EOG recordings were typically measured by placing the electrode in the middle of turbinate II′ or III (see Figure 1B, using the nomenclature of Ressler et al. 1993), and the position of the electrode was adjusted to measure negative EOGs in response to the stimuli. We defined a response as a negative deflection of more than twice the magnitude of the peak-to-peak noise of the recording (the smallest response we

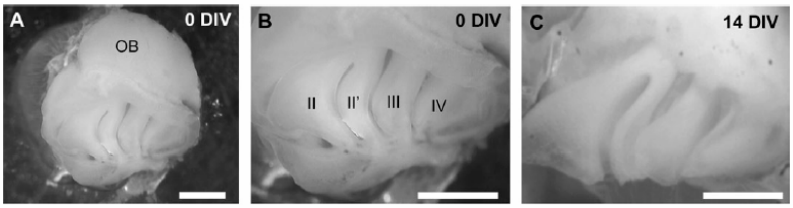

Figure 1 Comparison of an acute explant of the mouse OE connected to the OB with an organotypic culture. **(A)** Photomicrograph of the OE preparation connected to the OB acutely isolated (0 DIV). **(B)** and **(C)** The olfactory turbinate system in the 0 DIV preparation (same OE as in A) and in a 14 DIV culture. Roman numbers indicate individual turbinates using the nomenclature of Ressler et al. (1993). Scale bar in A, B, C: 2 mm.

considered was −50 μV). Electrical signals were passband filtered at 0.1 Hz–1 kHz, digitized at 10 kHz (Digidata 1200, Axon Instruments), stored in a personal computer, and analyzed with pClamp 8.2 (Axon Instruments) or with Igor Pro software (WaveMetrics, Lake Oswego, OR).

For odorant stimulation, we used 2 odorant mixtures. Mixture 1 was composed of 3 odorants: cineole, acetophenone, and amylacetate, each present at 1 mM; mixture 2 was composed of 17 odorants: amylacetate, 2-heptanone, S-(+)carvone, R-(−)carvone, isoamylacetate, cineole, acetophenone, eugenol, octanal, R-(+)limonene, 1-octanol, nonanal, 1-heptanal, citral, geraniol, (−)menthone, and decanal, at 100 μM each. All odorants were prepared in dimethylsulfoxide (DMSO) at 0.5 M and diluted to the final concentration in Ringer's solution. The total concentration of DMSO in the mixtures was never more than 0.6% and had no effect on EOGs (data not shown). All odorants and DMSO were from Sigma.

The IBMX stock solution was prepared in Ringer's solution at 1 mM and diluted to final concentrations. Niflumic acid (NFA; Sigma) was prepared in DMSO at 200 mM as a stock and diluted to the final concentration in Ringer's solution.

To compare different treatments or populations, we used analysis of variance (ANOVA). Significance of differences between individual data points was determined using unpaired *t*-tests. P values <0.05 were considered significant. Data are reported as mean ± standard deviation and the total number of responsive OEs (N).

Results

We set up a preparation by explanting one-half of the entire olfactory system from cranial bones. It included all turbinates, covered by olfactory neuroepithelium, and the corresponding hemisphere of OB, as illustrated in the photomicrograph in Figure 1A. The overall morphology of the OE at 0 DIV and at 14 DIV appeared largely similar (Figure 1B,C).

To assess the functionality of cultured mouse OEs, we recorded the EOG in response to the exposure of odorants or to the phosphodiesterase inhibitor IBMX and compared these results with controls performed in acute preparations. The EOG is an extracellular field potential originating from the summated activities of many OSNs near the recording electrode at the surface of the epithelium and provides a good quantitative test of the neurons' functionality (Ottoson 1955; Scott and Scott-Johnson 2002; Nickell et al. 2006). EOG responses were recorded from turbinates II' or III (Figure 1B).

EOG responses to odorants

In a first set of experiments, we tested the physiological response to odorants. Figure 2 shows representative recordings of EOG responses to 2 different odorant mixtures, whose composition was selected to increase the probability that a large number of OSNs respond to the stimulus. Odorant mixture 1 was composed of 1 mM cineole, amylacetate, and acetophenone. Very high odorant concentrations (1 mM) were included in this mixture to increase the probability of obtaining responses also from OSNs expressing odorant receptors with a low sensitivity to the selected odorants. Indeed, it is well known that about 1000 different odorant receptors are expressed in various neurons and that each OSN has a specific dose–response curve for various odorants (Firestein 2001; Mombaerts 2004). For example, it has been shown that the odorant concentration necessary to activate half of the maximal current in individual neurons ranges from 3×10^{-6} to 9×10^{-5} M (Firestein et al. 1993) and, more recently, that 100 μM was not sufficient to reach saturation in dose–response curves measured with EOG recordings from mouse OEs (Munger et al. 2001). Recordings in Figure 2A show that the shapes of the EOGs from cultured OEs at different DIV were quite similar to those of EOGs from acute preparations, that is, it was characterized by a steep negative deflection of the polarization that reached a peak and then repolarized. We measured EOGs in response to the odorant mixture 1 in 10 acute preparations from different mice and found 9 responsive OEs, corresponding to 90% functional preparations, with an average response of −249 ± 94 μV (N = 9). Eight cultured OEs, ranging from 2 to 5 DIV, obtained from different mice were tested with

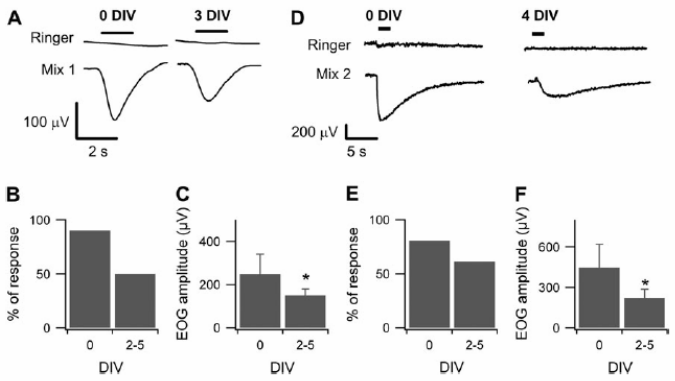

Figure 2 EOG responses to odorants in mouse acute isolated and cultured OEs. **(A)** Recordings from an acute OE (0 DIV, first column) and a 3 DIV OE (second column). For each OE, Ringer alone was first applied for 2 s as a control for perfusion artifacts (upper traces), and then odorant mixture 1 composed of 1 mM acetophenone, amylacetate, and cineole in Ringer was applied for 2 s (lower traces). The time of application of the stimulus is indicated with the black horizontal bars. **(B)** Percentage of responsive preparations at 0 DIV or between 2 and 5 DIV, as indicated. **(C)** Average amplitude of EOG responses at 0 DIV or at 2–5 DIV was significantly different (*t*-test: $P < 0.05$). The same type of experiments was repeated with odorant mixture 2 composed of 17 odorants each at 100 μM: amylacetate, 2-heptanone, S-(+)carvone, R-(−)carvone, isoamylacetate, cineole, acetophenone, eugenol, octanal, R-(+)limonene, 1-octanol, nonanal, 1-heptanal, citral, geraniol, (−)menthone, and decanal. **(D)** The percentage of responsive preparations and the average EOG amplitudes at various DIV were plotted in **(E)** and **(F)**, respectively. As in (C) the average amplitude of EOGs at 0 DIV and at 2–5 DIV was significantly different (*t*-test: $P < 0.05$).

odorants, and 4 epithelia (50%) responded with a negative EOG to the applied stimulus (Figure 2B). The average EOG response to odorant mixture 1 in cultures between 2 and 5 DIV was −150 ± 30 μV ($N = 4$), significantly lower than the average amplitude measured at 0 DIV (*t*-test: $P < 0.05$) (Figure 2C).

It could be of interest to note that we tested 3 more epithelia that remained in culture up to day 8, 10, and 14, and we found that all 3 responded to the odorant mixture, although we did not systematically investigate responses in long-living cultures.

We performed a second set of experiments using a different mixture, composed of 17 odorants, each present at 100 μM (see odorant composition in the legend of Figure 2 or Materials and methods), to increase the probability to obtain a response from more OSNs that could express odorant receptors nonsensitive to mixture 1. As shown in Figure 2D, the shape of the EOGs was similar to that previously recorded with mixture 1 (Figure 2A), both in acute and cultured OEs. Moreover, also with odorant mixture 2, we measured a reduction in the percentage of cultures responding to odorants between 2 and 5 DIV compared with 0 DIV (Figure 2E) and a significant decrease in the average amplitude of EOGs (Figure 2F). Indeed, the average EOG response to odorant mixture 2 in cultures between 2 and 5 DIV was −225 ± 63 μV ($N = 8$), significantly lower than −445 ± 174 μV ($N = 28$) measured at 0 DIV (*t*-test: $P < 0.05$).

Therefore, for both mixtures, the percentage of cultures responding to odorants was lower than that for acute preparations. Moreover, also the average EOG amplitude of the responsive cultures was significantly lower than that measured at 0 DIV.

It would be interesting to determine dose–response relations in response to odorants; however, previous experiments with EOG measurements could not determine useful dose–response curves because saturation was never effectively achieved (Munger et al. 2001). We therefore did not attempt to measure dose–response relations in response to odorants, but we obtained dose–response relations in response to IBMX, as described in detail in the following paragraphs.

EOG responses to IBMX

IBMX is widely used to activate the cyclic nucleotide second messenger cascade bypassing the activation of odorant receptors in OSNs (Firestein, Darrow, and Shepherd 1991; Firestein, Zuffall, and Shepherd 1991; Chen et al. 2000). IBMX is an inhibitor of PDE, and because in the cilia of functional OSNs there is an endogenous activity of both adenylate cyclase and PDE, the inhibition of PDE causes an increase in the intraciliary cAMP concentration due to basal production of cAMP by adenylate cyclase. The increased cAMP concentration causes the opening of CNG channels and the depolarizing influx of Na and Ca ions in the cilia (Schild and Restrepo 1998; Firestein 2001). We investigated the functionality of OSNs by measuring EOG responses to the application of IBMX. Figure 3A shows representative recordings of EOG responses to IBMX in an acute preparation and after 5 days in culture. As previously observed for the responses to odorants (Figure 2), also the shapes of the

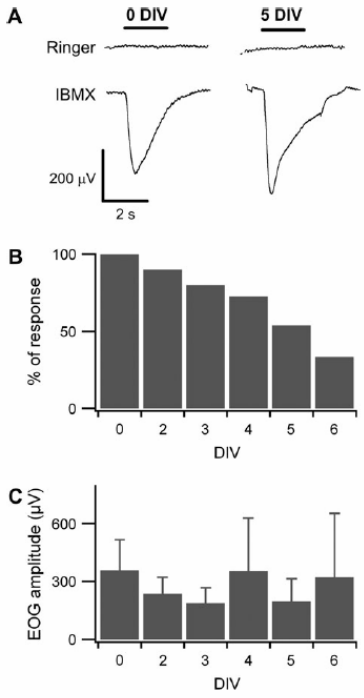

Figure 3 **(A)** EOG responses to IBMX application. Recordings from a 0 DIV (first column), and from a 5 DIV OE (second column). For each OE, Ringer alone was first applied for 2 s as a control for perfusion artifacts (upper traces), then 500 μM IBMX in Ringer was applied for 2 s (lower traces). The time of application of the stimulus is indicated with the black horizontal bars. **(B)** Percentage of responsive preparations at various DIV as indicated. **(C)** Average amplitude of EOGs in 500 μM IBMX in responsive acute preparations at various DIV was not significantly different (1-way ANOVA: $P = 0.36$) (0 DIV, $N = 10$; 2 DIV, $N = 6$; 3 DIV, $N = 4$; 4 DIV, $N = 5$; 5 DIV, $N = 7$; and 6 DIV, $N = 5$).

EOGs measured in response to IBMX from cultured OEs were similar to those of EOGs from acute preparations. We tested the response to 500 μM IBMX, a concentration giving saturation of the dose–response curve as shown in Figure 4B, in 10 acute OEs from different mice, and we found a response in every OE, with an average value of −358 ± 158 μV ($N = 10$). We analyzed the percentage of OEs responding to stimulation with IBMX at 0 DIV and after various days in culture (Figure 3B). At 0 DIV all OEs responded; between 2 and 4 DIV, we measured a response to IBMX in about 80% of the cultures; whereas after 5 DIV, the percentage of responsive cultures decreased to about 33% at 6 DIV. Therefore, a decrease in responses appears to be correlated to the longer time in vitro. The analysis of the average EOG amplitudes (Figure 3C) of the responsive cultures shows that the average amplitude was not significantly different at various DIV up to at least 6 DIV (1-way ANOVA: $P > 0.05$).

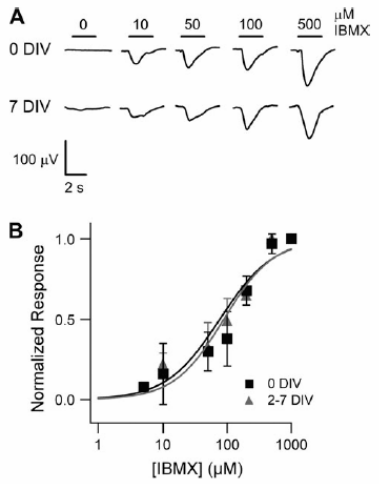

Figure 4 The dose–response relations for IBMX. **(A)** Comparison of EOG responses to different concentrations of IBMX from an acute OE (upper traces) and from a 7 DIV OE (lower traces). Black horizontal bars indicate the time of application of IBMX in Ringer. Numbers represent the IBMX concentrations (in micromoles). **(B)** EOG amplitudes induced by various concentrations of IBMX were normalized to the maximal response. Symbols plot the average responses from 4 acute (squares) and 6 cultured (triangles) OEs tested between 2 and 7 DIV. Lines were the best fit of the Hill equation to the data with $K_{1/2} = 76$ μM, $n = 1.3$, for acute and $K_{1/2} = 88$ μM, $n = 1.1$, for cultured epithelia.

It could be of interest to note that we tested some additional epithelia that remained in culture up to day 13 and found that some of them responded to IBMX, although we did not systematically investigate responses in long-living cultures.

IBMX induces similar dose–response relations in both acute and organotypic preparations

A further important test of the functional properties of OSNs is the measurement of the dose–response relations. Various concentrations of cAMP in OSNs were produced applying different concentrations of IBMX ranging from 5 μM to 1 mM. We therefore measured the EOGs in response to various concentrations of IBMX on the same epithelium. Figure 4 shows EOG recordings for different concentrations of IBMX in an acute (Figure 4A, upper traces) and in a 7 DIV OE (Figure 4A, lower traces). Several dose–response relations were measured both in acute and in cultured OEs. The average normalized peak responses at various IBMX concentrations were plotted versus the IBMX concentration (Figure 4B), and data were fitted with the Hill equation: $V/V_{max} = c^n/(c^n + K_{1/2}{}^n)$, where V is the peak EOG response measured at the concentration c, V_{max} is the maximal peak EOG response, $K_{1/2}$ is the IBMX concentration

producing 50% of the maximal response, and n is the Hill coefficient. The best fit gave $K_{1/2}$ = 76 μM, n = 1.3 for measurements from 4 fresh epithelia and $K_{1/2}$ = 88 μM, n = 1.1 for 6 epithelia in culture. These experiments demonstrate that in cultured OEs the dose–response relation for IBMX was very similar to that measured in acute OEs.

NFA reduces the EOG amplitude in both acute and organotypic preparations

To further investigate the pharmacology of olfactory signaling in cultured and acute preparations, we analyzed in more detail a commonly used blocker of the response. Indeed, it has been recently reported that the EOG response is primarily caused by a depolarizing Cl current (Nickell et al. 2006) that can be blocked by NFA, a well-known blocker for Ca-activated Cl channels involved in olfactory transduction (Kleene 1993; Kurahashi and Yau 1993; Lowe and Gold 1993; Zhainazarov and Ache 1995; Reisert et al. 2003; Pifferi et al. 2006; Boccaccio and Menini 2007). We therefore analyzed the effect of NFA on EOG recordings in organotypic cultures stimulated with IBMX. Perfusion for 5 min of 300 μM NFA in Ringer caused a great reduction of EOG responses both in acute preparations and in cultured OEs (Figure 5A). The block was largely reversible after extensive wash with Ringer's solution for 20–30 min. On average, NFA reduced the EOG amplitude by 74 ± 9% (N = 11) in acute preparations and by 58 ± 17% (N = 5) in cultured OEs (up to 5 DIV); the difference was not significant (t-test: P > 0.05) (Figure 5B). These results indicate that the Ca-activated Cl component of olfactory transduction in responsive organotypic cultures (at least up to 5 DIV) is similar to that measured in acute preparations.

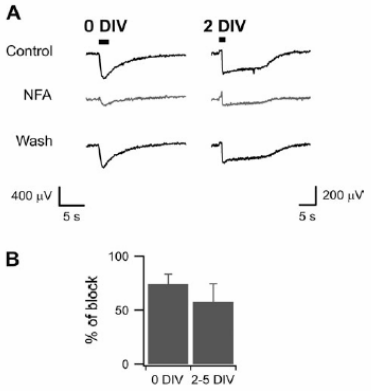

Figure 5 Reduction of EOG response amplitude by NFA. **(A)** EOG recordings from a 0 DIV (first column) and from a 2 DIV OE (second column) in response to 500 μM IBMX. Filled horizontal bars indicate the time of application of IBMX. A control EOG was first recorded, and then 300 μM NFA was added to the bath for 5 min. The EOG in response to IBMX was recorded again in the presence of NFA (middle traces), finally, the recovery of the EOG response to IBMX was tested after washing out NFA by 20- to 30-min perfusion of Ringer alone (lower traces). **(B)** Average percentage of EOG amplitude blocked by NFA at 0 DIV and between 2 and 5 DIV was not significantly different (unpaired t-test: P = 0.08; 0 DIV, N = 11; 2–5 DIV, N = 5).

Discussion

Our data show that it is possible to record EOG in response to odorants and to IBMX from organotypic cultures of the OE connected to its OB obtained from postnatal mice. To the best of our knowledge, EOG responses to odorants from organotypic cultures of OEs from postnatal mice have previously been reported only by Josephson et al. (2004). The olfactory organotypic culture system of Josephson et al. (2004) was different from that employed in our study because it was composed of pieces of OE and OB instead of the entire OE connected to the corresponding OB (Josephson et al. 2004). Moreover, they used a different way to apply odorants to the OE cultures: they recorded EOG in response to puffs of vapor from a 16 mM odorant mixture solution containing ethyl butyrate, eugenol, (+) carvone, and (−) carvone and they used a salt solution without calcium and magnesium. In contrast, we applied the stimuli dissolved in solution and used also other compounds to block or activate the transduction cascade (Chen et al. 2000; Lin et al. 2007). The percentage of cultures responding to odorants in Josephson et al. (2004) was 43%, whereas in our work, the total percentage of cultures responding to odorant mixtures was 57%. Therefore, a large reduction in the number of cultures responding to odorants was observed in both types of cultures. We did not detect any evident morphological difference between responding and nonresponding cultures. It is possible that damage of axonal connections between OE and OB could cause nonresponsive cultures, but we did not investigate the cause of the reduction of responses in cultures, which will open an interesting area for further studies.

We further investigated the EOG responses of organotypic cultures by using IBMX instead of odorants. The relationship between the number of DIV and the ability to respond to IBMX was investigated in detail, and we found that the percentage of cultures responding to IBMX decreased from about 80% between 2 and 4 DIV to about 33% at 6 DIV. We did not examine the causes of the reduction in the percentage of responsive cultures, which remain to be further investigated.

Our data showed that dose–response relations in response to IBMX were similar in acute and in cultured OEs (up to at least 7 DIV). Because IBMX induces an electrophysiological response bypassing the activation of odorant receptors and G proteins, the similarity of dose–response relations in response to IBMX indicates that the transduction cascade after activation of adenylyl cyclase is functional both in acute and in responsive organotypic preparations. Therefore, our results indicate that, although not every culture is functional,

at least those responding to IBMX appear to have a dose–response similar to acute preparations. The responsive OEs are likely to be useful in studies in which the function of some protein involved in the second part of the transduction cascade has been modified by using molecular biology techniques. For example, previous work has used differences in the dose–response to IBMX between wild-type and knockout mice for the subunit CNGA4 to show that the CNGA4 subunit contributes to the high cAMP sensitivity of the native olfactory channel (Munger et al. 2001). In their study, Munger et al. (2001) used IBMX because it induced response in all olfactory neurons, whereas useful dose–response relationships could not be determined for odors because saturation was never effectively achieved. The possibility of using of RNA interference (RNAi) on cultured OEs, instead of producing knockout mice, and the subsequent electrophysiological measurements, could be a powerful experimental tool to measure the functional consequences of modifying proteins that may be involved in olfactory transduction and signaling. Therefore, although further detailed studies of each step of the transduction cascade will be necessary to fully validate the use of this model, our EOG recordings show the ability of OE organotypic cultures to maintain their functionality over time in vitro and that this model is likely to be useful to help identifying the contribution and the identity of several proteins involved in the transduction cascade.

Finally, in this study, to further investigate the olfactory signaling in cultures, we measured the percentage of EOG response to IBMX blocked by NFA, a blocker of Ca-activated Cl channels, and found that the culture conditions did not significantly modify it. This property could be useful to help establishing the molecular identity of the Ca-activated Cl channel. Indeed, although recent work has suggested that bestrophin-2 is a candidate olfactory Ca-activated Cl channel (Pifferi et al. 2006), the molecular identity of this channel has not been definitely established yet. These cultures may be appropriate for using RNAi techniques to reduce the expression of a particular gene, such as VMD2l1 or other genes, and to analyze the effect the gene has on a function measured by EOG recordings. Indeed, this culture system is appropriate for the delivery of genes or of other substances and for the assessment of functional properties. The use of RNAi on cultured OEs could be a powerful experimental tool to measure the functional consequences of inactivating proteins that may be involved in olfactory transduction and signaling.

A further new area of investigation will also be the measurement of electrophysiological responses of neurons in the OB connected to the OE in this organotypic cultures.

Funding

European Commission (ERG 11-505935); Italian Institute of Technology (IIT 2007); Italian Ministry of Education Research and University (COFIN 2006).

Acknowledgements

We thank Anna Boccaccio for comments on the manuscript, Beatrice Pastore for technical help, and Manuela Schipizza-Lough for checking the English.

References

Ache BW, Young JM. 2005. Olfaction: diverse species, conserved principles. Neuron. 48:417–430.

Boccaccio A, Lagostena L, Hagen V, Menini A. 2006. Fast adaptation in mouse olfactory sensory neurons does not require the activity of phosphodiesterase. J Gen Physiol. 128:171–184.

Boccaccio A, Menini A. 2007. Temporal development of cyclic nucleotide-gated and Ca2+-activated Cl- currents in isolated mouse olfactory sensory neurons. J Neurophysiol. 98:153–160.

Buck LB. 2004. Olfactory receptors and odor coding in mammals. Nutr Rev. 62:S184–S188.

Chen S, Lane AP, Bock R, Leinders-Zufall T, Zufall F. 2000. Blocking adenylyl cyclase inhibits olfactory generator currents induced by "IP(3)-odors". J Neurophysiol. 84:575–580.

Chuah MI, David S, Blaschuk O. 1991. Differentiation and survival of rat olfactory epithelial neurons in dissociated cell culture. Brain Res Dev Brain Res. 60:123–132.

Farbman AI. 1977. Differentiation of olfactory receptor cells in organ culture. Anat Rec. 189:187–199.

Firestein S. 2001. How the olfactory system makes sense of scents. Nature. 413:211–218.

Firestein S, Darrow B, Shepherd GM. 1991. Activation of the sensory current in salamander olfactory receptor neurons depends on a G protein-mediated cAMP second messenger system. Neuron. 6:825–835.

Firestein S, Picco C, Menini A. 1993. The relation between stimulus and response in olfactory receptor cells of the tiger salamander. J Physiol. 468:1–10.

Firestein S, Zufall F, Shepherd GM. 1991. Single odor-sensitive channels in olfactory receptor neurons are also gated by cyclic nucleotides. J Neurosci. 11:3565–3572.

Gahwiler BH. 1981. Organotypic monolayer cultures of nervous tissue. J Neurosci Methods. 4:329–342.

Goetze B, Breer H, Strotmann J. 2002. A long-term culture system for olfactory explants with intrinsically fluorescent cell populations. Chem Senses. 27:817–824.

Gong Q, Liu WL, Srodon M, Foster TD, Shipley MT. 1996. Olfactory epithelial organotypic slice cultures: a useful tool for investigating olfactory neural development. Int J Dev Neurosci. 14:841–852.

Gonzales F, Farbman AI, Gesteland RC. 1985. Cell and explant culture of olfactory chemoreceptor cells. J Neurosci Methods. 14:77–90.

Hegg CC, Greenwood D, Huang W, Han P, Lucero MT. 2003. Activation of purinergic receptor subtypes modulates odor sensitivity. J Neurosci. 23:8291–8301.

Josephson EM, Yilma S, Vodyanoy V, Morrison EE. 2004. Structure and function of long-lived olfactory organotypic cultures from postnatal mice. J Neurosci Res. 75:642–653.

Kleene SJ. 1993. Origin of the chloride current in olfactory transduction. Neuron. 11:123–132.

Kleene SJ, Gesteland RC. 1983. Dissociation of frog olfactory epithelium. J Neurosci Methods. 9:173–183.

Kurahashi T, Yau KW. 1993. Co-existence of cationic and chloride components in odorant-induced current of vertebrate olfactory receptor cells. Nature. 363:71–74.

Li CX, Parker A, Menocal E, Xiang S, Borodyansky L, Fruehauf JH. 2006. Delivery of RNA interference. Cell Cycle. 5:2103–2109.

Lin W, Margolskee R, Donnert G, Hell SW, Restrepo D. 2007. Olfactory neurons expressing transient receptor potential channel M5 (TRPM5) are involved in sensing semiochemicals. Proc Natl Acad Sci USA. 104:2471–2476.

Lledo PM, Gheusi G, Vincent JD. 2005. Information processing in the mammalian olfactory system. Physiol Rev. 85:281–317.

Lowe G, Gold GH. 1993. Nonlinear amplification by calcium-dependent chloride channels in olfactory receptor cells. Nature. 366:283–286.

Ma M, Chen WR, Shepherd GM. 1999. Electrophysiological characterization of rat and mouse olfactory receptor neurons from an intact epithelial preparation. J Neurosci Methods. 92:31–40.

Menini A. 1999. Calcium signalling and regulation in olfactory neurons. Curr Opin Neurobiol. 9:419–426.

Menini A, Lagostena L, Boccaccio A. 2004. Olfaction: from odorant molecules to the olfactory cortex. News Physiol Sci. 19:101–104.

Michel V, Monnier Z, Cvetkovic V, Math F. 1999. Organotypic culture of neuroepithelium attached to olfactory bulb from adult mouse as a tool to study neuronal regeneration after ZnSO4 neuroepithelial trauma. Neurosci Lett. 271:195–198.

Mombaerts P. 2004. Genes and ligands for odorant, vomeronasal and taste receptors. Nat Rev Neurosci. 5:263–278.

Munger SD, Lane AP, Zhong H, Leinders-Zufall T, Yau KW, Zufall F, Reed RR. 2001. Central role of the CNGA4 channel subunit in Ca2+-calmodulin-dependent odor adaptation. Science. 294:2172–2175.

Nickell WT, Kleene NK, Gesteland RC, Kleene SJ. 2006. Neuronal chloride accumulation in olfactory epithelium of mice lacking NKCC1. J Neurophysiol. 95:2003–2006.

Nickell WT, Shipley MT, Behbehani MM. 1996. Orthodromic synaptic activation of rat olfactory bulb mitral cells in isolated slices. Brain Res Bull. 39:57–62.

Noble M, Mallaburn PS, Klein N. 1984. The growth of olfactory neurons in short-term cultures of rat olfactory epithelium. Neurosci Lett. 45:193–198.

Ottoson D. 1955. Analysis of the electrical activity of the olfactory epithelium. Acta Physiol Scand Suppl. 35:1–83.

Pifferi S, Pascarella G, Boccaccio A, Mazzatenta A, Gustincich S, Menini A, Zucchelli S. 2006. Bestrophin-2 is a candidate calcium-activated chloride channel involved in olfactory transduction. Proc Natl Acad Sci USA. 103:12929–12934.

Pinato G, Midtgaard J. 2005. Dendritic sodium spikelets and low-threshold calcium spikes in turtle olfactory bulb granule cells. J Neurophysiol. 93:1285–1294.

Pixley SK, Pun RY. 1990. Cultured rat olfactory neurons are excitable and respond to odors. Brain Res Dev Brain Res. 53:125–130.

Reisert J, Bauer PJ, Yau KW, Frings S. 2003. The Ca-activated Cl channel and its control in rat olfactory receptor neurons. J Gen Physiol. 122:349–363.

Ressler KJ, Sullivan SL, Buck LB. 1993. A zonal organization of odorant receptor gene expression in the olfactory epithelium. Cell. 73:597–609.

Ronnett GV, Parfitt DJ, Hester LD, Snyder SH. 1991. Odorant-sensitive adenylate cyclase: rapid, potent activation and desensitization in primary olfactory neuronal cultures. Proc Natl Acad Sci USA. 88:2366–2369.

Schild D, Restrepo D. 1998. Transduction mechanisms in vertebrate olfactory receptor cells. Physiol Rev. 78:429–466.

Scott JW, Scott-Johnson PE. 2002. The electroolfactogram: a review of its history and uses. Microsc Res Tech. 58:152–160.

Trombley PQ, Westbrook GL. 1991. Voltage-gated currents in identified rat olfactory receptor neurons. J Neurosci. 11:435–444.

Vargas G, Lucero MT. 1999. A method for maintaining odor-responsive adult rat olfactory receptor neurons in short-term culture. Chem Senses. 24:211–216.

Zhainazarov AB, Ache BW. 1995. Odor-induced currents in Xenopus olfactory receptor cells measured with perforated-patch recording. J Neurophysiol. 74:479–483.

Accepted January 17, 2008